A new approach to predictive modelling of flow of hydrophobically associating polyacrylamide polymers in porous media.

AFOLABI, R.O.

2022

A New Approach to Predictive Modelling of Flow of Hydrophobically Associating Polyacrylamide Polymers in Porous Media

Richard O. Afolabi

PhD 2022

A New Approach to Predictive Modelling of Flow of Hydrophobically Associating Polyacrylamide Polymers in Porous Media

Richard O. Afolabi

A thesis submitted in partial fulfilment of the
requirements of
Robert Gordon University
for the degree of Doctor of Philosophy

Funding
The Petroleum Technology Development Fund (PTDF)

April 2022

DECLARATION

I, **Richard O. Afolabi**, declare that this thesis titled "*A New Approach to Predictive Modelling of Flow of Hydrophobically Associating Polyacrylamide Polymers in Porous Media*" and the work presented in it are my own and has been generated by me as the result of my original research.

I confirm that:

1. This work was done wholly while in candidature for a doctorate at Robert Gordon University.
2. Where I have consulted the published work of others, this was always clearly attributed, cited, and referenced.
3. Where I have quoted from the work of others, the source was always given. Except for such quotations, this thesis is entirely my work.
4. I have acknowledged all primary sources of funding for this research work.
5. Parts of this work has been published and being considered for publication as:
   a) **Afolabi, R. O.**, Oluyemi, G. O., Officer, S., & Ugwu, J. O. (2019). Hydrophobically Associating Polymers for Enhanced Oil Recovery – Part A: A Review on the Effects of Some Key Reservoir Conditions. *Journal of Petroleum Science and Engineering, 180*, 681-698.
   b) **Afolabi, R. O.**, Oluyemi, G. O., Officer, S., & Ugwu, J. O. (2019). Hydrophobically Associating Polymers for Enhanced Oil Recovery – Part B: A Review of Modelling Approach to Flow in Porous Media. *Journal of Molecular Liquids, 293*, 111495.
   c) **Afolabi, R. O.**, Oluyemi, G. O., Officer, S., & Ugwu, J. O. (2020). Determination of a Critical Separation Concentration for Associative Polymers in Porous Media Based on Quantification of Dilute and Semi-Dilute Concentration Regimes. *Journal of Molecular Liquids, 317*, 114142.
   d) **Afolabi, R. O.**, Oluyemi, G. O., Officer, S., & Ugwu, J. O. (2021). A New Approach for Quantitative Mapping of Retention Mechanisms of Associative Polymers in Porous Media. *Journal of Molecular Liquids, 343,* 117685.

DEDICATION

To God Almighty,
The Creator of the ends of the earth,
From whom all blessings flow.

"His understanding is unsearchable. He gives power to the weak,
And to those who have no might, He increases strength.
Even the youths shall faint and be weary, and the young men shall utterly fall,
But those who wait on the Lord, shall renew their strength"
Isa 40:28-31a (NKJV)

To the entire faculty and staff of the School of Engineering, Robert Gordon University.
To my wife, Esther O. Afolabi, for your patience and understanding during the past three years.
To my parents, Prince (Late) Emmanuel O. Afolabi and Mrs. Helen A. Afolabi.

ACKNOWLEDGEMENTS

First, I would like to express my sincere gratitude to the Petroleum Technology Development Fund (PTDF) for the Overseas Scholarship Scheme (OSS) under the grant number PTDF/ED/PHD/ARO/1387/18. This funding allowed me to pursue my doctorate at Robert Gordon University (RGU), Aberdeen, United Kingdom. The scholarship scheme has enabled me to experience a different culture in addition to my primary academic purpose. I would like to thank Dr Andrew Lamb and his team of professionals at the graduate school for the series of unending development programmes to ensure that every moment of my research journey was impactful. Specifically, I would like to thank Mrs Dorothy McDonald, Dr Lesley Dickson, Mr Martin Simpson and Mrs Andrea MacMillan for their tireless support and commitment in ensuring a smooth doctorate journey. Further, I would like to thank my supervisory team comprising Dr Gbenga F. Oluyemi, Dr Simon Officer, and Dr Johnson O. Ugwu for their consistent support and guidance during this project's running and thoughtful comments on this thesis and the subsequent publications from it. I am also thankful to the technical services team of the School of Engineering, Mr Alan McClean, and Mr David Howie, for all their thoughtful guidance in the setup and running of my laboratory experiments. I would like to especially appreciate Mr Alan McClean for his doggedness in ensuring health and safety procedures are followed to the latter. In addition, my appreciation goes to Dr Yakubu Balogun for his assistance with the core flooding setup and for always being available for inquiries. My deep appreciation also goes to the administrative team of the School of Engineering comprising of Dr Rosslyn Shanks, Mrs Petrena Morrison, and Mrs Kirsty Stevenson for their apt attention as it relates to administrative matters affecting my research. My gratitude also extends to my colleagues and friends I have made during my research journey, namely Mr Mutiu Adegboye, Mr Emmanuel Eke, Mrs Priscilla Ogunlude, Mr Auwalu Mohammed and Mr Promise Oyama. I appreciate every moment we have had to rub minds on our research works and post-doctorate journey. To conclude, I cannot forget to thank my family for all the unconditional support in this very intense academic journey. To my wife, Esther O. Afolabi, I express my sincere gratitude for your patience and understanding during the past three years. Finally, I acknowledge my mother, Mrs Helen Afolabi, for her endless prayers during my doctorate journey. To everyone I cannot mention due to space constraints and has contributed formally or informally to the success of my doctorate journey, I am indeed grateful.

ABSTRACT

Associative polymers provide a high resistance factor due to their thickening effect. However, the high resistance factor may simply reflect pore plugging in the porous media. This offers a significant limitation for the deep propagation of the beneficial effect of viscous thickening arising from associative interactions of the polymer molecules. Consequently, sustaining this beneficial effect of associative interactions remains an active area of research. In this work, a novel predictive approach was developed for quantitative mapping of the various retention mechanisms and flow regimes connected with the transport of hydrophobic interactions in associative polymers. As a result, the methodology for this research work was developed in three stages. Firstly, a novel dimensionless variable was defined for quantifying hydrophobic interactions between associative polymer molecules. This was achieved with the knowledge of the critical aggregation concentration of the polymer molecules. Secondly, the structural kinetic theory was adopted in mapping static to dynamic retention in the porous media. This was achieved by relating the characteristic time scale for static and dynamic retention to the variation in polymer and reservoir properties, thus making it possible to correlate static retention results to large-scale dynamic retention with minimal fitting parameters. In this predictive model, the in-situ entrapment was linked to the effective pore radius and the hydrodynamic size of the polymer molecules. Thirdly, a similar structural kinetic theory was employed for the quantitative description of hydrophobic interactions under shear thinning, shear thickening, and shear degradation flow regimes in the porous media. Likewise, the degradation of hydrophobic interactions was predicted based on the individual expressions for the different flow regimes. Finally, an optimization approach was developed to sustain hydrophobic interactions in the porous media by combining the predictive models for hydrophobic interactions lost to polymer retention and the hydrophobic interactions gained due to elongation effects in the porous media. The research findings showed that the hydrophobic interactions lost to different retention mechanisms play a significant role in pore damage. The proportion of hydrophobic interactions lost to polymer retention at 25 ℃ varied from 0.04 to 0.56 for polymer concentrations from 50 to 1,000 ppm. This amounted to an estimated damaged pore volume ranging from 0.21 to 0.46 PV and a porosity reduction from 0.364 to 0.19. The quantitatively mapped adsorption accounted for 99.9, 98.5 and 91.5 % of the total damaged pore volume for 300, 500 and 750 ppm, respectively, while entrapment amounted to 0.1, 1.5 and 8.5 % of the damaged pore volume. The optimized condition for hydrophobic

interactions in a porous media was obtained when the correction factor related to the net hydrophobic interactions lost to polymer retention and the net hydrophobic interactions gained from elongation effects was unity ($\omega_a = 1$). As a result, the optimized polymer concentrations at 25 ℃ for 1, 3 and 6 mL/min were 420, 560 and 740 ppm, respectively. The observed outcomes imply that the hydrophobic interactions lost to the retention and gained due to elongation thickening in the porous media play a significant role in the sustainability of these interactions in porous media. Furthermore, the optimization approach enabled further sustainability of hydrophobic interactions deep into the porous media by ensuring that the net hydrophobic interactions lost to retention were equally gained from the elongation thickening effect, thus ensuring pre-injection levels hydrophobic interactions can be maintained deep in the porous media. This research outcome gives a new insight into the proper planning, design, and optimisation of associative polymers for oil recovery operations.

Keywords: Associative Polymers; Polyacrylamide; Hydrophobic Interactions; Porous Media; Predictive Modelling.

TABLE OF CONTENTS

LIST OF TABLES

LIST OF FIGURES

NOMENCLATURE

Abbreviations

AA	Acrylic Acid
AM	Acrylamide
$AMC_{12}S$	2-(acrylamido)-dodecanesulfonic acid
AMPS	2-acrylamido-2-methyl propane sulfonate
ASE	Alkali Swellable Emulsion
API	American Petroleum Institute
ANOVA	Analysis of Variance
BBD	Box-Behnken Design
CAC	Critical Aggregation Concentration
CAT	Critical Association Temperature
DOAC	*N,N*-dimethyloctadeyl allyl ammonium chloride
DPP	1-(4-dodecyloxy-phenyl)-propenone
DF	Dilution Factor
DPV	Damaged Pore Volume
EOR	Enhanced Oil Recovery
cEOR	Chemical Enhanced Oil Recovery
EUR	Ethoxylated Urethane
FTIR	Fourier Transform Infrared
HAPAM	Hydrophobically Associating Polyacrylamide
HPAM	Hydrolysed Polyacrylamide
HEC	Hydroxyethyl cellulose
HRTEM	High Resolution Transmission Electron Microscope
HTHS	Hight Temperature High Salinity

IPV	Inaccessible Pore Volume
IFT	Interfacial Tension
LCST	Lower Critical Solution Temperature
NDS	3-(diallyl-amino)-2- hydroxypropyl sulfonate
NIMA	3-(2-(2-Heptadec-8-enyl-4,5-dihydro-imidazol-1-yl) ethyl carbamoyl) acrylic acid
NIPA	*N*-isopropylacrylamide
NMR	Nuclear Magnetic Resonance
NIDAQ	National Instruments Data Acquisition System
PAM	Polyacrylamide
PAA	Poly Acrylic Acid
PEG	Polyethylene Glycol
PEF	Polymer Enhanced Foam
RPM	Revolution per Minute
RF	Resistance Factor
RRF	Residual Resistance Factor
RSD	Response Surface Design
SFB	Synthetic Formation Brine
SSS	Sodium 4-styrenesulfonate
TEM	Transmission Electron Microscope
TGA	Thermogravimetric Analysis
TDS	Total Dissolved Solids
UCST	Upper Critical Solution Temperature

A	Cross Sectional Area of Core Holder, $\mathbf{cm^2}$
A_{pr}	Polymer Activity, $\mathbf{wt.}\ \%$
a	Recovery Constant during Shear Thinning, $\mathbf{1/s}$
ΔP	Differential Pressure across Core Holder, **Pa**
ΔPV	Differential Number of Pore Volume for Effluent Cut, **(PV)**
b	Breakdown Constant during Shear Thinning **(-)**
B	Empirical Fitting Coefficient, $\mathbf{g/\mu g}$
B_a and k_a	Parameter Constants for Arrhenius Equation
Ca	Capillary Number
C_{ag}	Critical Aggregation Concentration, **ppm**
C_d	Concentration of Diluted Polymer Solution, **ppm**
C_{pe}	Effective Polymer Concentration, **ppm**
C_i	Concentration of Individual Salts in Ionic Solution, **ppm**
C_s	Weighted Sum of Ionic Concentrations in Solution, **ppm**
C_p	Polymer Concentration, **ppm**
$C_{p,i}$	Initial Polymer Concentration, **ppm**
$C_{p,f}$	Final Polymer Concentration, **ppm**
$C_{sep,c}$	Critical Separation Concentration, **ppm**
C_{ps}	Concentration of Stock Polymer Solution, **ppm**
C_{p-eff}	Effluent Polymer Concentration from Porous Media, **ppm**
C_{tr-eff}	Effluent Tracer Concentration from Porous Media, **ppm**
C_{p-inj}	Injected Polymer Concentration to Porous Media, **ppm**
C_{tr-inj}	Injected Tracer Concentration to Porous Media, **ppm**

D_{rot}	Rotational Diffusion Coefficient, $\mathbf{(Rad^2/s)}$
D_g or R_{gr}	Average Rock Grain Size, $\boldsymbol{\mu m}$
E_{PV}	Excluded Pore Volume for Effective Polymer Concentration, **(PV)**
E_a	Activation Energy, $\mathbf{J/mol.K}$
f_{rup}	Polymer Rupturing Rate, $\mathbf{1/s}$
g	Extension Parameter during Shear Thickening, **(-)**
h	Contraction Constant during Shear Thickening, $\mathbf{1/s}$
H_i	Intermolecular Interactions, **(-)**
H_{app}	Apparent Hydrophobic Interactions, **(-)**
H_μ	Hydrophobic Interactions - Normalized Remaining Viscosity, **(-)**
$H_{C_{pD}}$	Hydrophobic Interactions - Dimensionless Concentration, **(-)**
H_0	Initial Hydrophobic Interactions, **(-)**
H_{sh}	Hydrophobic Interactions during Shearing Thinning, **(-)**
H_{el}	Hydrophobic Interactions during Shear Thickening, **(-)**
H_{max}	Maximum Hydrophobic Interactions, **(-)**
IPV or I_{PV}	Inaccessible Pore Volume, $\mathbf{cm^3}$
I_I	Intramolecular Interactions, **(-)**
k_B	Boltzmann Constant ($1.380 \times 10^{-23} \mathbf{m^2 kg s^{-2} K^{-1}}$)
k_b	Rock Permeability to Brine, **mD**
k_d	Damaged Rock Permeability, **mD**
k_0	Initial Rock Permeability, **mD**
K'	Mark-Houwink Constant, $\mathbf{dL/g}$
k	Number of Factor in Experimental Design, **(-)**
L_p	Average Pore Length in Porous Media, **cm**

L	Length of Core Holder, **cm**
M_1	Mass of Empty Measuring Cylinder, **g**
M_2	Mass of Cylinder and Sand Grains, **g**
M_{gr}	Mass of Sand Grains, **g**
M_{gr+Wat}	Mass of Grains and Brine, **g**
m	Recovery Exponent during Shear Thinning, **(-)**
m_g	Extension Exponent during Shear Thickening, **(-)**
M_{w0}	Reference Polymer Molecular Weight, $\mathbf{g/mol}$
M_w	Measured Polymer Molecular Weight, $\mathbf{g/mol}$
$\overline{M_w}$	Average Polymer Molecular Weight (Manufacturer), $\mathbf{g/mol}$
n	Breakdown Exponent during Shear Thinning, **(-)**
n_h	Contraction Exponent during Shear Thickening, **(-)**
N_A	Avogadro's Constant ($6.022 \times 10^{23} \mathbf{mol^{-1}}$)
N_{De} or N_D	Deborah Number, **(-)**
PV_{gr}	Grain Pore Volume, $\mathbf{cm^3}$
PV_{inj}	Number of Pore Volumes Injected, **(PV)**
PV_{pb}	Number of Pore Volumes to Polymer Breakthrough, **(PV)**
PV_{bb}	Number of Pore Volumes to Brine Breakthrough, **(PV)**
R_g	Gas Constant, $\mathbf{Jmol^{-1}K^{-1}}$
R_h	Hydrodynamic Radius of Polymer Molecules, **µm**
R_p	Effective Pore Radius, **µm**
v_p	Average Pore Velocity, $\mathbf{m/s}$
V_{gr}	Bulk Volume of Sand Grain, $\mathbf{cm^3}$
V_{po}	Volume of Pore Spaces, $\mathbf{cm^3}$

Q_b	Brine Flowrate, $\mathbf{cm^3/s}$
R^2	Coefficient of Determination, **(-)**
${R_{adj}}^2$	The Adjusted R^2 Value, **(-)**
${R_{pred}}^2$	The Predicted R^2 Value, **(-)**
$Ret_{C_{pi}}$	Cumulative Retained Polymer Molecules in the Porous Media, **(-)**
T	Temperature, **K**
$t_{max-ret}$	Time for Maximum Retention under Static Conditions, **s**
t_{sol}	Polymer solution flow time in a Ubbelohde viscometer, **s**
t_{slv}	Solvent flow time in a Ubbelohde viscometer, **s**
V_m	Volume Occupied per Polymer Chain, $\mathbf{cm^3}$
W_d	Weight of Diluted Polymer Solution, **g**
W_{gr}	Weight of Rock Grains, **g**
W_p	Weight of Polymer Solutions, **g**
W_d	Weight of Empty Ceramic Dish, **g**
W_{d+HS}	Weight of Ceramic Dish and Polymer Granules, **g**
W_{d+DS}	Weight of Ceramic Dish and Polymer Granules after Heating, **g**
W_{pr}	Weight of Polymer Granules, **g**
W_s	Weight of Stock Polymer Solution, **g**
W_{bs}	Weight of Brine Solution for Dilution, **g**
W_{bd}	Weight of Brine Solution for Dilution, **g**
X_i	The Coded Independent Variables, **(-)**
X_iX_j	The Coded Interaction Terms, **(-)**
${X_i}^2$	The Coded Quadratic Terms, **(-)**
$y(\lambda_1)$	Box-Cox Transformation Parameter, **(-)**

Greek Symbols and Units

α	Dimensionless Parameter for Effective Salinity **(-)**
σ	Mark-Houwink Constant, $\mathbf{dL/g}$
β_1	Polymer Relaxation Time, $\mathbf{s}$
β_2	Stretching Constant, $\mathbf{1/s}$
β_3	Critical Time for the Onset of Polymer Degradation, $\mathbf{s}$
β_a	Tuning Parameter (Theoretical Value: 0.144$\mathbf{Kmol^{-1}J^{-1}}$)
β_b	Tuning Factor for Uncertainties in the Pore Structure
β_o	Intercept Coefficient of the Statistical Model, **(-)**
β_i	Linear Coefficient of the Statistical Model, **(-)**
β_{ii}	Squared Coefficient of the Statistical Model, **(-)**
β_{ij}	Interaction Coefficient of the Statistical Model, **(-)**
β_1 to β_6	Parameters of the Statistical Model in Uncoded Units, **(-)**
ϕ	Rock Porosity, **(-)**
ϕ_d	Damaged Rock Porosity, **(-)**
ϕ_0	Initial Rock Porosity, **(-)**
Γ_{DPV}	Damaged Pore Volume, $\mathbf{cm^3}$
Γ_{PV}	Fractional Pore Volume Occupied by Polymer Molecules, **(-)**
Γ_p	Polymer Adsorbed, $\mathbf{\mu g/g}$
ρ_{gr}	Rock Grain Density, $\mathbf{g/cm^3}$
ρ_{poly}	Polymer Density, $\mathbf{g/cm^3}$
τ_p	Polymer Relaxation Time, $\mathbf{s}$
τ_c	Contact Time, $\mathbf{s}$
τ_{ct}	Characteristic Flow Time, $\mathbf{s}$
τ_r	Pore Residence Time, $\mathbf{s}$

τ_{el}	Elongational Relaxation Time, **s**
μ_{agg}	Apparent Polymer Viscosity at the CAC, **Pas**
μ_{app}	Apparent Polymer Viscosity, **Pas**
μ_{sh}	Shear Thinning Polymer Viscosity, **Pas**
μ_{el}	Elongational Polymer Viscosity, **Pas**
μ_0	Zero Shear Rate Viscosity, **Pas**
μ_{min}	Minimum Polymer Viscosity, **Pas**
μ_{max}	Maximum Polymer Viscosity, **Pas**
μ_{rel}	Relative Polymer Viscosity, **(-)**
$[\mu]$	Polymer Intrinsic Viscosity, $\mathbf{dL/g}$
μ_s	Solvent Viscosity, **Pas**
μ_{sp}	Specific Viscosity, **(-)**
μ_w	Viscosity of Deionized Water, **Pas**
θ_i	Parameter that Depends on the Valency of the Ions in Solution, **(-)**
λ	Dependency of Molecular Weight on Hydrophobic Degradation, **(-)**
λ_1	Optimal Value for the Determination of $y(\lambda_1)$, **(-)**
ω_a	Correction Factor for Hydrophobic Interactions, **(-)**
γ	Polymer Shear Rate, $\mathbf{1/s}$
γ_c	Critical Shear Rate for Onset of Shear Thickening, $\mathbf{1/s}$
$\gamma_{c,deg}$	Critical Shear Rate for Onset of Shear Degradation, $\mathbf{1/s}$
γ_{deg}	Shear Rates under Degradation Flow Regime, $\mathbf{1/s}$
γ_{el}	Shear Rates under Elongation Flow Regime, $\mathbf{1/s}$
γ_{sh}	Shear Rates under Shear Thinning Flow Regime, $\mathbf{1/s}$

CHAPTER ONE

1.0. Introduction

1.1. Research Background and Focus

A common trend during the transport of polymers in porous media is that hydrodynamic forces act differently on the polymeric species[1] because of their size distribution (Abidin et al., 2012; Kamal et al., 2015; Lohne et al., 2017; Silva et al., 2018). The outcome of this flow induced separation is that the injected polymer solution is split into three phases: a polymer-rich phase, a polymer-depleted phase, and a solvent (water or brine) phase (Lohne et al., 2017). The solvent phase, being propagated at a low flowrate, will occupy the micropores of the porous media that are completely inaccessible to the polymer molecules (Taylor and Nasr El-Din, 1998; Levitt and Pope, 2008; Wever et al., 2013; Al-Sabagh et al., 2016; Raffa et al., 2016; Lohne et al., 2017). These pores occupied by the solvent do not necessarily translate to the overall inaccessible pore volume but rather a component of the overall inaccessible pore volume. The individual components of the overall inaccessible pore volume arise because polymer entrapment also contributes to the overall inaccessible pore volume in porous media. For the polymer-depleted phase, this fills the pore surface and represents practically the immobile phase of the polymer solution. Finally, the polymer-rich layer is sterically excluded from the remaining two layers and flow at the centre of the pores. This observed phenomenon arises due to the size distribution of the polymer molecules in solution (Yin et al., 2006; Zhang et al., 2008; Gong and Zhang, 2009; Skauge et al., 2018). The sterically excluded polymer-rich phase occurs for associative polymers due to the large proportion of hydrophobic interactions between polymer molecules. The network of polymer chains that constitute this phase flow as a single entity in the porous media, thereby maintaining some level of viscous thickening. Furthermore, the segregation of polymer molecules during flow in porous media explains why the effective viscosities measured during core floods may differ from the corresponding bulk viscosity values. The segregation of polymer molecules means that the injected associative polymer solutions exhibit an in-situ concentration (or effective concentration). Also, the strength of the molecular interactions that constitute this phase is related to the molecular size and distribution of hydrophobic moieties on the backbone of the molecules (Taylor and Nasr El-Din, 1998; Levitt and Pope, 2008; Wever et al., 2013; Al-Sabagh et al., 2016; Raffa et

[1] Polymeric species, polymer molecules and polymer chains were used interchangeably and mean the same thing.

al., 2016; Lohne et al., 2017). Large hydrophobic blocks on the polymer chain mean sizeable molecular interaction and vice versa (Delamaide et al., 2013; Liao et al., 2017; Zhong et al., 2017; Bai et al., 2018; Li et al., 2018). However, the polymer units within the polymer-depleted phase remain close to the pore surface and interface with the polymer-rich layer, where the exchange of polymer molecules and associative interactions occurs depending on the reservoir conditions (Lohne et al., 2017). Also, the polymer molecules within this depleted phase maintain a lower proportion of hydrophobic interactions than the polymer-rich phase. Overall, the transport of associative polymers in porous media leads to the separation of hydrophobic interactions, which are split between the polymer-rich phase and the polymer-depleted phase (Lohne et al., 2017). Previous studies show that the proportion of these hydrophobic interactions within the polymer-rich phase depend on local variation in the reservoir parameters such as temperature, salinity, permeability, porosity, pH and hardness (Sun et al., 2015; Akbulut and Temizel, 2017; El-Hoshoudy et al., 2017; Li et al., 2018). However, under these reservoir conditions, there is still limited understanding of the distribution, propagation and the sustainability of these hydrophobic interactions deep in a porous media despite numerous scientific works on associative polymers (Zhou et al., 2008; Gao, 2011; Kang et al., 2016). According to Seright et al. (2011), two reasons may contribute to the limited understanding of the distribution, propagation and the sustainability of these hydrophobic interactions in a porous media. Firstly, the existing experimental approach used in numerous scientific works reported over the last decade was limited to short cores with external pressure taps to evaluate hydrophobic interactions inside the porous media. Thus, the high resistance factor (RF) exhibited by such polymers may simply reflect pore plugging in the porous media and, as such, provides a limited understanding of the beneficial effect of associative interactions propagated deep in porous media (Dupuis et al., 2010; Dupuis et al., 2011; Seright et al., 2011; Dupas et al., 2013). In other words, the high RFs reported in the literature using short cores may indicate that polymer retention dominates or contribute significantly to the RF compared to the desired effect of viscous thickening for mobility control. Different retention mechanisms have been reported with associative polymers, including multilayer adsorption, entrapment and plugging (Wei et al., 2007; Zhou et al., 2008; Delamaide et al., 2013). However, it is not a straightforward approach using experimental analysis in identifying if polymer retention or viscous thickening contributes significantly to the RF experienced in a porous media as determination of the RF takes a generalized approach. Secondly, the rapid and abrupt increase in polymer viscosity with concentration above the critical aggregation

concentration (CAC) leads to concerns about controlling the performance of the polymer during flooding operations (Taylor and Nasr El-Din, 1998; Levitt and Pope, 2008; Wever et al., 2013; Al-Sabagh et al., 2016; Raffa et al., 2016; Lohne et al., 2017). Adequate control of these hydrophobic interactions is crucial as small operational errors could result in polymer injectivity issues when polymer concentration exceeds a target and may provide insufficient mobility when the concentration is low (Dupuis et al., 2011; Seright et al., 2011; Patokina, 2015; Guo et al., 2018). For such operational errors, predictive control becomes significant and this would extend beyond the existing limitations of known experimental approaches in forecasting the performance of associative polymers deep in a porous media. However, a distinct quantitative parameter for the estimation and monitoring of these changes in hydrophobic interactions during flow in a porous media is required. The applicability of existing quantitative metrics to control the in-situ hydrophobic interactions between the polymer molecules may not uniquely capture the transient behaviour of these interactions within the distributed phases identified earlier. For example, previous experimental studies on associative polymers using core flooding have used parameters such as the RF as a measure of hydrophobic interactions between polymer molecules (Taylor and Nasr El-Din, 1998; Guo et al., 2012; Ye et al., 2013; Chen, 2016; Dai et al., 2017). As mentioned previously, these experimental studies use short cores in which the high values of the RF may be an indication of plugging rather than viscous thickening or a combination of both (Seright et al., 2011). In this case, using the RF as a measure of the in-situ hydrophobic interactions may not indicate its distribution within the polymer phases identified but rather a generalised outcome. The distribution of hydrophobic interactions within these phases is crucial in understanding its sustainability and propagation deep into a reservoir. As such, the use of the RF as a measure of changing hydrophobic interactions may not adequately capture the behaviour of these hydrophobic interactions within the distributed phases described for associative polymer transport in a porous media. Thus, limiting the overall understanding of the sustainability of these hydrophobic interactions deep in a reservoir. Nonetheless, the RF remain the only experimental parameter known for describing polymer in-situ behaviour during transport in a porous media (Taylor and Nasr El-Din, 1998; Levitt and Pope, 2008; Wever et al., 2013; Al-Sabagh et al., 2016; Raffa et al., 2016; Lohne et al., 2017). Therefore, predictive estimates and numerical quantification of these molecular interactions would require modification of these parameters where possible. However, identifying a quantifiable parameter, which can be related to viscosity or RF, remains paramount for achieving predictive control of hydrophobic interactions.

1.2. Research Statement of Problem

The desired goal of polymer flooding for enhanced oil recovery (EOR) is to provide appropriate mobility control. This improved mobility can be manifested in a high resistance factor through viscous thickening. Also, associative polymers reported from numerous experimental studies to provide such high values compared to non-associative polymers such as hydrolysed polyacrylamide (HPAM). Also, these high RFs connected to associative polymers have been reported to take place under known severe degradation and retention conditions in reservoirs (Oruwori and Ikiensikimama, 2010; Wever et al., 2011; Lai et al., 2013; Choi et al., 2014; Al-Sabagh et al., 2016; Raffa et al., 2016; Das et al., 2017; Sarsenbekuly et al., 2017; Bai et al., 2018; Silva et al., 2018). Thus, this makes associative polymers a potentially desirous ingredient for chemical enhanced oil recovery involving polymer flooding. The field trials on chemical flooding operations have seen an unprecedented shift towards the application of associative polymers in the last decade (Yin et al., 2006; Zhang et al., 2008; Gong and Zhang, 2009; Skauge et al., 2018). However, the high resistance factors associated with associative polymers may not necessarily be the desirous beneficial effect needed for enhanced oil recovery. This unbeneficial effect from the high RFs may indicate the loss to large polymer aggregates formed due to hydrophobic interactions to polymer retention mechanisms such as entrapment rather than the desirous viscous thickening effect for mobility reduction. Previous research works have indicated that these aggregates are lost to retention a few meters from the injection point, thus putting in doubt the ability of these associative polymers to propagate their improved rheological properties deep into a reservoir (Seright et al., 2011; Wever et al., 2011; Wever et al., 2013; Li et al., 2017; Silva et al., 2018; Sharafi et al., 2018). Unfortunately, this may have limited the use of associative polymers to experimental studies and field trials with no reported concrete field application (Yin et al., 2006; Zhang et al., 2008; Gong and Zhang, 2009; Seright et al., 2011). Consequently, there is a clear gap in research in understanding the in-situ behaviour of these hydrophobic interactions between associative polymer molecules. Filling this knowledge gap is critical in optimising the performance of associative polymers, as it would give an insight into how different polymer retention mechanisms and flow regimes would affect the propagation of hydrophobic interactions between associative polymers. As a result, this identified gap in the transport of associative polymers in porous media formed the basis of this research work.

1.3. Research Aim and Objectives

This research aimed to carry out a systematic modelling and optimization of the propagation of hydrophobic interactions between associative polymer molecules in a porous media. The specific objectives achieved by this research work include the following as itemized below:

a) Define a dimensionless parameter based on measurable entities to quantify the proportion of hydrophobic interactions and extend the dimensionless parameter to incorporate polymer and porous media properties.
b) Develop a model for predicting in-situ pressure drop based on the effect of in-situ hydrophobic interactions on the different polymer retention mechanisms and polymer flow regimes in porous media.
c) Examine and validate the predictions of the developed model and the associated effects of the components describing the effects of hydrophobic interactions on polymer retention and flow regimes using existing and modified experimental procedures.
d) Enhance and optimize the propagation of hydrophobic interactions between associative polymers within the limits of the developed model predictions, considering the effects of polymer retention and viscosity thickening.

1.4. Research Approach and Workflow

The approach used in achieving the overall research aim and the underlying specific objectives identified was a mix of modelling, statistical and experimental methods. The research approach was developed using the methodical workflow in Figure 1.1 below. The various components of the workflow are summarized into the following sections:

a) **Parameter Identification**: This step was carried out to define a dimensionless parameter to quantify the proportion of hydrophobic interactions between associative polymer molecules within a given polymer concentration. The defined dimensionless parameter was only used to quantify the proportion of hydrophobic interactions between molecules and does not consider the magnitude of the strength of this type of intermolecular association. As such, the output of this dimensionless parameter has values between 0 and 1 with values closer to one, indicating that associative hydrophobic interactions dominate the overall molecular interactions and values closer to zero indicating non-associative intramolecular interactions dominating.

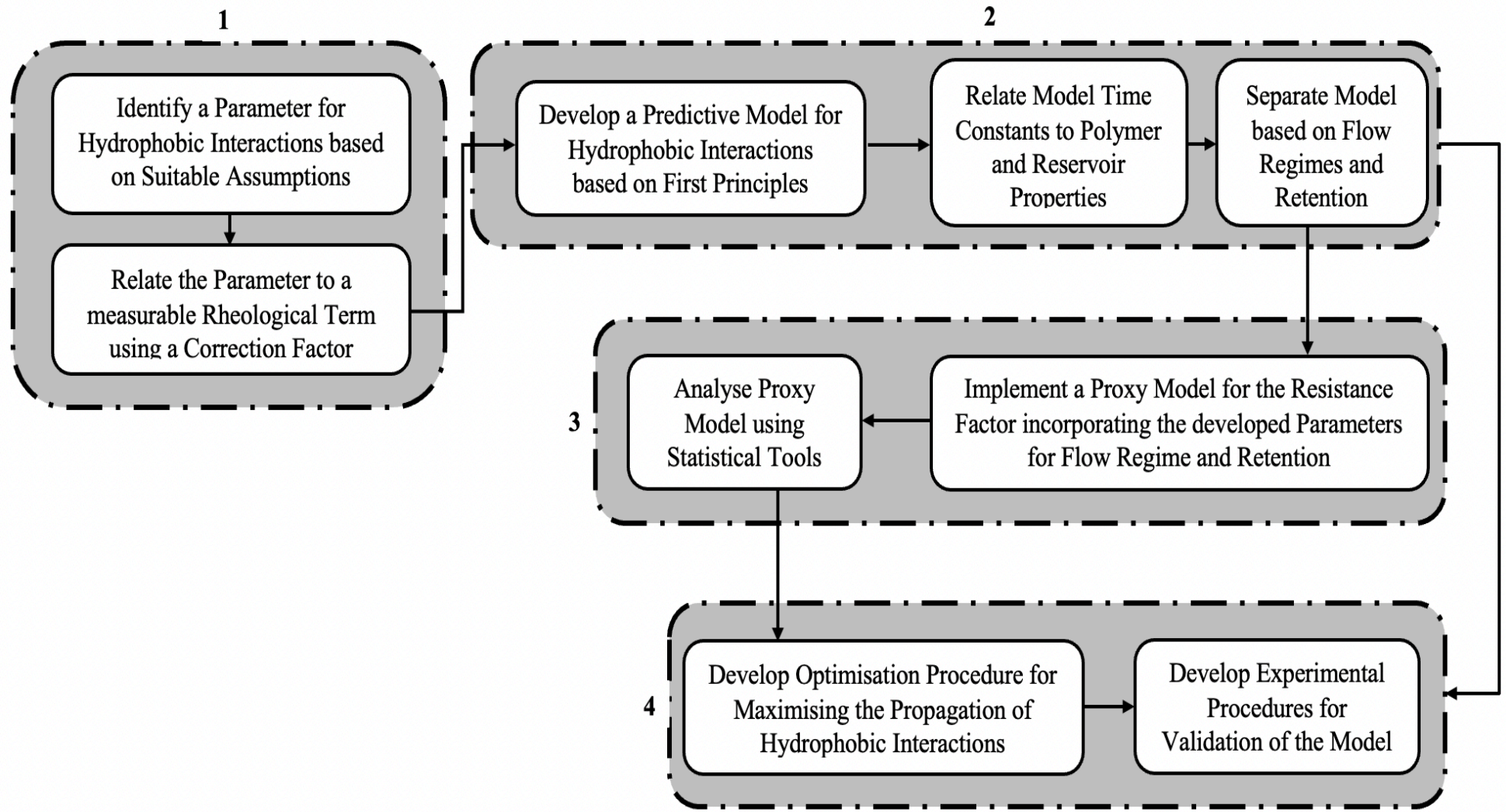

***Figure 1.1**: Research approach and workflow: (1) Parameter identification (2) Predictive modelling (3) Proxy modelling and (4) Experimental validation*

b) **Predictive Modelling from First Principles**: The modelling approach was based on the application of the structural kinetic theory. This theory was applied to develop correlations relating the dimensionless parameter to the effects of polymer retention and the various flow regimes associated with the transport of polymers in porous media. The associated model constants were related to:
    i. Reservoir and field operating conditions: temperature, brine salinity and ion concentration, flow rate (or shear rate) and polymer concentration.
    ii. Polymer and reservoir properties: polymer molecular weight, porosity, and permeability.

c) **Proxy Modelling of Resistance Factor**: This aspect involved using a statistical design of experiment to develop a proxy model for the resistance factor (and pressure drop) incorporating the dimensionless parameters for the flow regimes and polymer retention. The type of statistical design chosen was based on the number of experimental runs, cost, and availability of crucial ingredients for the experiments. The application of the regression analysis (proxy modelling) was made to connect the individual models developed from the first principles to the overall pressure drop (or resistance factor) across the porous media. This approach helps to identify whether polymer retention or viscosity thickening has the most significant contribution to the in-situ pressure drop, thereby optimising the propagation of associative polymers in porous media.

d) **Experimental Validation**: The various procedures used to validate the developed model predictions were structured according to the American Petroleum Institute (API) Specification 63 (Recommended Practices for the Evaluation of Polymers used in Enhanced Oil Recovery Operations). The adopted procedures from the API specification 63 were structured along two lines. Firstly, characterisation of the polymer and porous media material. This ensured the determination of crucial polymer properties such as intrinsic viscosity (or molecular weight) and porous media properties such as porosity and permeability. Secondly, determination of polymer retention, degradation, and in-situ viscosity (and resistance factor). This allowed for the validation of the novel approach for mapping the various retention mechanisms connected with associative polymers, the model predictions of the pressure drop and onset of polymer degradation.

The workflow presented here was simply a summary of the methodology employed in this research work. The details of the component of each workflow are comprehensively described in chapter three and four of this thesis.

1.5. Research Outcomes, Significance and Publications

A key parameter in the design of a polymer flood system for mobility control is the cost-effectiveness of the system. The cost-effectiveness of the system is determined by the cost of the polymer and the corresponding resistance factor provided by the chosen polymer solution at conditions in the reservoir. Consequently, associative polymers offer a much higher resistance factor than non-associative polymers such as HPAM. However, the high resistance factor may not necessarily indicate the desired mobility control but rather a significant loss of hydrophobically induced polymer aggregates to retention. Thus, these hydrophobically induced aggregates are specifically responsible for the cost-effectiveness of the polymer. This research work was able to quantitatively identify the contributions of hydrophobically induced polymer aggregates to polymer retention and effective viscosity, thereby optimizing the mobility control of associative polymers with minimizing loss of aggregates to retention. Thus, an optimum polymer concentration can be defined for the injected slug, which is also an underlying factor in the success of any polymer flooding project. The outcome of this research work was the improvement and enhancement of the overall cost-effectiveness of associative polymers compared to non-associative polymers. Besides, these findings negate the need for compositionally tuned polymer slugs which has been suggested in literature for improving in-situ viscosity when propagated deep in the reservoir. Also, the concept of compositionally tuned slugs has a couple of uncertainties surrounding the number of injected slugs (leading and trailing slugs), the composition of injected slugs, the size of the injected slugs and the number of cycles of injected slugs needed to sustain hydrophobic interactions. These uncertainties would limit the economic viability of applying the concept of compositionally tuned polymer slugs. However, the knowledge of the in-situ behaviour of hydrophobic interactions would mean reduced uncertainty on the overall economics of the polymer flooding project. The following research publications represent some of the significant output of this work:

a) **Afolabi, R. O.**, Oluyemi, G. O., Officer, S., & Ugwu, J. O. (2019). Hydrophobically Associating Polymers for Enhanced Oil Recovery – Part A: A Review on the Effects of Some Key Reservoir Conditions. *Journal of Petroleum Science and Engineering, 180*, 681-698.
b) **Afolabi, R. O.**, Oluyemi, G. O., Officer, S., & Ugwu, J. O. (2019). Hydrophobically Associating Polymers for Enhanced Oil Recovery – Part B: A Review of Modelling Approach to Flow in Porous Media. *Journal of Molecular Liquids, 293*, 111495.

c) **Afolabi, R. O.**, Oluyemi, G. O., Officer, S., & Ugwu, J. O. (2020). Determination of a Critical Separation Concentration for Associative Polymers in Porous Media Based on Quantification of Dilute and Semi-Dilute Concentration Regimes. *Journal of Molecular Liquids, 317*, 114142.

d) **Afolabi, R. O.**, Oluyemi, G. O., Officer, S., & Ugwu, J. O. (2021). A New Approach for Quantitative Mapping of Retention Mechanisms of Associative Polymers in Porous Media. *Journal of Molecular Liquids, 343,* 117385.

1.6. Research Contributions to Knowledge

This research work has given new insights into the transport of hydrophobically associating polymers in porous media. Furthermore, these insights are significant for optimising and maximising hydrophobic interactions between polymer chains during transport in porous media. The substantial and impactful contributions of this research work to the body of knowledge include the following:

a) Identifying a unique and measurable parameter for quantifying the proportion of hydrophobic interactions between associative polymer molecules during flow in porous media. Also, the total proportion of molecular interactions in terms of associative and non-associative was computed as unity. Therefore, for a given estimation of associative hydrophobic interactions, the corresponding balance of non-associative interactions can also be calculated. Furthermore, this parameter does not indicate the magnitude or strength of the interaction between the polymer molecules.

b) Development of a novel experimental approach to estimate fractional damaged pore volume based on accurate mapping of static polymer retention to dynamic polymer retention. The mapping of static retention to dynamic retention involves using the same solid to liquid ratio and retention time. The dynamic retention time was calculated using Pore Volume (PV) to the total static retention time for maximum retention to the flow conditions under dynamic conditions.

c) Based on the unique predictive approach for estimating fractional damaged pore volume, a novel method was developed to map the various types of polymer retention mechanisms (monolayer and multilayer adsorption, polymer mechanical entrapment and polymer pore plugging) using the distribution of hydrophobic interactions between retained polymer molecules. Besides, a new equation was also developed to predict the onset of mechanical entrapment and the onset of pore plugging. This was achieved with

the knowledge of the associative interactions that exist between the retained polymer molecules.

d) The development of a new model for predicting hydrophobic interactions between associative polymers under different flow regimes (shear thinning, shear thickening and degradation) during transport in a porous media with minimal fitting parameters. The fitting parameters incorporate primary reservoir conditions and polymer properties known to affect the performance of associative polymers. The knowledge of the amount of in-situ hydrophobic interactions allowed for the computation of the effective polymer concentration during transport in a porous media.

e) A novel approach for predicting the onset of shear thickening and the onset of shear degradation. Predicting the onset of shear degradation depends on the proportion of hydrophobic interactions as defined by the identified dimensionless parameter from (a). However, the onset of shear thickening was based on the ratio of the characteristic times, which represents the fitting parameters in the developed model for flow regimes in (d). This showed that the onset of shear thickening was independent of the proportion of hydrophobic interactions.

f) An optimisation approach for maximising the propagation of associative interactions based on the identified contributory effect to polymer retention and effective viscosity. Optimal conditions were defined based on the point at which the impact on polymer retention on hydrophobic interactions cancel out the corresponding effect of flow regimes on the hydrophobic interactions, thereby ensuring that propagation of associative interactions was significantly maintained at the pre-injection estimate of the interactions.

1.7. Research Thesis Structure

The research thesis is divided into nine Chapters, with the details of each Chapter outlined below:

a) **Chapter One - Introduction**: The introductory Chapter focussed on the background to the research where the knowledge gap which formed the basis for the study was identified. Also, these gaps in knowledge were uniquely detailed in the problem statement, thereby laying the foundation for the research aim and the specific objectives achieved in this work. Furthermore, the approach taken by this research and the significance of the outcomes to the overall understanding and application of associative

polymers was discussed. These outcomes have manifested in the outlined contributions to the body of scientific knowledge.

b) **Chapter Two - Literature Review**: The review Chapter focuses on the current state of the art related to the experimental investigations of associative polymers for potential application in chemically enhanced oil recovery. The effect of reservoir conditions such as temperature, divalent ion concentration and salinity were discussed with further highlights on polymer retention mechanisms (adsorption, entrapment and plugging) arising from the propagation of associative polymers in porous media. The Chapter concluded with reported works of the effects of reservoir heterogeneity on the propagation of associative polymers and a summary of the key findings from the review.

c) **Chapter Three - Parameter Identification and Predictive Modelling**: The model development encompassed a combination of first principles and a statistical approach in identifying a predictive approach to understand the propagation of hydrophobic interactions between associative polymers in porous media. The first-principles approach was based on using suitable assumptions and existing correlations in relating established and known reservoir conditions and polymer properties to associative hydrophobic interactions. Also, the statistical method was applied in relating the developed numerical quantities using the first principles to the pressure drop across the porous media.

d) **Chapter Four - Research Materials and Experimental Procedures**: This Chapter discussed the experimental procedures used in validating the developed models, and any modification carried out on the existing approach to suit this purpose. The various practical methodology adopted in this work were formulated according to the American Petroleum Institute (API) Specification 63 (Recommended Practices for Evaluation of Polymers used for Enhanced Oil Recovery Operations). Modification of existing methods defined in API – 63 was only carried out to incorporate the identification of the effects of hydrophobic interactions.

e) **Chapter Five - Material Characterization and Properties**: This Chapter examined the outcomes of applying experimental characterization techniques on silica sand and associative polymer. The characterization of the polymer materials included the use of analytical techniques such as Fourier Transform Infrared (FTIR) spectroscopy and Raman spectroscopy and the determination of the molecular weight. Furthermore, the characterization of the porous media material involved the determination of the material porosity and permeability.

f) **Chapter Six - Quantitative Characterization of Polymer Concentration Regimes**: The identified parameter for quantifying hydrophobic interactions was discussed in mapping the different polymer concentration regimes. The effect of various conditions such as temperature, salinity and shear rates on the different concentration regimes was also addressed with a novel plot indicating how concentration regimes transit with a variation of these conditions developed. The recovery of hydrophobic interactions was also investigated and how this translates to the reversibility of these interactions stated in this Chapter.

g) **Chapter Seven - Quantitative Mapping of Retention Mechanisms in Porous Media**: This Chapter discussed applying the predictive approach developed in Chapter 3 to map the various types of retention mechanisms in porous media. In addition, critical concentrations which marks the onset of the different types of retention mechanisms were also identified and discussed in detail. Furthermore, the novel experimental procedure described in Chapter 4 was applied in validating the predictions obtained.

h) **Chapter Eight - Hydrophobic Interactions during Flow in a Porous Media**: The Chapter examined the application of developed models for characterising the different flow regimes associated with associative polymers in porous media. The models accurately captured the onset of the various flow regimes, and this was emphasised in the Chapter. Additionally, the model for the flow regimes was applied in conjunction with that developed for polymer retention in identifying the contribution of shear thickening and retention to the overall pressure drop (and Resistance Factor) in the porous media. The Chapter concluded with an optimization approach for maximizing the propagation of hydrophobic interactions between associative polymers in porous media.

i) **Chapter Nine – Research Conclusion and Recommendations**: The concluding Chapter identified the key findings of this research and its beneficial effect on the entire field application of associative polymers for chemical enhanced oil recovery. The research conclusion included the key finding on the optimisation of associative polymer properties, which would enable the deep propagation of the unique hydrophobic interactions between the polymer molecules. Furthermore, recommendations for further works were given, and this applies to studies on different porous media materials and polymer transport in the presence of oil (multi-phase flow).

CHAPTER TWO

2.0. Literature Review

2.1. Associative Polymers

Conventional polymers such as polyacrylamide (PAM), hydrolysed polyacrylamide (HPAM) and Xanthan Gum employed for EOR operations have several associated challenges. PAM/HPAM polymers are susceptible to loss of viscosity under extreme reservoir conditions. On the other hand, while Xanthan Gum may withstand high salinity conditions, its biodegradability has hampered its sustained use for EOR operations. These strengths and weaknesses are reflected in their field applications, as shown in Table 2.1. From Table 2.1, Xanthan Gum and hydroxyethyl cellulose (HEC) offer good field applicability under high salinity conditions compared to HPAM/PAM. Above all, the need to mitigate the challenges associated with the use of PAM/HPAM polymers for EOR purpose has necessitated increased research into chemical derivatives of polyacrylamide (Taylor and Nasr El-Din, 1998; Guo et al., 2012; Ye et al., 2013; Chen, 2016; Dai et al., 2017). An integral derivative is a hydrophobically associating polyacrylamide (HAPAM). The underlying goal for these derivatives was to improve the thickening capability of polyacrylamides under harsh reservoir conditions such as high-temperature high salinity (HTHS) (Wever et al., 2013; Chen, 2016; Dai et al., 2017). The improved thickening capability of associative polymers ensures a higher mobility reduction than HPAM polymers. This increased mobility reduction by associative polymers translates to higher incremental oil recovery compared to HPAM polymers. Recently, it has been shown that for viscoelastic polymers, there is a transition from steady laminar flow to a strongly fluctuating flow consistent with elastic turbulence (Clarke et al., 2015; Cui et al., 2016). The onset of this elastic turbulence (or flow fluctuations) has been identified as the mechanism behind the additional mobilisation of trapped oil (capillary desaturation through destabilisation of trapped oil). At a flow rate greater than the onset for shear thickening, extensional viscosity cannot be taken as the reason for additional oil recovery when the capillary number (Ca) is less than the threshold ($\mathrm{Ca} \leq 1$). Thus, the degree of trapped oil mobilisation is a function of the extent of elastic turbulence generated. Therefore, the gradual recovery of associating polymers could be due to the additional effect of intermolecular association (hydrophobic interaction) on elastic turbulence for flow in porous media. Laboratory studies on HAPAM, as shown in Table 2.2, are numerous; however, comparison with Table 2.1 indicates limited field application.

***Table 2.1**: Example of field applications of different polymer types under different conditions (modified from Kamal et al., 2015).*

Country	Field	Polymer Type	T (°C)	Formation Salinity (mg/L)	Reference
China	Daqing	HPAM	45.0	9000	(Pu and Xu, 2009)
	Gudong	HPAM	68.0	3022	(Zhijian et al., 1998)
	Bohai Bay	HPAM	65.0	6070	(Mogollon and Lokhandwala, 2013)
	Xing Long Tai	HPAM	56.6	3112	(Zhang et al., 1999)
	Bohai oil field	HAPAM	65.0	32423	(Han et al., 2006)
	Henan oil field	HPAM	75.0	5060	(Chen et al., 1998)
	Shengli	HPAM	70.0	10000	(Gao, 2014)
USA	Cambridge Minnelusa	PAM	55.6	Not specified	(Vargo et al., 2000)
	Tambaredjo	HPAM	36.0	Not Specified	(Mogollon and Lokhandwala, 2013)
	Tanner	PAM	80.0	66800 (P)[a]	(Pitts et al., 2006)
	West Khiel	HPAM	57.0	46,480 (P)[a]	(Meyers et al., 1992)
Canada	Pelican	HPAM	23.0	6800	(Mogollon and Lokhandwala, 2013)
	David pool	PAM	31.0	6660 (I)[b]	(Pitts et al., 2004)
Germany	Eddesse-Nord	Xanthan Gum	22.0	120,000	(Abbas et al., 2013)
	Vorhop-Knesebeck	Xanthan Gum	56.0	210,000	(Abbas et al., 2013)
Austria	Matzen	HPAM	50.0	20,000	(Kornberger et al., 2013)
India	Viraj	HPAM	81.0	13,250	(Pratap and Gauma, 2004)
	Sanand	PAM	85.0	Not specified	(Tiwari et al., 2008)
Russia	Romashkino (Tatarstan)	HEC	36.0	250,000	(Abbas et al., 2013)

[a]Produced water salinity. [b]Injection water salinity.

***Table 2.2**: Core flooding studies on some selected polymers (modified from Kamal et al., 2015).*

Polymer Type	Polymer Concentration (ppm)	T (° C)	Salinity (mg/L)	Core Type	Recovery [a] (%)	Reference
Xanthan Gum	500	50	-	Sandstone	66 T	(Austad et al., 1997)
HAPAM	1000	50	-	Sandstone	53.6 T	(Austad et al., 1997)
HAPAM	5000	60	5000	Sandstone	8.5	(Liu et al., 2012)
HAPAM	2000	60	5000	Sandstone	11	(Sabhapondit et al., 2003)
HPAM	2000	70	10000	Sandstone	34	(Gong et al., 2008)
HAPAM	7000	60	5000	Sandstone	10.6	(Ye et al., 2013)
HPAM	1100	75	12000	Sandstone	9.8	(Chen et al., 1998)
HPAM	2500	45	508 - 6778	Sandstone	16.7	(Yang et al., 2006; Liu et al., 2007)
HPAM	4500	38	30700	Carbonate	45	(Panthi et al., 2013)
HAPAM	2000	60	-	Not specified[b]	12	(Liu et al., 2013)
HAPAM	2000	60	-	Not specified[b]	18	(Liu et al., 2013)
HAPAM	2000	65	5000	Sandstone	5.7	(Lai et al., 2013)

[a]Recovery reported with T as total recovery while remaining value are additional recovery due to PF. [b]Not indicated in the corresponding article.

More importantly, this comparison indicates that with the level of scientific research on HAPAM, it would eventually replace HPAM for polymer flooding operations. These associative polymers are synthesised or produced with the incorporation of hydrophobic comonomers along the polymer backbone. Accordingly, these hydrophobic monomers contribute to the overall molecular weight of the polymers. In addition, HAPAM polymers are characterised by a CAC (see Figure 2.1). The enhanced rheological properties of HAPAM are apparent above the CAC, which can be traced to the intermolecular association between polymer chains (Zhu et al., 2014; Cui et al., 2016; Wever et al., 2011). However, these interactions between polymer chains above the CAC is dependent on the distribution of the hydrophobic comonomers along the polymer chain. These distributions can be random or block-like, and it is determined by the conditions of the synthesis procedure

(Wever et al., 2011). As mentioned earlier, the method of synthesising HAPAM polymers significantly influences the hydrophobe distribution on the polymer chain.

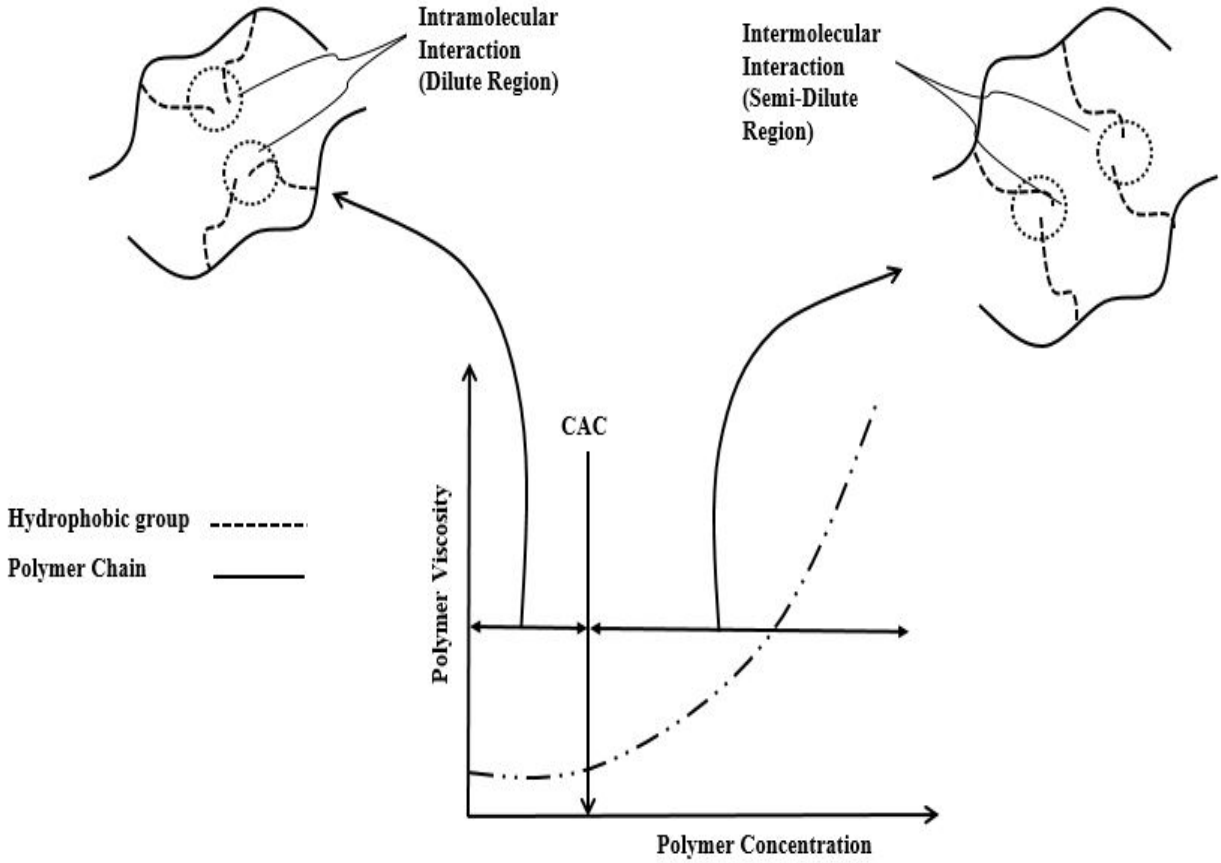

Figure 2.1*: Viscosity behavior of hydrophobically associating polymers (HAPAM) before and after the critical aggregation concentration*

The chemical synthesis of polyacrylamide is via a free radical polymerisation (Giz et al., 2001; Qavi et al. 2014; Rintoul, 2017; Yamamoto et al., 2017; Shatat and Niazi, 2018). Notwithstanding, the insoluble nature of the hydrophobic comonomer has led to the chemical modification of the synthesis route for HAPAM polymers (Zhang et al., 2017). Hence, the different methods available for synthesising HAPAM polymers include homogeneous, heterogeneous and micellar copolymerisation (Taylor and Nasr El-Din, 1998; Wever et al., 2011). Each method ensures the solubility of the hydrophobe with either a surfactant or co-solvent, as in the case of micellar and homogenous copolymerisation respectively. However, the heterogeneous copolymerisation method does not use any additive in ensuring the dispersion of the hydrophobic comonomer. The most widely used polymerisation technique for HAPAM is the micellar copolymerisation method compared with the other techniques (Candau et al., 1994; Candau and Selb, 1999; Taylor and Nasr El-Din, 1998; Wever et al., 2011; Chen, 2016). Significantly, the key advantage of this method is that the produced polymer ends up with a block-like distribution of the hydrophobic

comonomer on the polymer chain. However, this is particularly dependent on the molar ratio of the surfactant employed to the hydrophobic comonomer (Candau et al., 1994; Taylor and Nasr El-Din, 1998; Candau and Selb, 1999; Wever et al., 2011; Kamal et al., 2015). A molar ratio involving a single hydrophobic unit contained in a single micelle would increase the randomness of the distribution of hydrophobe on the polymer chain. On the other hand, where the number of hydrophobe units in a particular micelle is greater than one, a block-like distribution of the hydrophobe would be obtained. Alternatively, while micellar copolymerisation uses a surfactant in solubilising the hydrophobe, another modification to the process involves using a polymerisable surfactant (Wever et al., 2011). The use of a polymerisable surfactant ensures that the purification process of the final polymer product for the removal of surfactants may not be required. Nevertheless, this approach's challenge lies in identifying the desired polymerisable surfactant (Wever et al., 2011). Other parameters that affect the synthesis of HAPAM polymers via micellar copolymerisation include the type of initiator, temperature, type and content of surfactant and the molar ratio of monomers (Candau et al., 1994; Taylor and Nasr El-Din, 1998; Wever et al., 2011; Kamal et al., 2015). Another synthesis approach to HAPAM polymers involves the technique of template copolymerisation (Yan and Row, 2006; Hood et al., 2014; Feng et al., 2017; Szymański et al., 2018). A template predefines the molecular configuration of the associating polymer, which ensures that the block-like distribution of the hydrophobe constituents is well ordered. The consequence of this is that the block of hydrophobe content on the polymer chain can be extensive. The thickening capability of water-soluble polymers relates to its hydrodynamic volume in an aqueous solution (Deen 2012; Chen, 2016; Feng et al., 2017). PAM/HPAM polymers depend on electrostatic repulsion between charged carboxylate groups along the chain (Abidin et al., 2012; Choi et al., 2015; Gong et al., 2017). In the case of HAPAM, this can be achieved using zwitterion monomers, which have negative and positive charges. The thickening ability is controlled by external parameters on the polymers, such as ionic strength and pH (Nesrinne and Djamel, 2017). However, polymers for EOR applications would require that the thickening ability of the polymers is independent of/or can tolerate these conditions. Therefore, having HAPAM polymers with charge distribution along the polymer chain would ensure control over the rheology in an aqueous solution (Wever et al., 2011). In addition, the associative behaviour of HAPAM polymers can be increased by the amount of hydrophobe (hydrophobicity) present in the polymer chain. Whereas, when the hydrophobe length on the polymer chain becomes too long, the polymer's solubility is affected, which may result in polymer dissolution

challenges for field application. Consequently, there is a need for an optimum hydrophobe content when synthesising HAPAM polymers. The determination of this optimum concentration of hydrophobic comonomer required has not been a subject of extensive research. However, the synthesis of associating polymers for EOR application would require the knowledge of the predefined conditions of oil reservoirs. This is important as an excess amount of hydrophobe content may have far-reaching implications when the solubility of HAPAM polymers is considered. In like manner, the thickening properties of HAPAM polymers can be influenced by the introduction of water-soluble chemical spacers in the molecular configuration (Li-Bin et al., 2010; Wever et al., 2011). The chemical spacers are there to link the hydrophilic backbone of the polymer to the hydrophobic group. Li-Bin et al. (2010) investigated the effect of ethylene oxide spacer length on the solution properties of water-soluble hydrophobically associating poly (acrylic acid-co-Rf-PEG Macromonomer) containing fluorocarbon. The authors discovered that the hydrophobic association increased with ethylene-oxide spacer length from the rheological study carried out. This, in turn, influences the thickening performance of the polymer with a similar result on the effect of spacer length reported by Noda et al. (2001). Characterisation of the hydrophobic interactions has been investigated extensively using pyrene, a probe employed for fluorescence spectroscopy (Prazeres et al., 2001; Tang et al., 2003; Pandey et al. 2003; Bains et al., 2011; Mei et al., 2016). The low solubility of pyrene in water and its unique emission spectrum makes it the preferred choice to study hydrophobic interactions in molecules (Siu and Duhamel, 2008; Jordan and Gibb, 2015). The fluorescence spectroscopy studies on hydrophobically associating polymers using pyrene have shown that three distinct flow regimes characterise such polymers (Gong and Zhang, 2009; Duhamel, 2012). At polymer concentration below the CAC, the associative interactions are more intramolecular. It has been discovered that the onset of hydrophobic association between polymer chains occurs at concentration values closer to the CAC (Taylor and Nasr El-Din, 1998). This is manifested in a shift in the emission spectrum associated with the solubilisation of pyrene by hydrophobic clusters using fluorescence spectroscopy. Between this onset concentration value and the CAC, there exists some form of hydrophobic interactive influence, but its dominant effect is minimal. Although CAC is regarded as the threshold for associative characteristics in associative polymers, the proper characterisation of the onset concentration value mentioned earlier may change this knowledge. Furthermore, the minimal hydrophobic clusters may not solubilise pyrene enough to detect a unique emission spectrum. This onset concentration value differs from the CAC based on

the extent of hydrophobic association and may be classified as a transition period. At polymer concentrations above the CAC, there tends to be an extensive network of intermolecular association between polymer chains, which leads to an increase in the polymer viscosity. This is captured in fluorescence spectroscopy by a characteristic emission spectrum, not the case at the onset concentration value. Table 2.3 presents some of the comonomers usually employed in modifying the rheology of both acrylamide-based polymers and other types of polymers made from the different monomeric units.

Table 2.3*: Examples of monomers employed in polymer modification.*

Monomer	**Reference**
N, *N*-dimethyl Acrylamide	(Algi and Okay, 2014; Fang et al., 2016)
2-vinylnaphtahlene	(Zeng et al., 2002)
Methacrylic Acid	(Fernyhough et al., 2009; Bang et al., 2017)
N-vinylpyrrolidinone	(Taghizadeh and Foroutan, 2004; Willersinn and Schmidt, 2017)
4-vinylbenzenesulfonate	(Kang et al., 2015)
2-Acrylamido-2-methyl-1-propanesulfonic acid	(Çavuş, 2010; Kundakci et al., 2011)
Methyl methacrylate	(Cilurzo et al., 2014; Khromiak et al., 2018)
Poly(propylene glycol) methacrylate	(Shemper et al., 2002)
Sodium vinylsulfonate	(Mori et al., 2010; Mori et al., 2012)
Carboxymethyl cellulose	(Han et al., 2010; Han et al., 2013)
N-phenylacrylamide	(Zhou and Lai, 2004)
N-tert-Octylacrylamide	(Zhu et al., 2012)
N-dodecylacrylamide	(Wan et al., 2014)
N-methyl-*N*-vinyl acetamide	(Pavlov et al., 2018)
N-(n-octadecyl)acrylamide	(Principi et al., 2000)

Additionally, these comonomers ensure that the modified polymer is resistant to conditions, initiating chemical and mechanical degradation. Moreover, these comonomers ensure that the modified polymer maintains a substantial part of its hydrodynamic volume, hence its viscosity, under the conditions obtainable in an oil reservoir (Kamal et al., 2015; Das et al.,

2017; Sarsenbekuly et al., 2017; Bai et al., 2018; Silva et al., 2018). Characterisation of the molecular architecture of HAPAM polymers has been conducted using infrared (IR) spectroscopy and nuclear magnetic resonance (NMR) spectra (Lai et al., 2013). This allows the determination of the chemical bonding arising from the presence of specific functional groups. FTIR alone cannot give a complete description of the molecular structure of a polymer; hence, it is used along with NMR for a complete characterisation of the molecular configuration. This was the case when Quan et al. (2019) characterised hydrophobically associating polymers which were abbreviated as HPAAT. The polymer was synthesised from acrylamide (AM), allyl polyethylene-1000 (APEG), octadecyl dimethyl allyl ammonium chloride (DMDAAC-18) and sodium styrene sulfonate (SSS) using FTIR and ^{1}H-NMR spectroscopy. Figure 2.2 shows the FTIR spectrum of the synthesised polymer with the absorption bands at 1715 cm^{-1} and 3448 cm^{-1} corresponding to C=O and N-H stretching vibrations of the amide groups.

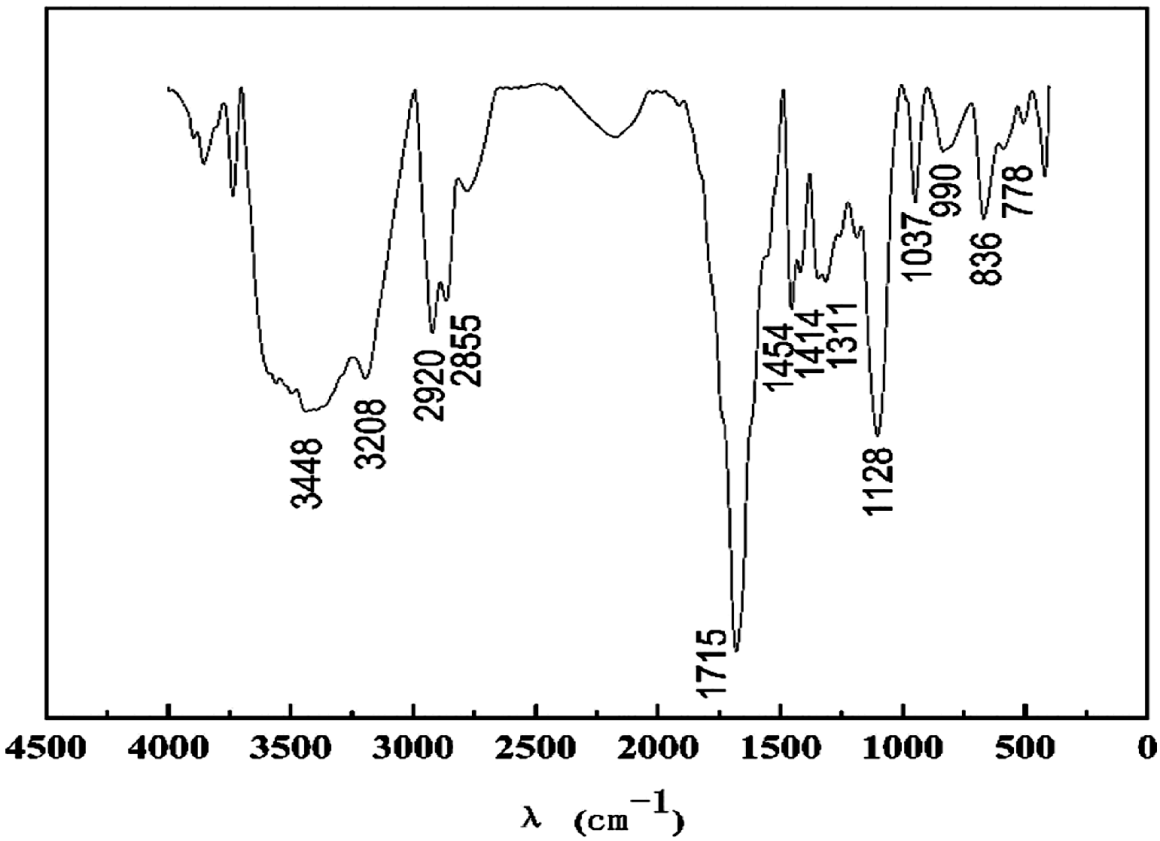

***Figure 2.2**: FTIR spectrum of a hydrophobically associating polymer (HPAAT) (Quan et al., 2019)*

The peaks at 778 cm^{-1} and 1414 cm^{-1} corresponds to a benzene ring and S=O, which confirms the presence of SSS. Furthermore, the peak at 1128 cm^{-1} shows C-O-C stretching vibrations which confirms the existence of APEG in the associative polymer HPAAT. The peaks at 2920 cm^{-1} and 2855 cm^{-1} indicate hydrocarbon groups –CH_3 and –CH_2- in the

polymer. The result of the characterization study using FTIR was consistent with the molecular design structure of the polymer, as shown in Figure 2.3.

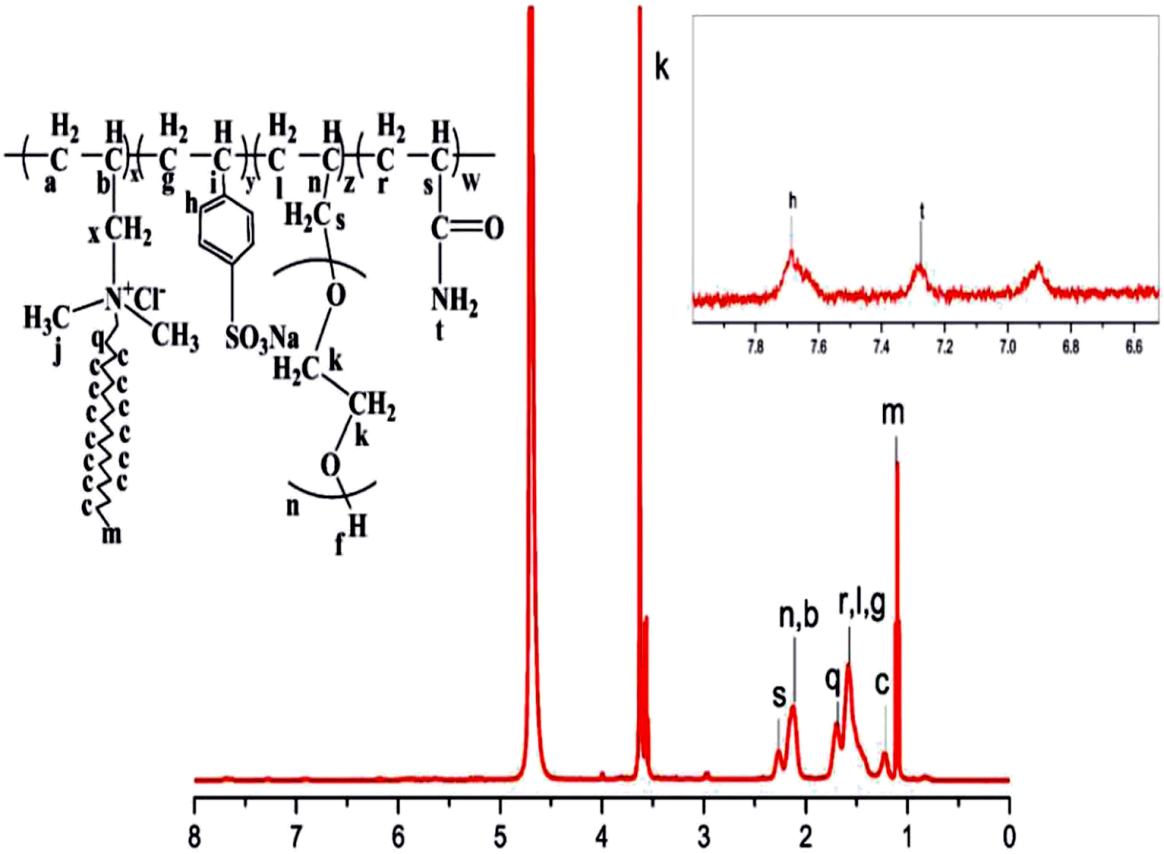

***Figure 2.3**: [1]H-NMR spectrum of a hydrophobically associating polymer HPAAT by (Quan et al., 2019).*

Equally important is the [1]H-NMR analysis of the HPAAT polymer carried out by the authors. Their analysis indicates a shift of the hydrogen spectrum of the associative polymer in the following manner: 1.09(m, –CH3), 1.25–1.36 (c, –(CH2)15–), 1.62 (r, l, g, –CH_2–CH–C–O–NH_2, –CH_2–CH–CH_2–, –CH_2–CH–C), 1.71 (q, –N–CH_2–CH_2–), 2.14 (n, b, –CH–CH_2–O–, –CH–CH_2–N), 2.26 (s, –CH–C–O–NH2), 3.22 (z, x, –n–CH_2–, CH_2–N–), 3.30 (j, –N–CH_3), 3.63 (k, –CH_2–O–, –CH_2–CH_2–O–), 7.21 (t, –NH_2), 7.67 (h, –CH–CH–C). Similarly, El-Hoshoudy et al. (2015) used FTIR, ^{13}C-NMR, [1]H-NMR, scanning electron microscopy (SEM), thermogravimetric analysis (TGA) and high-resolution transmission electron microscope (HRTEM) to characterize a HAPAM polymer (acrylamide-4-dodecyl-benzenesulfonate-1-vinylimidazol-3-ium-divinyl sulfone). Using a similar approach to Quan et al. (2019), the authors used the FTIR and [1]H-NMR spectra to propose a chemical structure for the associative polymer. Similarly, the studied HAPAM polymer SEM image indicated a 3-dimensional structure arising from intra and intermolecular association between polymer chains. The authors concluded that the mesoporous structure of the

polymer surface from the SEM analysis could be attributed to the crystallinity of the polymer due to the polar amide group, which ensures an attractive secondary force arises from hydrogen bonding. This was also the case for studies on other types of polyacrylamide based hydrophobically associating polymers (El-Hoshoudy et al., 2017). However, Sheng (2011) reported that the 3-dimensional structural network formed by hydrophobically associative polymers occurs due to a combination of strong electrostatic force, hydrogen bonding and van der Waals forces. Other forms of associating polymers based on ethoxylated urethane (EUR), hydroxyethyl cellulose (HEC) derivatives and alkali swellable emulsion (ASE) have been described in the literature (Tam et al., 1998; Xu et al., 1996; Kastner et al., 1996; Ihara et al., 2004; Kawakami et al., 2006; Zhao and Chen, 2007; Kjoniksen et al., 2008; Wever et al., 2011). Some of these polymers were produced because of the demand for eco-friendly materials. Associating polymers based on EUR are classified as telechelic associative polymers with enhanced rheological features even at low concentration and molecular weight. Moreover, these unique characteristics have made hydrophobically modified EUR polymers the focus of research for various commercial applications (Wever et al., 2011; Wang et al., 2016). Hydrophobically modified EUR polymers synthesis results in a hydrophilic polyethylene glycol (PEG) main chain with hydrophobic groups attached to the polymer chain through the urethane functional group (Barmar et al. 2010; Wang et al. 2016). Additionally, the associative behaviour in these polymers occurs at low concentration values of CAC. Above the CAC, the molecular arrangement of these polymers in aqueous solution ranges from flower-like micelles with micellar cores of hydrophobes to flower-loops of the hydrophilic main chain. Moreover, there is a critical percolation concentration aside from the CAC where polymer viscosity increases (Wang et al. 2016). However, hydrophobically modified EUR polymers for polymer flooding are not known despite their enhanced rheological attributes. Similarly, hydrophobically modified ASE polymers made up of three components, mainly methacrylic acid, ethyl acrylate, and a hydrophobic group, is insoluble under low pH conditions. Therefore, its solubility under high pH conditions would benefit polymer flooding in high salinity oil reservoirs. Overall, the use of hydrophobically associating EUR, HEC, and ASE for enhanced oil recovery is not well known. Currently, the domain of polymer research is focused on the application of HAPAM polymers for EOR operations. As a result, the remainder of this review would be focused on hydrophobically associating polyacrylamide.

2.2. Effect of Reservoir Conditions on Associative Polymers

As mentioned before, the rheological behaviour of hydrophobically associating polyacrylamide is governed by the CAC. The hydrophobic blocks on the polymer chain confer on it its unique solution properties. Accordingly, at low polymer concentrations, which represents the dilute region, the viscosity of the polymer is low (as well as its hydrodynamic volume). Here, intramolecular association dominates the rheological behaviour. In contrast, high polymer concentration above the CAC (semi-dilute region) would bring about a sharp increase in polymer hydrodynamic volume due to the intermolecular association between polymer chains. Consequently, the viscosity of HAPAM is increased, and application of these polymers would require that their solution properties arising from hydrophobic interactions withstand the conditions inherent in an oil reservoir.

2.2.1. Effect of Salinity and Hardness

Ordinarily, increasing the concentration of salts and divalent ions causes a reduction in the viscosity of HPAM due to the screening effect of the cations present in the solution. However, the rheological behaviour of HAPAM polymers under increasing salinity and divalent ion concentration often exhibits different trends depending on some factors such as the type of hydrophobe, the molecular structure of the HAPAM polymer and polymer concentration (Jincheng et al. 2018). Deng et al. (2014) conducted the synthesis of acrylamide based associating polymer using sodium 2-acrylamido-2-methylpropanesulfonic sulfonate as the hydrophobic comonomer. The viscosity of a 1 wt.% solution of the prepared HAPAM polymer decreased with increasing NaCl concentration (up to 0.2 wt.% NaCl) under various shear rates. Between 0.2 and 0.4 wt.% NaCl, the viscosity of the associating polyacrylamide solution increased. Likewise, Quan et al. (2016), El-Hoshoudy et al. (2017) and Sarsenbekuly et al. (2017) reported similar trends with HAPAM polymers in solutions containing monovalent and divalent ions. According to El-Hoshoudy et al. (2017), acrylamide-based poly (4-dodecyl-benzenesulfonate-3-[5-(butane-2-sulfonyl)-3-carbamoyl-1-methyl-heptyl] imidazol-3-ium) showed an initial decrease in polymer viscosity with NaCl concentration, after which the viscosity increased with increasing NaCl concentration. The same effect was also reported for HAPAM polymers written by Sarsenbekuly et al. (2017) and Quan et al. (2016). This phenomenon associated with HAPAM polymers was attributed to:

a) **Screening/Shielding Effect**: Cations in salts reduce the electric double layer and hydration layer, reducing the electrostatic repulsion between charged groups on the polymer chain (Quan et al. 2016; El-Hoshoudy et al. 2017; Sarsenbekuly et al. 2017). In effect, chain contraction is experienced, and a reduction in the hydrodynamic volume of the polymer in solution. This initial effect was responsible for the reduction of the polymer viscosity.
b) **Hydrophobic Associative Effect**: A further increase in the concentration of salt and divalent ions would ensure contact of the hydrophobic groups on the polymer chain. The effect of this was the formation of aggregates of polymer chains (El-Hoshoudy et al., 2017). The impact of this aggregation of polymer chains was that it nullifies the initial screening effect, which brought about the reduction in the hydrodynamic volume of the polymer through a contraction. As a result, the polymer is stretched, and its hydrodynamic volume was increased.

The various polymer solutions containing salts described above can simply be prepared by dissolving the polymer in an appropriate amount of salt/divalent ion solution. Other approaches include adding a sufficient quantity of salt to an already prepared polymer solution or adding salt water to the polymer solution. Nevertheless, the method used in preparing HAPAM polymers both in aqueous and brine solutions has been demonstrated to affect the rheological behaviour of the HAPAM polymers (Maia et al. 2005; Wever et al. 2011). Maia et al. (2005) synthesized an acrylamide-*N, N*-dihexylacrylamide copolymer and evaluated its rheological behaviour under monovalent (Na^+) ion concentration. The authors applied the three procedures mentioned earlier in assessing how the mode of contact of HAPAM polymers with Na^+ ions affect its rheology. The copolymer exhibited different tolerances to Na^+ ions. Firstly, with the copolymer dissolved in a salt solution, the viscosity of the polymer solution decreased with increasing NaCl concentration. This was ascribed to the screening effect of the cations on the charged moieties present on the polymer chain. Secondly, when the salt powder was added to the copolymer solution, the viscosity increased up to a maximum, after which there was a reduction. The authors explained why the viscosity passed through a maximum and identified the presence of surfactant in the solution. Thirdly, when salt water or brine solution was added to the polymer solution, the viscosity of the polymer increased with increasing salinity. The authors attributed this third phenomenon to "*Easiness of Interaction*" when salt and polymer exist already in solutions, which leads to the formation of a network of polymer chains. Al-Sabagh et al. (2016) evaluated the effect of divalent ions (Ca^+) at 30 ^{0}C and shear rate of 6 s^{-1} on HAPAM

polymers with different type and quantities of hydrophobic monomers. A general observation was that the associative effects of the polymers (or cation resistance) could only be maintained at low concentrations of divalent ions compared to monovalent ions. This was the case irrespective of the type of hydrophobic content of the polymer. This can be explained in terms of the strong shielding effect of divalent ions compared to monovalent ions. Aside from the authors' findings, there is limited understanding of this phenomenon associated with HAPAM polymers. In addition to the preparation method, the concentration regime (dilute or semi-dilute) of hydrophobically associating polymers plays a role in its salt tolerance (Kamal et al., 2015). In general, the salt-thickening ability of associating polymers in brine solutions can be maintained up to a particular concentration of monovalent or divalent ion depending on the type of hydrophobic comonomer employed (Wyatt et al., 2011; Chen et al., 2012; Zhong et al., 2014; Kamal et al., 2015). However, beyond this salt concentration value, the polymer viscosity thins out with increasing salinity in the presence of monovalent and divalent ions. The ensuing effect is sometimes the precipitation of HAPAM polymers out of solutions (salting-out effect), which can impact the polymer concentration required. With polymer concentration often limited in high permeable reservoirs, improving the salt-thickening capability of hydrophobically associating polyacrylamide had resorted to cross-linking of the polymer chains (Zhong et al., 2014). The essence of cross-linking of HAPAM polymer chains is to:

a) Offset the effect of having an extended hydrophobic group on the polymer backbone, which might minimize its solubility in solution.
b) Decrease the volume available per molecule without necessarily increasing the polymer concentration.
c) Ensure that the salt-thickening capability of HAPAM polymers is enhanced (over a wide range of salinity) within a predetermined polymer concentration value in porous formations.

The molecular conformation of the cross-linked polymer enables it to have an expanded configuration compared to linear associative polymers without side chains. This ensures the average diameter of the polymer aggregates is higher under monovalent or divalent conditions. Therefore, the salt-thickening capability of the associative polymer is increased when cross-linked. However, the resulting molecular weight of cross-linked polymers may be too high as control over the degree of cross-linking can be challenging to maintain. This may subsequently cause formation damage in sections of oil reservoirs with low permeability. With applied polymer concentration in most permeable formations

constrained to ensure salt tolerance, a proper understanding of CAC under aqueous and high salinity conditions is required (Zhong et al., 2014). The salinity effect on the CAC of some polymers from the work of Rashidi et al. (2010) are presented in Table 2.4.

Table 2.4*: Critical Aggregation Concentration (ppm) data as a function of salinity for the studied sulfonated polymers (AN105 – AN132) at 20 ^{0}C (Rashidi et al., 2010).*

Polymers	**Solvents**	
	CAC (at 0.1 wt.% NaCl)	**CAC (at 10 wt.% NaCl)**
AN105	264	625
AN113	250	556
AN125	244	527
AN132	200	434

As seen from the table, the CAC of the polymers were observed to increase with the degree of salinity. The increment in CAC can be ascribed to an increase in charge density on the polymer chain, which decreases polymer hydrodynamic volume. As such, a higher threshold value of CAC would be required for a meaningful hydrophobic associative effect to take place. To express this, a mathematical relationship by Hayahara and Takao (1968) can be used as shown in Equation (2.1):

$$V_m = \frac{M_w}{C_{ag} N_a} \quad (2.1)$$

Where V_m is the volume available per polymer chain, M_w is the molecular weight of the polymer, C_{ag} is the CAC of the polymer and N_a is Avogadro's number. An increase in the CAC (denoted by C_{ag}) would decrease the volume available per polymer chain, V_m and vice versa. When V_m is reduced polymer chains come together, and the hydrophobic associative effect is enhanced. This cumulative effect of salinity on CAC was also validated by the work of Saeed et al. (2017). However, the implication of this on EOR operations would mean:

a) High polymer concentration would be needed, if not above the limit for EOR operations, which could be detrimental to the economics of the flooding process.

b) Polymer injectivity would be affected, and this is often constrained by formation fracture pressure.

Ultimately, a salt-tolerant HAPAM polymer is one whose thickening properties are enhanced under increasing salinity. However, the choice of a particular HAPAM for high salinity condition depends on several factors inherent in both the polymer architecture (and hence its synthesis method) and reservoir. As such, the applicability of associating polymers for EOR operations would essentially be specific to the reservoir conditions.

2.2.2. Effect of Temperature

Thermal effects on the rheological properties of HAPAM polymers have been reported widely in the literature (Taylor and Nasr El-Din, 1998; Hourdet et al., 2005; Al-Sabagh et al., 2016; Dai et al., 2017; Bai et al., 2018). Various HAPAM polymers with different hydrophobic moieties on the polymer backbone have been reported with diverse response under varied temperature conditions. However, the temperature dependence of HAPAM polymers is affected by the concentration regime (dilute and semi-dilute regime). When polymer concentration is less than the CAC of the HAPAM polymer, there is a decrease in polymer viscosity with increasing temperature. Yang et al. (2015) demonstrated this using synthesised hydrophobically associating cationic perfluorinated polyacrylamide (HACFP). The polymer viscosity at a concentration of 0.2 wt.% (< CAC value of 0.24 wt.%) decreased with temperature over the range of 20 – 85 ^{0}C. The authors attributed this phenomenon to a weak intermolecular associative effect between hydrophobic groups in the dilute concentration regime (C_p < CAC, where C_p is polymer concentration). Besides the explanation offered by the authors, this could also be attributed to the intramolecular associative effect being an endothermic process under this concentration regime. Polymer chains would coil up under these conditions, thereby reducing the hydrodynamic volume and the polymer solution's viscosity. With further increase in temperature, the thermal-induced motion of water molecules and the polymer chains would further strengthen the hydrodynamic volume reduction by clustering coiled polymer chains, further reducing the polymer viscosity. A similar phenomenon was reported for HAPAM modified with 2-phenoxylethylacrylate by Dai et al. (2008) at a polymer concentration less than the CAC. A consensus in the literature on the thermal behaviour of HAPAM polymers is that the viscosity of the polymers increases with temperature up to a maximum, after which there is a decrease in viscosity with a further increase in temperature. Such a trend is obtainable when the polymer concentration exceeds the CAC, i.e., semi-dilute concentration regime.

El-Hoshoudy et al. (2017) revealed this fact with synthesised acrylamide-based poly(4-dodecyl-benzenesulfonate-3-[5-(butane-2-sulfonyl)-3-carbamoyl-1-methyl-heptyl] imidazol-3-ium) through evaluation of its thermal resistance between 25 and 100 ^{0}C at a concentration of 2 g/L and a shear rate of 7.34 /s. The viscosity of the HAPAM polymer increased up to a maximum of 50 ^{0}C after which there was a decrease in viscosity up to 100 ^{0}C. This can be explained by the endothermic driven process of hydrophobic intermolecular association between polymer chains in solution. This leads to a network/micro-domain of polymer chains with an increase in hydrodynamic volume regarding polymer viscosity. When the temperature exceeds the 50 ^{0}C mark, the thermal-induced motion of the water molecules will weaken the super-aggregate structure formed by the hydrophobic interactions between the polymer chains, thereby weakening the intermolecular association between the chains. The outcome of this is a reduction in polymer viscosity with increasing temperature. Equally, Lai et al. (2013), Zou et al. (2013) and Sun et al. (2015) reported a similar trend for synthesised HAPAM polymers poly (AM-NaAA-DNDA), cyclodextrin functionalised associating acrylamide, and poly (AM-AMC$_{12}$S-DPP) respectively. The maximum viscosity for the HAPAM polymers was obtained at 40 ^{0}C [for poly (AM-NaAA-DNDA)], 80 ^{0}C [for cyclodextrin functionalized associating acrylamide polymer] and 35 ^{0}C [for poly (AM-AMC$_{12}$S-DPP)]. Additionally, Gou et al. (2015) reported maximum viscosity at temperatures of 35 and 42 ^{0}C respectively for poly (AM-AA-NDS-NIMA) and poly (AM-AA-NIMA). Therefore, the type, amount and molecular composition of the hydrophobic comonomers employed in the synthesis of HAPAM polymers play a role in its temperature tolerance. Table 2.5 shows the maximum temperature tolerance of some HAPAM polymers in the semi-dilute concentration regime. The copolymerisation of acrylamide with these hydrophobic comonomers is partly aimed at improving its temperature tolerance. However, some of the HAPAM arising from the copolymerisation process may not achieve high polymerisation activity and, thus, experience low intrinsic viscosity and molecular weight (Zhong et al., 2014; Li et al., 2017). The implication of this is that the maximum temperature tolerance of some of these polymers may vary, as indicated in Table 2.5.

***Table 2.5**: Maximum temperature tolerance of some selected HAPAM polymers. Polymers were evaluated under a shear rate of 170 /s and temperature range of 20 – 140 ^{0}C.*

Polymer*	Maximum Temperature (℃)	CAC (g/L)	Concentration Regime	Reference
AM-AA-NIMA [1]	42	0.80	Semi-dilute	(Gou et al. 2015)
AM-AA-NDS-NIMA [2]	35	1.00	Semi-dilute	(Gou et al. 2015)
AM-AMC$_{12}$S-DPP [3]	35	0.20	Semi-dilute	(Sun et al. 2015)
AM-DOAC-SSS [4]	80	1.65	Semi-dilute (0.3 wt.%)	(Quan et al. 2016)
	100		Semi-dilute (0.4 wt.%)	
	120		Semi-dilute (0.5 wt.%)	

***The abbreviations denoting the polymers are:*

1. *AM-AA-NIMA – HAPAM containing 3-(2-(2-heptadec-8-enyl-4,5-dihydro-imidazol-1-yl)ethylcarbamoyl)acrylic acid (NIMA) and acrylic acid (AA)*
2. *AM-AA-NDS-NIMA – HAPAM containing 3-(2-(2-heptadec-8-enyl-4,5-dihydro-imidazol-1-yl)ethylcarbamoyl)acrylic acid (NIMA), 3-(diallyl-amino)-2-hydroxypropyl sulfonate (NDS) and acrylic acid (AA)*
3. *AM-AMC$_{12}$S-DPP – HAPAM containing 1-(4-dodecyloxy-phenyl)-propenone (DPP) and 2-(acrylamido)-dodecanesulfonic acid (AMC$_{12}$S)*
4. *AM-DOAC-SSS – HAPAM containing ionic hydrophobic monomer N,N-dimethyloctadeyl allyl ammonium chloride (DOAC) and the anionic monomer sodium 4-styrenesulfonate (SSS)*

As such, thermo-thinning defects tend to set in beyond temperature values for maximum viscosity. Furthermore, the molar ratio of hydrophobic comonomers employed in the copolymerization process is in the range of 10 – 30 % (Li et al., 2017). While an increment would improve the performance of the polymer, it may create additional cost for production. The temperature effect on the CAC of HAPAM is limited and not widely reported. Nevertheless, this may have a significant impact, in the same manner, as earlier reported for salinity effects. El-Hoshoudy et al. (2017) reported the temperature tolerance of synthesized acrylamide-based poly (4-dodecyl-benzenesulfonate-3-[5-(butane-2-sulfonyl)-3-carbamoyl-1-methyl-heptyl] imidazol-3-ium) at the critical aggregation concentration.

However, there was no reported indication of its effect on the CAC of the polymer. A general understanding of this effect could be linked to the description given by Hourdet et al. (2005). The dynamics of the associative network formed by HAPAM polymers are tied to the hydrophobic interactions' strength (as measured as the binding energy/energy barrier) between polymer chains. Accordingly, Andrade's Equation (Equation 2.2) can be applied to hydrophobically associating polymers, where the activation energy can be closely compared to the energy barrier.

$$\mu = B_a e^{\left(\frac{E_a}{k_a T}\right)} \quad (2.2)$$

Where μ is the polymer viscosity, E_a is the activation energy (kJ/mol), B_a and k_a are constants, T is the temperature in kelvin. The relationship between the CAC of associating polymers and the intrinsic viscosity is represented in Equation (2.3):

$$C_{ag} = \frac{1}{[\mu]} \quad (2.3)$$

Where the CAC is C_{ag} and the intrinsic viscosity of the polymer solution $[\mu]$ is represented in Equation (2.4) where μ_s is the viscosity of the solvent:

$$[\mu] = \lim_{C_p \to 0} \left(\frac{\mu - \mu_s}{\mu_s}\right) \quad (2.4)$$

From the expressions in Equations (2.2) to (2.4), the dynamics of the hydrophobic association between polymer chains is dependent on temperature and the degree of hydrophobicity (which is described by the activation energy). The outcome can be described in two ways:

a) For a given degree of hydrophobicity, an increase in temperature would bring about a reduction in polymer viscosity, μ, likewise the intrinsic viscosity, $[\mu]$. This would imply an increase in the critical aggregation concentration, C_{ag}. This simply means that a higher polymer concentration would be required to sustain the associative effect of the hydrophobic groups present in the polymer backbone.
b) The degree of hydrophobicity increases, and the energy barrier/activation energy intensifies, likewise the intrinsic viscosity. As such, the critical aggregation concentration would decrease. However, polymers with a high degree of hydrophobicity would experience a larger drop in viscosity with temperature.

While these are plausible theoretical explanations of thermal effects on the CAC of associating polymers, further research into this trend would be beneficial where polymer injectivity is paramount. As previously stated, EOR involving polymers requires concentration values set to a particular limit based on the economics of the project. In

improving the thermal resistance of hydrophobically associating polymers, grafting of the copolymers with a temperature-responsive side chain have been reported (Barker et al., 2003; Hourdet et al., 2005; Brassinne et al., 2014; Lee et al., 2015; Victor et al., 2016; Li et al., 2017). Such *"smart polymers"* are characterized by a critical association temperature (CAT) above which polymers self-assemble into hydrophobic micro-domains (Hourdet et al., 2005; Li et al., 2017). In other words, there is a change in character from hydrophilicity to hydrophobicity (Li et al., 2017). This CAT is determined by the critical solution temperature of the graft monomer employed. *N*-isopropylacrylamide (NIPA) is a commonly employed monomer in preparing thermos-responsive polymers, and it is characterized by a low critical solution temperature (LCST) (Oh et al., 2013; Zhang and Hoogenboom, 2015; Victor et al., 2016; Badi, 2017; Santis et al., 2017). The LCST represents the temperature value below which components of a mixture are miscible. In addition, some monomers are characterized by an upper critical solution temperature (UCST) above which components in the mixture are miscible in all proportions (Badi, 2017; Niskanen and Tenhu, 2017). The smart tuning of the viscosity of these polymers ensures that they are applicable in high-temperature oil reservoirs. However, the critical solution temperature values of the grafted polymers are dependent on the degree of polymerization, branching and polydispersity. As such, some HAPAM molecules grafted with thermos-responsive comonomer may still exhibit low molecular weight with high polymer concentration needed for thermo-thickening. Further to this, Li et al. (2017) pointed out that an expensive coupling agent is necessary for the polymerization process of thermo-responsive polymers and reactions are conducted at low polymer loadings. Increasing the hydrophobic length would strengthen the intermolecular associative effect for high-temperature applications; however, there is a limit to ensure polymer solubility is maintained. In addition, some grafted polymers may exhibit an LCST lower than the UCST. This simply means such polymers can only exhibit thermo-thickening over a particular temperature interval while thermo-thinning will set in at lower and higher temperatures. For polymers exhibiting both LCST and UCST, a favourable disposition is for LCST to be higher than the UCST. This would ensure the temperature tolerance of the polymer at high temperatures. Some thermo-responsive associating polymers may require some stimulating effect for thermal response between grafts on the polymers (Li et al., 2017). This may limit the acceptance of thermo-responsive hydrophobically associating polymers in the oil and gas industry as this would contribute to cost. The long-term stability of HAPAM polymers in porous media depends on the sustainability of its associative characteristics under different conditions of temperature,

salinity, pH and divalent ion concentration. In addition, the CAC, which is a critical parameter of associative polymers, have been reported in the literature to be susceptible to reservoir conditions (El-Hoshoudy et al., 2017; Saeed et al., 2017). However, an explanation for the susceptibility of the CAC to different reservoir conditions could mean that intramolecular interactions could transit to intermolecular interactions and vice versa. Recently, Guo et al. (2016) showed this possibility by conducting core flooding through three serially mounted cores with very similar rock properties (permeability and porosity). It was observed that for associative polymers, HNT-3.28 and HNT-4.32 (containing 3.28 and 4.32 mol % hydrophobic monomer respectively), the resistance factors (RF) of the polymers were much greater in the second and third cores compared to the first core. A plausible explanation given by the authors was the conversion of intramolecular interactions to intermolecular interactions due to elongational or extensional flow in the porous media. However, this transition between the two interactions depends on the hydrophobic monomer content. It was observed that a similar trend of transition was not observed with associative polymers HNT-1.1 and HNT-2.2 (containing 1.1 and 2.2 mol % hydrophobic monomer) respectively. The authors put forward that this may be due to low intramolecular interactions such that any transition to intermolecular interaction has been counteracted by polymer-rock interaction such as adsorption. Similarly, this trend of intramolecular to intermolecular transition and vice versa may explain why the CAC of associative polymers change under different reservoir conditions. However, an understanding of this phenomenon could eventually explain the stability of associative polymers under different reservoir conditions.

2.2.3. Effect of pH

The charged nature of polyelectrolytes makes them easily affected by the degree of ionization of solution (Wever et al., 2011). Polyelectrolytes with more than one negative group (polyanion) experience high viscosity at high pH and low viscosity at low pH (Wever et al., 2011). In contrast, polycations experience low viscosity at high pH and high viscosity at low pH (Wever et al., 2011). However, typical polyelectrolytes are polyanionic with pH response as earlier described for polyanions. Zhou et al. (2001) showed this with polyacrylic acid, with the polymer viscosity increasing with pH up to a maximum at pH values between 8 and 9. The decrease in the viscosity value beyond the pH value was attributed to the salting out effect, similar to what is obtained from NaCl. The response of hydrophobically associating polymers to pH is rather complex (Zhou et al., 2001). A balance between electrostatic repulsion between charged moieties on the chain and hydrophobic interactions

characterizes the pH responsiveness of HAPAM (Branham et al., 1996; Smith and McCormick, 2001; Zhou et al., 2001; Zhuang et al., 2001; Huaiping et al., 2008; Wever et al., 2011). In other words, the viscosity of hydrophobically associating polymers with an increase in pH is dependent on the transition between intramolecular and intermolecular interaction. In demonstrating this effect, Zhou et al. (2001) synthesized a copolymer of acrylic acid and 2-(*N*-ethylperfluorooctanesulfoamido) ethyl acrylate or 2-(*N*-ethylperfluorooctanesulfoamido) ethyl methacrylate. It was observed that two increments in polymer viscosity were achieved. Beyond a pH value of 4, polymer viscosity increased to a maximum in the range of 5 – 6. Further increment leads to a decrease in polymer viscosity followed by another increase beyond pH of 11. This behaviour of the polymer is captured in Figure 2.4.

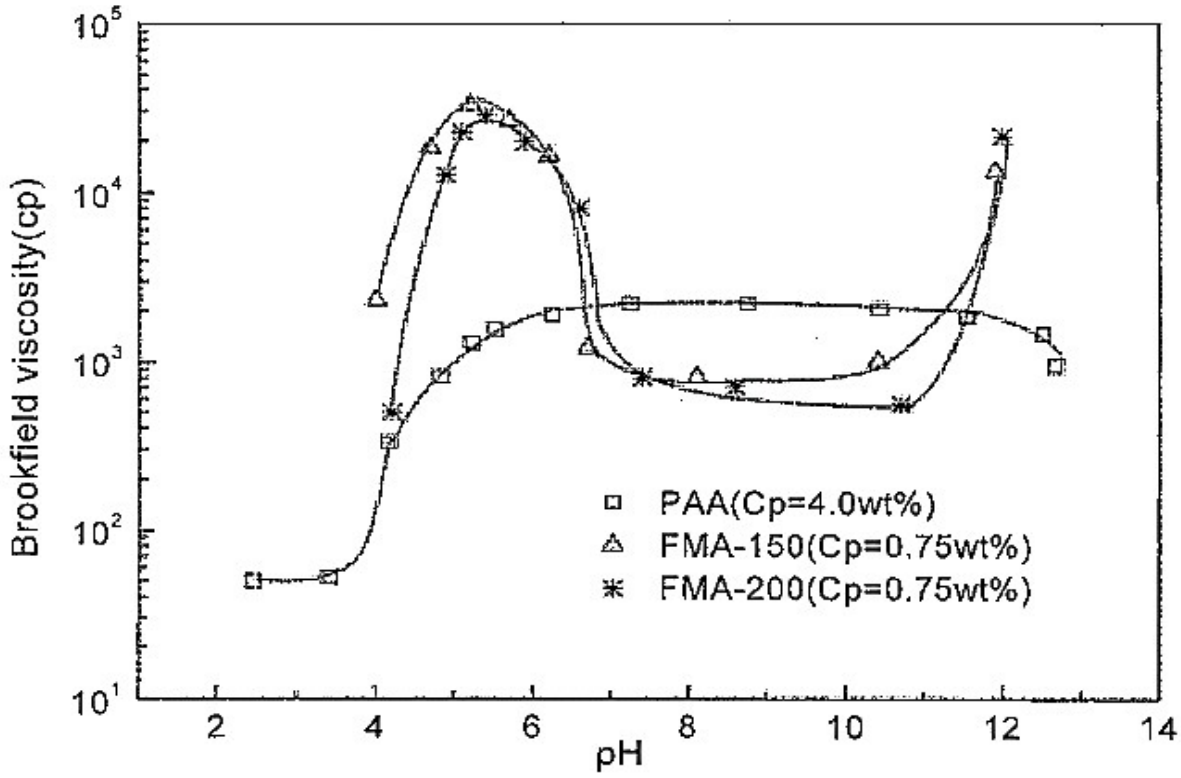

Figure 2.4*: Effect of pH on the solution viscosity of poly (acrylic acid) (PAA) and their modified polymers (FMA) at temperature 25 ^{0}C and a shear rate of 0.4 /s (Zhou et al., 2001).*

An explanation for this trend can be grouped into three categories according to the authors:

a) Between pH 5 – 7, the ionic character of the polyacrylic acid copolymers is not fully developed and as such, hydrophobic interactions occur in solution.
b) Between pH 7 – 11, the polyelectrolyte character of the copolymers is developed with chain expansion. However, a lack of mobility prevents the hydrophobic interaction.

c) Beyond pH 11, the screening effect similar to what is experienced under increasing salinity allows for the exposure of hydrophobic groups for associative interaction.

Although, the authors did not discuss the pH range of 1 – 4, however under this condition, the intramolecular associative effect is dominant; hence the viscosity of the HAPAM is low without any noticeable increase. Similarly, Zhuang et al. (2001) demonstrated the above trends highlighted from (a) to (c) using poly (acrylate-co-alkyl acrylate) as shown in Figure 2.5.

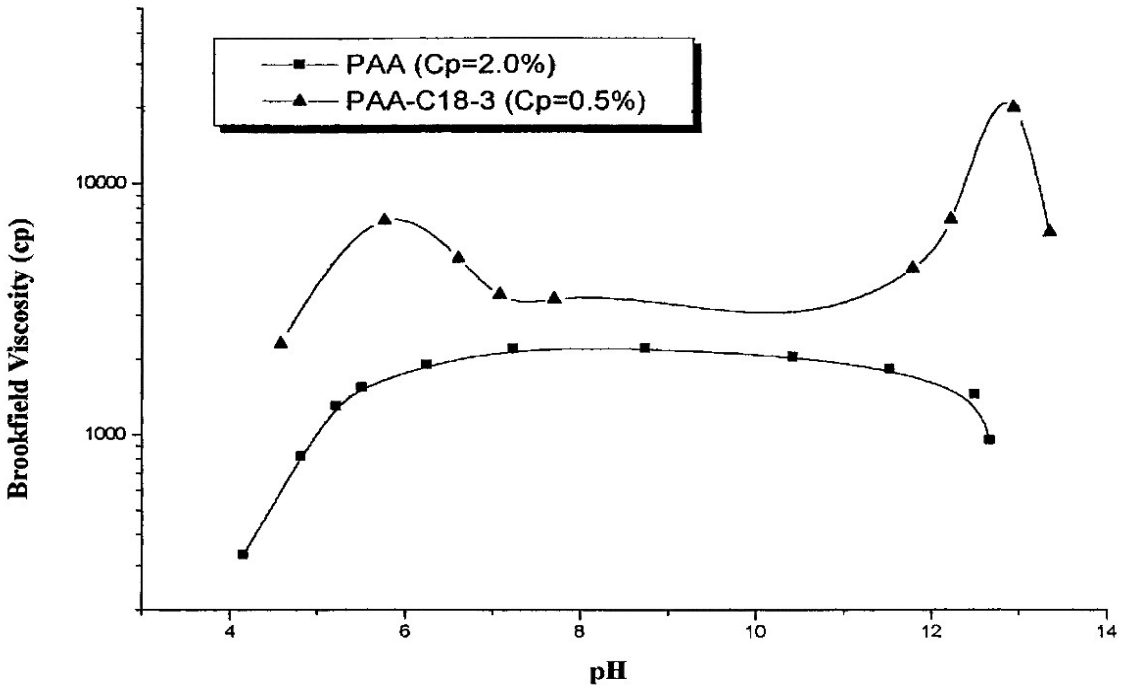

Figure 2.5: *Effect of pH on polymer viscosity of PAA and PAA modified with n-dodecyl acrylate/2-ethylhexyl acrylate (PAA-C) (Zhuang et al. 2001).*

For the poly acrylic acid (PAA) polymer, under low pH conditions (acidic conditions), there is a low charge density due to the undissociated state of the carboxylic groups on the polymer chain. This minimizes electrostatic repulsion hence chain retraction resulting in a decrease in polymer viscosity. As the pH increases, there is a gradual increase in charge density due to the gradual dissociation of the carboxylic groups on the polymer chain. At maximum viscosity, there is complete dissociation of the carboxylic groups, and a further increase in pH would result in a salting out effect on the polymer. This is similar to the effect reported by Zhou et al. (2001) on PAA polymers in Figure 2.4. However, the modified PAA copolymers, i.e. poly (acrylate-co- alkyl acrylate) by Zhuang et al. (2001), showed the same trend described by Zhou et al. (2001). The behaviour of the associating polymer is

essentially a balance between electrostatic repulsion between charged moieties on the chain and hydrophobic interactions.

2.3. Inaccessible Pore Volume of Associative Polymers

The IPV can be described as the fraction of the rock pore volume, which remain inaccessible to the polymer due to the polymer size (Pancharoen et al., 2010; Sheng, 2011; Al-Hajri et al., 2018; Torrealba and Hoteit, 2019). According to Sheng (2011), polymer molecules cannot flow through those pores when polymer molecular sizes are larger than some pores in a porous medium. Consequently, the volume of those pores that polymer molecules cannot access is called the IPV (Sheng, 2011). Aside from the polymer size, this phenomenon depends on salinity, divalent ion concentration, rock surface effect, temperature, polymer charge and concentration and the pore-size distribution of the rock (including dead-end pores) (Al-Hajri et al., 2018; Torrealba and Hoteit, 2019). Pancharoen et al. (2010) studied the effect of different associating polymers on the IPV of a sand-packed column with an absolute permeability of 21.6 D. The molecular weight of associating polymers was identified as a critical factor that influences the IPV of associating polymers. High molecular weight associating polymers are characterised by sizeable molecular volume and more hydrophobic regions on the polymer chain. As such, associating polymers with large molecular weight would result in polymer chains with large molecular clew dimension compared to pore throat sizes. According to the experimental work of Pancharoen et al. (2010), low molecular weight associating polymers displayed 12 and 20 % of IPV using superposition and simulation methods respectively. However, the high molecular weight associating polymers showed IPV between 33 – 49 % depending on the approach used. An explanation for this could still be explained in terms of the hydrophobic interactions, which increases with polymer molecular weight. In like manner, the concentration regime of associating polymers, either dilute or semi-dilute, can influence the IPV. At concentrations representative of dilute regime, hydrophobic interactions are absent, polymer resistance factor is reduced, and injectivity increases, thereby reducing IPV. However, when polymer concentration represents the semi-dilute regime, hydrophobic interactions dominate, and polymer resistance factor is increased and as such injectivity decreased thereby increasing IPV. The IPV represents one of many mechanisms of polymer transport in porous media, and where this is dominant, it may lead to polymer acceleration. This would occur when polymer solution is injected at salinity lower than the reservoir

salinity. However, where polymer adsorption is dominant, the process of polymer transport is different, as discussed below.

2.4. Retention Properties of Associative Polymers

The size of associating polymer cluster depends on polymer concentration and the level of hydrophobe content that can lead to polymer adsorption and retention in porous media (Taylor and Nasr El-Din, 1998). This is mainly the case when the hydrophobe distribution along the polymer chain is blocky rather than random. In the case of block distribution of hydrophobe content, the concept of multilayer adsorption has been proposed as an explanation (Page et al., 1993; Volpert et al., 1998; Dupuis et al., 2011; Kamal et al., 2015; Zhao et al., 2017). The adsorbed layer of the associating polymer has a segment of the hydrophobic group interacting with the rock surface. In contrast, another portion of the hydrophobic group interacts with other polymer chains, forming another adsorption layer. As a result, an increase in the polymer concentration of associating polymer would continuously increase polymer adsorption on the rock surface. Most of the experimental studies on HAPAM have focused on using sand-pack columns. As such, the mechanism of polymer-rock interaction for hydrophobically modified polymers may differ for calcite, sandstone, and dolomite reservoirs. El-Hoshoudy et al. (2015) reported the interaction of associative polymers with sandstone rocks. The polymers exhibited -50.3 and -21.8 mV from Zeta potential measurements with an average value of – 46.3 mV. Thus, such associative polymers are capable of causing a wettability alteration on positively charged sandstone reservoirs during polymer flooding processes. However, at a pH value greater than 2, it was reported that sandstone rock could exhibit a negatively charged surface in which the positively charged nitrogen bases can adsorb on the rock surface and alter wettability (El-Hoshoudy et al., 2015). In addition, Chiappa et al. (1999) reported the effect of polymer charge (anionic, weakly anionic and cationic) from a 2 % KCl solution on its adsorption on a quartzite rock surface, which was negatively charged at pH greater than 2. It was evident from their findings that polymer adsorption increases from anionic to weakly anionic to cationic polymers. However, when these polymers were exposed to reservoir sand (49 wt.% Quartz and 21 wt.% Calcite), the anionic polymer exhibited negligible adsorption phenomenon while adsorption increased from the weakly ionic to the cationic polymer. It should be noted that calcite has a positively charged surface at pH values less than 9.5. Therefore, polymer interaction with the rock surface may reflect a much more complex behaviour at the calcite surface. The presence of divalent ions can enhance the

adsorption of anionic polymers onto a quartzite surface which can be achieved in two ways (Chiappa et al., 1999). Firstly, the divalent ion creates a link (or act as a bridge) between the anionic polymer and the negatively charged quartz surface. Secondly, the divalent ions can neutralize part of the negative sites on the anionic polymer, thereby reducing electrostatic repulsion. Similarly, the adsorption of crude oil tends to reduce the tendency of polymer-rock interaction (Chiappa et al., 1999; Taheri-Shakib et al., 2019(a); Taheri-Shakib et al., 2019(b)). Quan et al. (2019) reported the use of HAPAM polymers in the acidification process of carbonate rocks. The adsorption of the associative polymer was such that it forms a protective film on the carbonate rock. The authors reported that the adsorption and desorption of associative polymers on the carbonate surface influence the reaction rate between the acid and the carbonate. However, after the desorption process at the end of the reaction, small amounts of the associative polymers remain on the rock surface, thereby creating cracks and voids (Figure 2.6).

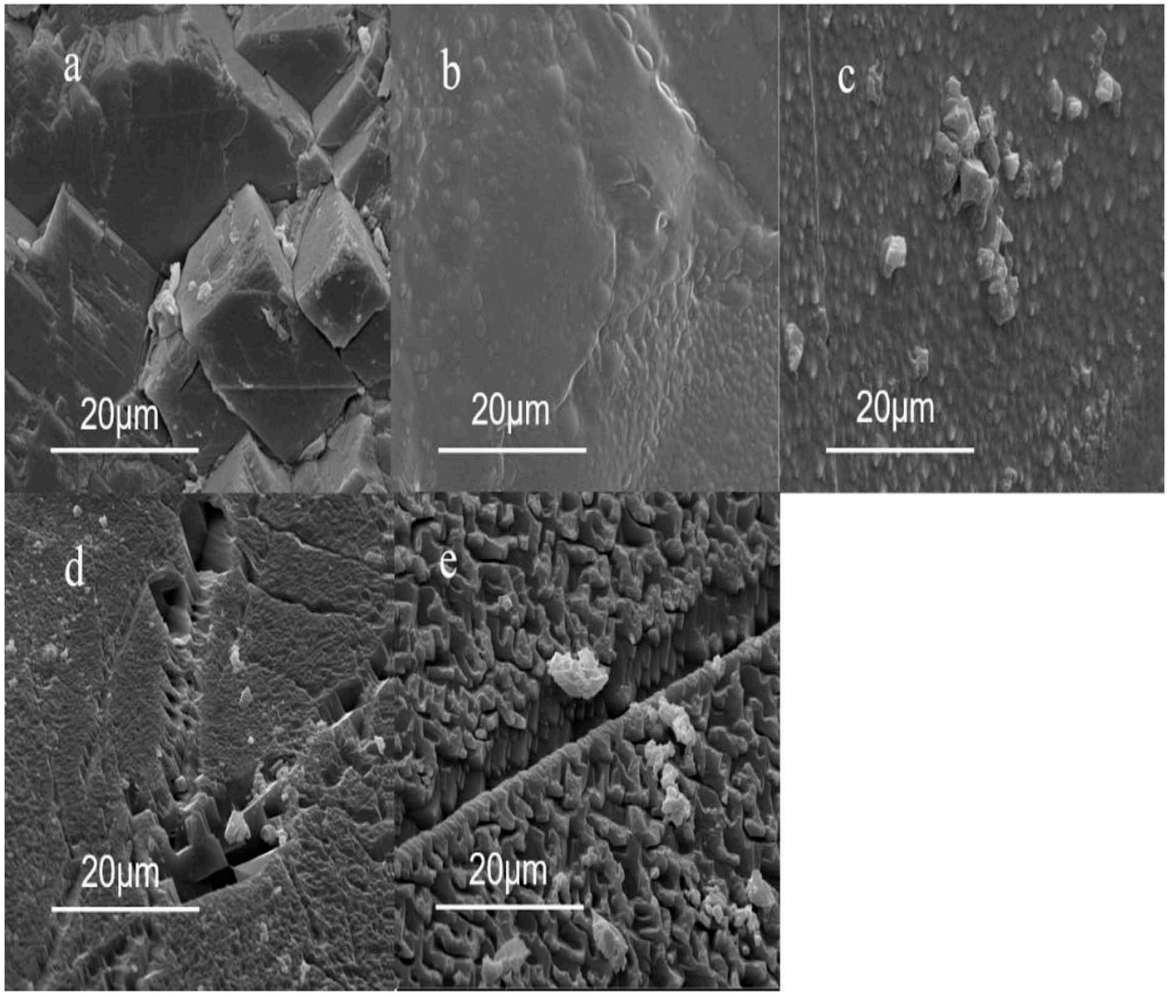

Figure 2. 6*: SEM images of the associative polymer (HPAAT) at various dissolution times: (a) the untreated carbonate sample, (b) 5000 mg L^{-1} HPAAT-40 min (c) 8000 mg L^{-1} HPAAT-50 min, (d) 5000 mg L^{-1} HPAAT-55 min, and (e) 8000 mg L^{-1} HPAAT-65 min. (Quan et al., 2019).*

The adsorption isotherm of HAPAM polymers does not follow the classical approach, often characterized by a plateau region. This is often attributed to the continuous interaction between the hydrophobic regions of the polymer chains in solution. Concerning this, Volpert et al. (1998) reported on the interaction between HAPAM polymers and an alumina silicate surface. The adsorption isotherm of the HAPAM was characterized by a continuous increase in the adsorbed polymer and the absence of a plateau region. This phenomenon was explained in terms of classical multilayer adsorption due to the hydrophobic interaction between polymer chains. However, recent studies on the rock adsorption (in sand-pack column) phenomenon associated with hydrophobically modified polymers has been attributed to some *"minor polymeric species"* (Dupuis et al., 2011; Seright et al., 2011). This implies that for hydrophobically associating polymers, adsorption does not mean the deposition of a substantial quantity of polymer molecules from solution to the rock surface. Accordingly, Dupuis et al. (2010) experimentally showed that the classical theory of multilayer adsorption does not apply to hydrophobically associating polymers. Instead, adsorption of hydrophobically associating polymers is controlled by the presence of *"minor polymeric species"*. The authors injected an associating polymer with sulfonated polyacrylamide backbones and alkyl hydrophobic side chains into a cylindrical chamber with granular packs. As expected, a high resistance factor was obtained with the associating polymers. However, core plugging did not occur as evident from the stabilization trend obtained from the resistance factor curves and no loss in viscosity of the polymer effluent. The polymer effluent was re-injected into a new core, and resistance factor values were stable with no increase. According to Dupuis et al. (2011) and Seright et al. (2011), removal of these *"minor polymeric species"* with an appropriate filtration method without degrading the thickening capability of the polymer will ensure more negligible adsorption. However, the selection of a proper filtration method, which will ensure that the associating polymers do not lose their viscous properties, may be challenging. Moreover, investigating the origin of these *"minor polymeric species"* would help understand how to properly design the synthesis and treatment process of hydrophobically associating polymers. Core flooding experiments carried out show an irreversible reduction in permeability without filtration of the precursor polymer solution. The resistance to adsorption of associating polymers can also be improved by using hydrophobes, which contain sulfonate groups (Taylor and Nasr El-Din, 1998; Seright et al., 2011; Wever et al., 2011). The use of 2-acrylamido-2-methyl propane sulfonate (AMPS) as a comonomer in modifying polyacrylamide has been reported to produce more negligible adsorption than HPAM polymers. However, this phenomenon

appears to be peculiar with associating polymers made of 2-acrylamido-2-methyl propane sulfonate. Other factors such as salinity may influence the adsorption of associating polymers in porous media (Rashidi et al., 2009; Li et al., 2016; Akbari et al., 2017; Amirian et al., 2018). This may manifest in the form of ion competition with polymer molecules for adsorption sites and may result in less adsorption (Torrealba and Hoteit, 2019). It has been reported that where polymer adsorption is the prevailing transport mechanism in porous media, an injection of polymer solution at salinities lower than that of the reservoir would lead to polymer retardation where the salinity front accelerates faster than the polymer front.

2.5. Polymer Injectivity and Permeability Reduction

Polymer injectivity can be predicted and monitored from values obtained for resistance factor (RF) and a residual resistance factor (RRF) (Al-Shakry et al., 2019). The injectivity of associating polymers is low compared to conventional HPAM polymers and is characterised by large RFs (Seright et al., 2011; Azad and Trivedi, 2017). Furthermore, this low injectivity can be attributed to the nature of the polymer hydrophobic interaction, which is concentration-dependent (Dupuis et al., 2011; Xie et al., 2016; Azad and Trivedi, 2017). Azad and Trivedi (2017) carried out an injectivity study on associative polymers compared to HPAM polymers. It was observed that at a concentration of 2000 ppm, the associative polymers exhibited higher RFs than HPAM polymers at the concentration for all shear rates studied. Furthermore, the concentration value of 2000 ppm represents the CAC of the associative polymer, and the polymer showed decreased resistance for values at high shear rates. The reduced values of the RFs can be explained in terms of a transition of the associative effect from intermolecular to intramolecular interaction at high shear rates (Seright et al., 2011; Reichenbach-Klinke et al., 2016; Azad and Trivedi, 2017). However, at a concentration of 1000 ppm for the associative polymers and HPAM, the RFs exhibited by both polymers were similar. For the associative polymer, this could be explained by intramolecular interaction dominating the rheology of the polymer. On the other hand, the amount and type of hydrophobe content in the polymer could also play an essential role in the injectivity of associative polymers. Reichenbach-Klinke et al. (2016) investigated the performance of different associative polymers in terms of molecular weights and hydrophobic contents. The RF and viscosity were observed to increase with hydrophobic content, and the reverse was the case with polymer injectivity (Seright et al., 2011; Reichenbach-Klinke et al., 2016; Azad and Trivedi, 2017). However, in oil saturated cores, it has been reported that the presence of oil weakens the intermolecular interactions, with

the degree of weakening dependent on the hydrophobic content (Reichenbach-Klinke et al., 2016). Also, surfactants tend to reduce the high RF of associative polymers by competing with the hydrophobic interactions, thereby creating a surfactant-polymer interaction. Equally significant from the work of Reichenbach-Klinke et al. (2016) is the impact of associative polymer on permeability reduction. Using polymer concentrations of 1000 and 2000 ppm for the associative polymer and HPAM respectively showed that associative polymers have higher values for the RRF compared to HPAM. This was explained in terms of the mechanism of multilayer adsorption, which is further enhanced by hydrophobic interactions. However, this phenomenon of multilayer adsorption remained debatable, as shown by the works of Dupuis et al. (2011) and Seright et al. (2011), who attributed the permeability reduction to the presence of some *"minor polymeric species"*. Therefore, permeability reduction by associative polymers depends on the hydrophobic comonomer that makes up the polymer chain. In like manner, at a concentration of 1000 ppm, the HPAM showed higher values for the RRF compared to the associative polymer. This implies that the dilute concentration regime where intramolecular interaction dominates ensures that the RRF is low. Under these circumstances discussed, it is evident that the properties of associative polymers can be tuned and adjusted to achieve the desired injectivity, propagation, RF and RRF. Further to this, the mechanism of polymer-rock interaction (IPV and adsorption), as discussed earlier, can be employed in improving the injectivity and propagation of associative polymers as proposed by Torrealba and Hoteit (2019). The authors proposed a compositionally tuned polymer injection process, which considers polymer transport under salinity, adsorption and IPV. This takes explicitly into account polymer retardation and acceleration effects arising from adsorption and IPV respectively. The proposed injection scheme appears viable under simulation. However, an experimental study is still required in validating the outcome. The application of this study to associative polymers would require optimising in terms of slug composition, injection cycle size and number of cycles.

2.6. Emulsion Properties of Associative Polymers

A challenge associated with polymer flooding is the separation of water from crude oil. This difficulty is traced to the interfacial tension (IFT) characteristics of polymers to enhance the stability of oil emulsions (Deng et al., 2002; Meiqin et al., 2008; Pancharoen, 2009; Pancharoen et al., 2010; Al-Sabagh et al., 2016). The interfacial tension characteristics of associating polymers are attributed to the distribution of hydrophilic and hydrophobic

blocks along the polymer backbone (Pancharoen, 2009; Pancharoen et al., 2010). According to Pancharoen et al. (2010), the hydrophobic groups on the polymer backbone align themselves in the oil phase, which contains active interfacial components such as asphaltenes and resins, while the hydrophilic part remains in the aqueous phase. This behaviour of associating polymers reduces the contact area between oil and water, thereby reducing the interfacial tension and enhancing crude oil emulsion stability. Comparison with low molecular weight surfactants shows that the abilities of these polymers in reducing IFT was less. Therefore, the authors pointed out the magnitude of this IFT reduction does not appear to be significant enough to contribute to added oil recovery. However, the strength of the emulsion stability effect of associative polymers depends on several factors, such as the type of associative polymer and polymer concentration. Meiqin et al. (2008) investigated the effect of polymer concentration on the interfacial tension characteristics of associative polymers. The measured interfacial shear viscosity of the water-oil film was used to characterise the stability of the water-oil emulsion. It was observed that the interfacial shear viscosity of the oil-water film increased with associative polymer concentration hence its emulsion stability. Consequently, the rate of demulsification and the rate of oil-water separation would decrease with increased polymer concentration. Thus, the strength of the emulsion stability caused by increased polymer concentration can be explained by the increased number of hydrophobic groups available to the oil phase. As such, IFT reduction does not contribute to the mechanism by which associating polymers improves oil recovery (Pancharoen et al., 2010). However, Reichenbach-Klinke et al. (2016) reported that additional oil recovery using associative polymers could occur with a combination of IFT reduction and mobility reduction. While this remains debatable, the increased oil-water emulsion stability arising from associating polymers remains a challenge towards its application. A foam can be described as having a gas phase dispersed in a liquid phase and often used in improving the mobility of gas (such as CO_2) during EOR operations (Zhang et al., 2015; Xu et al., 2016; Ahmed et al., 2017). However, the foam must remain stable in oil as its longevity is what determines its efficiency. Ahmed et al. (2017) compared the use of conventional HPAM polymer with an associative polymer in the preparation of polymer enhanced foams (PEFs) with polymer concentration kept at 2000 ppm and operating temperature and pressure at 80 ^{0}C and 14.5 psi respectively. Figures 2.7 and 2.8 show the comparison between HPAM and HAPAM polymers regarding foam stability and foam volume respectively. The stability of the PEF was observed to be more pronounced using an associative polymer compared to a HPAM polymer.

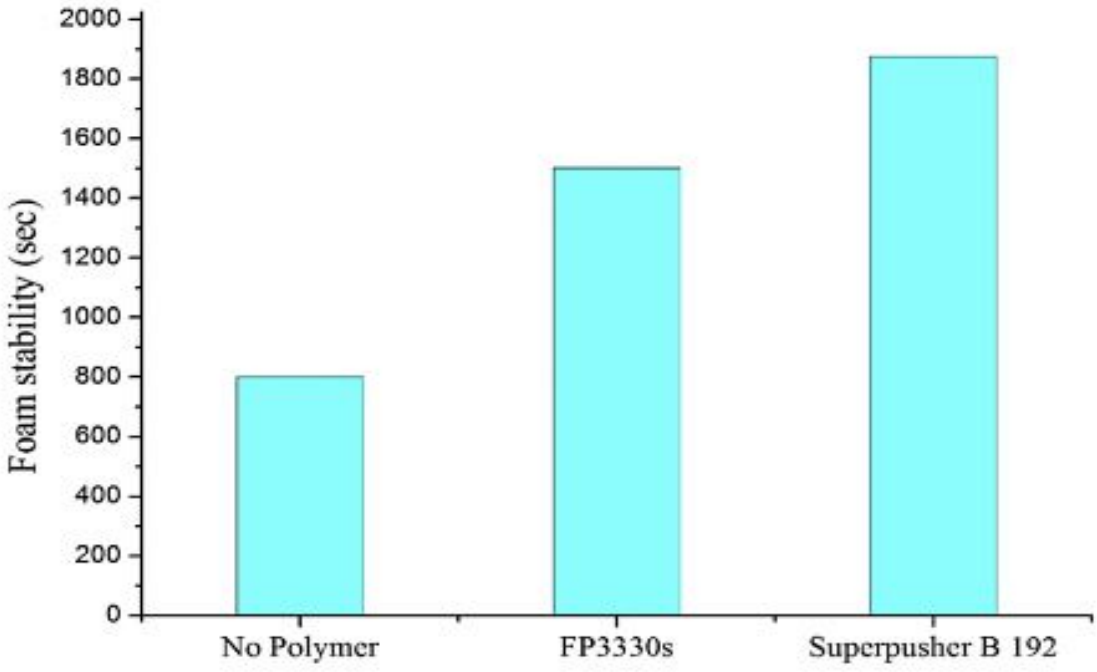

Figure 2.7: *Foam stability comparison of PEFs containing no polymer, conventional polymer (FP3330s) and associative polymer (Superpusher B192) CO_2 foams. The polymer concentration was 2000 ppm at 3 wt% NaCl, 80 ^{0}C and 14.5 psi (modified from Ahmed et al. (2017)).*

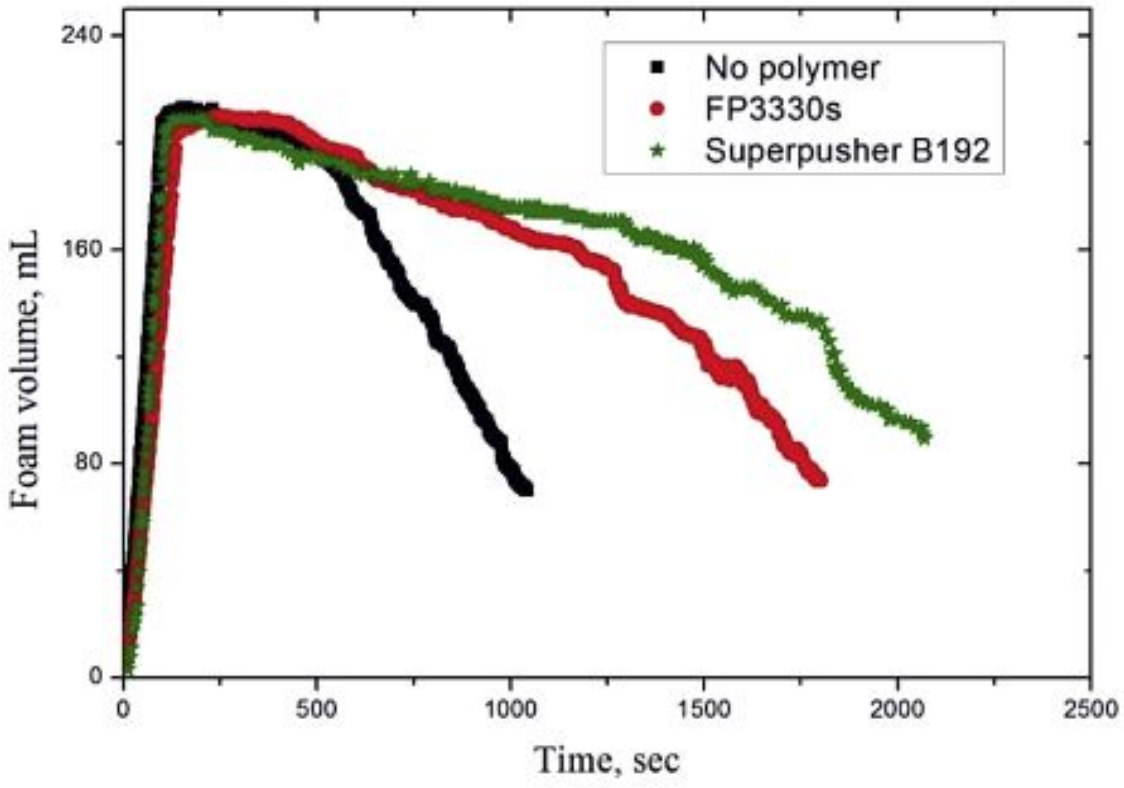

Figure 2.8: *Foam volume comparison of PEFs containing no polymer, conventional polymer (FP3330s) and associative polymer (Superpusher B192) CO_2 foams. The polymer concentration was 2000 ppm at 3 wt% NaCl, 80 ^{0}C and 14.5 psi (modified from Ahmed et al. (2017)).*

This can be explained by the enhanced thickening ability (arising from hydrophobic interactions) of the associative polymer compared to HPAM. This enhanced thickening effect of the associative polymer tends to limit gas diffusion, thereby enhancing foam stability through a gradual reduction in foam volume. However, the thickening capability of associative polymers differs for different hydrophobic content and under varying reservoir conditions. Hence, enhancing the performance of PEFs would require optimizing for different hydrophobe content and reservoir conditions.

2.7. Heterogeneity of Reservoirs on Associative Polymers

The influence of polymer concentration and reservoir heterogeneities on polymer flooding performance are among paramount factors that determine the success of the oil recovery process (Han et al., 2006; Wei et al., 2007; Wassmuth et al., 2012; Patokina, 2015; Xie et al., 2016). Reservoir heterogeneities arise from the oil formation's depositional history, which creates a difference in physical properties between the high permeability layer and low permeability layer (Xie et al., 2016). For a homogenous reservoir with uniform rock properties, the propagation of hydrophobically associating polymers depends on polymer concentration (Wassmuth et al., 2012). Furthermore, the molecular interaction/aggregation of associating polymers for mobility control can be regulated by changing the polymer concentration. Xie et al. (2016) evaluated the applicability of hydrophobically associating polymers in a heterogeneous reservoir system. It was confirmed by the authors that there exists compatibility between polymer molecular aggregation/association and pore-throat size. In other words, there exists a matching relationship between the size of an associated polymer cluster and the size of the pore-throat of the reservoir. Where the size of the associative polymer cluster matches well with the pore-throat size, the pressure drop was observed to be stable as pore volume increased. Alternatively, at a given polymer concentration, there could be a mismatch between the size of the cluster and the pore-throat; therefore, the pressure drop due to polymer injection increases with pore volume. Thus, a heterogeneous reservoir provides a scenario where rock properties play an essential role with polymer concentration (Wassmuth et al., 2012; Xie et al., 2016). A change in polymer concentration will control the mobility of polymer solution in the different permeable layers of the reservoir. Accordingly, Xie et al. (2016) considered the following as crucial for associating polymer in a heterogeneous reservoir:

a) The size of the associating polymer cluster is regulated from polymer concentration, thereby ensuring passage through low pore-throat zones.

b) Reservoir fluid diversion arising from polymer jam/retention in high permeability zone. This is a result of the size of the associating polymer cluster.

Thus, the different molecular association between polymer molecules and the size of the associating polymer cluster arises from varied polymer concentrations. The size of the associating polymer cluster at a given concentration needs to be optimally matched with the average heterogeneities and permeability of the different layers in the reservoir. The essence of optimally matching the size of the aggregates arising from the associating polymer clusters and the reservoir heterogeneities can be tied to the following:

a) High polymer concentration would be needed, if not above the limit for EOR operations, which could be detrimental to the economics of the flooding process.
b) For a heterogeneous reservoir, finding an optimum concentration for associating polymers would help prevent the occurrence of a profile reversal where polymer mobility is enhanced in the permeable layer with little residual oil.
c) In addition, polymer injectivity would be affected, and this is often constrained by formation fracture pressure. Furthermore, high polymer injection pressure can make associating polymers lose their space-network structure resulting in a reduced hydrodynamic size for the polymer molecules.

2.8. Performance of Associative Polymers under Alkali/Surfactant Flooding

The use of HAPAM polymers for Alkaline Surfactant Polymer (ASP) flooding is not common compared to the use of HPAM polymers, and its usage has been limited to laboratory studies and field trials (Feng et al., 2013; Guo et al., 2017). Feng et al. (2013) compared the use of HAPAM to HPAM polymers in an ASP flooding trial project in a Daqing class II reservoir ($100 – 300\ x10^{-3} \mu m^2$) containing heavy alkyl benzene sulfonate. The authors evaluated the HAPAM polymer under laboratory and field conditions. Figures 2.9(a) and (b) show the effect of the ASP system containing HAPAM and HPAM on the interfacial tension under laboratory conditions respectively. The associative polymer in Figure 2.9(a) offers good compatibility with heavy alkyl benzene sulfonate, which can ensure very low interfacial tension over a wide range of alkali/surfactant concentration. When aged for 120 days, the viscosity of the associative polymer is improved; however, the interfacial tension remained the same. A flooding experiment was conducted using a 1000 mg/L HAPAM-ASP system containing 1.0 % NaOH and 0.3 % alkyl benzene sulfonate. Figure 2.10 show that using 0.3 PV of ASP fluid improved the recovery of oil by 26 %.

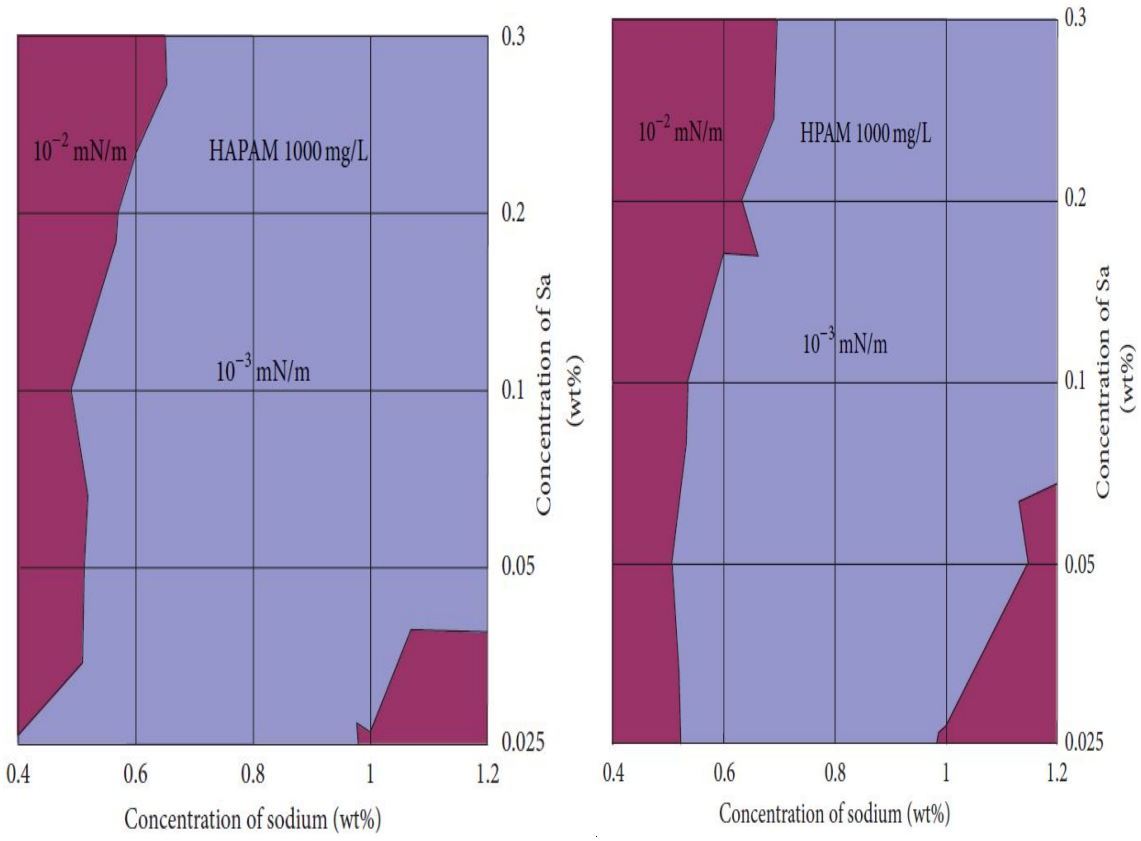

***Figure 2.9**: Interfacial tension of a 1000 mg/L ASP flooding system containing (a) HAPAM and (b) HPAM (Feng et al. 2013).*

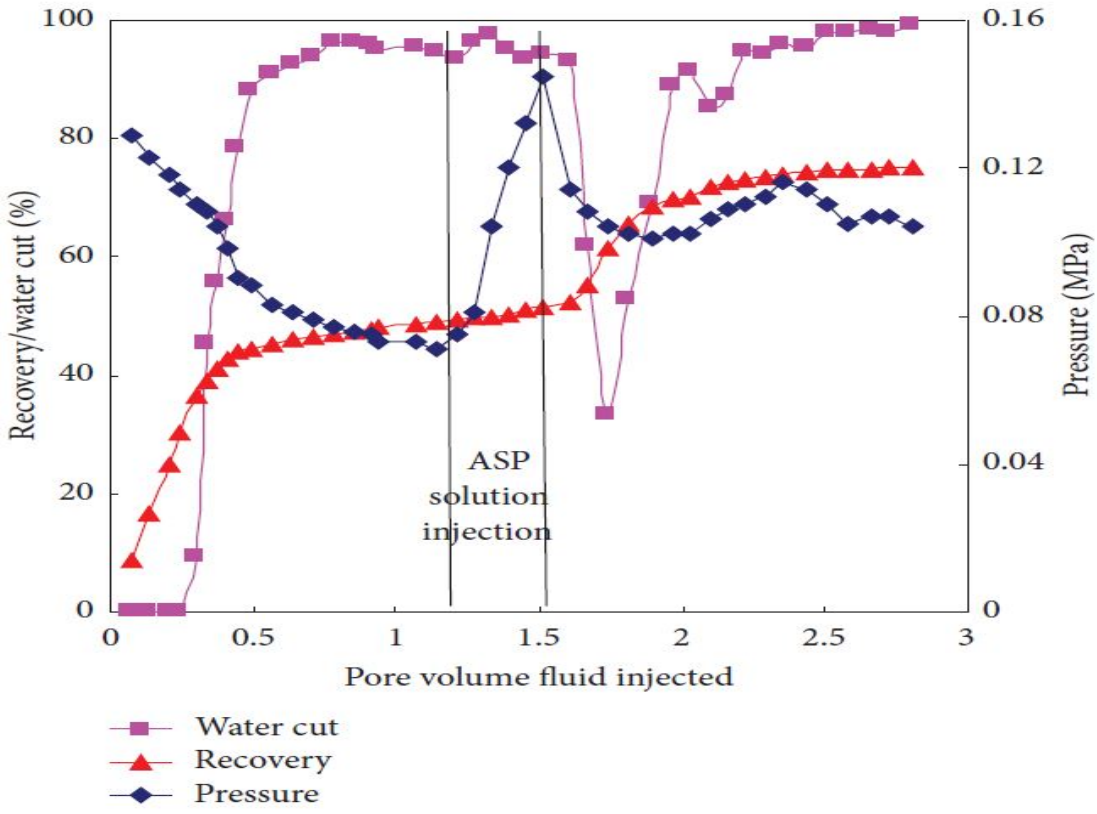

***Figure 2.10**: Core flooding results for the ASP system containing associative polymer as studied by Feng et al. (2013).*

The mechanism by which ASP systems containing associative polymers improve oil recovery is summarized in Figures 2.11 and 2.12.

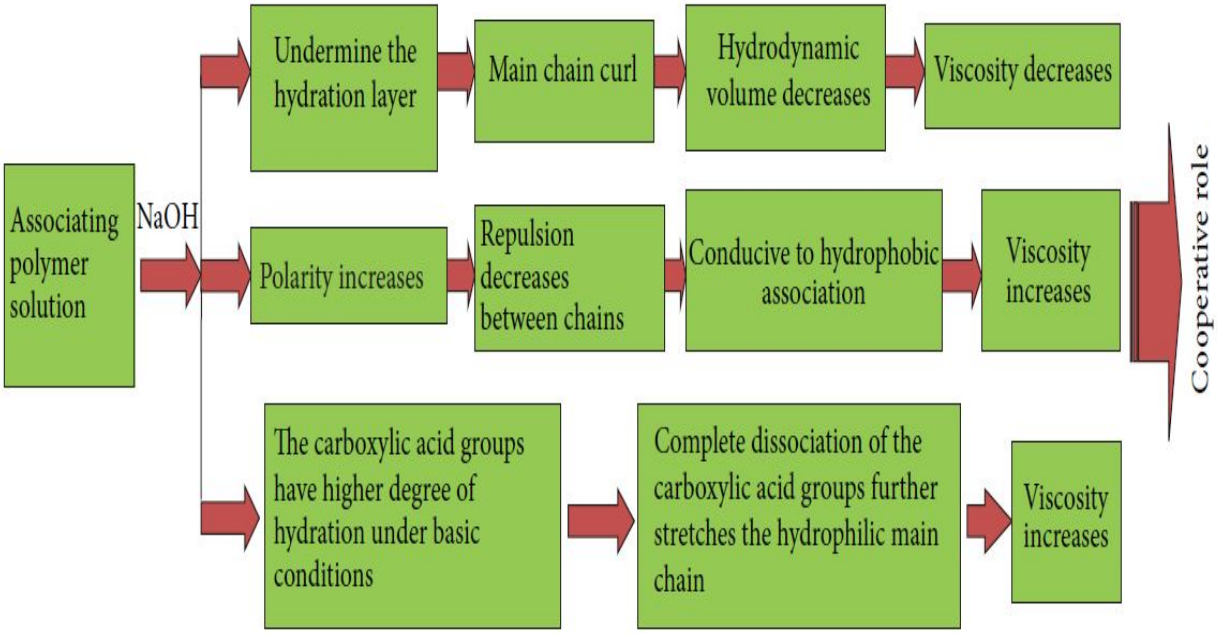

***Figure 2.11**: The effect of alkali on the viscosity of the associating polymer solution (Feng et al., 2013)*

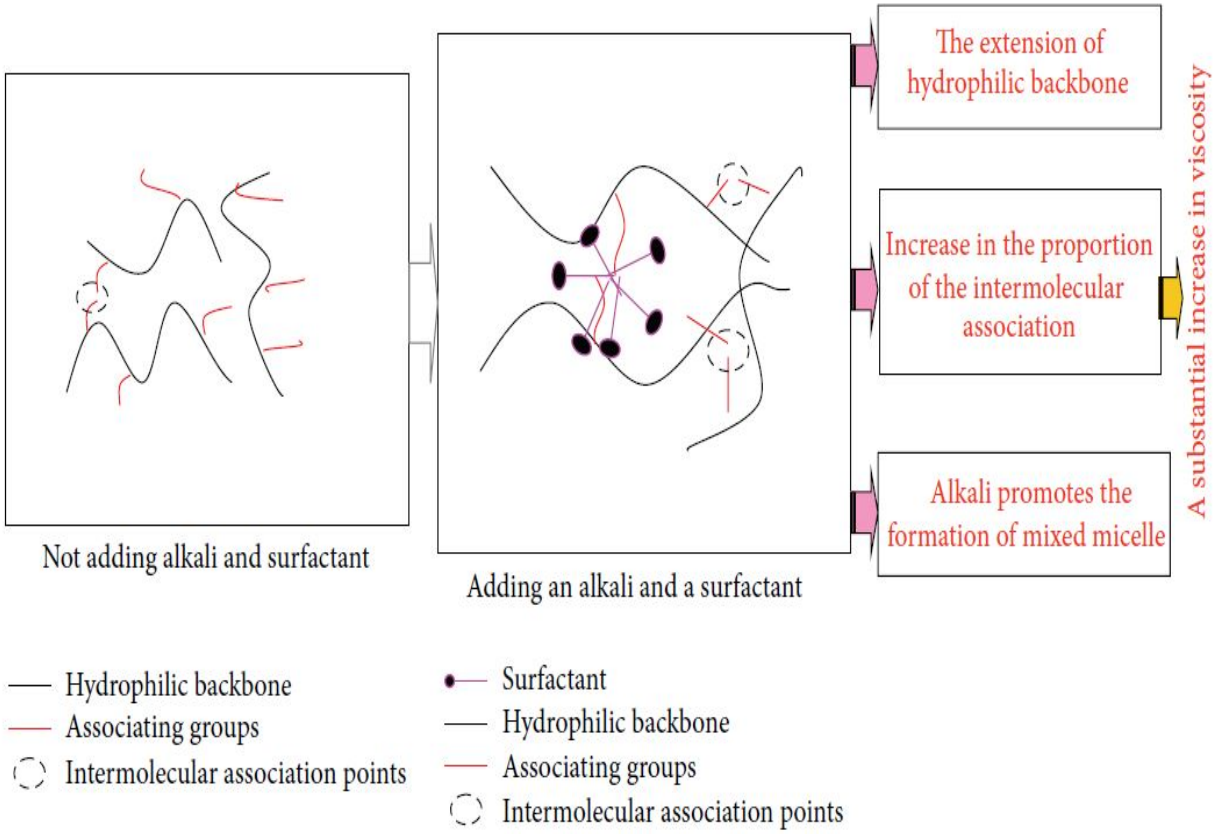

***Figure 2.12**: The effect of alkali mixed surfactant on the status of the associating polymer solution (Feng et al., 2013)*

In the presence of the base and the surfactant, the viscosity of the ASP fluid is increased due to the higher hydration degree of the carboxylic groups under basic conditions. This ensures that the carboxylic groups on the hydrophilic main chain on the associative polymer are entirely dissociated, thereby enabling polymer chain extension. Therefore, the surfactants present in the ASP system interact with the associative polymer's hydrophobic components, thereby resulting in more intermolecular association, which significantly increases the fluid's viscosity, as shown in Figure 2.12. However, it should be noted the rheological improvement of the ASP system containing associative polymers depend on the type and composition of the surfactant (Feng et al., 2013). In addition, the composition and kind of hydrophobic monomer in the associative polymer is also essential when considering the performance of the HAPAM-ASP system.

2.9. Solution Properties of Associating Polymers from Produced Fluids

The associated goal of a polymer flooding design is the reduction in the amount and cost of chemicals employed. In other words, the cost-effectiveness of a polymer flooding project design is crucial to its successful deployment and application. In addition, another identified challenge with polymer flooding design is the disposal of produced fluid containing the residual polymer. The associative characteristics of hydrophobically associating polymers have been shown to maintain the viscous properties of such polymers above the critical aggregation concentration. However, Lu et al. (2010) postulated that the successful characterization and reuse of hydrophobically associating polymers in produced fluids mean that:

a) The phenomenon of hydrophobic association exists in porous media. Nevertheless, the authors did not mention this depends on how it is propagated in a porous media. The propagation of associating polymers deep into a reservoir may affect the hydrophobic interactions between polymer chains (in-situ) and when produced (ex-situ).
b) The possibility of a change in the critical aggregation concentration of the produced associating polymer and what this change means on the solution properties of the polymer. These changes, if they occur, may be attributed to changes in the hydrophobe content when the polymer flows through the porous media.

Studies by Lu et al. (2010) have shown that hydrophobically associating polymers obtained from produced fluids have lower hydrophobic content than pre-flooding conditions. This indicates that the compositional homogeneity of the polymers is affected, which further explains the reduced associative effect of the polymers. However, the CAC of the

associating polymer from the produced fluid was similar to its pre-flooding value. Although the reported results show that hydrophobically associating polymers can be reused; however, the study did not indicate if such property can be maintained in deep reservoirs. In addition, the well spacing in most oil fields would require deep propagation of polymers before the breakthrough of solutions from the producer well. Where the hydrophobic associative features are lost after flowing a short distance, its mobility control cannot be sustained far from the wellbore where most of the oil is displaced (Seright et al., 2011).

2.10. Modelling the Flow of Associating Polymers in Porous Media

2.10.1. In-Situ Rheology of Associative Polymers

To properly account for polymer rheology, the concept of in-situ viscosity has been coined to describe flow behaviour in porous media in comparison to bulk viscosity. The in-situ viscosity can be defined as the average viscosity inside a porous media and is also described as the apparent viscosity. This differs from the effective viscosity, which can be related to the viscosity of the polymer in a pore throat. Figure 2.13 shows a typical flow curve for a polymer solution in porous media displaying viscoelastic behaviour at a steady-state.

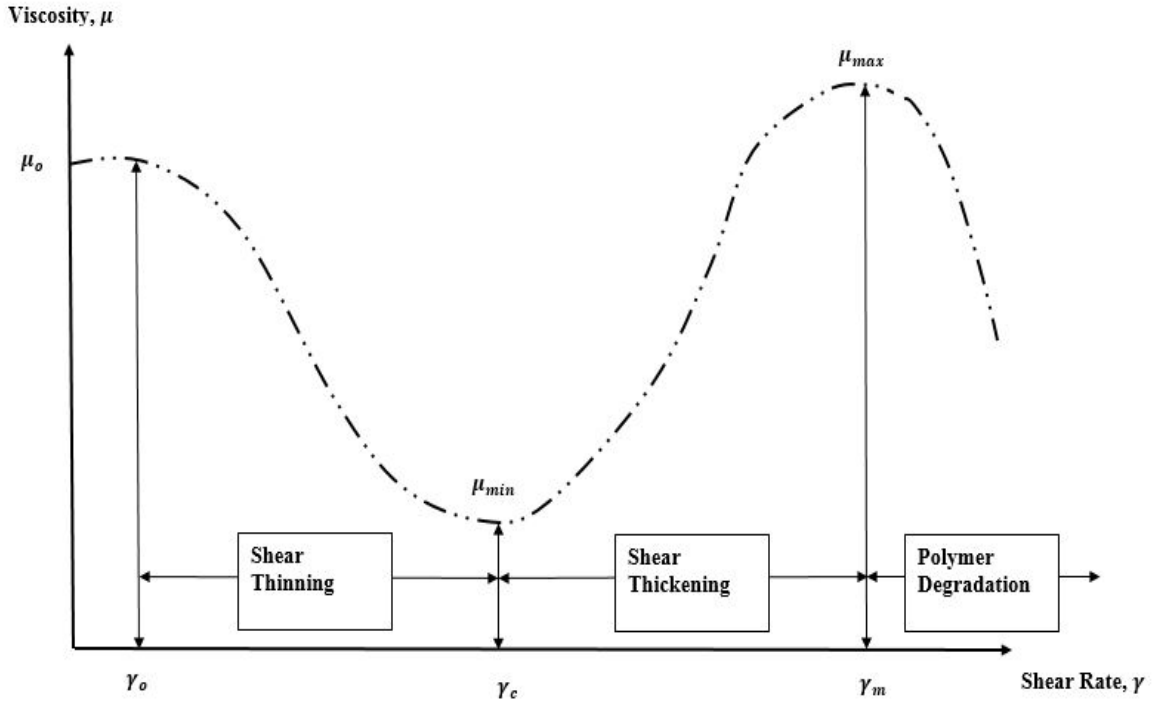

***Figure 2.13**: A typical plot of viscosity versus shear rate for a polymer solution that exhibits shear thickening. γ_c is the first critical shear rate which marks the onset of shear thinning. The increase in viscosity begins at the critical shear rate γ_c, after a minimum viscosity, μ_{min} and shear thinning resumes after shear rate, γ_m at maximum viscosity, μ_{max}. μ_o represents polymer viscosity at low shear rate.*

Similar trends in porous media have been reported (Edwards et al., 2002; Jiang et al., 2003; Khamees and Flori, 2018). The identifiable flow regimes in porous media can be classified as Newtonian, Shear Thinning, Shear Thickening and Mechanical Degradation (Hatzignatiou et al., 2013). The Newtonian regime is apparent at low shear rates. Still, beyond the initial critical rate γ_o, shear-thinning is apparent until polymer viscosity reaches a local minimum at a critical shear rate value of γ_c. This critical shear rate, which is one out of three, represents the threshold for the onset of shear thickening. A local maximum for the polymer viscosity is obtained at a third critical rate γ_m. Beyond γ_m, there is another decrease in polymer viscosity; this shear rate is characterized as the onset of mechanical degradation (Dupas et al., 2012; Brakstad and Rosenkilde, 2016; Lohne et al., 2017; Skauge et al., 2018). Many factors, including shear-thickening, influence polymer injectivity in porous media. Injection rates above the critical rate for the onset of shear thickening may reduce polymer injectivity for field application (Skauge et al., 2018). At this point, polymers undergo an irreversible thickening effect which culminates into degradation after a given period. The critical shear rate for the onset of dilatant behaviour in porous media depends on polymer, solvent and rock properties. However, in the case of associative polymers, some of the concerns, according to Seright et al. (2011), are related to:

a) Maintaining the enhanced viscous properties (long-term stability) and ensuring its propagation in porous media under varied reservoir conditions.
b) The effect of polymer concentration regime on polymer injectivity. An understanding of its effect on the onset of shear thickening in porous media.

As mentioned in (b), the effect of the concentration regime of associative polymer flow on the onset of shear thickening is limitedly understood. However, this can be complicated given that specific oil field parameters such as temperature and salinity have been reported to alter the CAC of associating polymers (Zou et al., 2013; Gou et al., 2015; Sun et al., 2015; Quan et al., 2016).

2.10.2. Existing Models for In-Situ Polymer Rheology

Due to the time-consuming nature of in-situ measurement techniques, in-situ polymer rheology has often been evaluated analytically and numerically (Skauge et al., 2018). The difficulty with modelling polymer rheology lies in the fact that they are non-Newtonian fluids and the porous media in which they flow is a non-uniform pore geometry (Lohne et al., 2017; Skauge et al., 2018). The analytical study of polymer flow in porous media involves using time-independent models with the addition of some viscoelastic attributes

(Delshad et al., 2008; Sochi, 2010; Hatzignatiou et al., 2013; Yang et al., 2015). This can be represented as shown in equation (2.5):

$$\mu_{app} = \mu_{sh} + \mu_{el} \quad (2.5)$$

Where μ_{sh} represents the shear-thinning component. Modelling the shear-thinning features of polymer flow has been captured using the Power law or Carreau model (Skauge et al., 2018). μ_{el} represents the elongational or extensional viscosity attributed to shear-thickening. In another approach, the flow of polymer in porous media is represented as the product of the shear and elastic components as shown in equation (2.6) (Lohne et al., 2017):

$$\mu_{app} = \mu_{sh}(\mu_{el}) \quad (2.6)$$

However, regardless of the approach employed (either equation (2.5) or (2.6)), a general classification of viscosity models for polymer flow in porous media was grouped into two by Yang et al. (2015). This classification was based on the number of parameters contained in the model: two-parameter and multi-parameter models. The only known two-parameter model describing polymer flow in porous media takes the form of the power-law model in describing shear-thinning and shear-thickening as shown below in equation (2.7):

$$\mu_{app}(\gamma) = \begin{cases} K_1(\gamma)^{n_1-1}, & \gamma < \gamma_c,\ n_1 < 1 \\ K_2(\gamma)^{n_2-1}, & \gamma > \gamma_c,\ n_2 > 1 \end{cases} \quad (2.7)$$

Where K_1, K_2, n_1, and n_2 are the consistency and flow index parameters representing the model. These parameters are similar to what is obtainable in the power-law viscosity model. The model is simplistic in form, and its application is limited due to a lack of clarity in differentiating between the shear thinning and shear thickening stage (Yang et al., 2015). In other words, accurate prediction of the onset of shear thickening is not captured by the model. The multi-parameter models take into account variations of polymer viscosity at relatively large shear rates. Table 2.6 presents known models that make up the shear thinning, and shear thickening components of various multi-parameter models used in describing polymer flow in porous media. The multi-parameter models generally give a full description of polymer flow from shear-thinning to shear thickening and even polymer degradation. However, many model parameters can be challenging, and it may be difficult to estimate them. In like manner, Lohne et al. (2017) described a similar challenge with such models when applied for polymer flow in porous media.

***Table 2.6**: Proposed models for polymer flow in porous media. Modified from Skauge et al., (2018)*

Model Form	Shear Component (μ_{sh})	Elastic Component (μ_{el})	Comment	Reference
$\mu_{app} = \mu_{sh}(\mu_{el})$	$\mu_{sh} = Hu^{n-1}$	$\mu_{el} = \frac{1}{1 - N_D}$	The model predicts an infinite value for the elongation viscosity with increasing Deborah Number, N_D	(Hirasaki and Pope, 1974)
$\mu_{app} = \mu_{sh}(\mu_{el})$	$\mu_{sh} = \frac{\bar{S}_{sw}}{\dot{\gamma}_a}$	$\mu_{el} = C(N_D)^{m_c}$	$\bar{S}_{sw}$ is average shear stress at wall of channels, $\dot{\gamma}_a$ apparent shear rate in porous media. C and m_c are parameter constants	(Masuda et al., 1992)
$\mu_{app} = \mu_{sh} + \mu_{el}$	$\frac{\mu_{sh} - \mu_\infty}{(\mu_0 - \mu_\infty)} = (1 + [\lambda_1\gamma]^2)^{(n_1-1)/2}$	$\mu_{el} = \mu_{max}(1 - e^{[-(\lambda_2\tau_r\gamma)^{(n_2-1)}]}$	This particular model was able to predict a maximum value for μ_{el} ($\mu_{el} = \mu_{max}$)	(Delshad et al., 2008)
$\mu_{app} = \mu_{sh} + \mu_{el}$	$\frac{\mu_{sh} - \mu_\infty}{(\mu_0 - \mu_\infty)} = (1 + [\lambda_1\gamma]^2)^{(n_1-1)/2}$	$\mu_{el} = (\lambda_2\gamma)^m$	m is the elongation exponent, $1/\lambda_2$ marks the onset of shear-thickening	(Stavland et al., 2010)

In their analogy, the manual tuning of each parameter for accurate flow description can be challenging and time-consuming for simulation purposes. However, the existence of a large number of parameters tends to quantify better the uncertainties surrounding polymer flow in porous media. For associating polymers, the contributions of the hydrophobic interactions to the apparent polymer rheology must be described with sufficient parameters in the model. In addition, variation in oil field parameters (porosity, permeability, temperature, salinity and ion concentration) alter polymer rheology and need to be captured in analytical models. For example, temperature conditions within a reservoir are usually much higher than the injected polymer solution; likewise, the ion concentration of the injected solution is much lower than what is obtainable in the reservoir. These variations, as earlier mentioned, would alter the solution properties (especially the CAC) of hydrophobically associating polymers and must be captured in the models. Furthermore, the elastic contributions of hydrophobically associating polymers to flow resistance are

more significant than hydrolysed polyacrylamide. Therefore, it becomes imperative to have a suitable model for predicting the onset of mechanical degradation since polymer mechanical degradation occurs after shear thickening; however, the time scale for the start of mechanical degradation depends on the elastic contribution of the polymer. Apparently, polymer mechanical degradation is significant in relation to injection facilities where polymer solutions are exposed to high flow rates and possibly to turbulent conditions. Moreover, the extent of degradation is a function of the polymer architecture and reservoir properties around the well region. In minimising the number of parameters associated with a model, Lohne et al. (2017) suggested that the time constants defining the transition between flow regimes be expressed as a function of polymer and reservoir properties. As such, the time constants of an appropriate model should capture the effect of the concentration regime of associating polymers (dilute and semi-dilute) and the impact of varying molecular weight (hydrophobic character) in addition to the rock properties. The advantage of this approach is that the number of parameters associated with a rheological model would be significantly reduced while allowing for a more straightforward regression of experimental results.

2.10.3. Predicting Critical Aggregation Concentration of Associating Polymers

The Huggins equation is employed to dilute polymer concentrations in the estimation of the intrinsic viscosity $[\mu]$, which is related to the polymer concentration C_p in Equation (2.8)

$$\mu_0 = \mu_s + \mu_s\left(k_0[\mu]C_p + k_1[\mu]^2{C_p}^2\right) \quad (2.8)$$

Where k_0 is equal to one, μ_s is the solvent viscosity and k_1 is the Huggins constant. Estimating a value for the CAC of associating polymers involves fitting the Huggins equation to rheological data for dilute polymer concentration. However, a predictive approach for estimating the CAC of associating polymers remains absent. The terms $k_0[\mu]C_p$ and $k_1[\mu]^2{C_p}^2$ characterises the dispersity of polymer chains with varying length in solution. Predicting the onset of associative interaction between polymer chains can be considered the concentration at which a single polymer chain interacts with another. This can be predicted by equating the terms $k_0[\mu]C_p$ and $k_1[\mu]^2{C_p}^2$ respectively as shown below in (2.9)

$$k_0[\mu]C_p = k_1[\mu]^2{C_p}^2 \quad (2.9)$$

The critical aggregation concentration, C_{ag} can be simplified from (2.9) as shown in (2.10) and (2.11) respectively

$$C_{ag} = \frac{k_0}{k_1[\mu]} \quad (2.10)$$

$$C_{ag} = \frac{1}{k_1[\mu]} \quad (2.11)$$

The critical aggregation concentration can be said to be inversely proportional to the intrinsic viscosity of the polymer. The impact of oil field parameters (such as temperature, salinity, pH and ion concentration) on the CAC of hydrophobically associating polymers has been comprehensively reported (Wyatt et al., 2011; Chen et al., 2012; Zhong et al., 2014; Kamal et al., 2015; Gou et al., 2015; Quan et al., 2016). However, the susceptibility of CAC to changing oil field parameters would have implications on the polymer injectivity and overall economics of the EOR operations. Also, the extent to which the CAC of associating polymers become vulnerable to oil field parameters is a function of the type and quantity of hydrophobic comonomer employed in the polymer synthesis. More importantly, there exists no independent model which correlates the CAC to the various oil field parameters. Using existing viscosity models (such as Power Law, Carreau, Ellis and Cross) would only relate the model parameters to the CAC or oil field parameters. Therefore, using a specific generic rheological model in its present form would allow for a parameterisation of the effect of oilfield parameters on the CAC of associating polymers. However, the aim would be to directly relate the CAC to the influence of the oil field parameters. Therefore, further research is necessary to accurately correlate the CAC of associating polymers to oil field parameters. To achieve this, a prediction methodology can be developed using multivariate regression analysis as shown in equation (2.12). A vital advantage of this approach is that the CAC is directly related to the oilfield parameters. The model constants arising from it are a function of the type and quantity of polymer used. The significance of this outcome is that the impact of oilfield parameters on the CAC can be directly inferred.

$$y(x_1, x_2, \dots x_n) = f(x_1, x_2, \dots x_n) \quad (2.12)$$

Where y is the CAC of the polymer, $x_1, x_2, \dots x_n$ represents the various field parameters associated with an oil reservoir. For example, considering the field parameters Temperature, T, and Salinity and Hardness, C_s, the CAC values can be made relative to a particular CAC measured for aqueous polymer solution at a given temperature, T_o, in Equation (2.13):

$$CAC_{T,C_s} = k_m CAC_{T_o} \quad (2.13)$$

Where CAC_{T,C_s} is the CAC at varied temperature, T and salinity conditions, C_s. k_m is the model coefficient which can be described as the ratio of CAC_{T,C_s} to CAC_{T_o}. Based on the obtained experimental data, the dependency of the dimensionless coefficient, k_m, on

temperature and salinity can be estimated. Therefore, equation (2.13) can be expressed as (2.14):

$$CAC_{T,C_s} = k_m CAC_{T_o} = f(\Delta T, \Delta C_s) CAC_{T_o} \quad (2.14)$$

Where $k_m = f(\Delta T, \Delta C_s)$, ΔT is the temperature difference and ΔC_s is the difference in the salinity concentration. Equation (2.14) represents a simple function for calculating the CAC at any temperature and salinity conditions. A proper form of $f(\Delta T, \Delta C_s)$ is vital for the prediction of CAC of associating polymers under varied temperature and salinity conditions. Therefore, the temperature and salinity influence on CAC would have to be analysed separately based on the experimental results, and a concrete form for $f(\Delta T, \Delta C_s)$ can be established. The model parameters that would arise from accurately determining the form for $f(\Delta T, \Delta C_s)$ would be dependent on the type of associating polymer and its response to temperature and salinity conditions.

2.10.4. Predicting the Onset of Shear Thickening using Rheological Models

Predicting the onset of various flow regimes associated with polymer flow in porous media is vital for designing chemical flooding operations. This is particularly significant for hydrophobically associating polymers where there are constrictions on polymer concentration and injectivity. Besides this, the literature has established that the onset of shear thickening marks the onset of associative hydrophobic interactions. The various flow regimes can be summarised by Equations (2.15) – (2.17) below:

$$\lim_{\gamma \approx 0} \mu_{app} = \mu_0 \quad (2.15)$$

$$\lim_{\gamma \approx \gamma_c} \mu_{app} = \mu_{min} \quad (2.16)$$

$$\lim_{\gamma \approx \infty} \mu_{app} = \mu_{max} \quad (2.17)$$

Equation (2.15) simply refers to the Newtonian flow regime and the onset of shear thinning. In Equation (2.16), this marks the onset of shear thickening (where μ_{min} is the minimum viscosity) is provided, whilst Equation (2.17) refers to the maximum value for viscosity (μ_{max}) after which shear degradation sets in. Therefore, an apparent viscosity model describing the full spectrum of polymer flow in porous media should capture the highlighted regimes from equations (2.15) – (2.17). Studies on polymer flow in porous media have considered the onset of shear thickening and shear degradation as important to polymer flooding. For this review, a predictive approach to the onset of shear thickening is considered. Most predictive models employed in the study of polymer flow have considered using the Deborah Number (N_D) in predicting the onset of shear thickening. The Deborah

Number is defined as the ratio of the polymer relaxation time (τ_p) to the characteristic time of flow (τ_{ct}) as shown in Equation (2.18)

$$N_D = \frac{\tau_p}{\tau_{ct}} \quad (2.18)$$

Associating polymers with varying amounts of hydrophobic monomer will have a wide range of molecular weight leading to various relaxation times. In estimating the onset of shear thickening, some researchers have recommended using the longest relaxation time in estimating N_D (Skauge et al., 2018). However, the use of the longest relaxation time may lead to an overestimation of N_D at the onset of shear thickening. In addition to this, a wide range of N_D has been reported at the onset of shear thickening behaviour. The work of Heemskerk et al. (1984) captured this and reported that the use of different polymers in the same porous media yielded the same N_D and the reverse was the case when the same polymer was employed in different rocks leading to N_D values between 1 and 2. It was concluded that the concept of the N_D can only be used to estimate the critical flow rate because of the inadequacy of calculating the stretching rate. Similarly, Zamani et al. (2015) reported that estimation of the stretch rate is crucial towards calculating the N_D at the onset of shear thickening. The authors proposed a linear function to relate the stretch rate to the Darcy velocity, thereby obtaining the distribution of the stretch rate in the porous media. In summary, relaxation time alone in calculating the onset of shear thickening is not sufficient if the stretch rate cannot be estimated. Accordingly, Lohne et al. (2017) reported that the use of N_D in describing the onset of shear-thickening is limited as it only captures the insufficient relaxation time required to recover from its deformation arising from the previous pore throat entry. The reason for the adoption of N_D for predicting shear-thickening is that the events of insufficient relaxation time for recovery and the characteristic time for flow in a pore entrance are assumed to be close (Lohne et al., 2017). In other words,

$$N_D = \frac{\tau_p}{\tau_{ct}} \approx 1 \quad (2.19)$$

The model described by Delshad et al. (2008) is widely seen as a "unified model" applied to the full spectrum of the flow of polymers in porous media. However, the model's constitutive equations (shear and elongational viscosity models) were independently constructed for shear thinning and shear thickening. As a result, while the full spectrum of the polymer behaviour may be captured, its predictive capability for the various flow regimes depicted by equations (2.15) to (2.17) may not be entirely captured. Table 2.7

shows the predictability of models developed by authors from Table 2.6 based on equations (2.15) to (2.17).

Table 2.7*: Predictive capability of various proposed models for in-situ rheology of polymers in porous media*

Model Form	$\lim_{\gamma \approx 0} \mu_{app}$	$\lim_{\gamma \approx \gamma_c} \mu_{app}$	$\lim_{\gamma \approx \infty} \mu_{app}$
$*\ \boldsymbol{\mu_{app} = \left[\mu_\infty + (\mu_0 - \mu_\infty)(1 + [\lambda_1 \gamma]^2)^{(n_1-1)/2}\right]\left[\frac{1}{1-\tau_p \gamma}\right]}$ (Hirasaki and Pope, 1974)	μ_0	-	∞
$*\ \boldsymbol{\mu_{app} = \left[\mu_\infty + (\mu_0 - \mu_\infty)(1 + [\lambda_1 \gamma]^2)^{(n_1-1)/2}\right]\left[C(\tau_p \gamma)^{m_c}\right]}$ (Masuda et al., 1992)	0	-	∞
$**\boldsymbol{\mu_{app} = \left[\mu_\infty + (\mu_0 - \mu_\infty)(1 + [\lambda_1 \gamma]^2)^{(n_1-1)/2}\right] + \left[\mu_{max}(1 - e^{\left[-\langle \lambda_2 \tau_p \gamma \rangle^{(n_2-1)}\right]}\right]}$ (Delshad et al., 2008)	μ_0	-	μ_{max}
$**\boldsymbol{\mu_{app} = \left[\mu_\infty + (\mu_0 - \mu_\infty)(1 + [\lambda_1 \gamma]^2)^{(n_1-1)/2}\right] + [(\lambda_2 \gamma)^m]}$ (Stavland et al., 2010)	μ_0	-	∞

**Carreau model for shear thinning added to the elongational (or extensional) models by Hirasaki and Pope (1974) and Masuda et al. (1992). The Deborah number, $N_D = \tau_p \gamma$ for the extensional models*

***Models by Delshad et al. (2008) and Stavland et al. (2010). For Stavland et al. (2010),* $\gamma_c = {}^1/_{\lambda_2}$

The predictability of the proposed models by the various authors does not capture the three conditions completely. The proposed model by Hirasaki & Pope (1974) predicts at $\gamma \approx \infty$, an infinite value for the viscosity. In other words, the model cannot capture the onset of shear degradation. The same applies to the model proposed by Masuda et al. (1992) except at $\gamma \approx 0$. The model by Delshad et al. (2008) predicts μ_0 and μ_{max} for at $\gamma \approx 0$ and $\gamma \approx \infty$ respectively. This implies that it can describe the shear-thinning region and predicts the onset of shear degradation. The model by Stavland et al. (2010) predicts a value of μ_0 and ∞ at $\gamma \approx 0$ and $\gamma \approx \infty$ respectively. However, a critical issue that seems not captured is the

prediction of the onset of shear thickening. A model for in-situ rheology should capture the prediction of the start of shear thickening according to Equation (2.16) when

$$\mu_{sh} = \mu_{el} \tag{2.20}$$

The model proposed by Stavland et al. (2010) estimates the critical shear rate for the onset of shear thickening as

$$\gamma_c = \frac{1}{\lambda_2} = N_D \left(\frac{1-\emptyset}{\emptyset}\right)\left(\frac{6\propto\sqrt{\tau}}{\lambda_1}\right) \tag{2.21}$$

Where γ_c is related to rock properties such as porosity, $\emptyset$, $\propto$ is a tuning parameter and tortuosity, τ. λ_1 and λ_2 are parameter constants. A similar expression was proposed by Lohne et al. (2017) for estimating the critical shear rate, as shown in Equation (2.22)

$$\lambda_2 = \frac{1}{\gamma_c} = \frac{1}{N_D^c}\left(\frac{3}{5R_g}\right)\left(\frac{\emptyset}{1-\phi}\right)\left(\frac{\eta_s[\eta]M_w}{T}\right) \tag{2.22}$$

However, there may not be a synergistic relationship between what can be obtained by Equation (2.20) and that estimated by equations (2.21) and (2.22). Nonetheless, equations (2.21) and (2.22) depend on the Deborah number's proper estimation related to the stretch rate, as earlier mentioned. In addition, equating the elastic components and the shear components to obtain an expression for the critical shear rate may not yield an explicit expression. From the model of Delshad et al. (2008), this can only reduce to Equation (2.23)

$$\left[-\langle\lambda_2\tau_p\gamma\rangle^{(n_2-1)}\right] = \ln\left[1 - \frac{\mu_\infty+(\mu_0-\mu_\infty)\left(1+[\lambda_1\gamma]^2\right)^{(n_1-1)/2}}{\mu_{max}}\right] \tag{2.23}$$

An explicit expression for the critical shear rate cannot be obtained and can only be achieved through a numerical solution and may not necessarily tally with values obtained from equations (2.21) or (2.22). Apart from relating the parameter constants of the model to the rock and polymer properties, there is a need for the model to satisfy Equation (2.20) to describe the full spectrum of polymer flow in porous media and predict the minimum viscosity before shear-thickening sets in. Furthermore, the rheological models depicted in Table 2.7 do not have a parameter associated with the stretch rate of the polymer during in-situ flow in porous media. There is a need to simplify rheological models to account for the effect of polymer stretching on hydrophobic interactions.

2.10.5. Degradation of Associating Polymers in Porous Media

The degradation of polymers has been reported under thermal, chemical, and mechanical conditions (Brakstad and Rosenkilde, 2016; Lohne et al., 2017; Ferreira and Moreno, 2017). These conditions can take place in the form of high temperature (thermal conditions), high salinity and oxidative conditions (chemical conditions), fluid stresses in pumps, valves,

injection wellbore, sand face (mechanical conditions) or any combination of the above (Brakstad and Rosenkilde, 2016). A parameter that is used in describing the degradation of polymer molecules is their molecular weight. Specifically, polymer chains rarely have the same degree of polymerization and hence molecular weight. Therefore, there would always be a molecular weight distribution around an average value due to some polymer chains being longer than the others. The molecular weight distribution describes the relationship between the number of moles of each polymer species and the molecular weight of that species using a discretized log-normal distribution (Brakstad and Rosenkilde, 2016). Hence, the degradation of polymers can be described as the scission of long-chain polymers when exposed to the degradation conditions mentioned earlier (Vanapalli et al., 2006; Zaitoun et al., 2012). According to Lohne et al. (2017), a simple model based on Figure 2.14 for the degradation study of polymers can be described using Equation (2.24)

$$\frac{\mathrm{dM_w}}{\mathrm{dt}} = -f_{rup}\mathrm{M_w} \qquad (2.24)$$

Where $\mathrm{M_w}$ is the polymer molecular weight and f_{rup} is the polymer rupturing or degradation rate. Determination of the molecular weight of polymers requires using the Huggins equation in (2.8) to estimate the intrinsic viscosity [μ], and this is related to the molecular weight using the Mark-Houwink Equation. However, Equation (2.8) is truncated after the second term depending on the value of the coil overlap parameter ($[\mu]\mathrm{C_p}$). The coil overlap concentration refers to the polymer concentration where polymer coils begin to touch each other.

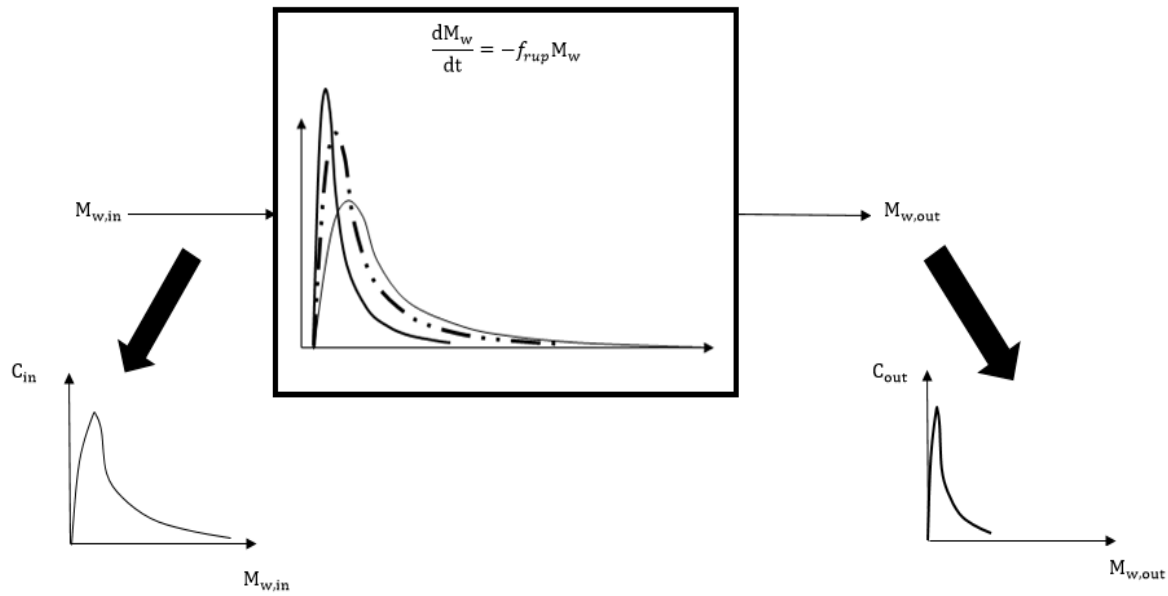

***Figure 2.14**: Flow of a polymer with its Molecular Weight Distribution (MWD) at the inflow, in a porous media and outflow. The thick square box represents the porous media with the changing MWD of the polymer subject to changing flow conditions.*

According to Brakstad and Rosenkilde (2016), when the value of $[\mu]C_p$ is less than 5, Equation (2.8) remains the expression for the Huggins equation. However, for associating polymers, modification of Equation (2.8) is necessary to account for semi-dilute or concentrated conditions. Consequently, Brakstad and Rosenkilde (2016) indicated that higher-order terms could be added to Equation (2.8) when $4 < [\mu]C_p < 15$ as shown in (2.25)

$$\mu_0 = \mu_s + \mu_s\left(k_0[\mu]C_p + k_1[\mu]^2{C_p}^2 + \mathbf{k_2}[\boldsymbol{\mu}]^{\mathbf{3}}\mathbf{C_p}^{\mathbf{3.8}} + \cdots\right) \quad (2.25)$$

The implication of this is that polymer intermolecular interaction on viscosity is considered with the higher-order terms. For $[\mu]C_p > 15$, the Martin equation is used as shown in (2.26) to describe a semi-dilute or concentrated regime. Here, the exponential term is used to capture the contribution of intermolecular association.

$$\mu_0 = \mu_s + \mu_s\left(k_0[\mu]C_p\right)\left(\mathbf{e}^{[\mathbf{bk_1}[\boldsymbol{\mu}]C_p]}\right) \quad (2.26)$$

As shown in Figure 2.14, the MWD of polymers differs under static and dynamic conditions. Therefore, Equation (2.8) discretisation would allow for computation of changing coil overlap parameter of the polymer molecules during flow. Equation (2.27) shows a discretised form of Equation (2.25).

$$\mu_0 = \mu_s + \mu_s(k_0\sum_{i=0}^{n}\langle[\mu]_i c_i\rangle + k_1\sum_{i=0}^{n}\langle[\mu]_i c_i\rangle^2 + \mathbf{k_2}\sum_{\mathbf{i=0}}^{\mathbf{n}}\langle[\boldsymbol{\mu}]_\mathbf{i}\mathbf{c_i}\rangle^{\mathbf{3.8}} + \cdots) \quad (2.27)$$

Overall, this higher-order form of the coil overlap parameter, $\langle[\boldsymbol{\mu}]_\mathbf{i}\mathbf{c_i}\rangle^{\mathbf{n}}$, can be used to indicate the degree of hydrophobic interaction between associating polymers and incorporated into the molecular weight distribution profile. This suggests that the intermolecular association has a multiplicative effect on polymer rheology. In addition, there is a need to integrate this degradation procedure in a suitable rheological model as the degree of hydrophobic interaction under static and dynamic conditions can be adequately studied. As mentioned earlier, an essential aspect of associative polymer research is how these hydrophobic interactions are sustained and propagated under dynamic conditions. Hence, a numerical approach remains a practical method in studying the dynamic nature of hydrophobic interactions during the flow of associating polymers in porous media. However, there is still a need for a qualitative approach for real-time study of this phenomenon in porous media. An existing approach that could be adapted for this is to measure the rheological properties of produced polymers and compare them with properties before injection. Nevertheless, this may not represent the real-time trend of hydrophobic interactions during flow in porous media. Therefore, a numerical approach remains a viable option and should follow the schematic modified from Brakstad and Rosenkilde (2016) in Figure 2.15.

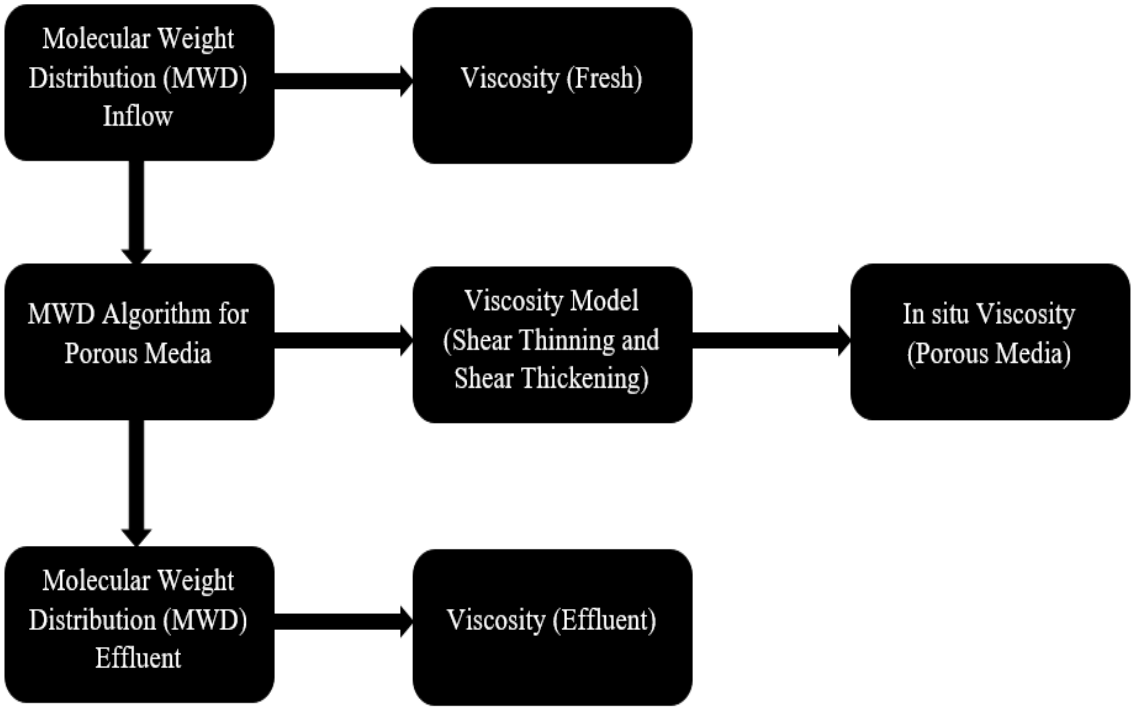

Figure 2.15*: A flow chart showing a proposed numerical approach to study of hydrophobic interaction between associating polymers during flow in a porous media.*

2.11. Porous Media Properties and its Impact on Polymer Flow

The nature of the porous media has an important influence on the flow of polymer solutions (Lai et al., 2013; Lohne et al., 2017; Skauge et al., 2018). The variation in the cross-sectional area of flow paths in the porous media ensures that polymer molecules undergo simultaneous acceleration and deceleration, leading to extensional or elongational flow (Seright et al., 2011; Lohne et al., 2017; Skauge et al., 2018; Al-Shakry et al., 2019). Consequently, a porous media can be considered a composition of simplified contraction-expansion channels of varied dimensions (Skauge et al., 2018; Afolabi et al., 2019). This explains the acceleration and deceleration of polymer molecules mentioned earlier. Furthermore, polymer molecules are compressed and stretched in the contraction channel with sufficient time to return to their original state if the flow velocity is below a critical value (Skauge et al., 2018; Afolabi et al., 2019). According to Skauge et al. (2018), polymer flow between contractions with enough time to return to its original state would mean that no stress is stored and no additional resistance to flow is observed. However, where polymer molecules cannot return to their original state, stress would be held, resulting in an increment in associated pressure drop and resistance to flow (Dupas et al., 2013; Azad & Trivedi, 2017; Skauge et al., 2018). This phenomenon explains how porous media properties contribute to polymer solutions' extensional and elongational flow. The

additional effect of the inherent nature of porous media is that polymer molecules are sheared near the wall of the pores and elongated or extended at the centre of the pores (Silva et al., 2018; Skauge et al., 2018. Consequently, molecular momentum is transferred through tangential and normal stress components in the porous media (Skauge et al., 2018).

2.12. Summary

The last two decades of research on hydrophobically associating polymers have witnessed polymers' development tolerant to a wide range of conditions reminiscent of an oil reservoir. The conditions of the reservoir would adequately define the required properties of these associating polymers. This, in turn, would determine the synthesis method/procedure, molecular structure and type of hydrophobic comonomer to be employed. In this regard, the rheological behaviour of hydrophobically associating polymers cannot be entirely linked to the molecular structure in an aqueous solution alone. Instead, the behaviour is a combination of the influence of oilfield parameters (such as temperature, salinity, ion concentration, pH and reservoir heterogeneity) and the polymer's molecular structure (arising from the synthesis method/procedure and the hydrophobic comonomer used). Therefore, finding an optimal scenario between the oilfield parameters and the molecular architecture of the polymer could define an appropriate use for associating polymers. This is imperative because a predominantly weak associative effect would not necessarily guarantee the needed rheological impact on recovery efficiency even if polymer injectivity is not affected. Also, an excessively strong associative effect may affect polymer injectivity and propagation even if the needed polymer mobility and oil recovery are obtained. Consequently, the following recommendations have been made based on the issues identified in this review:

a) The sensitivity of the critical aggregation concentration of associating polymers to oilfield conditions such as temperature, salinity/hardness, and pH. The impact of this on the performance of the polymers would be a key area of investigation.
b) Sustaining and maintaining the associative effect of these polymers (long-term stability) during propagation in porous media while considering the sensitivity of the critical aggregation concentration as highlighted in (a).
c) The associative effect on polymer injectivity as measured by polymer concentration above the critical aggregation concentration. An understanding of its effect on the onset

of shear thickening in porous media is essential. It has the potential to be a key focus of research activities in this field.

d) The possibility of a change in the critical aggregation concentration of the produced associating polymer and what this change means on the solution properties of the polymer.
e) Investigation of the effect of injection rate on the compatibility of the size of associating polymer cluster and reservoir pore-throat. Previous studies have focused on using a single injection rate to optimise solution properties of associating polymers and reservoir heterogeneity.
f) Investigation of the use of brackish water in the preparation of associating polymer solution. This study can help in investigating the influence of wastewater mineralisation and hardness on the properties of hydrophobically associating polymers.
g) Investigation of the origin of the *"minor polymeric species"* connected to hydrophobically associating polymers. These species are often tagged as *"pre-gel aggregates"; however*, understanding how to properly design the synthesis and treatment process of these hydrophobically associating polymers would reduce the likely occurrence of permeability impairment.
h) Develop a mathematical correlation of critical aggregation concentration to oil field parameters (such as temperature, salinity/hardness, and pH) and evaluate its suitability for predictive modelling.
i) Develop a qualitative approach to study the hydrophobic interactions between associative polymers under real-time flow conditions in porous media. The results of this approach should be compared to the quantitative approach described in this article.
j) Examine the impact of hydrophobic interactions on polymer injectivity as measured by polymer concentrations above the critical aggregation concentration. An understanding of its effect on the onset of shear thickening in porous media is essential. It has the potential to be a key focus of research activities in this field.
k) Investigate the possibility of a change in the critical aggregation concentration of the produced associating polymer and what this change means on the solution properties of the polymer. While previous works have indicated no noticeable change in CAC, the work was limited to a particular associating polymer.

CHAPTER THREE

3.0. Parameter Identification and Predictive Modelling

This Chapter focussed on the identification of a novel parameter for describing the proportion of hydrophobic interactions and the development of models which describes hydrophobic interactions during polymer retention and under different flow regimes.

3.1. Numerical Quantification of the Proportion of Molecular Interactions

This section focused on the basis and assumptions for identifying a parameter for quantifying hydrophobic interactions between associative polymers. The relevance, uniqueness and novelty of this parameter is a subject of validation in the subsequent Chapter on experimental results and discussion.

3.1.1. Polymer Concentration Regimes

Identifying a parameter that uniquely describes the hydrophobic interactions between associative polymers is crucial in understanding the sustainability and control of hydrophobic interactions when propagated deep into a reservoir. Achieving this requires an understanding of the various concentration regimes associated with polymers and the threshold of each regime. There are three known concentration regimes associated with polymers: dilute, semi-dilute, and concentrated (Afolabi et al., 2019). Although, some authors often categorize the semi-dilute and concentrated regime as similar, in this work, it was defined as a distinct concentration regime from the semi-dilute regime. The CAC remains the only intrinsic property by which hydrophobic interactions is distinguished from intramolecular interactions (Taylor and Nasr El-Din, 1998; Yabin et al., 2001; Feng et al., 2005; Lu et al., 2010; Afolabi, 2015). At polymer concentration above the CAC, the associative characteristics of the polymer come into effect. Likewise, at polymer concentration below the CAC, intramolecular association within polymer chains become dominant. It has been established from previous studies that the CAC of associative polymers responds to changes in temperature, salinity, and hardness. Consequently, the difference in the CAC of associative polymers can be applied towards the measure of changing hydrophobic interactions between polymer chains. Fundamentally, the variation in the CAC indicates a transition of polymer molecules to/from either concentration regimes. Computational modelling of these variations in hydrophobic interactions with time will be less challenging when such a parameter as CAC is applied. However, there exists

no known correlation between the CAC of associative polymers and parameters describing reservoir conditions. In defining a dimensionless parameter that quantifies the hydrophobic interactions between associative polymers, the following assumptions were made:

a) The proportion of intramolecular interactions in the dilute regime increases with polymer concentration, C_p and reaches a maximum at the critical aggregation concentration, C_{ag}.
b) The summation of the proportion of molecular interactions (hydrophobic and intramolecular) arising from polymer chain interaction that constitutes the semi-dilute concentration regime is assumed to be unity.
c) Intramolecular interaction occurs both in the dilute regime (C_p less than the critical aggregation concentration, C_{ag}) and the semi-dilute regime ($\mathrm{C_p}$ greater than the critical aggregation concentration, C_{ag}).
d) The hydrophobic interaction network between associative polymer chains occurs in semi-dilute and concentrated regimes, i.e., polymer concentration, C_p must be higher than the critical aggregation concentration, C_{ag}.
e) The value of the critical aggregation concentration, C_{ag}, is susceptible to local variation in reservoir conditions such as the concentration of salts, applied flow/shear rate, and temperature present in a reservoir.
f) The increase in the polymer concentration, C_p above the C_{ag} would lead to a rise in the proportion of hydrophobic interactions; however, the critical aggregation concentration, C_{ag} remain unaffected.
g) The onset of the concentrated regime is assumed to occur at the point where hydrophobic interactions start to dominate over the intramolecular interactions, i.e. this occurs at the point where hydrophobic and intramolecular interactions are equal.

Figure 3.1 shows the mapping of the various concentration regimes based on the stated assumptions.

3.1.1.1. Hydrophobic Interactions in the Semi-Dilute/Concentrated Regime

Based on the assumptions highlighted above, the dimensionless parameter H_i was used to quantify the hydrophobic interactions between associative polymer chains at a given condition as shown in equation (3.1).

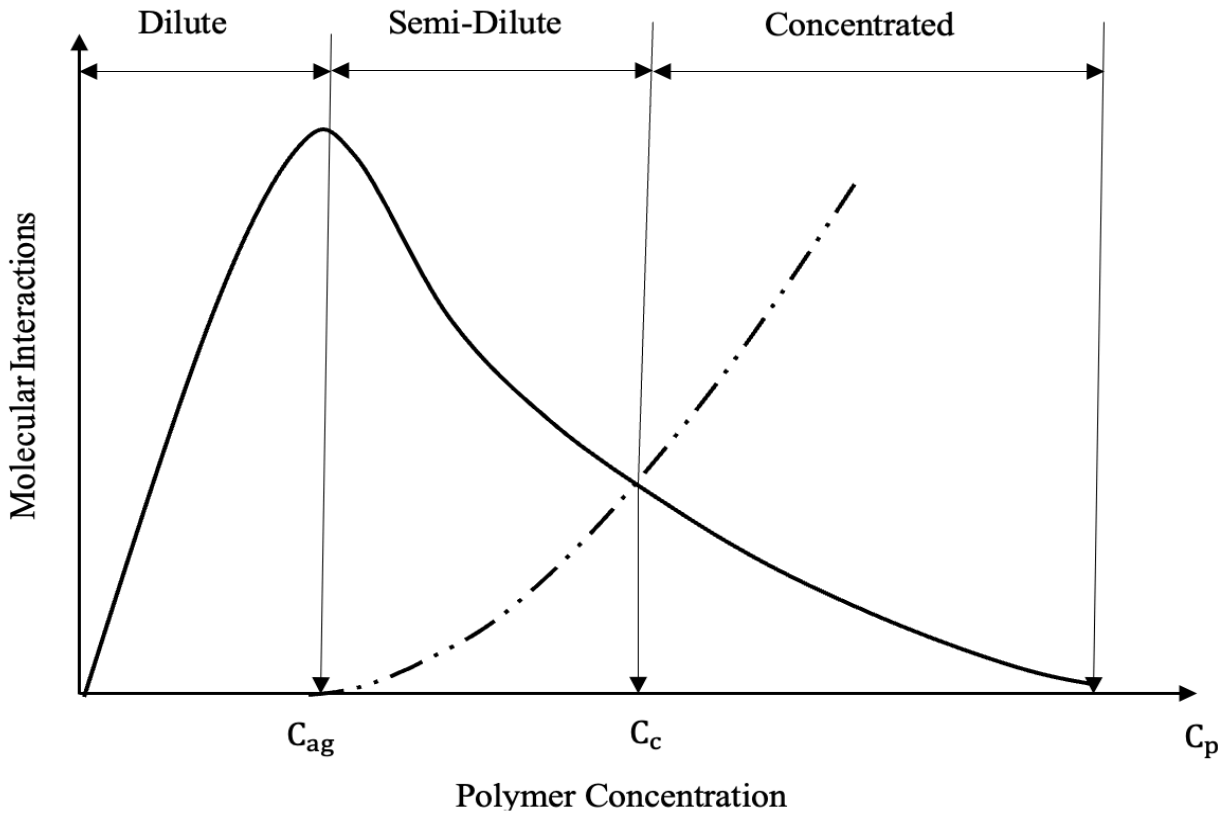

Figure 3.1*: Graphical description of the various polymer concentration regimes developed based on the assumptions.*

$$H_i = \frac{C_p - C_{ag}}{C_p} \begin{cases} C_p > C_{ag} \\ C_{ag} \neq 0 \end{cases} \quad (3.1)$$

Equation (3.1) applies to the semi-dilute and concentrated regimes ($C_p > C_{ag}$) where hydrophobic interactions are dominant. Equation (3.1) can be rewritten as follows in (3.2)

$$H_i = 1 - \left(\frac{C_{ag}}{C_p}\right) \quad (3.2)$$

Equation (3.2) represents a unique parameter for quantifying hydrophobic interactions in the semi-dilute regime. The identification of this parameter simply achieves the first objective of this research work. However, since the parameter was determined using suitable assumptions, validation of the outcomes using this parameter were discussed in Chapter 5.

3.1.1.2. Intramolecular Interaction: Dilute/Semi-Dilute/Concentrated Regime

A term can be defined to quantify the proportion of intramolecular interactions arising from polymer chains in the dilute regime. Thus, the numerical value of I_i can be estimated from equation (3.3):

$$\mathrm{I_i} = \left[\frac{\mathrm{C_{ag}}}{\mathrm{C_p}}\right]\begin{cases}\mathrm{C_p} > \mathrm{C_{ag}} \\ \mathrm{C_{ag}} \neq 0\end{cases} \tag{3.3}$$

Equation (3.3) applies in the semi-dilute regime where the polymer concentration, C_p is greater than the critical aggregation concentration, C_{ag}. However, when polymer concentration, C_p is less than the critical aggregation concentration, C_{ag}, equation (3.4) applies

$$\mathrm{I_i} = \left[\frac{\mathrm{C_p}}{\mathrm{C_{ag}}}\right]\begin{cases}\mathrm{C_p} < \mathrm{C_{ag}} \\ \mathrm{C_{ag}} \neq 0\end{cases} \tag{3.4}$$

Equation (3.4) applies strictly in describing intramolecular interactions in the dilute concentration regime.

3.1.1.3. Predicting the Onset of the Concentrated Regime

Based on the assumption made in (g) above, the balance in the proportion of molecular interactions in the semi–dilute regime is considered as the point where equations (3.2) and (3.3) are equal, as shown in (3.5)

$$\left[\frac{\mathrm{C_{ag}}}{\mathrm{C_c}}\right]\begin{cases}\mathrm{C_p} > \mathrm{C_{ag}} \\ \mathrm{C_{ag}} \neq 0\end{cases} = 1 - \left(\frac{\mathrm{C_{ag}}}{\mathrm{C_c}}\right)\begin{cases}\mathrm{C_p} > \mathrm{C_{ag}} \\ \mathrm{C_{ag}} \neq 0\end{cases} \tag{3.5}$$

This point of balance was employed in the determination of a critical concentrated concentration, C_c. The C_c marks the onset of the polymer concentrated regime and distinguishes it from the semi-dilute regime. Simplifying equation (3.5) for C_c yields (3.6)

$$\mathrm{C_c} = 2\mathrm{C_{ag}} \tag{3.6}$$

Equation (3.6) indicates the onset of the concentrated regime occurs at the polymer concentration value equivalent to twice the critical aggregation concentration, and this should happen when the proportion of hydrophobic and intramolecular interactions are 0.5 respectively. In addition, it is expected that the conditions that affect C_{ag} as described in Chapter 2 would also affect the C_c.

3.1.2. Description of Polymer Distributed Phases in Porous Media

Predicting hydrophobic interactions in a porous media requires relating it to the defined parameter in (3.1), a measurable entity in terms of polymer concentration. From Figure 3.2, this can be related to another defined another dimensionless parameter which is a measurable entity in terms of polymer viscosity, as shown in equation (3.7)

$$\frac{\mu_{ap}-\mu_{ag}}{\mu_0-\mu_s} = \omega_a\left(\frac{C_p-C_{ag}}{C_p}\right) \tag{3.7}$$

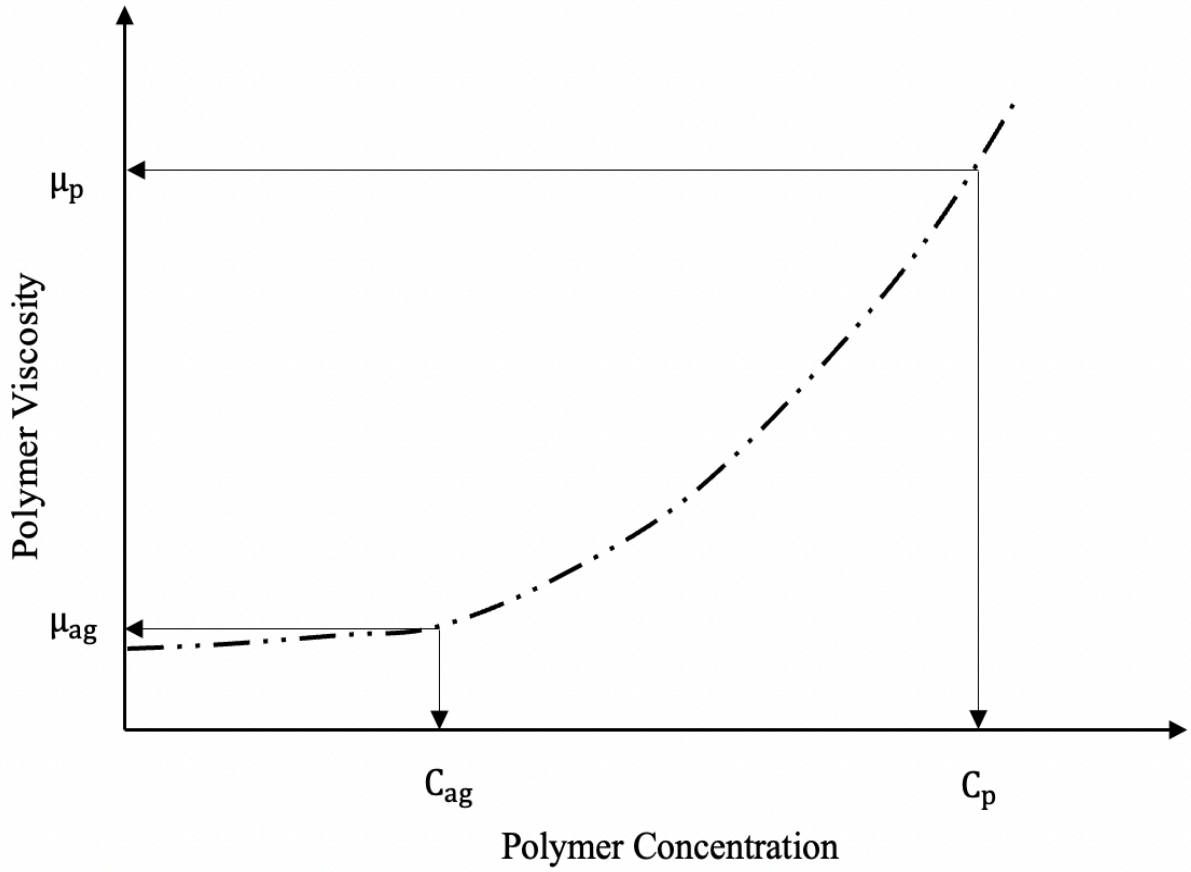

Figure 3.2*: Typical rheological profile for hydrophobically associating polymers*

Where μ_0 is the polymer viscosity at zero shear rate, μ_{ap} is the apparent viscosity of the polymer under flow, μ_{ag} is the viscosity at the critical aggregation concentration and ω_a is a correction factor used to correlate the hydrophobic interactions in terms of polymer concentration, H_{C_p} to hydrophobic interactions in terms of polymer viscosity, H_μ as shown in equation (3.8).

$$H_\mu = \omega_a\left(H_{C_p}\right) \tag{3.8}$$

In terms of bulk viscosity measurements, the correction factor should be unity indicating that $H_\mu = H_{C_p}$. Equation (3.8) was applied in the experimental validation of the predictive mapping of polymer concentration regimes as shown in Chapter Six. However, describing flow in porous media would mean that the correction factor would vary according to the distributed polymer phases (polymer-rich and depleted phases). This would indicate which in-situ phenomena affect the network of hydrophobic interactions in the injected polymer solution. For the polymer-rich phase, ΔH_μ was used to describe the differential change in the proportion of hydrophobic interactions under different flow regimes, as shown in equation (3.9).

$$\Delta H_\mu = \Delta\left(\frac{\mu_{ap}-\mu_{ag}}{\mu_0-\mu_s}\right) \tag{3.9}$$

In the case of the polymer depleted phase, ΔH_{C_p} was applied to describe the differential change in the proportion of hydrophobic interactions lost to different polymer retention mechanisms according to equation (3.10).

$$\Delta H_{C_p} = \Delta\left(\frac{C_p-C_{ag}}{C_p}\right) \tag{3.10}$$

However, ω_a would vary, indicating how hydrophobic interactions changes between the polymer-rich phase and the depleted phase, as shown in Table 3.1.

Table 3.1*: Interpretation of the correction factor in equation (3.8) and its implication for polymer retention and viscous thickening in porous media.*

Correction Factor, ω_a	**Dimensionless Parameters**	**Meaning**
$\omega_a < 1$	$\Delta H_\mu < \Delta H_{C_p}$	Indicates that more hydrophobic interactions are lost to polymer retention than it contributes to the thickening effect
$\omega_a = 1$	$\Delta H_\mu = \Delta H_{C_p}$	Indicates the ideal pre-injection situation and the optimized condition during injection in a porous media.
$\omega_a > 1$	$\Delta H_\mu > \Delta H_{C_p}$	Indicates that more hydrophobic interactions contribute to the thickening effect than what is lost to polymer retention

3.2. Modelling of Hydrophobic Interactions in Different Flow Regimes

The apparent network of hydrophobic interactions in a polymer solution, H_{ap} in a porous media was modelled to consist of two parts as shown in equation (3.11):

$$\mathrm{H_{ap}} = \mathrm{H_{sh}} + \mathrm{H_{el}} \tag{3.11}$$

H_{sh} represents the hydrophobic interactions during shear thinning and H_{el} represents the hydrophobic interactions during shear thickening. The suitability of a model for predicting apparent network of hydrophobic interactions during flow in a porous media would require that it satisfy the following conditions:

$$\lim_{\gamma \approx 0} \mathrm{H_{ap}} = \mathrm{H_0} \tag{3.12}$$

$$\lim_{\gamma \approx \gamma_c} \mathrm{H_{ap}} = \mathrm{H_{min}} \tag{3.13}$$

$$\lim_{\gamma \approx \infty} \mathrm{H_{ap}} = \mathrm{H_{max}} \tag{3.14}$$

Equation (3.12) simply refers to the Newtonian flow regime and the onset of shear thinning. The onset of shear-thinning is characterized as the reciprocal of the polymer relaxation time. In equation (3.13), this marks the onset of shear thickening (where H_{min} is the minimum value for the hydrophobic interactions, and equation (3.14) refers to the maximum value for the hydrophobic interactions (H_{max}) after which shear degradation sets in. Therefore, an apparent model describing the full spectrum of hydrophobic interactions during polymer flow in porous media should capture the highlighted regimes from equations (3.12) – (3.14).

3.2.1. Structural Kinetics during Shear Thinning

The structural kinetic theory proposed by Toorman (1997) was applied in this section. The theory was modified to account for hydrophobic interactions and applied for the shear thickening and degradation in sections (3.2.2) and (3.2.4) respectively. The non-dimensional parameter, H_i, is related to the change in the proportion of hydrophobic interactions between polymer molecules according to H_μ. This parameter, H_i describes the structural state of the polymer molecules during shear thinning and shear thickening flow. The structural state during flow is dependent on the state of hydrophobic interactions between polymer molecules under the flow conditions. The rate of structural breakdown, which characterizes the molecular coil disentanglement, is dependent on the shear rate of deformation, γ and fraction of polymer molecules interacting at that point in time, H_i. The rate of breakdown according to Toorman (1997) is expressed as shown in (3.15)

$$\frac{\mathrm{dH_i}}{\mathrm{dt}} = -\mathrm{b}\gamma \mathrm{H_i}^{n} \tag{3.15}$$

where b is the breakdown constant, and n is the breakdown exponent. The rate of recovery that characterizes the hydrophobic interaction is related to the fraction of polymer molecules available. Hence, the rate of recovery according to Toorman (1997) is expressed as shown in (3.16)

$$\frac{dH_i}{dt} = a(H_o - H_i)^m \quad (3.16)$$

where a is the recovery parameter, and m is the recovery exponent. The net rate expression is the difference between the rate of breakdown and that of recovery (3.17).

$$\frac{dH_i}{dt} = a(H_o - H_i)^m - b\gamma H_i{}^n \quad (3.17)$$

Assuming first-order rate kinetics for the breakdown and recovery expressions, $m = n = 1$, equation (3.17) becomes (3.18)

$$\frac{dH_i}{dt} = a(H_o - H_i) - b\gamma H_{i_i} \quad (3.18)$$

At equilibrium, the rate of breakdown equals the rate of recovery. Therefore, $\frac{dH_i}{dt} = 0$ and (3.18) becomes (3.19)

$$a(H_o - H_{sh}) = b\gamma_{sh} H_{sh} \quad (3.19)$$

The equilibrium structural parameter, H_{sh} is therefore expressed as (3.20)

$$H_{sh} = \frac{H_o}{1+\beta_1 \gamma_{sh}} \quad (3.20)$$

Where γ_{sh} is the shear rate under shear thinning, $\beta_1 = \frac{b}{a}$ and it is related to the polymer relaxation time. According to Lohne et al. (2017), the polymer rotational relaxation time expression can be related to a characteristic time scale of rotational diffusion, D_{rot} as shown in (3.21)

$$\beta_1 = \frac{1}{2D_{rot}} \quad (3.21)$$

This diffussion coefficient can be computed using the Einstein–Smoluchowski relation as shown in (3.22) below

$$D_{rot} = \frac{k_B T}{8\pi\mu_s R_h^3} \quad (3.22)$$

Where k_B is the Boltzmann constant and R_h is the hydrodynamic radius of a rigid sphere of a flexible polymer in solution. Substituting (3.22) into (3.21),

$$\beta_1 = \frac{4\pi\mu_s R_h^3}{k_B T} \quad (3.23)$$

The value of R_h is estimated using the expression given by Lohne et al. (2017) in equation (3.24)

$$R_h = \left(\frac{3}{10\pi N_A}\right)^{1/3} ([\mu]M_w)^{1/3} \quad (3.24)$$

Where N_A is the Avogadro's number. Combining (3.23) and (3.24), a new expression for β_1 is obtained beow

$$\beta_1 = \left(\frac{6}{5k_B N_A}\right)\left(\frac{\mu_s[\mu]M_w}{T}\right) \quad (3.25)$$

Thus the final expression for equation (3.25) becomes (3.26)

$$\beta_1 = \beta_a\left(\frac{\mu_s[\mu]M_w}{T}\right) \quad (3.26)$$

The constant $\left(\beta_a = \frac{6}{5k_B N_A}\right)$ in equation (3.26) is applied as a prefactor with a theoretical value of 0.144 $Kmol^{-1}J^{-1}$. This parameter is used as a tuning factor to account for the uncertainties in the molecular weights and eventual effects of solvent quality on polymer dispersion.

3.2.1.1. Effects of Salinity and Temperature

The effect of solution salinity is included in the model by making the solvent viscosity in equation (3.26) salinity dependent. For this purpose, μ_s is expressed as a power law of the total ion concentration according to Lohne et al. (2017), as shown below in (3.27)

$$\mu_s = \mu_w C_s^{\alpha} \quad (3.27)$$

The parameter μ_w refers to the viscosity of deionized water, C_s is an effective salinity parameter and α is a fitting parameter. The effective salinity C_s is the weighted sum of the ionic concentrations in solution as shown in (3.28).

$$C_s = \sum_i C_i\theta_i \quad (3.28)$$

Where C_i is the molar concentration of the salts and θ_i is a parameter that depends on the oxidation state of the ions present in the solution. Combining (3.25) and (3.27) yields (3.29)

$$\beta_1 = \left(\frac{6C_s^{\alpha}}{5k_B N_A}\right)\left(\frac{\mu_w[\mu]M_w}{T}\right) \quad (3.29)$$

This shows that the prefactor, β_a can be modified to account for the effect of salinity on interaction forces between polymer chains dispersed in solution. In the current model developed for β_1, the time constant is an inverse function of temperature since it was related to diffusion.

3.2.1.2. Disentanglement of Polymer Chains in Hydrophobic Network

The disentanglement of polymer molecules in hydrophobic interactions was model according to the structural kinetic theory by considering the fraction of polymer molecules dissociated from the network of hydrophobic interactions in solution. The disentanglement

procedure is modelled according to the differential equation in (3.15) as shown in equation (3.30) below:

$$\frac{dH_i}{dt} = -b\gamma H_i{}^n \quad (3.30)$$

Applying equation (3.30) for predicting the disentanglement of polymer molecules from the interaction network was based on the following rationale used by Lohne et al. (2017):

a) Short polymer chains with a small distribution of hydrophobic blocks have a more significant probability of dissociating from the hydrophobic network. This is captured by the term $H_i{}^n$
b) The breakdown or dissociation exponent n represents the dependency of the hydrophobic interaction network on disentanglement with values between $0 < n < 1$. A value close to 1 indicates a strong dependence and vice-versa. For this work, n is taken to have a value of 1, indicating a substantial dependency.
c) The dissociation of polymer molecules from the hydrophobic network occurs above a critical shear rate corresponding to $\gamma = {}^{1}/_{\beta_1}$.

Simplifying the differential equation in (3.30) yields equation (3.31)

$$H_i = H_0 e^{-b\gamma t} \quad (3.31)$$

With H_0 representing the initial proportion of hydrophobic interactions before disentanglement and t indicating the shearing or propagation time in a porous media.

3.2.2. Structural Kinetics during Shear Thickening

A porous media can be considered as geometry with numerous converging-diverging channels. In the converging section, there is a sharp acceleration at the entry point due to an abrupt change in diameter, which leads to an extension or stretching of polymer molecules. However, in the diverging section, there is a sharp deceleration at the entry of the diverging point due to an abrupt increase in diameter, ensuring that the polymer molecules contract. The rate of elongation of polymer molecules was modelled according to the structural kinetic theory of Toorman (1997) and modified to depend on the shear rate of elongation, γ_{el} and can be related to the fraction of polymer molecules remaining after an increase in the proportion of hydrophobic interactions due to polymer extension $(H_{max} - H_i)$. Hence, the rate of extension is expressed as shown in (3.32)

$$\frac{dH_i}{dt} = g\gamma_{el}(H_{max} - H_i)^{m_g} \quad (3.32)$$

where g is the extension parameter and m_g is the extension exponent. The rate of structural contraction of polymer molecules after removal of shear elongation forces is also dependent

on the proportion of hydrophobic interactions at any point in time, H_i. Therefore, the rate of structural contraction is expressed as shown in (3.33)

$$\frac{dH_i}{dt} = -hH_i^{n_h} \quad (3.33)$$

where h is the contraction constant and n_h is the contraction exponent. The net extension is the difference between the rate of contraction and that of extension, as shown in (3.34).

$$\frac{dH_i}{dt} = g\gamma_{el}(H_{max} - H_i)^{m_g} - hH_i^{n_h} \quad (3.34)$$

Assuming first-order rate kinetics for the contraction and extension expressions, $m_g = n_h = 1$, equation (3.34) becomes (3.35)

$$\frac{dH_i}{dt} = g\gamma_{el}(H_{max} - H_i) - hH_i \quad (3.35)$$

At equilibrium, the rate of contraction equals the rate of extension. Therefore, $\frac{dH_i}{dt} = 0$ and (3.35) becomes (3.36)

$$g\gamma_{el}(H_{max} - H_{el}) = hH_{el} \quad (3.36)$$

The equilibrium structural parameter, H_{el} is therefore expressed as (3.37) with $H_{max} = 1$

$$H_{el} = \frac{H_{max}\gamma_{el}}{\beta_2 + \gamma_{el}} \quad (3.37)$$

where $\beta_2 = h/g$ can be described as a rate constant, and it is a measure of the stretching of polymer molecules during elongational flow. A small value for β_2 would indicate a low stretching capacity of polymer molecules during elongational flow, meaning the hydrophobic interactions between polymer molecules would approach their maximum value at a low elongation rate. The reverse is the case for high values of β_2, meaning high stretching capacity of polymer molecules, indicating the interactions between polymer molecules would approach their maximum value at a high elongation rate.

3.2.2.1. Predicting the Onset of Shear Thickening/Hydrophobic Interactions

Setting $H_o = H_{max} = 1$ and equating equations (3.20) and (3.37) ensured that the shear rate which marks the onset of hydrophobic interactions in a porous media could be derived. Likewise, the onset of shear thickening, γ_c as shown in (3.38).

$$\frac{1}{1+\beta_1\gamma_c} = \frac{\gamma_c}{\beta_2+\gamma_c} \quad (3.38)$$

Simplifying,

$$\gamma_c = \sqrt{\frac{\beta_2}{\beta_1}} \quad (3.39)$$

The critical shear rate can be related to the polymer and rock properties. According to Lohne et al. (2017), computation of the pore residence time can be made based on the assumption

that the pore length, L_p is equal to the characteristic rock grain size, D_g (or R_g). The relationship between the effective pore radius, R_p and rock grain size, D_g is given in (3.40)

$$\frac{2\emptyset}{R_p} = 6\frac{(1-\emptyset)}{D_g} = 6\frac{(1-\emptyset)}{L_p} \tag{3.40}$$

Therefore, the pore residence time is computed using the expression in (3.41)

$$\tau_r = \frac{L_p}{v_p} = 12\left(\frac{1-\emptyset}{\emptyset\gamma}\right) \tag{3.41}$$

Where v_p is the average pore velocity and $\gamma = 4v_p/R_p$ relates the shear rate at the wall to the average pore velocity. The elongational relaxation time, τ_{el} is computed as the characteristic time scale of diffusion and simplified as equation (3.42)

$$\tau_{el} = \frac{36}{5}\left(\frac{\mu_s[\mu]M_w}{R_gT}\right) \tag{3.42}$$

The onset of hydrophobic interactions can be correlated with the dimensionless Deborah number. This Deborah number according to Lohne et al. (2017) is defined in (3.43)

$$N_{De} = \frac{\tau_{el}}{\tau_r} \tag{3.43}$$

Therefore,

$$12\left(\frac{1-\emptyset}{\emptyset\gamma_c}\right)N_{De} = \frac{36}{5}\left(\frac{\mu_s[\mu]M_w}{R_gT}\right) \tag{3.44}$$

Simplifying (3.44), the critical shear rate for the onset of hydrophobic interactions, γ_c is given in (3.45)

$$\gamma_c = \frac{5}{3}N_{De}\left(\frac{1-\emptyset}{\emptyset}\right)\left(\frac{R_gT}{\mu_s[\mu]M_w}\right) \tag{3.45}$$

In this case, the Deborah number, N_{De} was applied as a fitting parameter determined from experimental results. Equations (3.39) and (3.45) can be applied in predicting the onset of shear thickening. However, applying (3.39) would require determining the parameter β_2.

3.2.2.2. Derivation of the Rate Constant Parameter β_2

Comparing (3.39) and (3.45), an expression for the rate constant, β_2 can be obtained as shown in (3.46)

$$\beta_2 = \frac{25}{9}\left(\frac{\beta_a}{N_{De}}\right)\left[\frac{(1-\emptyset)}{\emptyset}\right]^2\left(\frac{T}{\mu_w[\mu]M_{w0}}\right) \tag{3.46}$$

Thus the final expression for equation (3.46) becomes (3.47)

$$\beta_2 = \beta_b\left[\frac{(1-\emptyset)}{\emptyset}\right]^2\left(\frac{T}{\mu_w[\mu]M_{w0}}\right) \tag{3.47}$$

Where $\beta_b = \frac{25}{9}\left(\frac{\beta_a}{N_{De}}\right)$. β_b was used as a tuning factor to account for the uncertainties in the pore structure. This was captured by applying the Deborah number as a fitting parameter.

This simply means that the rate coefficient, β_2 is dependent on both the polymer and rock properties.

3.2.3. Flow Regimes for Shear Thinning and Thickening in Porous Media

A new model was developed for predicting the changing hydrophobic interactions in the shear thinning and shear thickening flow regime using the findings based on the structural state of the polymers earlier discussed. The dimensionless shear-thinning parameter, H_{sh} can be defined as Equation (3.48)

$$\mathrm{H_{sh}} = \frac{\mathrm{H_o}}{1+\beta_1\gamma_{\mathrm{sh}}} \tag{3.48}$$

For the dimensionless elongational parameter, H_{el}, this is represented as shown in (3.49)

$$\mathrm{H_{el}} = \frac{\gamma_{\mathrm{el}}}{\beta_2+\gamma_{\mathrm{el}}} \tag{3.49}$$

Therefore, a new and simplified model for hydrophobically associating polymers during flow in porous media can be expressed as (3.50)

$$\mathrm{H_{ap}} = \frac{\mathrm{H_o}}{1+\beta_1\gamma_{\mathrm{sh}}} + \frac{\mathrm{H_{max}}\gamma_{\mathrm{el}}}{\beta_2+\gamma_{\mathrm{el}}} \tag{3.50}$$

Applying conditions (3.12) to (3.14) to Equation (3.50)

$$\lim_{\gamma\approx 0} \mathrm{H_{ap}} = \mathrm{H_0} \tag{3.51}$$

$$\lim_{\gamma\approx \gamma_c} \mathrm{H_{ap}} = \mathrm{H_{min}} = \frac{1}{1+\sqrt{\beta_1\beta_2}}(\mathrm{H_0} + \mathrm{H_{max}}) \tag{3.52}$$

$$\lim_{\gamma\approx \infty} \mathrm{H_{ap}} = \mathrm{H_{max}} \tag{3.53}$$

It was observed that the novel model developed contained fewer parameters. Although a higher number of parameters would reduce the uncertainties surrounding the model prediction, the tuning of each parameter for accurate flow description can be challenging and time-consuming. The novel feature of this model was that the definition of polymer characteristics and reservoir conditions was reduced to the model's time constants. As such, the time constant was related to the variation in reservoir conditions (such as porosity, temperature, salinity, and hardness) and polymer properties (concentration, intrinsic viscosity, and molecular weight) without introducing new fitting parameters.

3.2.4. Degradation of Hydrophobic Interactions in Porous Media

Equation (3.50) captured the changing hydrophobic interactions under the shear thinning and shear thickening/elongation flow regimes. Description of the degradation flow regime was done in two parts: predicting the onset of degradation of polymer molecules in the hydrophobic interaction network and a model for describing the degradation flow regime.

3.2.4.1. Predicting the Onset of Degradation of Hydrophobic Interactions

Degradation occurs when elongation forces are dominant over shear forces. Therefore, equation (3.50) reduced to (3.54) when $\gamma_{sh} = 0$:

$$\mathrm{H_{ap}} = \mathrm{H_o} + \frac{\gamma_{el}}{\beta_2 + \gamma_{el}} \tag{3.54}$$

The onset of degradation was predicted to occur when the proportion of hydrophobic interaction reached a maximum value of $H_{ap} = 1$ due to elongation of polymer molecules which exposes hydrophobic blocks to pronounced interactions. Therefore, equation (3.54) becomes (3.55)

$$1 = \mathrm{H_o} + \frac{\gamma_{deg}}{\beta_2 + \gamma_{deg}} \tag{3.55}$$

Where γ_{deg} is the critical rate for degradation. Simplifying (3.55) yields (3.56)

$$\gamma_{c\_deg} = \frac{(1-\mathrm{H_o})\beta_2}{\mathrm{H_o}} \tag{3.56}$$

Equation (3.53) indicates that the degradation of polymer molecules that constitute the hydrophobic interaction network is dependent on the proportion of interactions before injection (H_o) and polymer/porous media properties (β_2).

3.2.4.2. Degradation Flow Regime for Hydrophobic Interactions

According to the structural kinetic theory, the rate of structural breakdown, which characterizes the degradation flow regime, is dependent on the shear rate of degradation, γ and fraction of polymer molecules interacting at that point in time, H_i. The rate of breakdown follows similar expression obtained from Toorman (1997) as shown in (3.57)

$$\frac{\mathrm{dH_i}}{\mathrm{dt}} = -\mathrm{b}\gamma\mathrm{H_i}^{n} \tag{3.57}$$

where b is the breakdown constant, and n is the breakdown exponent. The rate of recovery that characterizes the hydrophobic interaction is related to the fraction of polymer molecules available. Hence, the rate of recovery is expressed as shown in (3.58)

$$\frac{\mathrm{dH_i}}{\mathrm{dt}} = \mathrm{a}(1 - \mathrm{H_i})^{\mathrm{m}} \tag{3.58}$$

where a is the recovery parameter, and m is the recovery exponent. The net rate expression is the difference between the rate of breakdown and that of recovery (3.59).

$$\frac{\mathrm{dH_i}}{\mathrm{dt}} = \mathrm{a}(1 - \mathrm{H_i})^{\mathrm{m}} - \mathrm{b}\gamma\mathrm{H_i}^{\mathrm{n}} \tag{3.59}$$

Assuming first-order rate kinetics for the breakdown and recovery expressions, $m = n = 1$, equation (3.59) becomes (3.60)

$$\frac{dH_i}{dt} = a(1 - H_i) - b\gamma H_{i_i} \quad (3.60)$$

At equilibrium, the rate of breakdown equals the rate of recovery. Therefore, $\frac{dH_i}{dt} = 0$ and (3.60) becomes (3.61)

$$a(1 - H_{deg}) = b\gamma_{deg} H_{deg} \quad (3.61)$$

The equilibrium structural parameter, H_{deg} is therefore expressed as (3.62)

$$H_{deg} = \frac{1}{1+\beta_3\gamma_{deg}} \quad (3.62)$$

Where γ_{deg} is the shear rate under degradation and β_3 is related to the critical shear rate for the onset of polymer degradation and β_2 as shown in (3.63)

$$\beta_3 = \frac{1}{\gamma_{c\_deg}} = \frac{H_o}{(1-H_o)\beta_2} \quad (3.63)$$

3.2.5. A New Model for Associative Polymers in Porous Media

Incorporating the effect of the shear degradation flow regime modifies equation (3.11) into (3.64) below.

$$H_{ap} = (H_{sh} + H_{el})H_{deg} \quad (3.64)$$

Substituting for H_{sh}, H_{el} and H_{deg} in (3.64) results in (3.65)

$$\mathbf{H_{ap}} = \left(\frac{\mathbf{H_o}}{\mathbf{1+\beta_1\gamma_{sh}}} + \frac{\boldsymbol{\gamma_{el}}}{\boldsymbol{\beta_2+\gamma_{el}}}\right)\left(\frac{\mathbf{1}}{\mathbf{1+\beta_3\gamma_{deg}}}\right) \quad (3.65)$$

Applying conditions like (3.12) to (3.14) to equation (3.65) results in the following expressions below

$$\lim_{\gamma_{el},\gamma_{deg}\approx 0} H_{ap} = \frac{H_o}{1+\beta_1\gamma_{sh}} \quad (3.66)$$

$$\lim_{\gamma_{sh},\gamma_{deg}\approx 0} H_{ap} = \frac{\gamma_{el}}{\beta_2+\gamma_{el}} \quad (3.67)$$

$$\lim_{\gamma_{sh},\gamma_{el}\approx 0} H_{ap} = \frac{H_o}{1+\beta_3\gamma_{deg}} \quad (3.68)$$

The developed model in (3.65) covers the entire flow regimes associated with polymer flow in a porous media. The advantage of this model is its simplicity with model parameters limited to the time constants (β_1, β_2 and β_3).

3.2.6. Effective Concentration of Polymer Propagation Front, C_{pe}

A concentration term, *"effective polymer concentration"*, is defined to quantify the concentration (and the hydrophobic interactions between molecules) of the polymer propagation front in the porous media. Therefore, the effective polymer concentration, C_{pe} at a given reservoir condition can be estimated as shown in equation (3.69) below:

$$C_{pe} = \frac{C_{ag}}{(1-H_{ap})} \quad (3.69)$$

Where C_{ag} is the critical aggregation concentration at a reference condition and H_{ap} is the apparent hydrophobic interaction at reservoir conditions. The equation was modified from the expression for hydrophobic interactions from (3.65). Substituting equation (3.65) into (3.69) gives (3.70)

$$C_{pe} = \frac{C_{ag}}{\left(1-\left[\frac{H_o}{1+\beta_1\gamma_{sh}}+\frac{H_{max}\gamma_{el}}{\beta_2+\gamma_{el}}\right]\frac{1}{1+\beta_3\gamma_{deg}}\right)} \quad (3.70)$$

Since the propagation front flows at the centre of the pores, the excluded volume effects, E_{PV} arising from IPV is incorporated into equation (3.70) using (3.71) below.

$$E_{PV} = 1 - I_{PV} \quad (3.71)$$

Therefore, Equation (3.70) becomes (3.72)

$$\mathbf{C_{pe}} = \left[\frac{C_{ag}}{\left(1-\left[\frac{H_o}{1+\beta_1\gamma_{sh}}+\frac{H_{max}\gamma_{el}}{\beta_2+\gamma_{el}}\right]\frac{1}{1+\beta_3\gamma_{deg}}\right)}\right]\mathbf{E_{PV}} \quad (3.72)$$

Equation (3.72) gives the effective concentration of polymer chains with hydrophobic interactions sufficient to propagate in porous media. This expression was applied in tracking the concentration of the polymer front as it propagates in the porous media.

3.3. Modelling of Hydrophobic Interactions in Polymer Retention

3.3.1. Mapping Static to Dynamic Retention

A constant denominator for static and dynamic retention is the "**Contact Time**" for surface interaction. This is further shown in Table 3.2 when comparing the various adsorption kinetic models.

Table 3.2*: Some of the known kinetic models used in the study of polymer adsorption (Kajjumba et al., 2018).*

Name	Equation	Parameters	Remarks
Pseudo First Order Model	$\frac{d\Gamma_t}{dt} = k(\Gamma_e - \Gamma_t)$	Γ_t is the adsorbate on adsorbent in time, t, Γ_e is the equilibrium adsorption capacity and k is the rate constant.	The common denominator to all the models is the time factor

Pseudo Second Order Model	$\frac{d\Gamma_t}{dt} = k(\Gamma_e - \Gamma_t)^2$	Γ_t is the adsorbate on adsorbent in time, t, Γ_e is the equilibrium adsorption capacity and k is the rate constant.
Elovich Model	$\frac{d\Gamma_t}{dt} = \alpha(\exp^{-\beta\Gamma_t})$	Γ_t is the adsorbate on adsorbent in time, t, α is the initial adsorption rate and β is the desorption constant.
Webb and Morris Model	$\Gamma_t = K_p\sqrt{t} + C$	K_p is the rate constant and C is the boundary layer thickness which determines the boundary layer effect.

Thus, the following general expression in equation (3.73) between the amount of polymer retained at a given time, Γ_p and the contact time for the static retention process, t_c.

$$\Gamma_p \propto t_c \tag{3.73}$$

Equation (3.73) can be simplified into (3.74) by introducing a constant, K_c as shown below:

$$\Gamma_p = K_c t_c \tag{3.74}$$

The rotational diffussion, D_{rot} of the polymer molecules can be related to t_c according to Lohne et al. (2017) as shown in (3.75)

$$t_c = \frac{1}{2D_{rot}} \tag{3.75}$$

This diffussion coefficient was computed using the Einstein–Smoluchowski relation in (3.76)

$$D_{rot} = \frac{k_B T}{8\pi\mu_s R_h^3} \tag{3.76}$$

Where k_B is the Boltzmann constant and R_h is the hydrodynamic radius of a rigid sphere of a flexible polymer in solution. Substituting (3.76) into (3.75) yeilds (3.77)

$$t_c = \frac{4\pi\mu_s R_h^3}{k_B T} \tag{3.77}$$

The value of R_h is estimated using the expression given by Lohne et al. (2017) in equation (3.78)

$$\mathrm{R_h} = \left(\frac{3}{10\pi \mathrm{N_A}}\right)^{1/3} ([\mu]\mathrm{M_w})^{1/3} \tag{3.78}$$

Where N_A is Avogadro's number. Combining (3.77) and (3.78), a new expression for t_c is shown in (3.79)

$$\mathrm{t_c} = \left(\frac{6}{5\mathrm{k_B N_A}}\right)\left(\frac{\mu_s[\mu]\mathrm{M_w}}{\mathrm{T}}\right) \tag{3.79}$$

Therefore, a modified relationship between the static retention, Γ_{p-st} and the contact time, t_c becomes Equation (3.80):

$$\Gamma_{\mathrm{p-st}} = \mathrm{K_c}\left[\left(\frac{6}{5\mathrm{k_B N_A}}\right)\left(\frac{\mu_s[\mu]\mathrm{M_w}}{\mathrm{T}}\right)\right] \tag{3.80}$$

According to Lohne et al. (2017), computation of the pore residence time for dynamic retention can be made based on the assumption that the pore length, L_p is equal to the grain size, D_g. As such, the pore radius, R_p is given in (3.81)

$$\mathrm{R_p} = \frac{\phi \mathrm{D_g}}{(1-\phi)} \tag{3.81}$$

The grain size, D_g or L_p can be calculated as the representative grain size for a packed bed of mono-sized spherical particles using the Blake-Kozeny Equation (Brakstad and Rosenkilde, 2016). Therefore, the pore residence time can be computed as shown in (3.82)

$$\frac{\gamma \tau_r}{12} = \left(\frac{1-\phi}{\phi}\right) \tag{3.82}$$

Where v_p is the average pore velocity and $\gamma = 4v_p/R_p$ relates the shear rate at the wall to the average pore velocity. Therefore, the contact time under dynamic conditions becomes (3.83):

$$\tau_c = 12\left(\frac{1-\phi}{\phi\gamma}\right) \tag{3.83}$$

Thus, a modified relationship between the dynamic retention, Γ_{p-dy} and the contact time, t_c becomes equation (3.84):

$$\Gamma_{\mathrm{p-dy}} = \mathrm{K_c}\left[12\left(\frac{1-\phi}{\phi\gamma}\right)\right] \tag{3.84}$$

Therefore, the correlation between static and dynamic retention was obtained as shown in (3.85):

$$\frac{\Gamma_{\mathrm{p-dy}}}{\Gamma_{\mathrm{p-st}}} = \frac{\mathrm{K_c}\left[12\left(\frac{1-\phi}{\phi\gamma}\right)\right]}{\mathrm{K_c}\left[\left(\frac{6}{5\mathrm{k_B N_A}}\right)\left(\frac{\mu_s[\mu]\mathrm{M_w}}{\mathrm{T}}\right)\right]} \tag{3.85}$$

The ratio of the contact times on the right-hand side (RHS) of equation (3.85) can be related to the Deborah number, N_{De} which is defined as the ratio of the polymer relaxation time to the pore residence time as shown in (3.86).

$$\mathrm{N_{De}} = \frac{\left[\left(\frac{6}{5\mathrm{k_B N_A}}\right)\left(\frac{\mu_S[\mu]\mathrm{M_W}}{\mathrm{T}}\right)\right]}{\left[12\left(\frac{1-\phi}{\phi\gamma}\right)\right]} \tag{3.86}$$

Therefore, equation (3.75) becomes (3.87)

$$\Gamma_{\mathrm{p-dy}} = \left(\frac{1}{\mathrm{N_{De}}}\right)\Gamma_{\mathrm{p-st}} \tag{3.87}$$

Thus, static retention can be mapped into dynamic retention using equation (3.87).

3.3.2. Quantification of Polymer Retention Mechanisms in Porous Media

3.3.2.1. Damaged Pore Volume and Interactions within Retained Polymer

Based on the assumptions highlighted above, the dimensionless parameter, H_{C_p} was used to quantify the hydrophobic interactions between retained associative polymer molecules as shown in (3.88):

$$\mathrm{H_{C_p}} = \frac{\mathrm{C_p - C_{ag}}}{\mathrm{C_p}} \begin{cases} \mathrm{C_p} > \mathrm{C_{ag}} \\ \mathrm{C_{ag}} \neq 0 \end{cases} \tag{3.88}$$

For accurate mapping of static to dynamic interactions, the fractional damaged pore volume (DPV or Γ_D) was related to (3.85) as shown in (3.89):

$$\Gamma_{\mathrm{D}} = \frac{\Gamma_{\mathrm{p-dy}}}{\Gamma_{\mathrm{p-st}}} = \frac{\mathrm{K_c}\left[12\left(\frac{1-\phi}{\phi\gamma}\right)\right]}{\mathrm{K_c}\left[\left(\frac{6}{5\mathrm{k_B N_A}}\right)\left(\frac{\mu_S[\mu]\mathrm{M_W}}{\mathrm{T}}\right)\right]} \tag{3.89}$$

The first order approximation of Huggins equation results in equation (3.90) for intrinsic viscosity

$$\lim_{\mathrm{C_p}\to 0} \frac{\mu_{sp}}{\mathrm{C_p}} = [\mu] \tag{3.90}$$

Modifying equation (3.89) was based on (3.88) and (3.90) results in (3.91):

$$\mathbf{1 - H_{C_p}} = \frac{\mathbf{5R_g T(1-\phi)\Gamma_D C_{ag}}}{\mathbf{3\mu_s \mu_{sp} \phi\gamma M_W}} \tag{3.91}$$

Equation (3.91) predicts the proportion of hydrophobic interactions between retained molecules. In other words, it gives the proportion of hydrophobic interactions lost to polymer retention in porous media.

3.3.2.2. Predicting Retention Mechanisms in Porous Media

Table 3.3 gives the various conditions for mapping the various mechanisms associated with polymer retention. The cumulative size distribution of the retained polymer molecules was

estimated based on the assumption that the cumulative amount of retained polymer molecules increases with injection concentration, as shown in (3.92)

$$\mathrm{Ret}_{(\mathrm{C_{pi}})} \cong \mathrm{Ret}_{\sum_{i=1}^{n} \mathrm{C_{p_{i-1}}}} \tag{3.92}$$

Table 3.3*: Conditions for distinguishing between the different retention mechanism in a porous media. R_h is the hydrodynamic size of the polymer; R_{hi} is the size of the retained polymer molecule and R_p is the pore size of the porous media.*

Conditions	**Meaning**
$\mathrm{R_{h}}i < \mathrm{R_p}$	Adsorption
$\mathrm{R_h} < \mathrm{R_{h}}i < \mathrm{R_p}$	Multilayer Adsorption
$\mathrm{R_{h}}i \approx \mathrm{R_p}$	Entrapment
$\mathrm{R_{h}}i > \mathrm{R_p}$	Pore Plugging

Where $Ret_{(C_{pi})}$ is the retained polymer at concentration C_{pi} and $Ret_{\sum_{i=1}^{n} C_{p_{i-1}}}$ is the cumulative retained polymer from concentrations value C_{po} up to C_{pi}. The size distribution of the retained polymer molecules, R_{hi} was estimated using a modified form of the expression by Lohne et al. (2017), as shown in (3.93)

$$\mathbf{R_{h}}i = \mathbf{R_h}\left[\frac{\mathbf{C_p}}{\mathbf{C_{ag}}}\right]^{\boldsymbol{H_{C_p}}} \tag{3.93}$$

Where R_h is the hydrodynamic radius of the molecules, which is given in equation (3.94) and H_{C_p} is the proportion of hydrophobic interactions among the retained molecules in (3.91).

$$\mathrm{R_h} = \left(\frac{3}{10\pi \mathrm{N_A}}\right)^{1/3} ([\mu]\mathrm{M_w})^{1/3} \tag{3.94}$$

Figure 3.3 shows the plot of the cumulative pore size distribution, $f(R_p)$ and the cumulative size distribution of the retained polymer molecules, $f(R_h)$. The pore fraction of entrapped molecules, Γ_{ent} up to R_2 can be predicted using equation (3.95)

$$\Gamma_{\mathrm{ent}} = \int_{\mathrm{R_{p1}}}^{\mathrm{R_{p2}}} \mathrm{f(R_p)} \Big/ \int_{\mathrm{R_o}}^{\mathrm{R_{h2}}} \mathrm{f(R_h)} \tag{3.95}$$

The inaccessible pore volume, I_{PV} is computed using Equation (3.96)

$$\mathrm{I_{PV}} = \int_{\mathrm{R_{p1}}}^{\mathrm{R_{p2}}} \mathrm{f(R_p)} \Big/ \int_{\mathrm{R_{p1}}}^{\mathrm{R_{p3}}} \mathrm{f(R_p)} \tag{3.96}$$

However, the I_{PV} in this work is defined as the sum of the pore fraction completely accessible to brine, I_{PVo} and that lost to entrapped molecules, Γ_{ent} as shown in (3.97)

$$I_{PV} = I_{PVo} + \Gamma_{ent} \quad (3.97)$$

From (3.97), I_{PVo} can be estimated. Considering Figure 3.3, the onset of polymer entrapment with reference to R_2 would commence at R_1 and the concentration value at this point is given in equation (3.98)

$$C_{p-ent} = C_{ag}\left[\frac{R_1}{R_h}\right]^{1/H_{R1}} \quad (3.98)$$

The point at which adsorption reaches its maximum and polymer entrapment becomes the dominant retention mechanism occurs at R_2 and the equivalent concentration value at this point is given in equation (3.99)

$$C_{p-ent} = C_{ag}\left[\frac{R_2}{R_h}\right]^{1/H_{R2}} \quad (3.99)$$

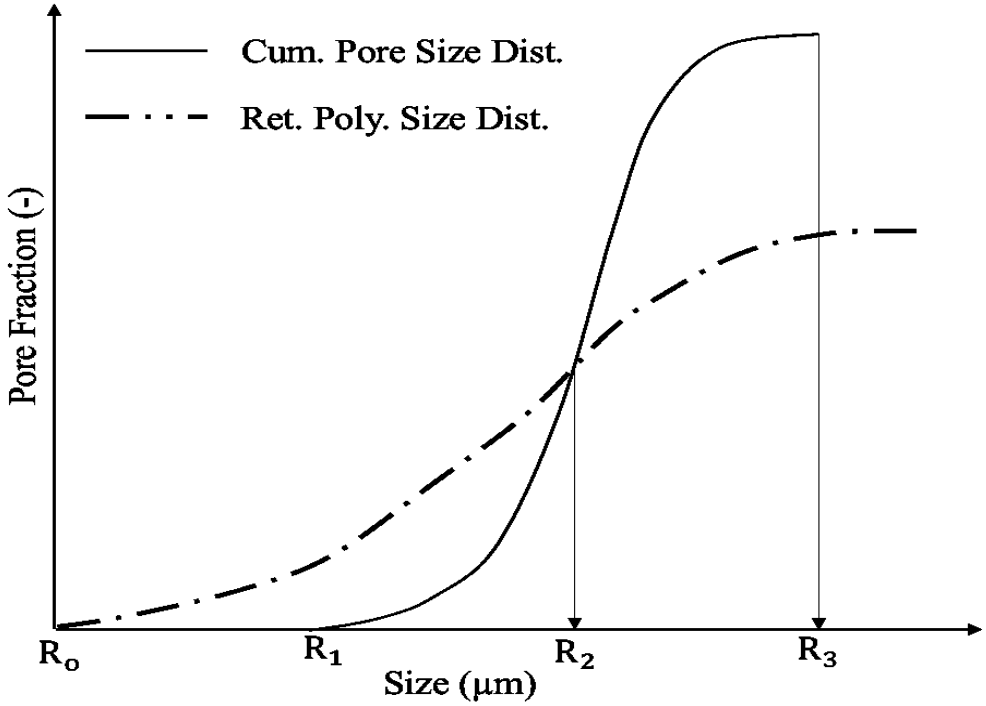

Figure 3.3*: Plot of pore size distribution and the cumulative size distribution of the retained polymer molecules in the porous media. The point R_2 was used as an illustration in predicting polymer entrapment.*

Similarly, pore plugging would occur at R_3 with an onset concentration shown in equation (3.100)

$$C_{p-plug} = C_{ag}\left[\frac{R_3}{R_h}\right]^{1/H_{R3}} \quad (3.100)$$

3.4. Predicting the Pressure Drop due to Retention and Thickening

An empirical model was developed for the pressure drop, ΔP in porous media using a statistical approach incorporating equations (3.65) and (3.91) for the shear viscosity and

retention respectively. This allowed an empirical identification of the contribution of polymer retention and shear thickening to the overall pressure drop.

3.4.1. Proxy Modelling of the Pressure Drop in the Porous Media

The Box-Behnken Design (BBD), which is a specific type of the response surface design (RSD), was employed to determine the significance of the dependency of ΔP on the specified parameters (H_μ, H_{C_p}, C_p and Q). The BBD was considered based on the following:

a) The BBD is a cheaper alternative rather than employing a full factorial design since it represents a fraction of a 3^k full factorial design and equipped with centre points for design balance.
b) It would be expensive and impractical to develop a large-scale design of experiment based on a 3^k full factorial design for k number of factors and the involvement of many experiments.

A non-linear regression analysis was performed using MINITAB to fit an empirical model to the data set according to a second-order polynomial equation in (3.101):

$$\Delta P = \beta_o + \sum_{i=1}^{3} \beta_i X_i + \sum_{i=1}^{3} \beta_{ii} {X_i}^2 + \sum_{i=0}^{2} \sum_{j=i+1}^{3} \beta_{ij} X_i X_j \qquad (3.101)$$

H_i: the predicted response; β_o: the intercept coefficient; β_i: the linear coefficient; β_{ii}: the squared coefficient; β_{ij}: the interaction coefficient; X_i: the coded independent variables; X_iX_j: the interaction terms; ${X_i}^2$: the quadratic terms. The model was evaluated and assessed using statistical tools such as the analysis of variance (ANOVA), coefficient of determination values (R^2), normality tests on the residuals and difference between model predictions and observed values.

3.4.2. Box-Cox Transformation of the Proxy Model

The Box-Cox transformation was applied to transform the non-normal response variable ΔP into a bell-shaped distribution. The most critical parameter of the Box-Cox transformation is the exponent, λ, with values ranging from -5 to 5. The transformation of the response variable (ΔP) has the form shown in (3.102):

$$y(\lambda) = \begin{cases} \frac{y^\lambda - 1}{\lambda}, & \lambda \neq 0 \\ \log y, & \lambda = 0 \end{cases} \qquad (3.102)$$

The optimal value for λ is the one that results in the best approximation of a normal distribution profile for the residuals of the model prediction of equation (3.101).

3.5. Summary

The efficiency of associative polymers depends significantly on the sustainability of these hydrophobic interactions in reservoirs. However, computational modelling and simulation of this network of interaction during transport in porous media are limited. In this chapter, a new mathematical approach was introduced for the numerical quantification, and predictive modelling of hydrophobic interactions. A summary of the key equations which constitute the model developed for the flow of associative polymers in porous media is given in Table 3.4 below.

***Table 3.4**: Summary of the main equations which constitute the predictive approach for the flow of associative polymers in porous media*

Description	Equation	Comments
Polymer Flow Regimes	$\mathbf{H_{ap} = \left(\frac{H_o}{1+\beta_1\gamma_{sh}} + \frac{H_{max}\gamma_{el}}{\beta_2+\gamma_{el}}\right)\left(\frac{1}{1+\beta_3\gamma_{deg}}\right)}$	Apparent hydrophobic interactions in porous media
	$\mathbf{C_{pe} = \left[\frac{C_{ag}}{(1-H_{ap})}\right]E_{PV}}$	Effective polymer concentration excluding retention effects
Polymer Retention	$\mathbf{\Gamma_D = \frac{\Gamma_{p-dy}}{\Gamma_{p-st}}}$	Damaged pore volume due to polymer retention
	$\mathbf{1 - H_{C_p} = \frac{5R_gT(1-\phi)\Gamma_D C_{ag}}{3\mu_s\mu_{sp}\phi\gamma M_W}}$	Hydrophobic interactions lost to polymer retention
	$\mathbf{R_{hi} = R_h\left[\frac{C_p}{C_{ag}}\right]^{H_{C_p}}}$	Effective size of retained polymer molecules

The development of this predictive approach was done under three steps. Firstly, the identification of a dimensionless parameter for the quantification of hydrophobic interactions. This was achieved by making suitable theoretical assumptions based on established finding reported in literature regarding associative polymers. Secondly, the identified parameter for quantifying hydrophobic interactions was related to the fractional damaged pore volume arising from polymer retention using the structural kinetic theory. The predictive tracking of hydrophobic interactions between the retained polymer molecules and pore surface ensured that the various retention mechanisms (adsorption and entrapment) can be accurately distinguished and quantified. Thirdly, the identified parameter for quantifying hydrophobic interactions was related to the different flow regimes

(shear thinning, thickening and degradation) using also the structural kinetic theory. The developed model for the flow regime enabled for an estimation of the effective concentration of the polymer propagation front in porous media. As such, the onset of hydrophobic interactions in a porous media can easily be tracked and monitored. The goal of developing the predictive approach was to optimise the propagation of hydrophobic interactions deep in a porous media and ensure its long-term sustainability. This was achieved with the aid of a correction factor which relates the hydrophobic interactions under polymer retention to the hydrophobic interactions under the polymer flow regimes. Existing experimental procedures were applied in validating the developed approach and where necessary, modification of the procedures was done as reported in the next chapter.

CHAPTER FOUR

4.0. Research Materials and Experimental Procedures

This chapter gives a detailed description of the experimental components of the methodology workflow presented in Chapter 1. The modelling component of the workflow is contained in Chapter 3 of this research work. The essence of the experimental section of this work was to validate the various components of the developed model as contained in Chapter 3.

4.1. Materials: Preparation and Characterization

This section gives details and procedures on preliminary laboratory tests to identify the associative polymers' properties under standard conditions. The details of the experimental techniques employed in the following subsections were according to the recommended practices for evaluating polymers for enhanced oil recovery (API Specification RP – 63). However, due to the novelty of most aspects of this work, existing techniques laid out in the recommended practice were modified where necessary to accommodate these new parameters.

4.1.1. Synthetic Formation Brine (SFB)

The salts employed in the preparation of synthetic formation brine (SFB) include analytical grade sodium chloride (NaCl), magnesium chloride ($MgCl_2$), calcium chloride ($CaCl_2$), potassium chloride (KCl), sodium sulphate (Na_2SO_4), sodium hydrogen carbonate ($NaHCO_3$) and strontium chloride ($SrCl_2$). These salts were purchased from Sigma Aldrich (UK) with the properties as provided by the supplier.

Materials and Apparatus

a) Fischer Scientific magnetic stirrer (Model: 11-102-50SH) with a coated magnetic bar.
b) Top loading laboratory balance (Maximum load: 2000 g; Sensitivity: 0.01g).
c) 1000 mL beaker and 2000 mL conical flask.
d) Millipore™ filter pumping and deionizing unit.

Experimental Procedure for the Preparation of Synthetic Brine

a) The base fluid (water) was deionized to a resistivity value of 18 MΩ-cm (a threshold for removing ions) using a Millipore™ pumping unit.
b) A given amount of deionized water in a 1000 mL beaker was placed on a magnetic stirrer containing coated magnetic bar.

c) Synthetic brine was formulated by dissolving the required amount of salts in the deionized water. The brine solutions were prepared to contain NaCl and $CaCl_2$ in the ratios 10 to 1, respectively.
d) The solution was stirred for approximately 20 minutes, after which it was filtered through the Millipore filter.
e) After stirring for the required time, additional deionized water was added to make up for the concentration of brine needed.
f) Before use, the synthetic brine solution was filtered through a 0.22 μm filter paper to ensure the removal of any particles present.

4.1.2. Associative Polymers

Two grades of hydrophobically associating polymers were used in this research work. These polymers, which are anionic polyacrylamide-based tetra polymer, include:

a) The Superpusher D118 (Degree of hydrolysis = 25 – 30 mol % at 25 ^{0}C; $\overline{M_w}$ = 16 – 20 x 10^6 g/mol; Appearance = white granular solid; Hydrophobe content = medium; Total anionic content = 15 - 25 mol.%).
b) The Superpusher C1205 (Sulfonic monomer = < 8 mol.% at 25 ^{0}C; $\overline{M_w}$ = 12 – 17 x 10^6 g/mol; Appearance = white granular solid; Hydrophobe content = 0.025 – 0.25 mol.%; Total anionic content = 15 - 25 mol.%).

SNF Floerger (France) supplied the associative polymers employed in this study. The properties of the polymers displayed are as obtained from the safety data sheet provided.

4.1.2.1. Determination of Polymer Activity, A_{pr}

The polymer activity represents the weight per cent of active solids, and this is usually assumed to be 100 wt.% in the absence of atmospheric exposure. However, dry polyacrylamide products have been reported to gain weight due to exposure to atmospheric conditions hence the need to adjust the polymer activity. Accurate estimation of the polymer activity is crucial in the computation of polymer concentration values.

Apparatus

The following apparatus was employed in the determination of the polymer activity:

a) Top loading laboratory balance (Maximum load: 2000 g; Sensitivity: 0.01g)
b) A ceramic dish and spatula
c) Desiccator with Silica gel desiccant
d) Oven

Experimental Procedure for Determination of Activity of Polymer Product (A_{pr})

a) An empty ceramic dish was weighed to the nearest 0.01g and recorded as W_d.
b) 10 g of the polymer sample was added to this dish and re-weighed. The new weight was recorded as W_{d+HS}.
c) The sample was allowed to dry for 2 hours in an oven, which is regulated and stabilized to 90 ^{0}C.
d) The sample was taken out of the oven after 2 hours and then cooled to room temperature in a desiccator containing silica gel.
e) The ceramic dish containing the sample was re-weighed and recorded as W_{d+DS}.

The activity of the polymers was estimated using equation (4.1) below:

$$A_{pr} = \frac{W_{d+DS} - W_d}{W_{d+HS} - W_d} \text{ x } 100 \qquad (4.1)$$

4.1.2.2. Determination of Chemical Composition of Polymers

The compositional analysis of the associative polymers was carried out to identify the functional groups present in the polymers and any interactions between them.

Materials and Apparatus

a) Associative Polymers (D118 and C1205).
b) Thermo Scientific Nicolet iS10 FTIR Spectrometer.
c) Avalon Raman Station (R3).

Experimental Procedure

a) The disaggregated polymer granules were dried in an oven using the approach in the determination of its activity in Section 4.1.2.1.
b) The dried polymer granules were packed in a plastic cavity, presented to the spectrometer by mounting the cavity.
c) The FTIR spectrum was presented as a plot of the percentage transmittance against wavenumber.
d) The Raman spectra were also generated using the Avalon Raman station as a plot of intensity against Raman shift.

4.1.2.3. Preparation of Stock and Dilute Polymer Solutions

The polymer solutions were prepared as a stock solution (approximately 5000 ppm) and diluted to test concentrations as required. Vigorous agitation was necessary for the initial dispersion of the dry polymer powder. The concentrated solutions of polymers were stored

at laboratory room temperature in brown glass bottles for 2 – 3 weeks without loss of effectiveness. However, diluted solutions were prepared the day they were used.

Apparatus

a) Magnetic stirrer (Hanna instruments– HI 190M with coated magnetic bar).
b) Top loading laboratory weighing balance (maximum load: 2000 g; sensitivity: 0.01 g).
c) Container: 2000 mL beaker.
d) Weighing cups.

Calculation for Preparation of Polymer Stock Solution (5000 ppm)

a) The amount of dry polymer product required to make up the appropriate amount of stock solution was calculated using equation (4.2):

$$W_{pr} = \frac{W_s \text{ x } C_{ps} \text{ x } 10^{-4}}{A_{pr}} \quad (4.2)$$

Where W_{pr} = weight of polymer product, g

W_s = weight of the stock solution to be made, g

C_{ps} = concentration of polymer in the stock solution, ppm

A_{pr} = activity of the polymer product, wt.%

b) The amount of makeup water to be used for the stock solution was calculated as follows from equation (4.3):

$$W_{bs} = W_s - W_{pr} \quad (4.3)$$

Mixing Procedure for Preparation of Polymer Stock Solution

a) A calculated amount of dry polymer product was weighed in a weighing cup, and the weight recorded.
b) The desired brine solution was calculated into a 2000 ml capacity beaker up to the lower meniscus of the 1000 ml mark. The weight was recorded, and a 1.5-inch coated magnetic stirring bar was added to the beaker.
c) The magnetic stirrer was used to adjust the vortex to extend 75% into the brine solution.
d) The polymer powder was sprinkled on the shoulder of the vortex for 30 seconds. The solution was observed to ensure no particles or *'fish-eyes* were present.
e) The solution was stirred using the magnetic stirrer at low speed (60 - 80 RPM) for about 2 – 3 hours to ensure complete dissolution.
f) The solution was left to sit overnight for proper hydration before diluting to the desired concentrations.

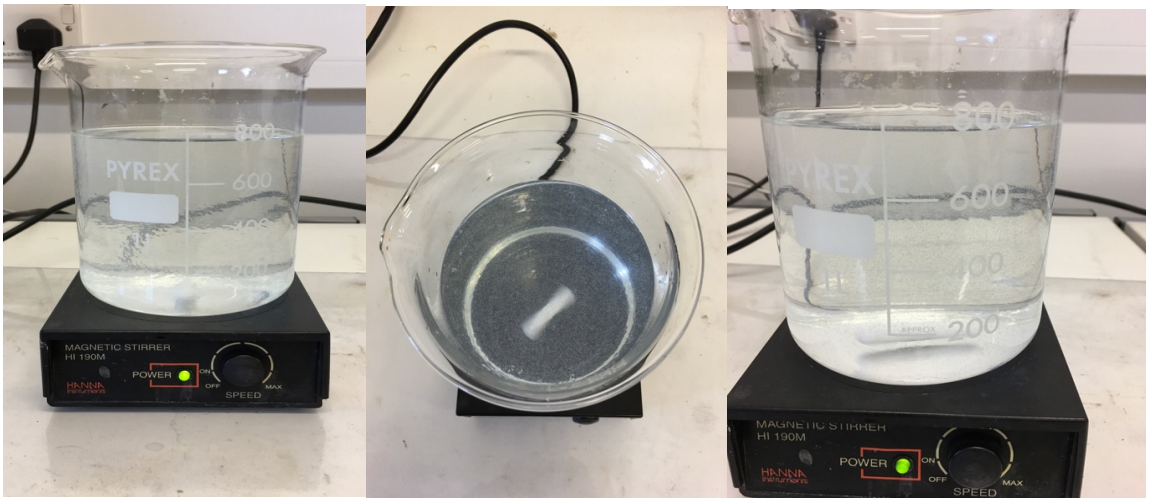

***Figure 4.1**: Preparation of stock polymer solution at room temperature*

Calculation for Preparation of Dilute Polymer Solution

a) Test concentrations of dilute polymer solutions to be used were prepared as required. The weight of stock solution required to make up the desired amount of diluted polymer solution was calculated using the relationship below from equation (4.4)

$$W_s = \frac{W_d \times C_d}{C_s} \quad (4.4)$$

Where:

W_d = weight of the diluted solution to be made, g.

C_d = concentration of polymer in diluted solution, ppm.

b) Equation (4.5) below was used to calculate the amount of makeup water required to make the desired diluted solution.

$$W_{bd} = W_d - W_s \quad (4.5)$$

Where: W_{bd} = weight of makeup water used in the diluted solution, g.

c) The solution was stirred using the magnetic stirrer at low speed (60 – 80 rpm) for about 10 minutes to ensure complete dissolution.

4.1.2.4. Estimation of Polymer Intrinsic Viscosity and Molecular Weight

The intrinsic viscosity of a polymer solution, [μ], may be used as an indirect indicator of polymer molecular weight for homologous linear polymers. To determine [μ], it was necessary to measure viscosities, μ of a series of polymer solutions at various polymer concentrations, C_p in a selected brine solvent. From these viscosities (see Appendix B), the relative viscosity, μ_{rel} was computed according to equation (4.6)

$$\mu_{rel} = \frac{\mu_{ap}}{\mu_s} \quad (4.6)$$

Where μ_{ap} and μ_s are the apparent polymer viscosity (at very low shear rate) and brine viscosity respectively. The values of $\ln(\mu_{rel})/C_p$ were plotted as functions of polymer concentration, C_p and a separate straight line was extrapolated to zero concentrations to obtain $[\mu]$ as shown in equation (4.7)

$$[\mu] = \lim_{C_p \to 0} \left[\frac{\ln(\mu_{rel})}{C_p}\right] \quad (4.7)$$

The y-intercept at $C_p = 0$ was the intrinsic viscosity estimate in units of inverse concentration.

Materials and Apparatus

a) Brookfield Digital Rheometer (Model DV-III; manufactured by Brookfield Engineering Laboratories) for measuring viscosities at low shear rates.
b) Synthetic brine containing 3 wt.% NaCl.
c) Polymer concentrations: 400, 300, 200, 150, and 50 ppm.
d) Temperature: 25 ℃ (77 °F).

Experimental Procedure for Determination of Polymer Intrinsic Viscosity $[\mu]$

a) A series of diluted polymer solutions with concentration ranging from 50 – 400 ppm (0.005 – 0.04 g/dL) were prepared in 3 wt.% NaCl brine using the procedure in paragraph 4.1.2.2.
b) The viscosities of each of these polymer solutions were measured using the Brookfield Digital Rheometer as a function of shear rate.
c) The temperature of the polymer solutions was kept at 25 ℃ by circulating water on the outer jacket of the viscometer cup containing the solution using the Medline Refrigerating & Heating Bath Circulator (Model: RW-0525G). This bath circulator was used for temperature control.
d) Using the very low or zero-shear-rate viscosities of the polymer solutions, the relative viscosity, μ_{rel} was computed at the given shear rate utilising the expression in Equation (4.6).
e) The values of $\ln(\mu_{rel})/C_p$ as a function of the polymer concentration, C_p was plotted. A linear model was fitted to the plot via regression analysis, and extrapolation was done according to Equation (4.7) to determine $[\mu]$ with units dL/g.

Experimental Procedure for Determination of Polymer Molecular Weight M_w

a) The polymer intrinsic viscosity, $[\mu]$ was estimated using the experimental procedure in the preceding section.

b) The intrinsic viscosity, $[\mu]$ was related to the Mark-Houwink Equation as shown in equation (4.8):

$$[\mu] = K'(M_w)^{\sigma} \quad (4.8)$$

Where K' and σ are the Mark-Houwink constants, and this depends on the polymer-solvent system. For solvents, a value of $a = 0.5$ is indicative of a theta solvent, and a value of $a = 0.8$ indicates a suitable solvent. For flexible polymers, $0.5 \leq a \leq 0.8$ and for semi-flexible polymers, $a \geq 0.8$.

c) If the degree of hydrolysis of the polymer is known, the Mark-Houwink constants K' and σ in Table 4.1 can be used to estimate the polymer molecular weight from Equation (4.8).

Table 4.1*: Mark-Houwink constants for polyacrylamide-based polymers*

% Hydrolysis	K'	a	Solvent
0.00	7.19×10^{-5}	0.770	3 wt.% NaCl
12.0	6.25×10^{-5}	0.810	
20.0	6.30×10^{-5}	0.825	
31.5	6.75×10^{-5}	0.830	
40.0	7.10×10^{-5}	0.833	

4.1.3. Determination of Critical Aggregation Concentration, C_{ag}

The critical aggregation concentration of the associative polymer was determined using the linearity deviation method. The plot of polymer viscosity against concentration has a low concentration region (dilute regime) and high concentration region (semi-dilute regime). In both concentration regimes, a linear relationship exists between polymer viscosity and concentration. The two linear models were fitted via regression analysis to the regions (dilute and semi-dilute region). This approximates a straight line in the plot of viscosity against polymer concentration. The critical aggregation concentration was approximated as the point of intersection of the fitted linear models.

4.1.3.1. Investigating Dependence of C_{ag} on Shear Rate

Materials and Apparatus

a) The Fann Viscometer (Model 35A/SR-12) with pre-set rates: 600, 300, 200, 180, 100, 90, 60, 30, 6, 3, 1.8, 0.9 RPM. Radius of bob: 1.7245 cm and Radius of Rotor: 1.8415 cm.

b) Brine: appropriate to conditions that apply.
c) Polymer Concentration: 150, 250, 500, 750, 1000, 2000 and 3000 ppm.
d) Temperature: appropriate to conditions that apply.

Experimental Procedure

a) The viscosity of the polymer solutions with concentrations under consideration was measured at a minimum of 12 shear rate values starting from the lowest and working upward (see Appendix C).
b) From the data obtained, polymer viscosity was plotted against polymer concentration at specified shear rates of the test.
c) The critical aggregation concentration, C_{ag} was estimated as the point beyond which the polymer viscosity shows a rapid increase.

4.1.3.2. Investigating Dependence of C_{ag} on Temperature

Materials and Apparatus

a) The Fann Viscometer (Model 35A/SR-12) with pre-set rates: 600, 300, 200, 180, 100, 90, 60, 30, 6, 3, 1.8, 0.9 RPM. Radius of bob: 1.7245 cm and Radius of Rotor: 1.8415 cm.
b) Brine: appropriate to conditions that apply.
c) Polymer Concentration: 150, 250, 500, 750, 1000, 2000 and 3000 ppm.
d) Temperature: 25, 50, 75 and 85 ℃.

Experimental Procedure

a) The viscosity of the polymer solution was measured at a given shear rate for the various polymer concentrations starting from the lowest and working upward at different temperatures.
b) From the data obtained, polymer viscosity was plotted against polymer concentration at specified temperatures of the test.
c) The critical aggregation concentration, C_{ag} was estimated as the point beyond which the polymer viscosity shows a rapid increase.

4.1.3.3. Investigating Dependence of C_{ag} on Brine Salinity.

Materials and Apparatus

a) The Fann Viscometer (Model 35A/SR-12) with pre-set rates: 600, 300, 200, 180, 100, 90, 60, 30, 6, 3, 1.8, 0.9 RPM. Radius of bob: 1.7245 cm and Radius of Rotor: 1.8415 cm.

b) Brine: Brine: S_1 (3.5% TDS), S_2 (3.8% TDS), S_3 (4.0% TDS) and S_4 (4.2% TDS). The ratio of NaCl to $CaCl_2$ was maintained at 10:1 (Table 4.2).

c) Polymer Concentration: 150, 250, 500, 750, 1000, 2000 and 3000 ppm.

d) Temperature: appropriate to conditions that apply.

Experimental Procedure

a) The viscosity of the polymer solution was measured at a given shear rate for the various polymer concentrations starting from the lowest and working upward.

b) From the data obtained, polymer viscosity was plotted against polymer concentration at the specified salinity of the test.

c) The critical aggregation concentration, C_{ag} was estimated as the point beyond which the polymer viscosity shows a rapid increase.

Table 4.2: *Synthetic brine composition for samples S_1 to S_4 prepared at 25 ^{0}C. The pH values for the brine samples S_1 to S_4 are 7.58, 7.92, 7.83 and 7.88 respectively.*

Composition of Synthetic Formation Brine				
Compound	**S_1 (wt.%)**	**S_2 (wt.%)**	**S_3 (wt.%)**	**S_4 (wt.%)**
Sodium Chloride, **NaCl**	2.266	2.553	2.739	2.925
Magnesium Chloride, **$MgCl_2$**	0.500	0.500	0.499	0.499
Sodium Sulphate, **Na_2SO_4**	0.394	0.394	0.394	0.393
Calcium Chloride, **$CaCl_2$**	0.236	0.255	0.275	0.294
Potassium Chloride, **KCl**	0.067	0.066	0.066	0.066
Sodium Hydrogen Carbonate, **$NaHCO_3$**	0.019	0.019	0.019	0.019
Strontium Chloride, **$SrCl_2$**	0.002	0.002	0.002	0.002
Total Dissolved Solids (TDS)	3.586	3.792	3.995	4.198

4.2. Porous Media: Preparation and Characterization

For laboratory screening of different polymers for mobility control, it was recommended (according to API Specification RP – 63) that Berea sandstone core be used as the standard porous media. However, due to the unavailability of Berea sandstone cores, other porous media materials had to be considered, with availability in large quantities being the selection criteria. Therefore, the porous media material considered for this study was disaggregated commercial silica sand due to its availability in sufficient quantities for the research work.

4.2.1. Commercial Silica Sand (40/60)

Commercial silica sands (40/60 mesh sizes) were used for the sand pack experiments and the sand particles were characterized for their petrophysical properties, mineralogical composition, and shape identification. The various experimental procedures for this analysis are detailed in the different sections below. The dataset for the sieve analysis of the sand grain types is contained in Appendix A.

4.2.1.1. Sieve Analysis and Grain Size Distribution

The estimation of the grain size distribution of the silica sand was carried out through a direct sieving process using a mechanical shaker with a sieve mesh arrangement.

Materials and Apparatus

a) The mechanical shaker with sieve mesh arrangement (mesh size: 50 – 900 μm).
b) Top loading laboratory weighing balance (maximum load: 2000 g; sensitivity: 0.01 g).
c) Disaggregated commercial silica sand (40/60 mesh size).
d) Oven.

Experimental Procedure for Determination of Sand Grain Size

a) The silica sand was dried in an oven at a high temperature of 70 ℃ to remove the coolant but low enough to prevent alteration of the sand material.
b) The weight of empty each sieve pans contained in the stack of meshes was taken before loading the sand grains on the top pan of the stack of meshes.
c) The dried and weighed sand sample was placed in the topmost (coarsest mesh) of a stack of meshes with decreasing sieve size mounted on the mechanical shaker.
d) The mechanical shaker was used to vibrate the stacked sieves such that given sand grains remain in each sieve after travelling downward through the stacked mesh.
e) The mechanical shaking process was continued (for about 60 minutes) until sand grains were retained on a mesh having a size less than the minimum grain size.
f) The mass of sand grains retained in each mesh was determined by weighing and converting the original test sample weight percentages.
g) The per cent weight of the sand grains on each mesh size was plotted against the mesh size resulting in a distribution curve.
h) Generally, the largest per cent weight determines the size of sand grains. Therefore, the largest weight per cent was taken as the grain size of the silica sand.

4.2.1.2. Optical Analysis of Sand Grains

The optical analysis of the unconsolidated sand grains was carried out to identify grain structural configuration and shape. This was important as grain geometry play a significant role in the porosity and specific surface of pore surface exposed to fluid flow in the porous media.

Materials and Apparatus

a) Leica DFC420 Digital Microsystems.
b) Disaggregated commercial silica sands (40/60 mesh size).

Experimental Procedure for Imaging Analysis

a) A small amount of the silica sand sample was loaded on an imaging glass and placed under the optical microscopy system.
b) High-resolution images of the sand grains were captured for shape identification and analysis.

4.2.1.3. Determination of Sand Pack Porosity and Grain Density

The silica sand porosity and grain density were determined using a direct method in both cases. The direct approach was chosen due to the simplicity of the methodology. The procedure for the direct method is detailed as follows:

Materials and Apparatus

a) Top loading laboratory weighing balance (maximum load: 2000 g; sensitivity: 0.01 g).
b) Disaggregated commercial silica sands (40/60 mesh size).
c) Measuring cylinders (100 mL).

Experimental Procedure for the Determination of Sand Grain Density

a) An empty measuring cylinder was weighed, and the mass recorded as M_1.
b) The empty cylinder was subsequently loaded with sand with the volume noted as V_{gr}
c) The mass of the sand loaded measuring cylinder sand taken and noted as M_2.
d) The sand grain density was estimated as shown in equation (4.11) below:

$$\rho_{gr} = \frac{M_2 - M_1}{V_{gr}} \quad (4.11)$$

e) The calculated grain density value was compared to known values in the literature for commercial silica sands.

Experimental Procedure for the Determination of Sand Porosity

a) The silica sand was loaded into a measuring cylinder, and the mass of sand noted as M_{gr} and the bulk volume of sand reported as V_{gr}.

b) Deionized water was added into the loaded sand contained in the measuring cylinder up to the sand meniscus level and new mas recorded as M_{gr+Wat}.

c) The mass of water occupying the pore spaces was computed by subtracting M_{gr} from M_{gr+Wat} and noted as M_{por}. Since the density of water is 1 g/cm^3, the pore volume, V_{por} is equal to M_{por};

d) The sand grain porosity was calculated using equation (4.12):

$$\phi = \frac{V_{por}}{V_{gr}} \tag{4.12}$$

4.2.2. Experimental Polymer Flooding

The polymer flooding was carried out using a flow rig constructed with components, as shown in Figure 4.1. The flow system was applied in the validation of the various models developed in Chapter 3 for hydrophobic interactions in a porous media.

4.2.2.1. Dynamic Flow System Description

The experimental flow rig setup employed in this research consist of several components, as shown in Figure 4.1.

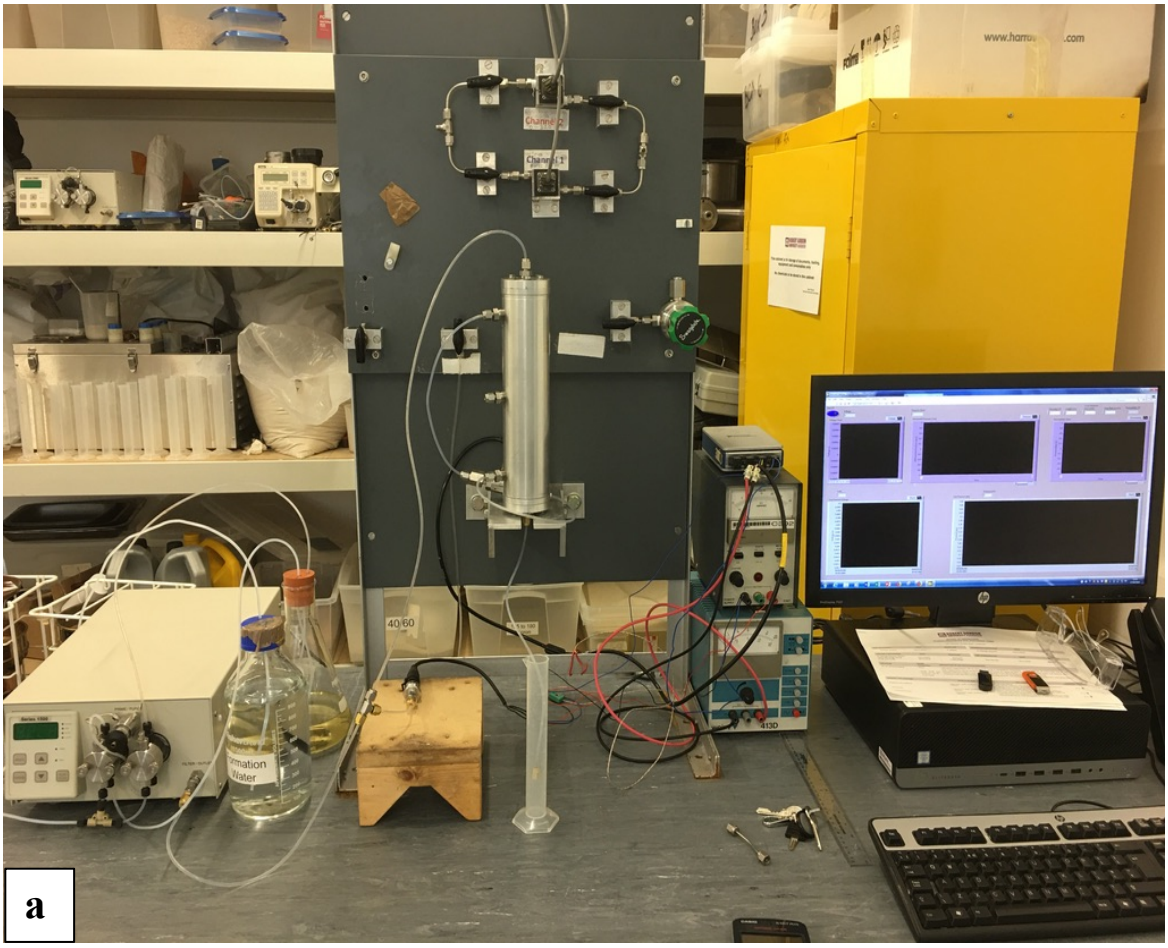

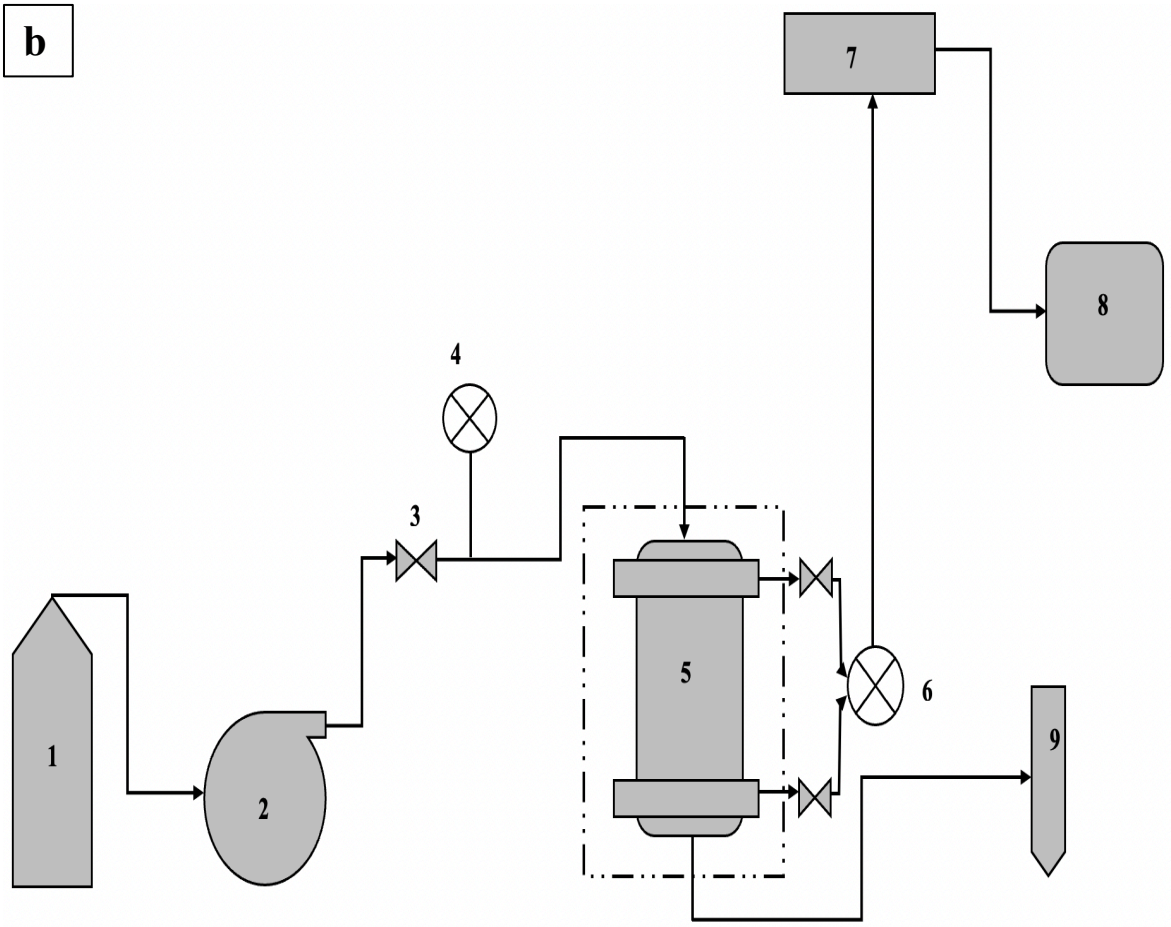

***Figure 4.2**: (a) Pictorial representation of the core flooding setup (b) Diagrammatic representation of the core flooding apparatus. 1) pump fluid, 2) pump, 3) valves, 4) pressure gauge, 5) core holder with sand pack, 6) pressure transducer, 7) NIDAQ data logger, 8) desktop computer, 9) effluent sample collector (test tubes). The dashed line – temp control.*

The description of the various vital components in the dynamic flow system is given in detail below:

a) **Flow Lines and Valves**: These lines and valves were set up to minimise dead volumes in which polymer solutions can be lost.

b) **Oven Cabinet**: This was an optional component of the flow system. This component became functional only when the temperature effect on the test core (sand packed medium) was to be studied.

c) **Stainless Steel Core Holder**: This was used to hold the silica sand and simulate the linear flow of polymer solutions during core flooding. The dimensions of the core-holder are a length of 10 cm, a diameter of 5.1 cm and a thickness of 1.9 cm. The core-holder was constructed with aluminium due to its lightweight (2.7 g/cm^3) and thermal conductivity (205 W/m-K) coupled with the corrosion-resistant nature of the aluminium metal.

d) **Dual Head Syringe Pump (Model HPLC 1500)**: This was used to deliver a predefined and varying volume of solutions at a constant flow rate across the core holder. The pump was made of stainless steel fitted with two 50 cm^3 pump heads that can run at a wide range of flow rates from 0.00167 to 1.67 cm^3 with 0.001 cm^3 increments and pressure range of 0 - 68.046 atm.

e) **Pressure Transducers**: This transducer was mounted across the core holder with its capacity chosen according to the requirements of the measurement resolution. Pressure monitoring was achieved using a Micro-Machined Silicon Wet/Wet Differential Pressure Transducer supplied by Omega with measurements recorded electronically through the aid of a high-speed National Instruments Data Acquisition System (NIDAQ) NI 9212. The differential pressure transducer ranges from 0 - 1.02 atm with an excitation voltage of 10 V DC supplied by a Weir 413D power supply. The transducer can operate within a temperature range of between -45 to 121°C.

f) **Data Acquisition System**: This was provided using a high-speed National Instruments Data Acquisition System (NIDAQ). This ensures that pressure monitoring and measurements from connected transducers were digitised and logged to a personal computer.

g) **Line Pressure Gauge:** A line pressure gauge was inserted at the outlet of the syringe pump. This gauge was necessary to monitor inlet pressure to the core holder and avoid over-pressurising the transducers.

4.2.2.2. Flow Leakage Test and Pressure Transducer Calibration

A flow leakage test and pressure transducer calibration were carried out before the start of core flooding experiments. The flow leakage test was done to maintain the integrity of the flow rig system, and the calibration of the pressure transducer was done to preserve its accuracy.

Materials and Apparatus

a) Druck DPI model 615 IS pressure calibrator.
b) LEAK-TEC detergent.
c) Flow system.

Experimental Procedure for Flow Leakage Test

a) The pressure calibrator was connected to the flow rig, and air pressure of 50 psi was applied and held for 5 minutes.
b) When there is a drop in the applied air pressure, it indicates leakage in the flow system.

c) Detection of the leak point was done by applying a solution of the LEAK-TEC detergent and look out for the formation of bubbles.
d) In the event of bubble formation, the fittings around it are tightened, and the steps (a), (b) and (c) were repeated until no drop in pressure was noticed.

Experimental Procedure for Pressure Transducer Calibration

a) The pressure transducer was positioned in the flow system in the orientation it is to be applied.
b) The electrical input was connected to the Druck DPI model 615 IS pressure calibrator, and the input signal was set to the minimum value of the range being used.
c) Once the appropriate supply pressure and input signals were set, the transducer's calibration began, and the output pressure was observed.
d) The pressure output was adjusted until reaching the minimum value while at a minimum electrical signal.
e) The electrical input signal was increased to its maximum value, and the output pressure was observed and adjusted where necessary until reaching maximum output pressure.

4.2.2.3. Determination of Brine Absolute Permeability, k_b

The absolute permeability of the silica sand to brine was determined using the flow system described in section 4.2.2.

Materials and Apparatus

a) Top loading laboratory weighing balance (maximum load: 2000 g; sensitivity: 0.01 g).
b) Disaggregated commercial silica sands (40/60 mesh size).
c) Edwards vacuum pump (Model ED50)
d) Dynamic Flow system.
e) Synthetic formation brine.

Experimental Procedure for the Determination of Brine Absolute Permeability

a) Silica sand was introduced into the core holder using the *"Dry-Packing Technique",* where sand grains were introduced through a funnel into the core holder.
b) When the sand grains had evenly dispersed and reached the desired level in the core holder, the flow of sand is stopped.
c) Shaking using the previously described mechanical shaker and tapping of the core holder continued for a given period until there was a complete settling of the sand grains in the core holder.

d) Two 180 μm screens were placed on both ends of the core-holder to act as fluid distributors and contain the core holder's sand without disrupting the fluid passage.
e) The core holder was mounted back into the flow system and placed under a vacuum pump to remove the air present. The presence of air/gas would reduce the brine permeability.
f) The prepared synthetic brine was injected through the sand pack starting at low flow rates and increased to moderate flow rates. Excessive flow rates were avoided to prevent sand fines migration or sand re-distribution with the core holder.
g) The pressure differentials were noted for different flow rates after steady-state conditions were attained.
h) The absolute permeability to brine, k_b was determined using Darcy's equation (4.13) by plotting the brine flow rate, Q_b (ranging from 0 to 12 mL/min) against the differential pressure, ΔP. This gave a straight line through the origin with slope, $\left(\frac{k_b A}{\mu_{app} L}\right)$ and no intercept.

$$Q_b = \left(\frac{k_b A}{\mu_{app} L}\right) \Delta P \qquad (4.13)$$

The apparent viscosity of the brine is μ_{app}, A is the internal cross-sectional area of the core holder (22.06 cm^2), and L is the length of the core holder (12 cm).

4.3. Determination of Polymer Retention

Experimental determination of the polymer retention was carried out (using API recommended practice for evaluation of polymer retention) in validating the various predictive or calculated outcomes for the quantification of polymer aggregates lost and the corresponding hydrophobic interactions lost due to the various polymer retention mechanisms (adsorption and entrapment) that exist in the porous media.

4.3.1. Experimental Static Retention Test

The static retention test can provide a preliminary screening of polymers. The tests are inexpensive and straightforward compared to procedures involving flow in cores. It is possible to hold the adsorbent constant for a series of tests, thereby isolating the polymer solution's changing properties.

Materials and Apparatus

a) Top loading laboratory weighing balance (maximum load: 2000 g; sensitivity: 0.01 g).
b) Disaggregated commercial silica sands (40/60 mesh size).

c) Glass conical funnel, 500 mL sample bottles and 10-micron filter papers.

d) Ubbelohde Viscometer, 5 mL Syringe container, stopwatch.

e) Polymer concentrations: 10, 50, 100, 300, 500, 750, and 1000 ppm.

Preparation of Samples for Static Retention

a) Dry silica sand (100 g) was weighed and poured into the sample bottles. Each sample bottle was labelled for each polymer concentration to be studied.

b) Aqueous polymer solutions (50 g) were added to each sample bottle for each polymer concentrations.

c) The bottles were capped and stored at representative temperatures for 4 days. The bottles were agitated along with their content periodically to maintain good contact between liquid and substrate.

d) The liquid was separated from the silica sands by filtering through a 10-micron filter paper.

Determination of Viscosity using Ubbelohde Viscometer

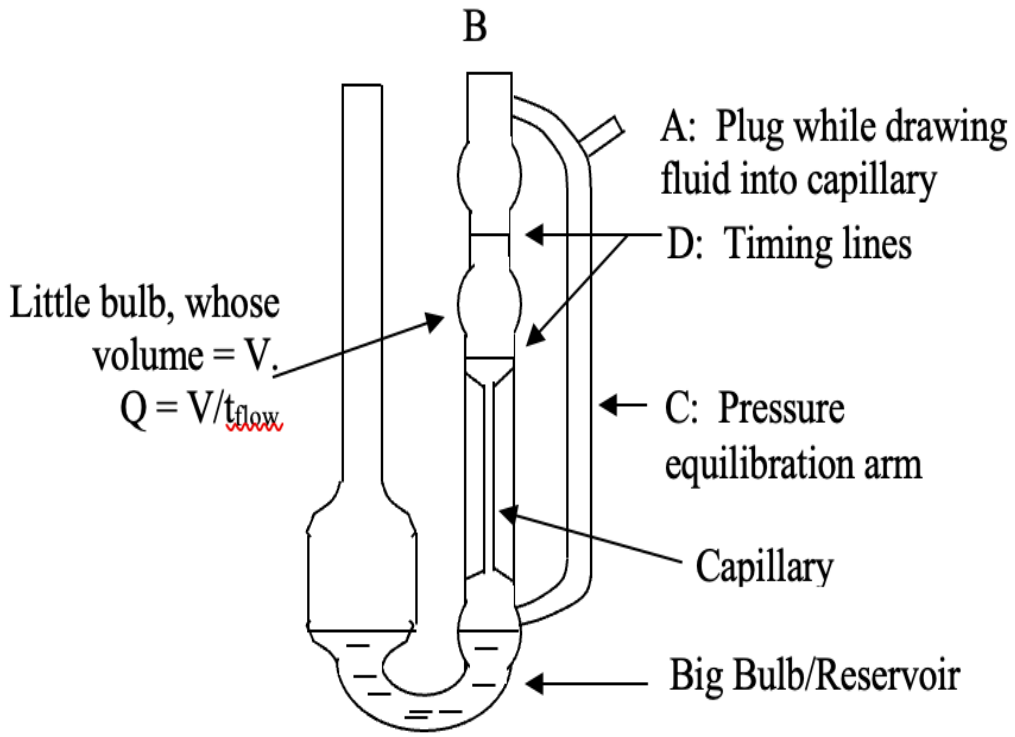

Figure 4.3*: Diagrammatic representation of the Ubbelohde viscometer used for this study*

a) The thermal control unit of the water bath was used to regulate the temperature of the content of the viscometer to the desired temperature of 25±0.05 ℃.

b) Determination of solvent (deionised water) flow time, t_{slv} in viscometer represented in Figure 4.3 was carried out as follow:

- The viscometer was loaded with solvent and placed in the temperature regulating bath and allowed to stand for about 10 min for equilibration.
- Most of the fluid resides in the big bulb and drawn up through the capillary by placing a finger over orifice "A" and applying suction (using a bulb) to orifice "B" (The air pressure keeps the fluid from rising into the pressure equilibration arm, "C").
- After the fluid has passed both indicator lines, "D", the suction from "B" was released while maintaining orifice "A" closed. The time it took for the solvent to pass through the indicator lines was noted. Afterwards, orifice "A" was released too. What little fluid had worked its way into the pressure equilibration arm "C" should quickly flow back to the reservoir, leaving the liquid in the capillary and top bulbs suspended.

c) The above determination was repeated at least 2 times until no more than 0.2 s deviation was found.

d) The viscometer was drained of any solvent and dry thoroughly using a vacuum oven.

e) A known volume of the polymer solution was transferred into the viscometer and allow to stand for 10 min for temperature equilibration.

f) The solution flow time, t_{sol} as an average was measured using the step (b) (If the solution flow time exceeds the flow time of the pure solvent by a factor of 2-5 then the result obtained is good or the viscometer was emptied, and the initial concentration was adjusted accordingly).

g) The solution flow time measurements were repeated until the standard deviation was < 0.2 s.

h) The polymer viscosity, μ_p was calculated as $\mu_p = (t_{sol}/t_{slv})\mu_w$.

Preparation of Standard Curve

a) 500 ppm of the stock solution of the appropriate polymer with identical composition to the unknown was prepared.

b) Standard solutions were prepared from the 500 ppm stock solution by diluting with brine to obtain concentrations of 0 to 500 ppm in 50 ppm increments.

c) The relative viscosity, μ_{rel} of the polymer solutions were computed from the solution flow times using the Ubbelohde viscometer, and $\ln(\mu_{rel})/C_p$was calculated for each polymer concentration.

d) The temperature of the polymer solutions was kept at 25 ℃ by circulating water on the outer jacket of the viscometer cup containing the solution using the Medline Refrigerating & Heating Bath Circulator for the temperature control.

e) The values of $\ln(\mu_{rel})/C_p$ as a function of the polymer concentration, C_p was plotted. A linear model was fitted to the plot via regression analysis, and a standard curve was obtained.

Determination of Residual Polymer Concentration from Standard Curve

a) For polymer samples with a concentration above 300 ppm, these were diluted to approximately 250 ppm with brine of the same composition. The dilution factor was calculated using equation (4.14).

$$\text{Dilution Factor (DF)} = \frac{\text{Mass of Diluted Sample (g)}}{\text{Mass of Initial Sample (g)}} \quad (4.14)$$

b) The final sample concentrations, $C_{p,f}$ were found by direct comparison of the sample relative viscosity, μ_{rel} with the standard curve obtained. These comparisons considered dilutions, which may have been necessary to reduce the sample concentrations to less than 300 ppm.

Procedure for Estimating Static Polymer Retention

a) Static polymer retention was calculated using equation (4.15):

$$\Gamma_{stat} = \frac{W_p(C_{p,i} - C_{p,f})}{W_{gr}} \quad (4.15)$$

Where W_p is the mass of polymer solution (g), W_{gr} is the mass of sand material (g), $C_{p,i}$ and $C_{p,f}$ are the initial and final polymer concentration respectively (ppm).

b) Estimation of static retention was also carried out for different polymer concentrations, and this was plotted against the concentration.

4.3.2. Experimental Dynamic Retention Test

The dynamic retention test is probably the most rigorous in determining the polymer loss; it is also the most time-consuming and probably requires the most analyses. However, this method also yields the inaccessible pore volume for a particular set of conditions, whereas the static retention test does not.

Materials and Apparatus

The materials and apparatus are like Section 4.2.2.3 with the inclusion of the following:

a) Ubbelohde Viscometer, 5 mL Syringe container, stopwatch.

b) Polymer concentrations: 10, 50, 100, 300, 500, 750, and 1000 ppm.

Experimental Procedure for Preparation of Core

a) The empty core holder was cleaned and dried, after which the dimensions of the core holder was measured.
b) Silica sand was introduced into the core holder using the *"Dry-Packing Technique"* where sand grains were introduced through a funnel into the core holder.
c) When the sand grains had evenly dispersed and reached the desired level in the core holder, the flow of sand is stopped.
d) Shaking and tapping of the core holder continued for a given period until there was a complete settling of the sand grains.
e) Two 180 µm screens were placed on both ends of the core holder to act as fluid distributors and contain the core holder's sand without disrupting fluid passage.
f) The core holder was mounted back into the flow system and placed under a vacuum pump to remove the air present. The presence of air/gas would manifest in higher permeability.
g) The core holder was evaluated for leakage using the procedure described in section 4.2.2.2.
h) The pore volume and permeability to brine of the sand pack was determined using the approaches described in Section 4.2.1.3 and 4.2.2.3.

Experimental Procedure for Preparation of Polymer Solutions

Selected polymer concentrations were prepared using the standard procedures described in Section 4.1.2.2.

Experimental Procedure for Polymer Injection

a) The pump in the flow system was set to the required injection rate, and synthetic brine was injected until the pressure stabilized.
b) Polymer injection of the desired concentration (**first polymer bank**) was started at the same flow rate until the pressure stabilized.
c) Effluent polymer cuts from the dynamic flow system were collected at regular time intervals in test tubes and marked to record events of the fluid and rate changes where necessary.
d) The pump rate was changed if different injection velocities are required and maintained until pressure again stabilizes. This sequence was continued until sufficient data was collected for the polymer concentration.

e) The pump was switched to brine using the same pump rate as the final polymer injection rate. This injection of brine was continued until pressure was stabilized and the presence of polymer is undetectable.

f) Steps (a) – (e) were repeated for a **second polymer bank to obtain polymer retention isotherms.**

g) The various steps from (a) to (f) were repeated for increasing polymer concentrations up to the maximum value considered in this work.

Determination of Effluent Polymer Concentration from Standard Curve

The effluent polymer concentration was determined by matching polymer relative viscosities to a standard concentration curve for the polymer solution. Details of this approach are contained in Section 4.3.1.

Calculation Procedure for Dynamic Retention and Inaccessible Pore Volume

a) The effluent polymer, $C_{p-eff-1}$ (relative to the injected concentrations, C_{p-inj}) was plotted against injected pore volumes, PV for the first polymer bank.

b) Similarly, the effluent polymer, $C_{p-eff-2}$ (relative to the injected concentrations, C_{p-inj}) was plotted against injected pore volumes, PV for the second polymer bank.

c) The inaccessible, I_{PV} was estimated from the cut off value of the normalized concentration at 0.5. This is given in equation (4.16) below:

$$I_{PV} = 1 - PV_{\frac{C_{p-eff-2}}{C_{p-inj}}=0.5} \quad (4.16)$$

d) Dynamic polymer retention (or adsorption), Γ_{dyn} was calculated as the area between the two plots of polymer concentration breakout curves. This is expressed in equation (4.17) below:

$$\Gamma_{dyn} = \left(\left\{\sum\left[\frac{C_{p-eff-2}\Delta PV}{C_{p-inj}} - \frac{C_{p-eff-1}\Delta PV}{C_{p-inj}}\right]\right\}\right)\frac{C_{p-inj}PV}{M_{gr}} \quad (4.17)$$

Where ΔPV is the incremental pore volume (the volume of each produced fraction of relative concentration $\frac{C_{p-eff}}{C_{p-inj}}$, and M_{gr} is the mass of the sand pack in the core holder.

e) The estimated polymer retention values were plotted against the polymer concentration values.

4.3.3. Correlating Static to Dynamic Retention and Damaged Pore Volume

The mapping of the static retention test to the dynamic retention test was done to achieve the following:

a) A first-order approximation of static to dynamic adsorption based on equal solid-liquid ratio and retention time.
b) A modified experimental approach for validating the novel equation developed in Chapter 3 for estimating the fractional damaged pore volume (DPV).

The various procedures defined previously for the quantification of static and dynamic retention were employed for this purpose. However, the only adjustment was to ensure that the solid-liquid ratio and retention time was the same. This represents a novel experimental approach that has not been reported in the literature.

Materials and Apparatus

a) Dynamic flow system, absorbance detector.
b) Top loading laboratory weighing balance (maximum load: 2000 g; sensitivity: 0.01 g).
c) Disaggregated commercial silica sands (40/60 mesh size).
d) Glass conical funnel, 500 mL sample bottles and 10-micron filter papers.
e) Ubbelohde Viscometer, 5 mL Syringe container, stopwatch.
f) Polymer concentrations: 10, 50, 100, 300, 500, 750, and 1000 ppm.

Procedure for Mapping Static to Dynamic Retention and Estimation of DPV

a) Static retention tests were conducted using the procedure set out in 4.3.1. for different polymer concentrations. This was done, ensuring that the solid to liquid ratio (volume of sand to the volume of the polymer solution was maintained at 1:2).
b) The volume of the core-holder defined the volume of sand employed. For each polymer concentration, they were contacted with 1 core-holder full of silica sand (1PV = 96.4 cm^3).
c) Plots of polymer retained during the static process against time were obtained for each concentration to estimate the time, $t_{max-ret}$ at which maximum retention was obtained.
d) The equivalent number of injected pore volumes, PV_{inj} during dynamic retention test required for the same solid to liquid ratio and retention time obtained during the static retention test is estimated from equation (4.18) below:

$$PV_{inj} = \frac{Q_{inj} t_{max-ret}}{96.4} \quad (4.18)$$

Where Q_{inj} is the injected flowrate. The flow rates considered in this study were 1, 3 and 6 mL/min.

e) The dynamic retention test was estimated with the procedure described in 4.3.2. The DPV (Γ_{DPV}) was estimated using equation (4.19):

$$\Gamma_{DPV} = \frac{\Gamma_{dyn}}{\Gamma_{stat}} \quad (4.19)$$

This was related to the damaged porosity, ϕ_d using (4.20)

$$\frac{\Gamma_{dyn}}{\Gamma_{sta}} = \frac{V_{dp}}{V_{po}} = \left[1 - \frac{\phi_d}{\phi_o}\right] \quad (4.20)$$

Where V_{dp} is the damaged pore volume, V_{po} is the pore volume and ϕ_o is the actual porosity of the medium before polymer retention.

A typical output from the correlation of the static to dynamic retention is shown in Figure 4.4 below. The mapping of the various retention mechanisms was done as follows:

a) **Mapping Adsorption**: adsorption is a function of the polymer contact time with the pore surface and polymer concentration.

b) **Mapping Polymer Entrapment**: entrapment is a function of the flow condition and polymer concentration in the porous media.

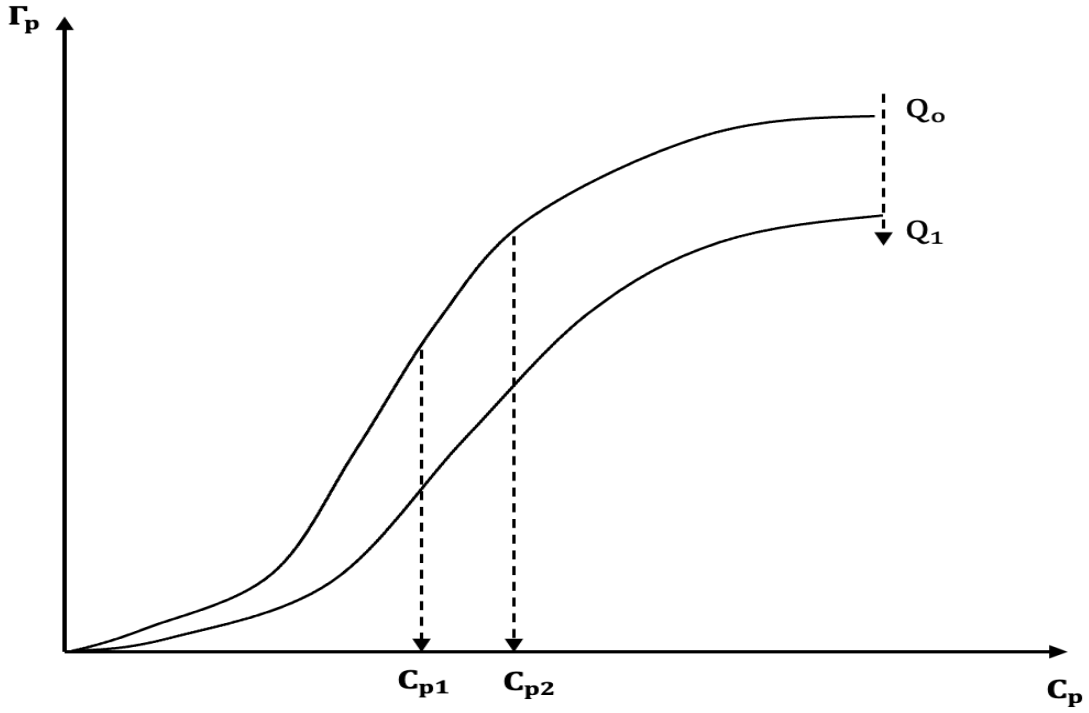

Figure 4.4*: Typical plot of polymer retention against concentration for static condition at Q_o and the correlated dynamic condition at flowrate Q_1.*

The rate-dependent entrapment, Γ_{ent} of polymer molecules was estimated using equation (4.21), and this encompasses the area created by the vertical decrease in adsorption from Q_o to Q_1 as shown in Figure 4.4.

$$\Gamma_{ent} = \sum \left[\left(\frac{\Gamma_p \Delta C_p}{C_p} \right)_{Q_o} - \left(\frac{\Gamma_p \Delta C_p}{C_p} \right)_{Q_1} \right] \quad (4.21)$$

Where Γ_p is the estimated retention as computed using effluent concentration analysis, C_p is the polymer concentration, Q_o refers to static retention condition (zero flow condition), Q_1 is the dynamic flow condition in the porous media, ΔC_p is the incremental polymer

concentration. The concentration-dependent entrapment of polymer molecules was computed using equation (4.22), and this signifies the increase in polymer concentration from C_{p_1} to C_{p_2} in Figure 4.4.

$$\Gamma_{ent} = \sum\left[\left(\frac{\Gamma_p \Delta C_p}{C_{p_2}}\right)_{Q_o} - \left(\frac{\Gamma_p \Delta C_p}{C_{p_2}}\right)_{Q_1}\right] - \sum\left[\left(\frac{\Gamma_p \Delta C_p}{C_{p_1}}\right)_{Q_o} - \left(\frac{\Gamma_p \Delta C_p}{C_{p_1}}\right)_{Q_1}\right] \qquad (4.22)$$

A summary of the modified experimental procedure is given in the flow diagram in Figure 4.5 below.

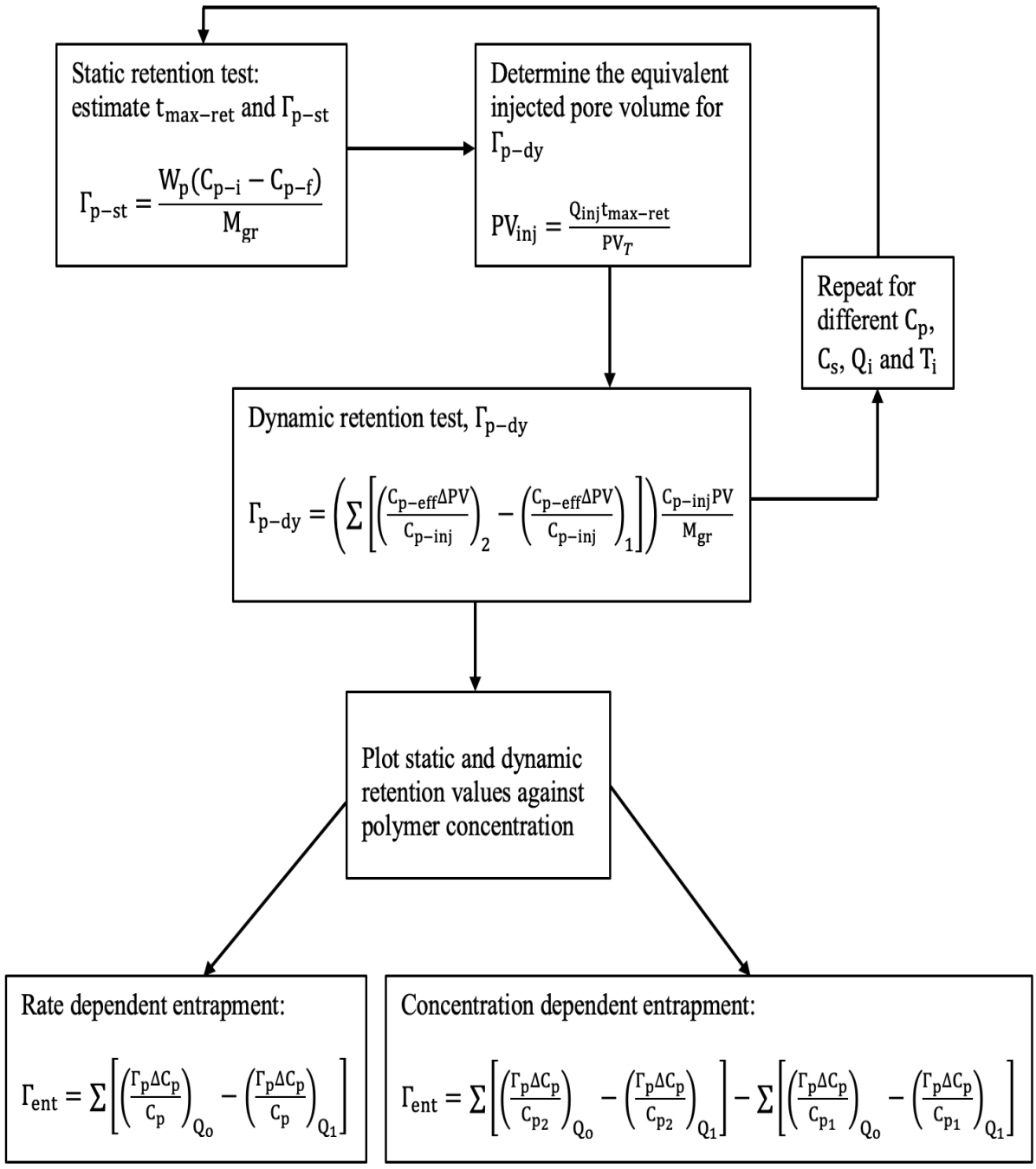

Figure 4.5*: A simplified flow diagram of the modified experimental approach which allows for the mapping of adsorption and entrapment mechanisms.*

4.4. Experimental Determination of Polymer Viscosity and Degradation

This section details the approach used in the estimation of the effective polymer viscosity and degradation. In addition, this approach was applied in the study of the propagation of hydrophobic interactions in a porous media.

4.4.1. Effective Polymer Viscosity and Hydrophobic Interactions

An experimental procedure was developed to quantify the proportion of residual hydrophobic interactions after injecting the polymer solution through a porous media. This was modified from the API specification for the evaluation of oilfield polymers.

Materials and Apparatus

a) Dynamic flow system.
b) Disaggregated commercial silica sands (40/60 mesh size).
c) Polymer concentrations: 10, 50, 100, 300, 500, 750, and 1000 ppm.

Experimental Procedure for the Estimation of Viscosity and Hydrophobic Interactions

a) Preparation of the polymer solutions and sand-packed media followed the procedures described in Sections 4.1.2.3 and 4.2.2 respectively.
b) The sand-packed media was flooded with 2.45 %TDS brine using the HPLC pump at different flow rates (1, 3, 6, 8, 10 and 11 mL/min) and the steady-state pressure drop, ΔP_{wo} noted for each flow rate.
c) After the imbibition process, the polymer solutions were injected at different flow rates (1, 3, 6, 8, 10 and 11 mL/min) and the steady-state pressure drop, ΔP_p was noted for each flow rate.
d) The polymer resistance factor (RF) was estimated using (4.23).

$$RF = \frac{\Delta P_p}{\Delta P_{wo}} \quad (4.23)$$

e) After the drainage process, brine solution (2.45 %TDS) was injected into the sand-packed media at the different flow rates considered (1, 3, 6, 8, 10 and 11 mL/min) and the steady-state pressure drop, ΔP_w was noted for each flow rate.
f) The polymer residual resistance factor (RRF) was estimated by comparing ΔP_w and ΔP_{wo} using (4.24).

$$RRF = \frac{\Delta P_w}{\Delta P_{wo}} \quad (4.24)$$

g) The effective viscosity, μ_{pe} of the polymer solution in the porous media was calculated using equation (4.25)

$$\mu_{pe} = \frac{RF}{RRF}\mu_s \quad \text{or} \quad \mu_{pe} = \frac{PV_{pb}}{PV_{bb}}\mu_s \tag{4.25}$$

Where μ_s is the viscosity of the brine solution, PV_{pb} and PV_{bb} is the number of pore volumes to breakthrough in the porous media for the polymer and brine solutions respectively.

h) The in-situ hydrophobic interactions were estimated using the normalised reduced viscosity (N_{RV}) developed in Chapter 3 and shown in equation (4.26)

$$N_{RV} = \frac{\mu_{pe} - \mu_{ag}}{\mu_{po} - \mu_s} \tag{4.26}$$

Where μ_{ag} is the polymer viscosity at the critical aggregation concentration, C_{ag} and μ_{po} is the pre-injection polymer viscosity.

4.4.2. Polymer Degradation Test

Materials and Apparatus

a) Dynamic flow system.
b) Disaggregated commercial silica sands (40/60 mesh size).
c) 500mL measuring cylinders, 500 mL beakers and 10-micron filter papers.
d) Polymer concentrations: 10, 50, 100, 300, 500, 750, and 1000 ppm.
e) The Fann Viscometer (Model 35A/SR-12) with pre-set rates: 600, 300, 200, 180, 100, 90, 60, 30, 6, 3, 1.8, 0.9 RPM.

Procedure for Evaluation of Polymer Degradation

a) Preparation of the polymer solutions and sand-packed media followed the procedures described in Sections 4.1.2.3 and 4.2.2 respectively.
b) The sand-packed media was flooded with 2.45 %TDS brine solution using the HPLC pump until 100 % brine saturation was achieved (approximately 45 minutes).
c) Polymer solutions were injected at different flow rates up to the maximum (30 mL/min) until steady-state pressure drop was achieved for each flow rate.
d) At stable differential pressure for each flow rate, 350 ml of effluent polymer solutions were collected for each polymer concentration for rheological analysis.
e) The effluent viscosity, μ_{eff} was determined using the Fann Viscometer (Model 35A/SR-12) at lowest shear condition (0.9 RPM) representative of zero shear rate, and the normalized effluent viscosity (N_{EV}) was computed using equation (4.27)

$$N_{EV} = \frac{\mu_{eff} - \mu_s}{\mu_{po} - \mu_s} \tag{4.27}$$

f) The normalized effluent viscosity was plotted against the values of the flow rates, Q considered. Equation (4.28) was fitted to the plots via regression analysis to determine the flow rate, Q_{dg} at the onset of polymer degradation.

$$N_{EV} = \left[1 + \left(\frac{Q}{Q_{dg}}\right)^2\right]^{-m/2} \quad (4.28)$$

Where m is a fitting parameter.

g) The equivalent critical shear rate for the onset of mechanical degradation, γ_{dg} was estimated using equation (4.29)

$$\gamma_{dg} = \frac{4\alpha Q_{dg}}{A\sqrt{8k\phi}} \quad (4.29)$$

Where ϕ is the porosity of the sand-packed media, k is the permeability of the medium, A is the cross-sectional area, and α is a dimensionless parameter.

4.5. Summary

In this chapter, a summary of the experimental procedures adopted in the study of associative polymers in porous media and validation of the predictive approach developed in chapter three were given. The various procedures were detailed according to the API specification for the analysis of oilfield polymers. In addition, a modified experimental approach for the estimation of rate and concentration-dependent polymer retention in porous media was developed. This was based on an accurate correlation of static to dynamic retention, which allowed for the corresponding mapping of the various retention mechanisms using well-established trends in literature. The unique outcome of the modified experimental procedure was the appropriate quantification of polymer adsorption in addition to the entrapment. This is significant compared to using a dynamic retention test that does not uniquely define the various retention mechanisms while giving a generalized outcome regarding incremental retention values. Consequently, proper economic planning and experimental evaluation of computational forecasting of the performance of polymers during chemical enhanced oil recovery operations can be made with the developed experimental approach.

CHAPTER FIVE

5.0. Material Characterisation and Properties

This chapter focussed on the characterisation of the polymer and sand materials along with the discussion on the observed trends and their likely implications for the propagation of hydrophobic interactions between associative polymers in a porous media.

5.1. Characterisation of the Polymer and Porous Media Material

The polymer and porous media material characterisation were done as a preliminary step before their application in the study of polymer transport in porous media. The characterisation study was intended to give the necessary insight into providing valuable explanation regarding the interaction between polymer and porous media material.

5.1.1. Associative Polymers

The characterization of the associative polymers was done to determine the functional group composition, molecular weight, and activity. The analysis reported in this section was on the solid polymer granules.

5.1.1.1. Molecular Weight and Intrinsic Viscosity of the Associative Polymers

The molecular weights and intrinsic viscosities of the associative polymers, D118 and C1205, were determined using simple capillary viscometry. The intrinsic viscosities were estimated by extrapolating to $C_p = 0$ from the plots of reduced viscosity, $ln(\mu_{rel})/C_p$ as a function of the polymer concentration, C_p as shown in Figure 5.1. Hence, the intercept of the plots corresponds to the intrinsic viscosities of the associative polymers. Therefore, the values for the intrinsic viscosities are 37.76 and 29.39 dL/g for polymers D118 and C1205 respectively. The intrinsic viscosity is a measure of the contribution of the polymer granules to its viscosity in solution. Consequently, careful observation of the intrinsic viscosities indicates that the granules of the D118 polymer would contribute more to the solution viscosity through hydrophobic interactions than the C1205 polymer type. As such, associative polymers with high intrinsic viscosities would provide solute particles with a high level of hydrophobic blocks on the polymer backbone. The molecular weights of the associative polymers were determined from the intrinsic viscosities using the Mark-Houwink equation in (4.8). Table 5.1 compares the estimated molecular weight of the

polymers with the manufacturers' range. From the relationship in (3.8), the molecular weight of an associative polymer is higher when the intrinsic viscosity is high.

***Table 5.1**: Comparison between the estimated polymer molecular weight and manufacturer range.*

Polymer Code	Intrinsic Viscosity (dL/g)	Molecular Weight (M_w)	Manufacturer's Specification (M_w)
D118	37.76	16.6 x 10^6 g/mol	16 – 20 x 10^6 g/mol
C1205	29.39	12.2 x 10^6 g/mol	12 – 17 x 10^6 g/mol

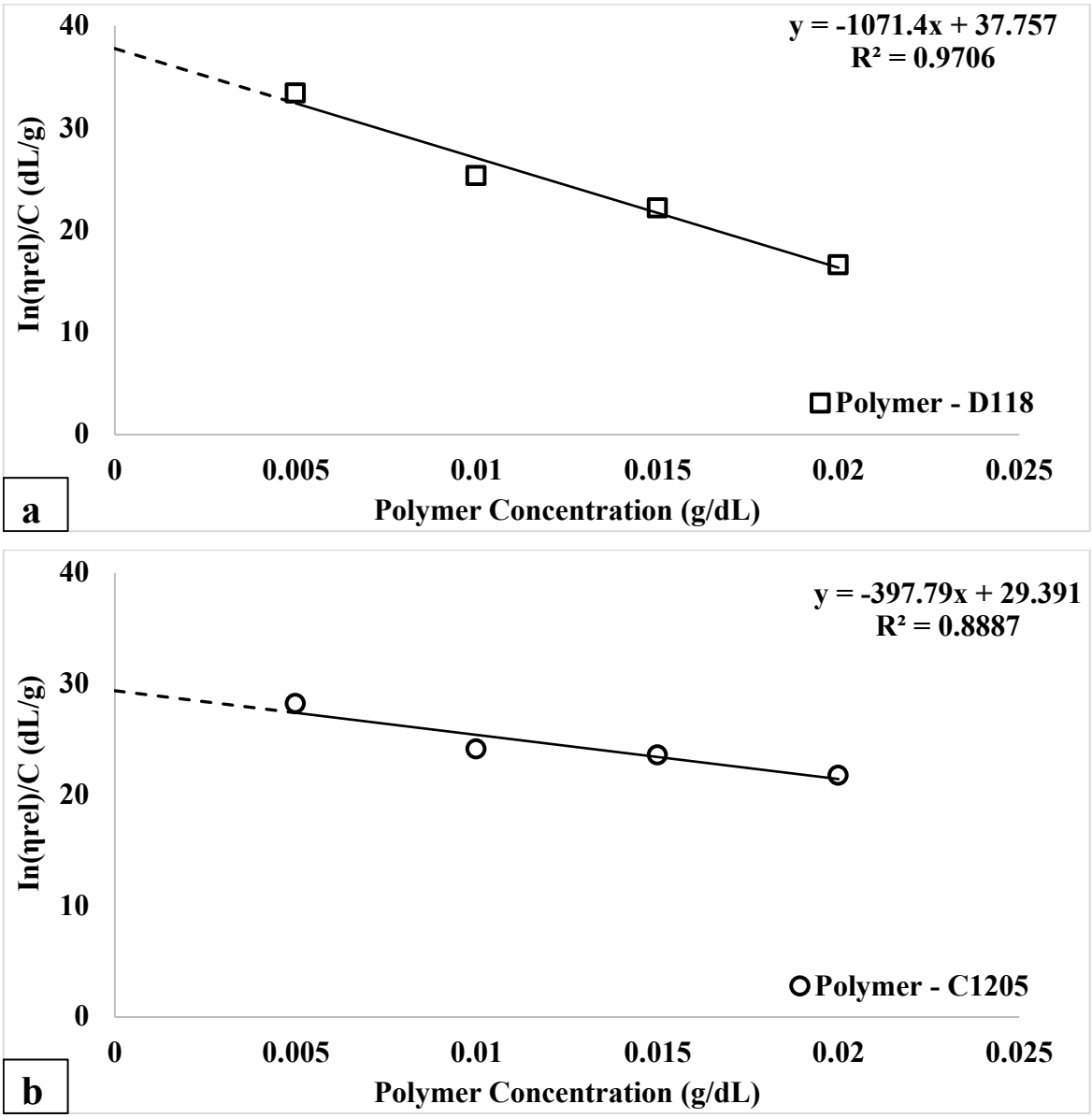

***Figure 5.1**: Plot of reduced viscosity against polymer concentration ($C_p < 500\ ppm$) at 25 ℃ and 3 wt.% NaCl (a) D118 and (b) C1205.*

5.1.1.2. Activity and Weight Loss of the Associative Polymers

The activity of polymer granules gives the percentage of active solids under different temperature conditions. Such a study provides an indicator of the ability of the associative polymers to withstand high reservoir temperatures. Therefore, the activity and weight loss curves for the two associative polymers (D118 and C1205) were obtained from their initial dry state respectively (Figure 5.2).

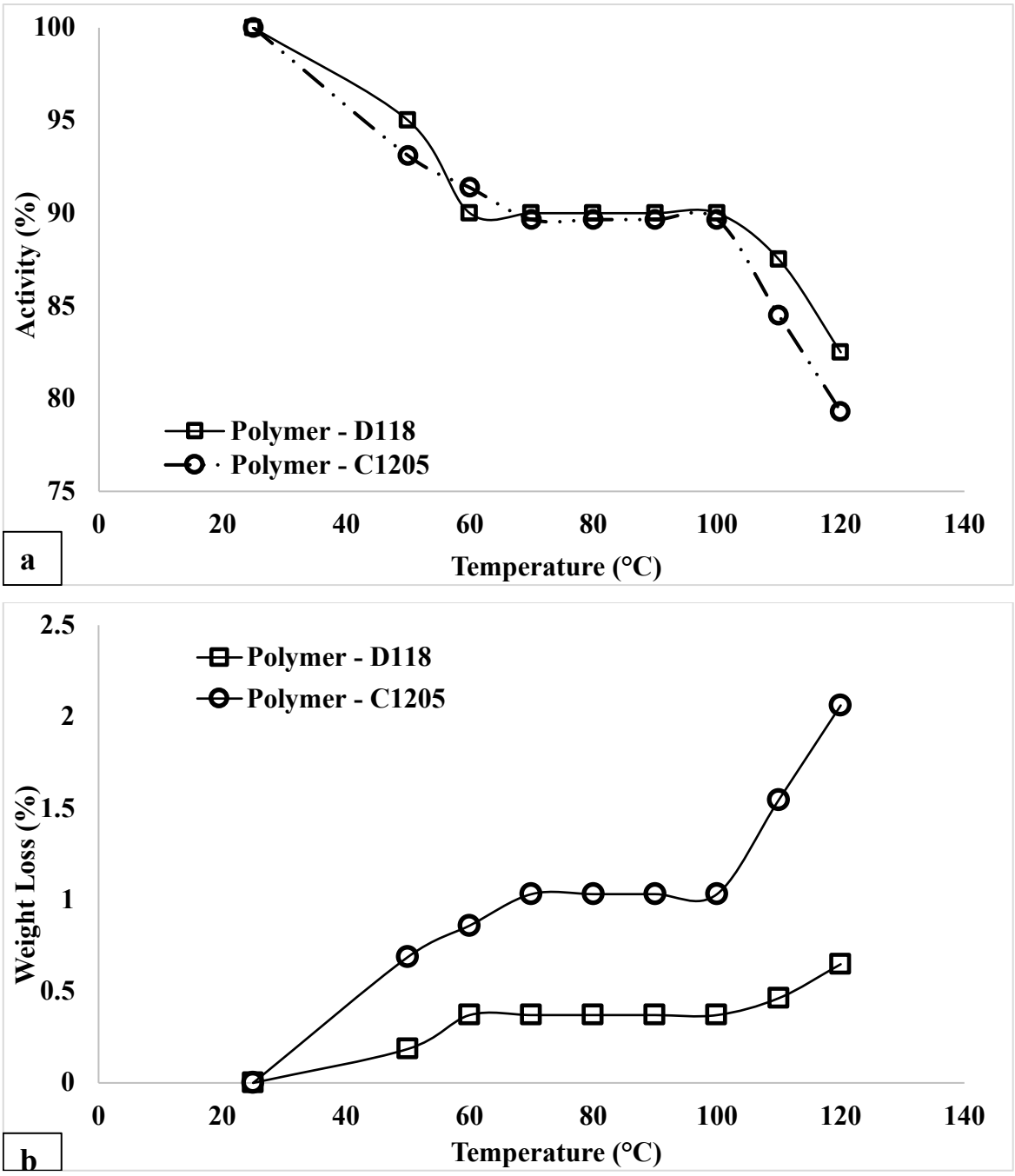

***Figure 5.2**: Plots of (a) activity and (b)weight loss for D118 and C1205 polymers respectively.*

From the weight loss curves, the amount of loss for both polymer samples were less than 3 wt.% at temperatures less than 120 ℃. Similarly, the activity curve for the polymer samples indicates that active solids were greater than 80 wt.% at temperatures less than 120 ℃. However, close observation of the curves indicated a two-stage decomposition of the associative polymer granules (D118 and C1205). These stages are 20 – 60 ℃ and 100 – 120 ℃ for D118 polymer while 20 – 70 ℃ and 100 – 120 ℃ for C1205 polymer respectively. The first-stage weight loss is related to the removal of water molecules, which are adsorbed on the surface of the polymer granules due to exposure to the atmosphere. These adsorbed water molecules can be likened to the bound water associated with the polymers. The equivalent water loss in both cases of polymers is 0.37 wt.% for D118 and 1.0 wt.% for C1205 respectively. The difference in weight loss may be credited to the difference in molecular architecture arising from different hydrophobic blocks on the polymer backbone. The second-stage weight loss can be explained in terms of depolymerisation and intermolecular dehydration reactions, which may lead to breaking any crosslinks between polymer chains. The equivalent weight loss in both cases of polymers is 0.27 wt.% for D118 and 1.03 wt.%for C1205 respectively. The application of polymers for oil and gas applications requires significant temperature stability because most polymeric materials tend to decompose (weight loss greater than 20 wt.%) significantly above 130 ℃. Therefore, the weight loss study suggests that the associative polymers have good thermal stability for reservoir temperatures up to 120 ℃, which is the temperature limit of the study. However, extrapolating the weight loss beyond 120 ℃ suggests that the associative polymers will remain stable up to temperatures of 200 ℃. The attendant weight loss at this temperature of 200 ℃ would still be less than 10 wt.%. The strength and distribution of the hydrophobic blocks of the polymer backbone play a significant role in the thermal stability of associative polymers.

5.1.1.3. Chemical Composition of the Associative Polymers

The active functional groups present in the associative polymers were analysed using the Fourier Transform Infrared (FTIR) and Raman spectroscopy. Figure 5.3 show the FTIR and Raman spectra for the associative polymer (D118). Analysis of the FTIR spectra in Figure 5.3a indicates that the polymers show peaks at 1399.16, 1545.73, 1653.73, 2913.07 and 3206.21 cm^{-1}. The peak at wavenumber 1653.73 cm^{-1} was assigned to the stretching vibrations of $C = O$ present in the amide group $-CONH_2$.

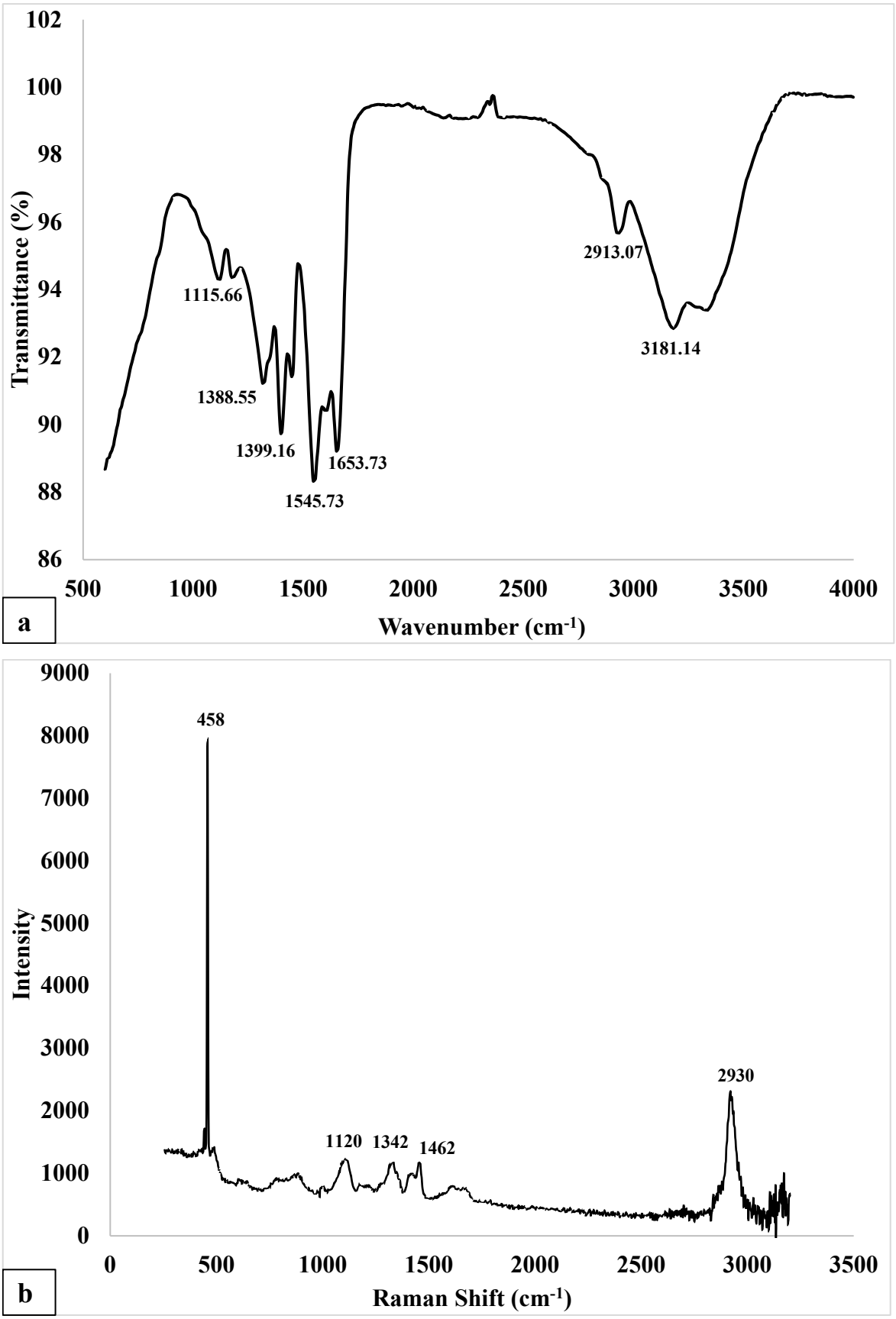

***Figure 5.3**: Compositional analysis of the associative polymers (a) FTIR spectra (b) Raman spectra.*

Furthermore, the peaks at wavenumbers, 2913.07 and 3181.14 cm^{-1} corresponds to the stretching vibration of $C-H$ in $-CH_3$ and $O-H$ in $-COOH$ respectively. The peaks at 1399.16 and 1545.73 cm^{-1} may indicate the presence of the $-SO_3$ group. Figure 5.3b shows the Raman spectra for the associative polymer. The strong peak at 458 and 2930 cm^{-1} indicate stretching vibrations arising from $S-S$ and $C-H$ respectively. This further validates the results obtained from the FTIR spectra regarding the presence of the functional groups $-CH_3$, $-SO_3$ and $-CONH_2$. The weak peak at 1120 cm^{-1} maybe due to the vibrational stretching of $C=S$. Similarly, the weak peak observed at 1342 cm^{-1} may correspond to $C-NO_2$ and the peak at 1462 cm^{-1} corresponds to δCH_2 and δCH_3 asym respectively. A summary of this spectra analysis and the corresponding functional groups identified is given in Table 5.2 below.

Table 5.2*: Summary of the identified peaks from the FTIR and RAMAN analysis and the corresponding functional groups.*

Peak (FTIR) cm^{-1}	**Peak (Raman) cm^{-1}**	**Functional Group**
1653.73	-	$-CONH_2$
2913.07	-	$-CH_3$
3181.14	-	$-COOH$
1399.16	-	$-SO_3$
1545.73	-	
-	458	$S-S$
-	2930	$C-H$
-	1120	$C=S$
-	1342	$C-NO_2$
-	1462	δCH_2, δCH_3

The FTIR and Raman spectroscopy combination has confirmed the presence of the functional groups $-CH_3$, $-SO_3$, $-COOH$ and $-CONH_2$. Therefore, the presence of the functional groups $-COOH$ and $-CONH_2$ may consequently explain the thickening ability of the associative polymers in solution. For non-associative polyacrylamide polymers, the repulsion between the carboxylate group, $-COOH$ and amide group, $-CONH_2$ would increase its hydrodynamic volume in solution hence, its viscosity. However, the scenario is different for hydrophobically associating polymer. In addition to the increase in hydrodynamic volume caused by the repulsion between the $-COOH$ and $-CONH_2$ groups, the repulsion of these groups exposes the hydrophobic blocks on the polymer chains to

intermolecular interactions. This phenomenon ensures that associative polymers show an enhanced thickening effect in solutions compared to non-associative polymers.

5.1.2. Silica Sands

The characterization of the silica sands was done to determine the mineralogical composition, structural configuration, and size distribution of the sand grains/particles. The analysis reported in this section was on the commercial silica sands.

5.1.2.1. Size Distribution of the Silica Sands

The particle size distribution (PSD) of the silica sands (40/60 and P230) are shown in Figure 5.4. The PSD is important in the understanding of the sand's physical and chemical properties (dataset of the sieve analysis is contained in Appendix A). The PSD plays an important role in the porosity and permeability of the prepared sand packs. For the 40/60 silica sand in Figure 5.4a, the mass mean diameter (MMD) or the D_{50} value was estimated as 350 μm. Thus, the average grain diameter for the 40/60 silica sand was estimated as 350 μm. In the case of P230 sand in Figure 5.4b, the D_{50} value was estimated as 250 μm hence, the grain size is 250 μm. The smaller grain size of the P230 sand compared to the 40/60 sand indicates that the P230 would have a tighter packing resulting in lower porosity and permeability than the 40/60 sand. The geometric standard deviation, σ_g for both sand types was estimated using equation (5.1) below:

$$\sigma_g = \frac{D_{84.13}}{D_{50}} \tag{5.1}$$

Where $D_{84.13}$ is the grain mass diameter at 84.13 % cumulative value. The values of σ_g for the 40/60 and P230 sands were 0.87 and 0.8 respectively. The geometric standard deviation describes how spread-out the various grain sizes are around the geometric mean. The value of σ_g was used in the computation of the relative standard deviation or degree of polydispersity, ϑ as shown in (5.2)

$$\vartheta = \frac{\sigma_g}{D_{50}} \tag{5.2}$$

The estimated degree of polydispersity for the 40/60 and P230 sand were 0.0024 and 0.0032 respectively. Since the degree of polydispersity values were less than 0.1, the sand grain particles in both cases were considered monodisperse. This means that the sand particles in both cases have the same size. The monodispersity of the sand grains implied that the porosity distribution of porous media prepared from such sands were uniform, thereby eliminating the prospect of heterogeneity.

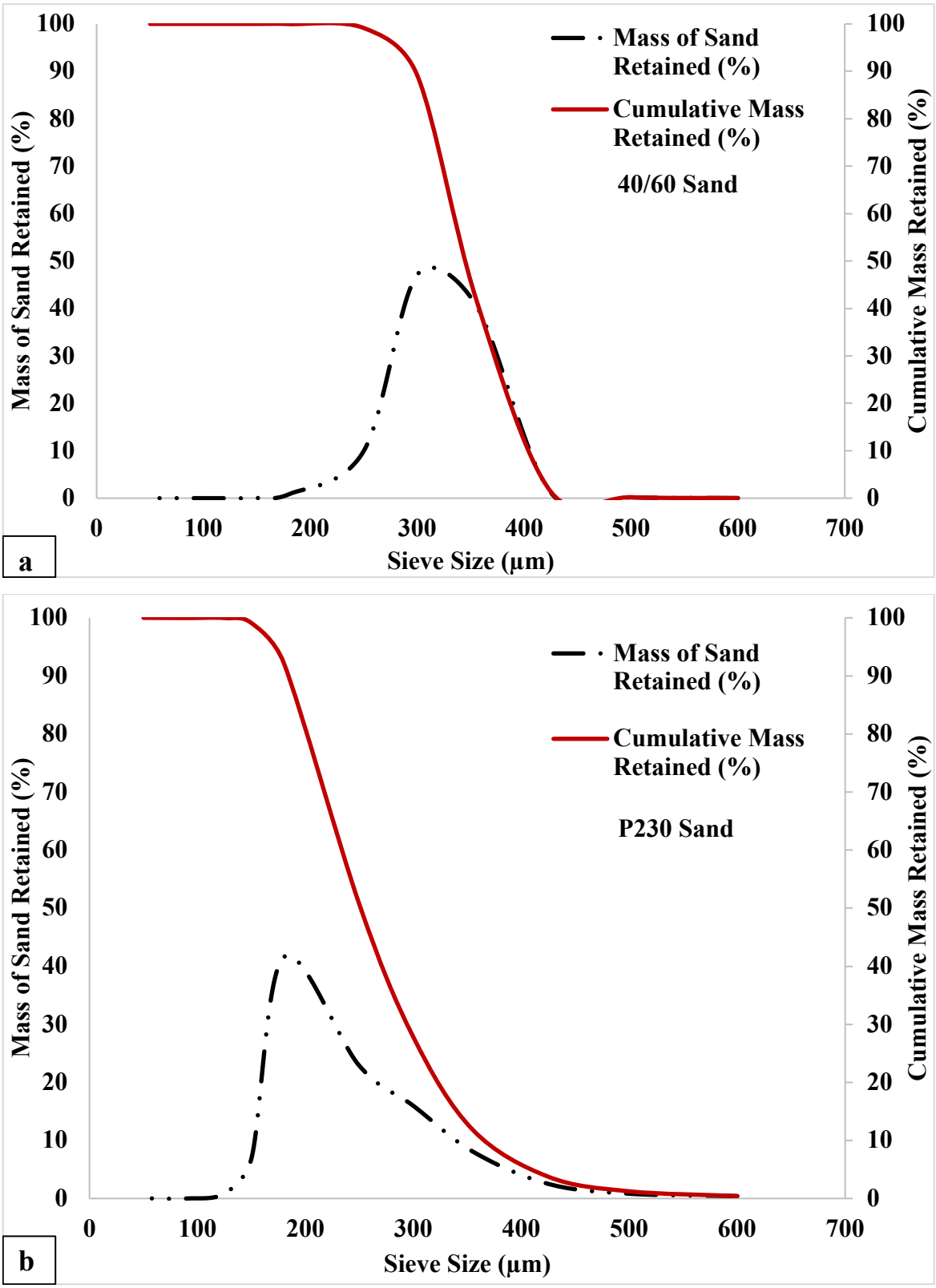

***Figure 5.4**: Particle size distribution of the studied sand grains (a) 40/60 sands (b) P230 sands.*

5.1.2.2. Topography and Surface Configuration of the Silica Sands

The study of the surface configuration of the sand grains was carried out using optical microscopy as captured in the high-resolution images in Figure 5.5. The images of the sand particles for both 40/60 and P230 indicate that the particle can be approximated as spherical. However, the P230 particles were observed not to be entirely spherical, with sharp edges noticeable. Furthermore, the image analysis also indicated that the sand particles are uncemented and unconsolidated with loose packing. Pictorially, the grains of the 40/60 sands were larger than the P230 sand and indicates that the specific surface of the 40/60 sand grains exposed to fluid flow within the pore space per unit pore volume was lower than the P230 sand grains. The consequence of the specific surface is that the sand grain with a large size (40/60) would provide a low surface area for polymer interaction. However, the P230 sand with a small size would give more surface exposure to polymer molecules, thereby increasing polymer interaction.

a. 40/60 Sand

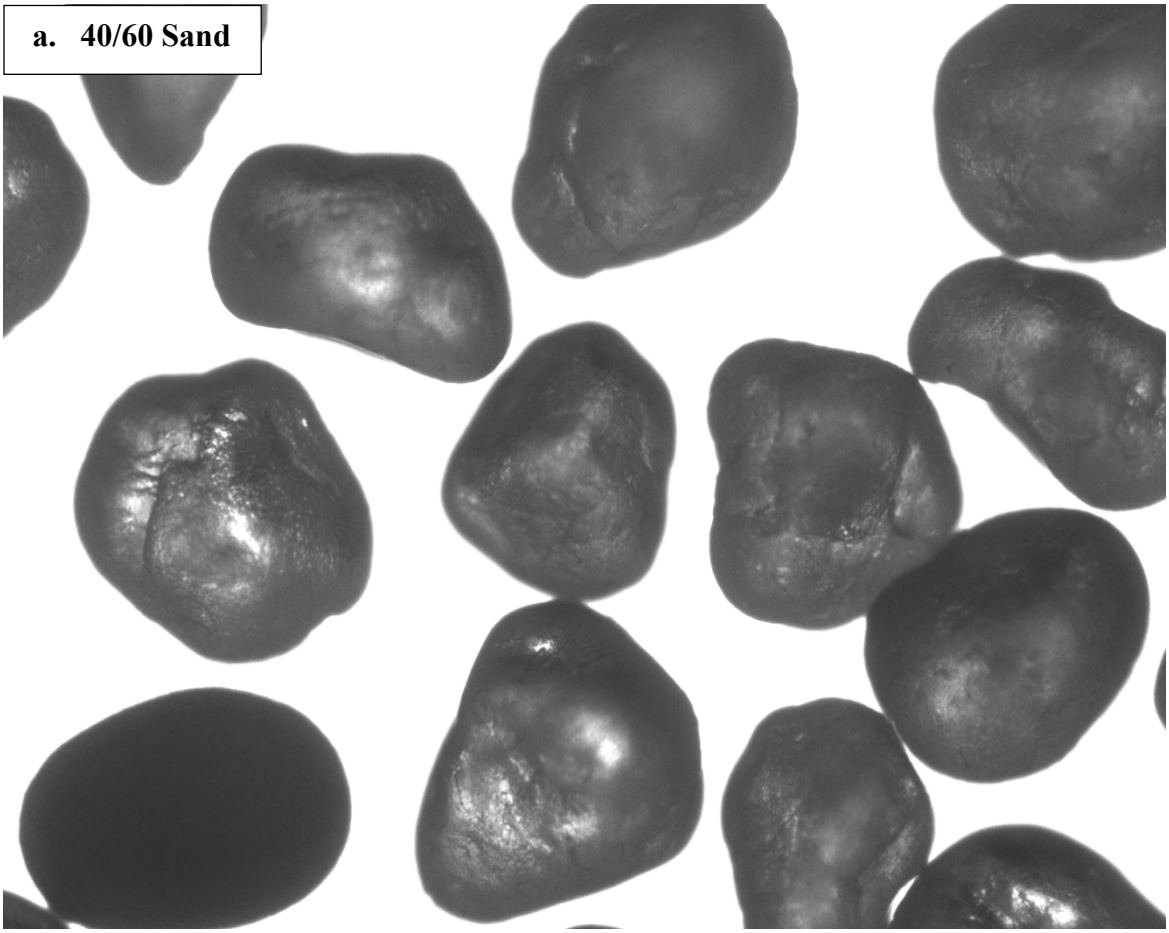

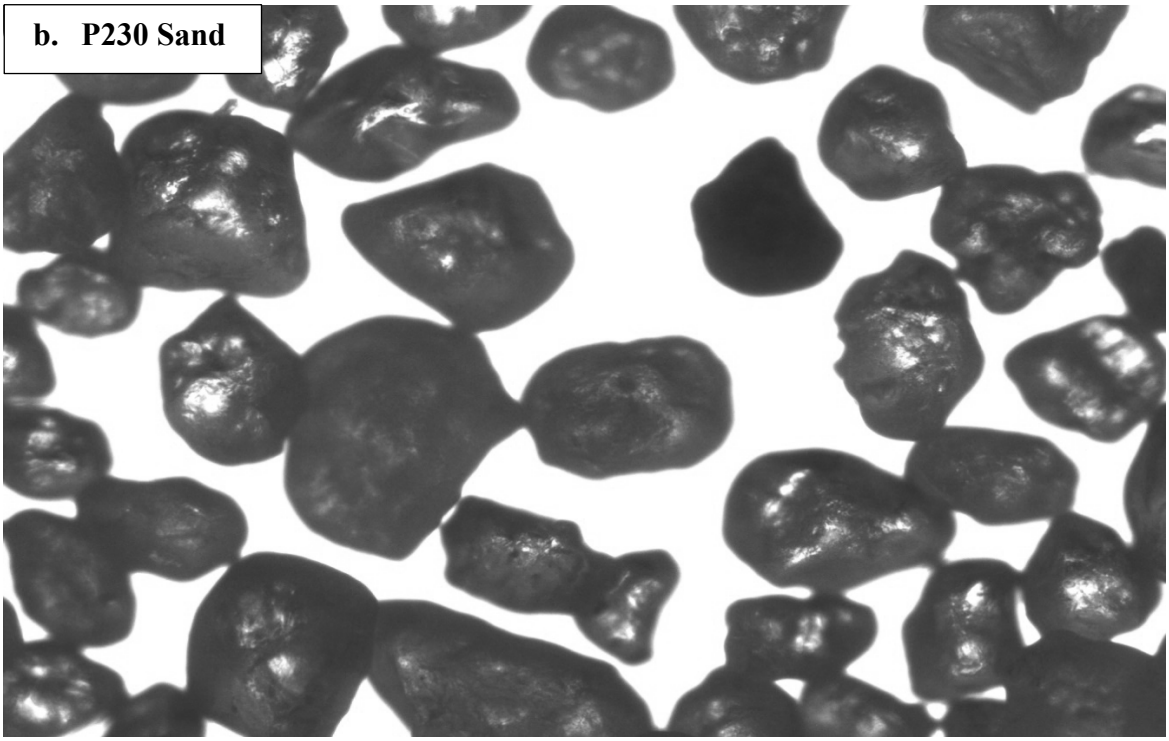

Figure 5.5*: Microscopic image of the silica sands (a) 40/60 sand (b) P230 sand (5x objective magnification.*

5.1.2.3. Mineralogical Composition of Silica Sand

The chemical composition of the silica sands is summarized in Table 5.2 as obtained from Idahosa (2015). From the table, the main mineral constituent of the sand is silica dioxide or quartz (SiO_2). Identifying the main mineral composition is critical in understanding the nature of polymer–rock interaction and brine–rock interactions. The quartz compound has been reported to exhibit a positively or negatively charged surface under certain pH conditions. This means that the surface wettability of the silica sands can be altered, and this can significantly affect its interaction with polymer molecules.

Table 5.3*: Chemical analysis of silica sands indicating the main elements (Idahosa, 2016)*

	Compound	**SiO_2**	**Al_2O_3**	**Fe_2O_3**	**TiO_2**	**CaO**	**MgO**	**LOI**
40/60 Sand	%	99.5+	0.06	0.02	0.012	<0.01	<0.01	0.1

	Compound	**SiO_2**	**Al_2O_3**	**Fe_2O_3**	**TiO_2**	**CaO**	**MgO**	**LOI**
P230 Sand	%	99.5+	0.06	0.02	0.012	<0.01	<0.01	0.1

5.1.2.4. Porosity and Absolute Permeability of Silica Sand

Figure 5.6 shows the plots to determine the average porosity and average absolute permeability to brine of the sand-pack porous media. The average porosity was determined by considering seven samples of varying bulk volumes of silica sand. These sands were contacted with brine (2.45 %TDS), and the pore volumes estimated and plotted against the bulk volumes as shown in Figure 5.6a. The average porosity was calculated as the slope of the plots, and these values correspond to 0.367 for the 40/60 sand and 0.323 for the P230 sand respectively. Similarly, the absolute permeability was estimated for both the 40/60 and P230 sand, as shown in Figure 5.6b. The procedure followed the description given in Chapter 4 with the pressure drop across the sand pack recorded at different flowrates. The absolute permeability was determined from the slope of the plot of flowrate against pressure drop. The estimated permeabilities for the 40/60 and P230 sands were 5.21 and 3.93 Darcy respectively.

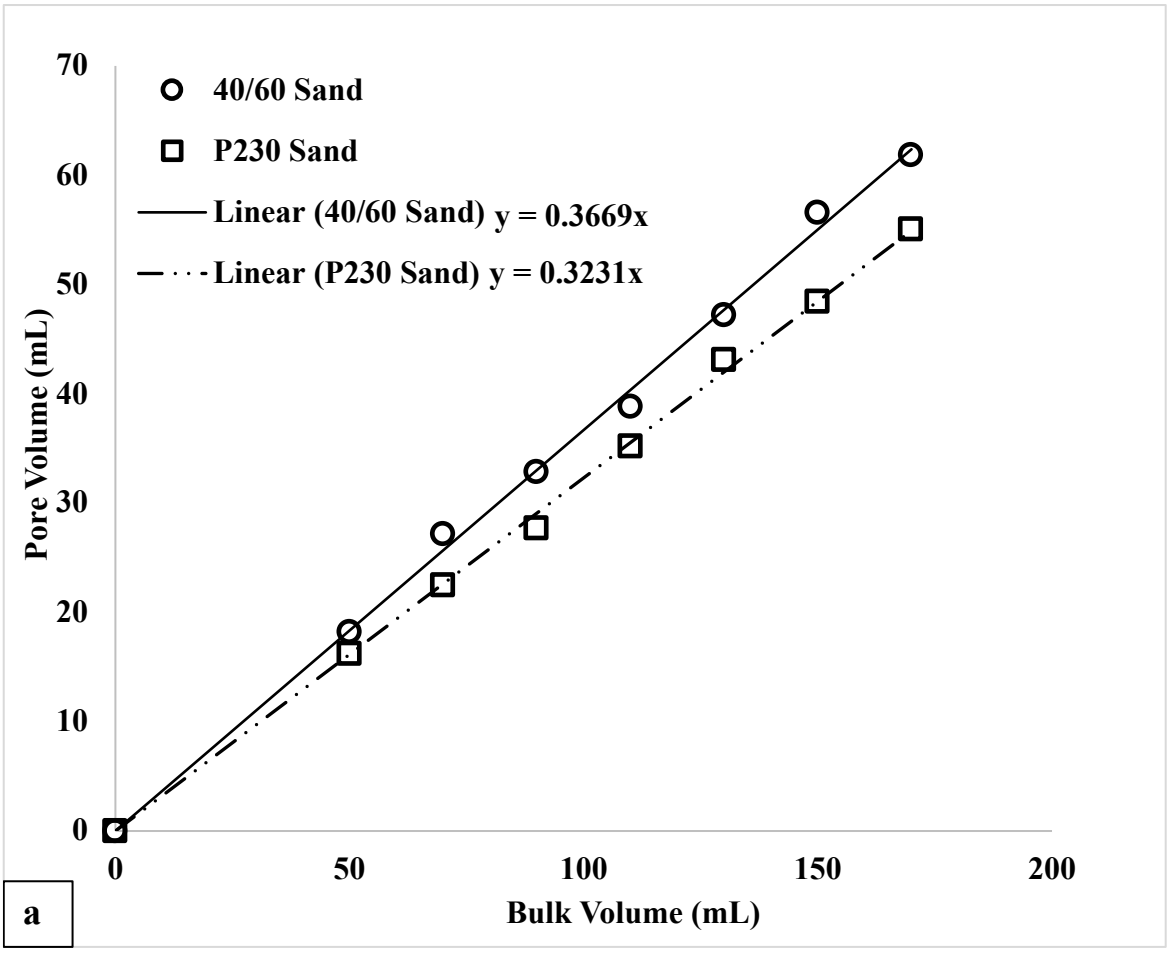

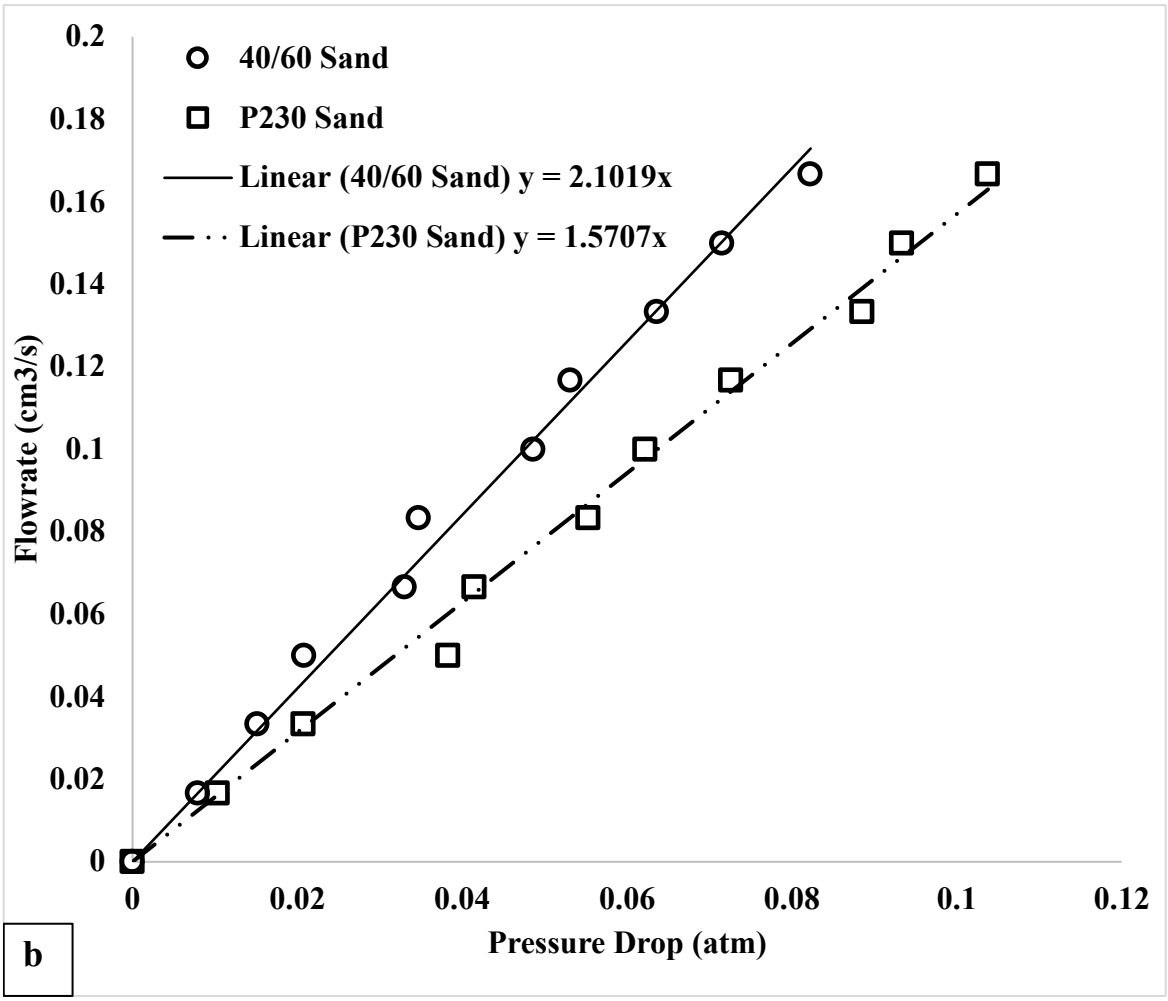

Figure 5.6*: Plots for the determination of the (a) average porosity and (b) absolute permeability of the 40/60 and P230 silica sands at 25* ℃ *and 2.45 %TDS brine salinity.*

5.1.2.5. In-Situ Shear Rates in Sand-Pack

The in-situ rheological behaviour of polymer solutions in porous media is a function of shear rate. Based on the API specification RP-63, Equation (5.3) was applied to determine the flowrate that would induce in-situ shear rates comparable to field application (between 10 and 100 /s).

$$\gamma = \left(\frac{3n+1}{4n}\right)\left(\frac{4\alpha Q}{A(8k\phi)^{0.5}}\right) \qquad (5.3)$$

where γ is the effective shear rate in the porous media; $\frac{3n+1}{4n}$ is the Rabinowitsch correction factor; ϕ is the porosity of the porous media; k is the permeability of the media; Q is the flowrate; A is the cross-sectional area of the media; α is the geometrical factor to account for the porous media structure (1.15 for sand pack). For the sand pack, it was observed that flowrates between 0.2 and 2 mL/min were estimated to induce shear rates between 10 and 100 /s comparable to field applications. Figure 5.7 shows the estimated shear rate plot

against the applied flow rate under different flow index. It was observed the relationship between the shear rate and flow rate was linear within the range studied (0 – 8 mL/min).

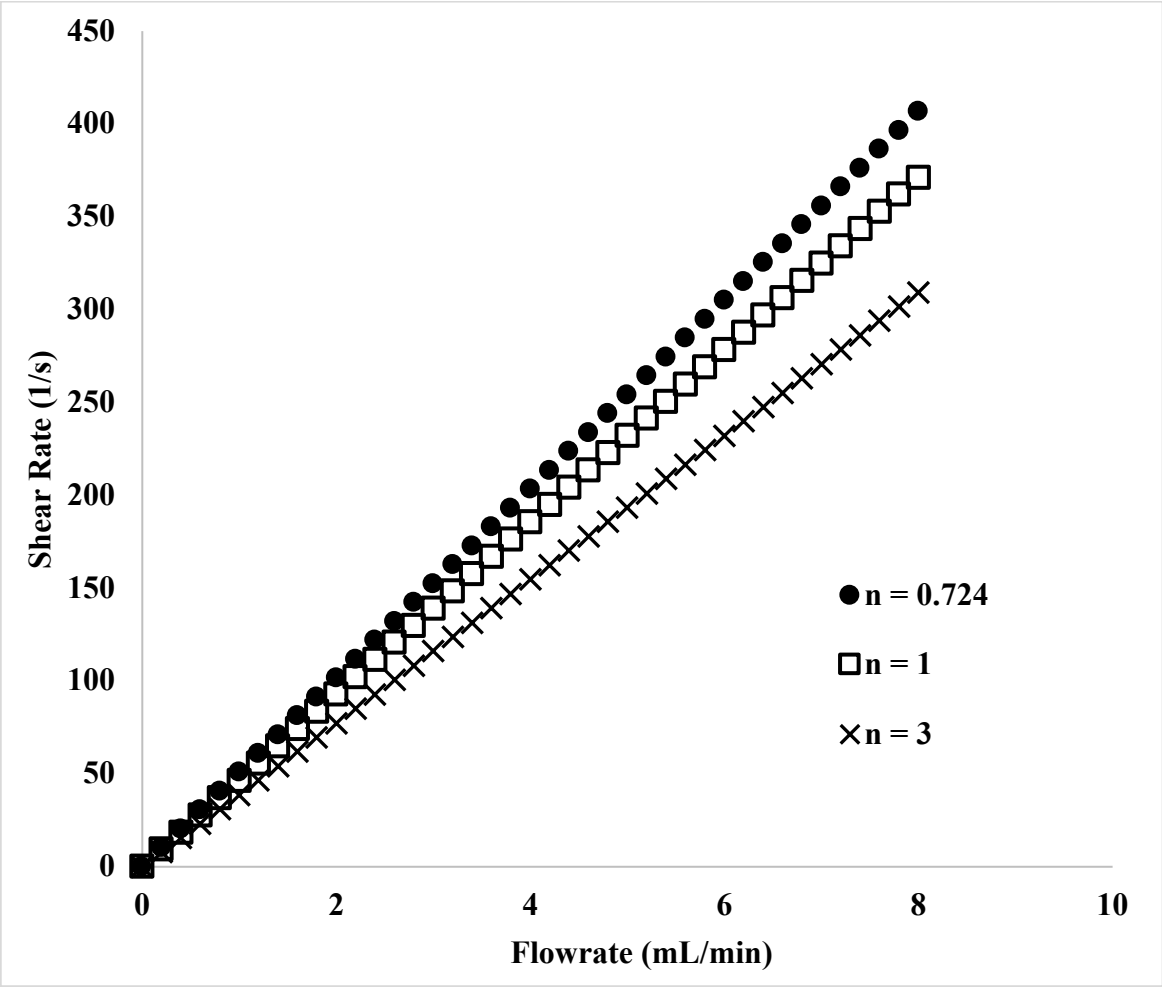

Figure 5.7*: In-situ shear rate simulation in the sand pack media at 25 ℃ and 2.45 %TDS. It was observed the relationship between the shear rate and flow rate was linear within the range studied (0 – 8 mL/min).*

5.2. Summary

The characterisation of the associative polymer and silica sand employed in this study was reported in this chapter. The hydrophobically associating polymers were characterised for their activity/weight loss, chemical composition and molecular weight using thermal analysis, FTIR/Raman spectroscopy, and viscometry. An essential outcome of this is that the polymer employed was a polyacrylamide based hydrophobically associating polymer. Similarly, the silica sand was characterised for its composition, size distribution, porosity, and absolute permeability to the brine solution. The outcome of the characterisation of the sand is the determination of the desired flow rates that would induce in-situ shear rates comparable to field application.

CHAPTER SIX

6.0. Quantitative Characterisation of Polymer Concentration Regimes

In this chapter, a quantitative description of the polymer concentration regimes was given and the effects of various conditions such as temperature, shear rates and brine salinity. This was analysed by considering the response of the critical aggregation concentration to the conditions identified.

6.1. Polymer Concentration Regimes

The two known concentration regimes discussed in this section are the dilute and semi-dilute concentration regimes. The threshold concentration and the effect of reservoir conditions are highlighted, likewise the distinguishing effect of the viscosity of each concentration regimes. Furthermore, a third concentration regime was discussed, and the overall significance of identifying the threshold concentration for the onset of the semi-dilute and concentrated regime.

6.1.1. Determination of the Critical Aggregation Concentration

The viscometry method was adopted in the determination of the critical aggregation concentration. This involved the understanding of the curvature of the plot of polymer viscosity against concentration. Two linear models were fitted via regression analysis to the identified concentration regions (dilute and semi-dilute region), which approximates a straight line in the plot of viscosity against polymer concentration. The critical concentration was approximated as the point of intersection of the fitted linear models. Figure 6.1 shows the approach taken to determine the critical concentration of the associative polymer under different temperatures (25, 50, 75, and 85 ^{0}C). It can be observed that the critical concentration increased with temperature from 25 to 85 ^{0}C. Similarly, the critical concentration was also determined for the associative polymer under different per cent of dissolved solids (3.6, 3.8, 4.0, and 4.2 % TDS), as shown in Figure 6.2. The approach also involved using the two linear models fitted via regression analysis to the regions (dilute and semi-dilute region), which approximates a straight line in the plot of viscosity against polymer concentration. It was observed that the critical concentration increased minimally with the percent dissolved solids. A similar approach was adopted in the determination of the critical aggregation concentration under different conditions of shear rates.

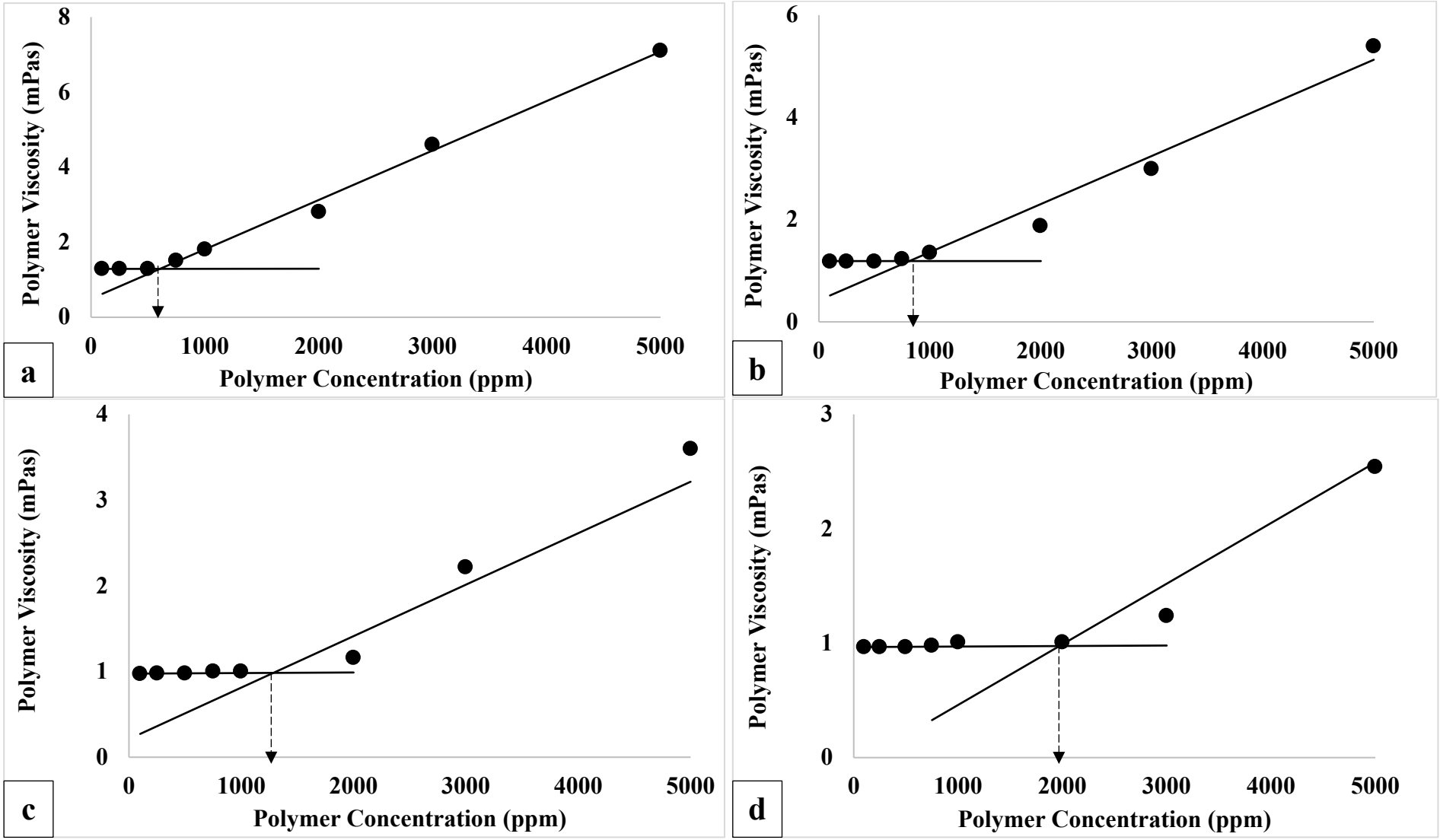

***Figure 6.1**: Determination of the critical aggregation concentration from the plot of polymer viscosity against concentration at (a) 25 ^{0}C (b) 50 ^{0}C (c) 75 ^{0}C (d) 85 ^{0}C. The measurement was taken at 3.6 % TDS and shear rate of 7.34/s.*

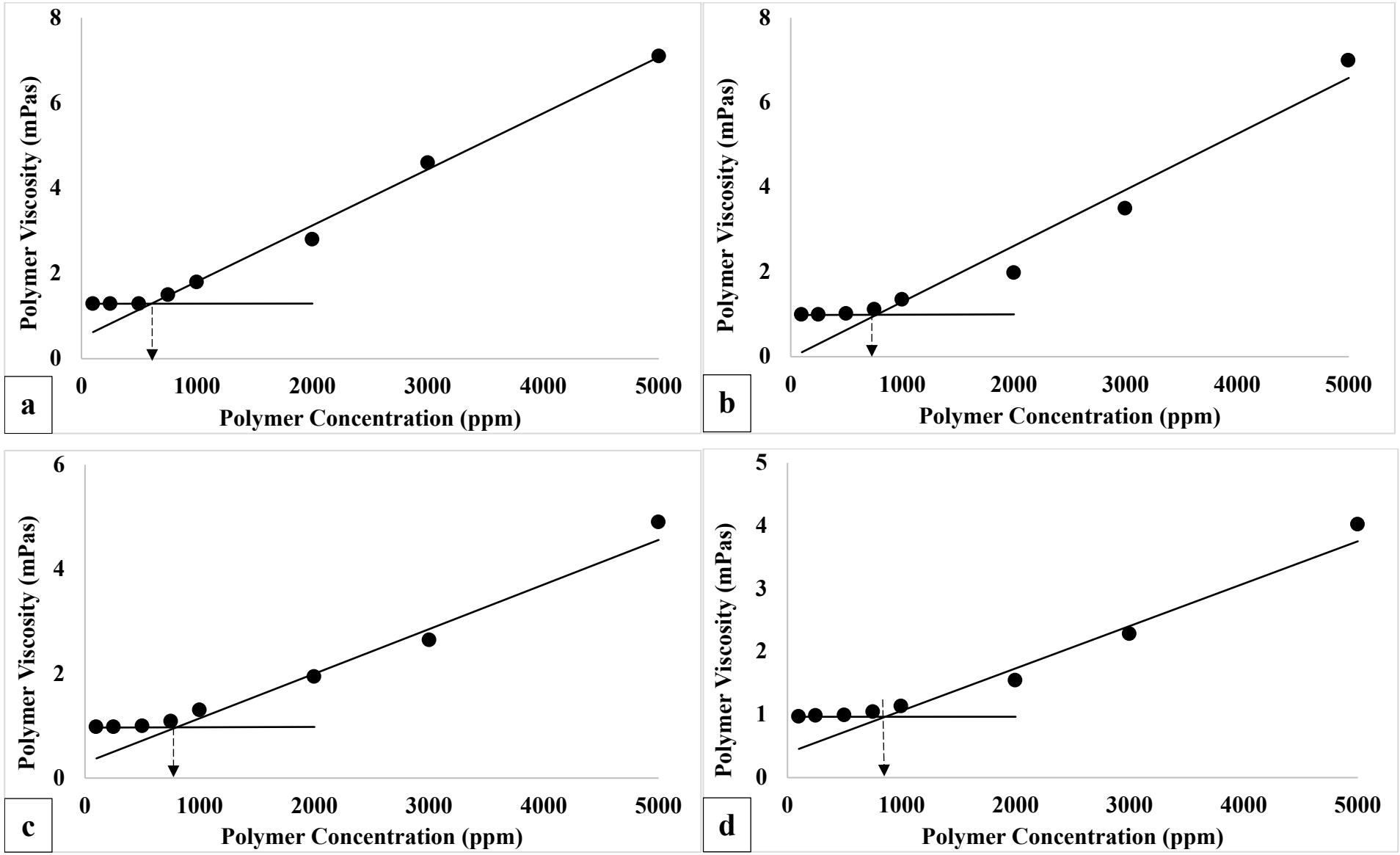

***Figure 6.2**: Determination of the critical aggregation concentration from the plot of polymer viscosity against concentration at (a) 3.6 % TDS (b) 3.8 % TDS (c) 4.0 % TDS (d) 4.2 % TDS. The measurement was taken at 25 ^{0}C and shear rate of 7.34/s.*

6.1.1.1. Effect of Temperature on the Critical Aggregation Concentration

The effect of temperature on the critical aggregation concentration of associative polymers is shown in Figure 6.3. The increase in the values of the critical aggregation concentration with temperature indicates a change in the polymer concentration regimes. As shown in Figure 6.3, the increment in the critical aggregation concentration with temperature was studied in three stages. Firstly, the increase in temperature from 25 to 50 ℃ (at 3.6 % TDS) means that the critical aggregation concentration increased from 260 to 740 ppm. This increment represents a change in the polymer concentration regimes, with the semi-dilute regime decreasing by 65 %. This means that some polymer chains, which interacted with each other in the semi-dilute regime, were severed from the network and exist as distinct polymer chains. As a result, the dilute concentration regime, which is characterised by separate polymer chains, increased by 65 %.

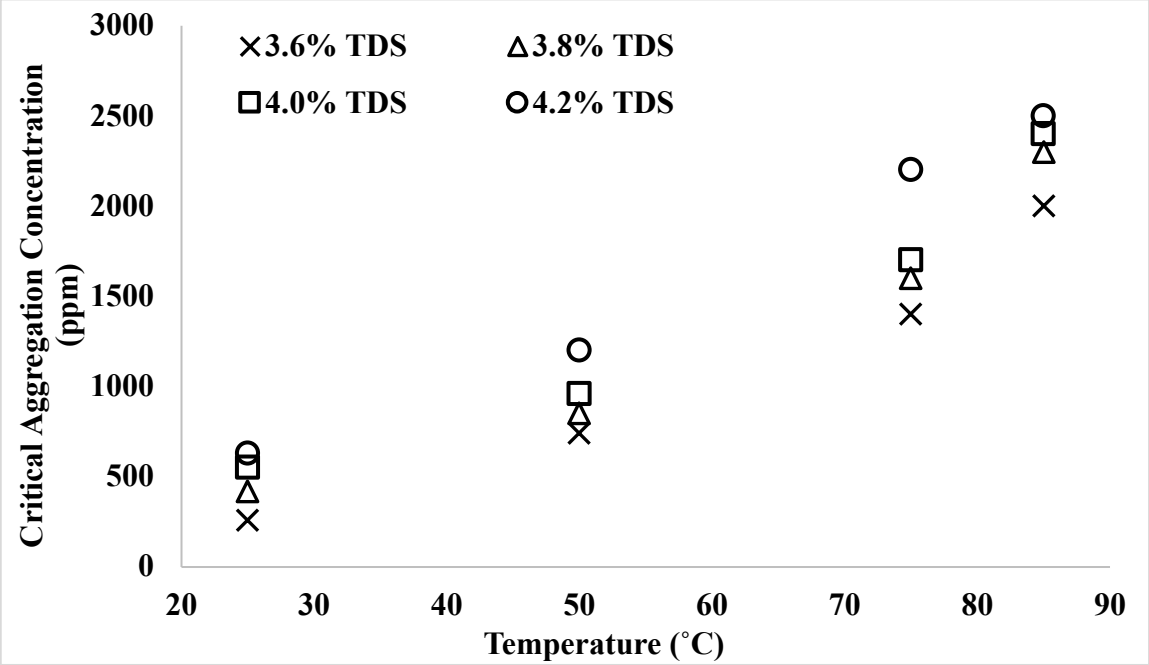

***Figure 6.3**: Effect of temperature on the critical aggregation concentration of studied associative polymer.*

Therefore, the change in the critical aggregation concentration represents a transition point for the concentration regimes. Secondly, an increase in temperature from 25 to 75 ℃ (at 3.6 % TDS) indicate that the critical aggregation concentration increased from 260 to 1400 ppm. Following from similar explanation, the semi-dilute regime decreased by 81.4 %, while the dilute regime increased by a similar percentage. Finally, an increase in temperature from 25 to 85 ℃ (at 3.6 % TDS) indicates that the critical aggregation concentration increased from 260 to 2,000 ppm. In this case, the semi-dilute regime

decreased by 87 %, while the dilute regime increased by a similar percentage. However, under different salinity conditions, the fractional change in the polymer concentration regimes tend to decrease. For example, an increase in temperature from 25 to 50 ℃ (at 3.6 % TDS) indicate a 65 % change in the critical aggregation concentration. However, a similar change in temperature under 3.8, 4.0, and 4.2 % TDS resulted in a 51, 47 and 43 % change in the critical aggregation concentration respectively. A plausible explanation for the temperature effects observed in Figure 6.3 was due to the gradual increase in the thermal energy of the polymer chains starting with the shorter chains up to the longer chains. When the distribution of thermal energy across the polymer chains is such that they are equal to the energy associated with the hydrophobic interactions, the break-off will not take place. However, when the thermal energy acquired by a given polymer chain exceeds the energy arising from the hydrophobic interactions, these polymer chains break off, and polymer viscosity is reduced. The break-off chains contribute to the dilute concentration regime, thereby increasing the critical aggregation concentration, as shown in Figure 6.3. Beyond this point, the increased mobility of the polymer chains arising from the thermal energy being more significant than the bond energy would lead to a structural rearrangement of the longer polymer chains in solutions. This led to a loss of associative interactions between polymer chains. This marked the further increase in the critical aggregation concentration shown in Figure 6.3, with a corresponding increase in the dilute concentration regime where the intramolecular association is dominant.

6.1.1.2. Effect of Salinity on the Critical Aggregation Concentration

Figure 6.4 shows the impact of brine salinity on the critical aggregation concentration of the studied associative polymer. The critical aggregation concentration of the associative polymer increased from 260 to 420 ppm when the total dissolved solids (TDS) increased from 3.6 to 3.8 %TDS (at 25 ℃). This change in the critical aggregation concentration resulted in a 38 % increase in the dilute concentration regime and an equivalent reduction in the semi-dilute concentration regime. Furthermore, an increase in the salinity from 3.6 to 4.0 %TDS and 3.6 to 4.2 %TDS (at 25 ℃) resulted in a 51 and 58 % increase in the dilute regime and equivalent reduction in the semi-dilute regime respectively. A similar trend was observed regarding the polymer concentration regimes concerning the dissolved solids under given temperatures (50, 75 and 85 ℃). The minimal change in the critical aggregation concentration of the associative polymer was indicative of its salt tolerance.

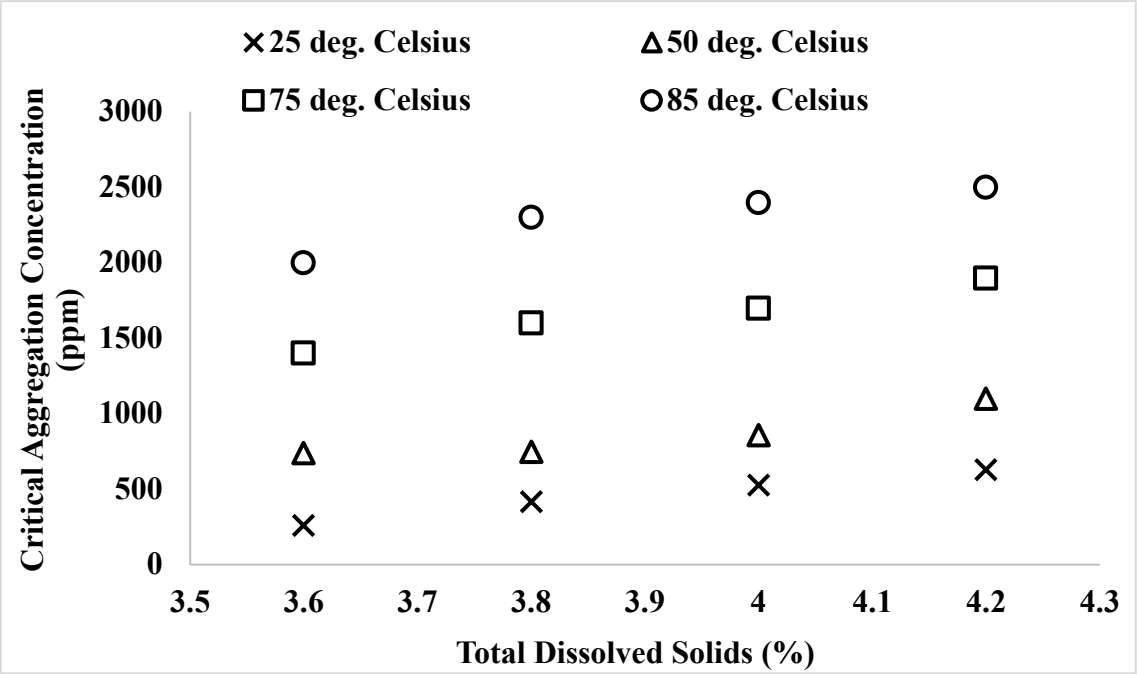

***Figure 6.4**: Effect of total dissolved solids on the critical aggregation concentration of associative polymer under given temperature conditions.*

The effect of salts on the critical aggregation concentration of associative polymers arises from the shielding or screening effect of the metallic ions present in the salts. The salt solutions considered for analysis contained Na^+ and Ca^{2+}/Mg^{2+} in the ratio 10:1 for 3.6, 3.8, 4.0 and 4.2 % TDS respectively. The observed critical aggregation concentration of associative polymers at given conditions was due to the electrostatic repulsive effect between carboxyl (COO^-) groups, which brings hydrophobic blocks on the polymer backbone closer for associative effect. This ensured that a given number of polymer chains with large hydrophobic blocks exist in the semi-dilute regime and others with smaller hydrophobic blocks remain in the dilute regime. However, the critical aggregation concentration was subject to change when monovalent and divalent ions are present in solutions. In this study, the concentration of monovalent (Na^+) ions ranged from 24,500 to 30,000 mg/L and that of divalent ions (Ca^{2+}/Mg^{2+}) were 2,450 to 3,000 mg/L. Monovalent ions present in the solution were attached to a single carboxylate group, thereby minimizing the repulsive effect; this reduced the semi-dilute regime and a subsequent increase in the dilute regime. In the case of divalent ions, two carboxyl groups shared a divalent ion (Ca^{2+}), and this further screened the repulsive effect between carboxyl groups on the chains. However, the transition of polymer chains from semi-dilute to the dilute regime under different salinity conditions was a function of the relative strength of the hydrophobic association. For shorter hydrophobic blocks on polymer chains, the screening

effect caused by the monovalent and divalent ions effectively negated the hydrophobic interactions that exist between chains. However, where the hydrophobic blocks on the backbone of polymer chains were large, the screening effect caused by the ions in solutions was not strong enough to negate the hydrophobic interactions between chains. Therefore, when the proportions of chains with large hydrophobic blocks were significant, the change in the critical aggregation concentration was minimal. This proposed mechanism explained the minimal change in the critical aggregation concentration shown in Figure 6.4. However, the increased thermal mobility of polymer chains arising from increased temperature further weakened the hydrophobic interactions, increasing the critical aggregation concentration. This explains the vertical increase in the critical aggregation concentration at temperatures of 25, 50, 75 and 85 ^{0}C in Figure 6.4.

6.1.1.3. Effect of Shear on the Critical Aggregation Concentration

The effect of shearing on the critical aggregation concentration of the studied associative polymer is shown in Figure 6.5.

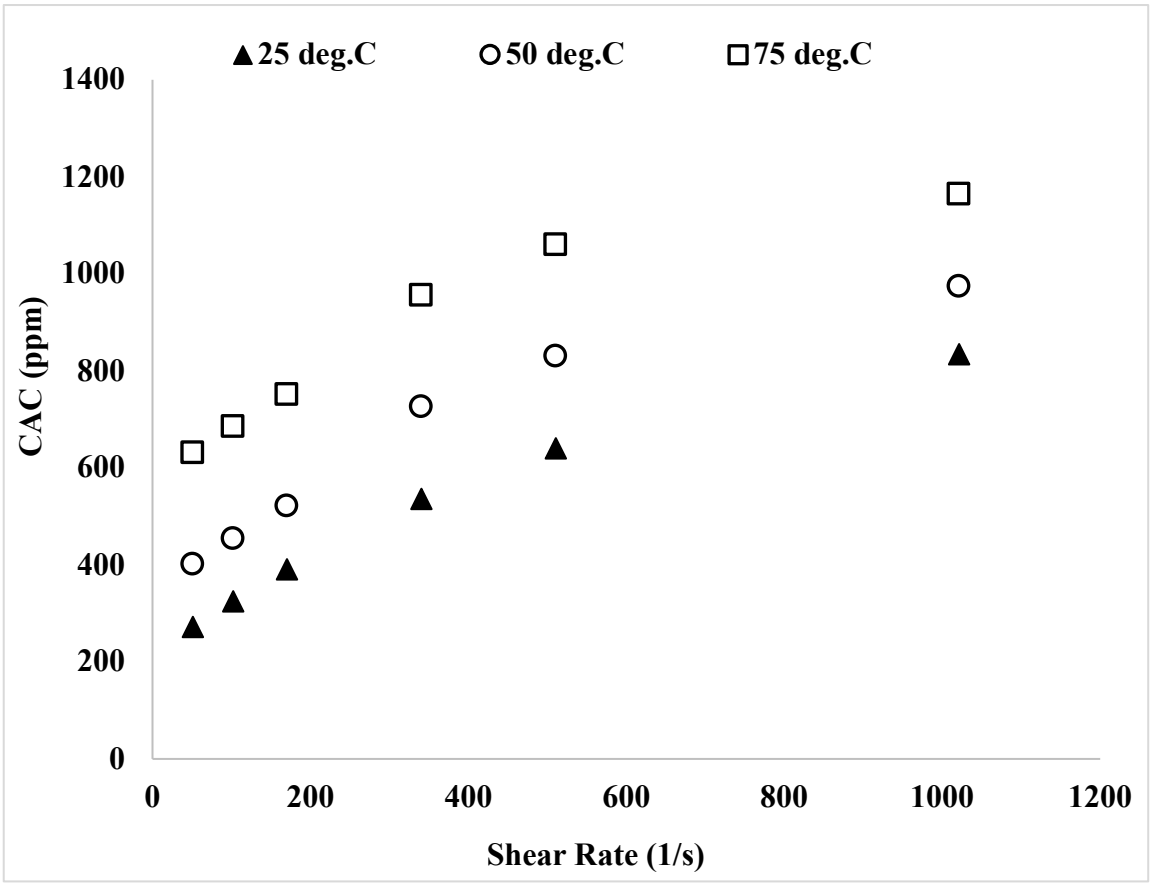

Figure 6.5*: Effect of shear rate on the critical aggregation concentration of the studied associative polymer under different temperature conditions.*

The critical aggregation concentration of the associative polymer increased from 260 to 530 ppm when the shear rate increased from 51 to 340 s^{-1} (at 25 ℃). This change in the critical aggregation concentration resulted in a 51 % increase in the dilute concentration regime and an equivalent reduction in the semi-dilute concentration regime. Furthermore, an increase in the shear rate from 51 to 510 s^{-1} and 51 to 1021 s^{-1} (at 25 ℃) resulted in a 57 and 68 % increase in the dilute regime and equivalent reduction in the semi-dilute regime respectively. A similar trend was observed regarding the polymer concentration regimes concerning the shear rates under given temperatures (50 and 75 ℃). The effect of shear rate on the critical aggregation concentration is explained by visualizing these polymer chains as entangled and single-independent coils. When subjected to flow, two competing forces arose. Firstly, the entropic force maintains the existing polymer configuration. This entropic force keeps the polymer chains independent from each other for the single-independent coils in the dilute regime. On the other hand, the magnitude of the entropic force in the semi-dilute regime is a function of hydrophobic interaction between polymer chains. The existing polymer configuration eventually gives rise to the critical aggregation concentration under these conditions. Secondly, a drag force comes into play when subjected to flow conditions. This drag force arises from the interaction between polymer molecules and the solvent in which it is dissolved. In the dilute regime, the drag force ensures the independent polymer chains are aligned in the flow direction. However, in the case of the semi-dilute regime, the drag force tries to disentangle the associated polymer chains in addition to aligning them in the flow direction. For polymer chains that are successfully disentangled and aligned in the flow direction, they become independent chains. As a result, the critical aggregation concentration of the associative polymer increases with the shear rate. Therefore, the effect of shear rate on the critical aggregation concentration is majorly the disentanglement of polymer chains in the semi-dilute regime. However, the application of higher shear rates could lead to polymer degradation in addition to disentanglement from the hydrophobic interaction network. The outcome of this process was the reduction in the semi-dilute regime and an increase in the dilute regime. This is essentially the phenomenon behind the shear thinning of associative polymers. However, given enough time to rest, associative polymer undergoes structural recovery and disentangled polymer chains transits from the dilute regime back to the semi-dilute regime. This is, however, dependent on the extent of mechanical degradation of the polymer chains. In the case of shear thickening in porous media, similar effects of drag force and entropic force are present; however, the torturous

nature of the porous media means that more hydrophobic blocks are brought closer together, thereby increasing the level of entanglement among polymer molecules.

6.1.2. Predicting the Onset of the Polymer Concentrated Regime

It is a fact that polymer molecules can exist as independent chains isolated from each other (dilute regime) or as aggregates of molecules (semi-dilute regime). However, the aggregation of polymer molecules in the semi-dilute regime does not necessarily imply that all polymer molecules in this regime are in an interactive state. Instead, the aggregation of polymer molecules due to hydrophobic interactions is a gradual build-up process. Beyond the critical aggregation concentration, the aggregation of polymer molecules into a network of aggregates commence. The number of molecules, which constitute these aggregates, depends on the concentration of the polymer solution. Figure 6.6 show the plots of molecular interactions for the dilute and the semi–dilute regimes as computed using the equations (3.1), (3.3), and (3.4) respectively. These plots were generated based on the susceptibility of the critical aggregation concentration to identified reservoir conditions as discussed in the preceding sections. The increase in the intramolecular interactions is indicative of the increase in the number of polymer chains with polymer concentration up to the critical aggregation concentration. At this state, hydrophobic interactions between polymer molecules are non-existent. This dilute state is characterized by the independence or isolation of polymer chains from each other. However, the intramolecular interaction begins to decrease beyond the critical aggregation concentration while the onset of hydrophobic interaction begins. This onset of hydrophobic interactions is marked by an increase in intermolecular association above the critical aggregation concentration. It is obvious from the plot that the onset of hydrophobic interactions between polymer molecules does not translate to an outright disappearance of intramolecular interaction within the polymer chains. Rather, polymer molecules gradually transit from intramolecular interaction to hydrophobic interactions at concentrations above the critical aggregation value. It was observed that these plots for the molecular interactions intersect at approximately 0.5 respectively and the estimated critical concentration, C_c at this point of intersection was 1 g/L (or 1,000 ppm), 1.7 g/L (1700 ppm) and 3.3 g/L (3300 ppm) at 25 ^{0}C (4.9 % TDS), 50 ^{0}C (4.9 % TDS) and 75 ^{0}C (4.9 % TDS) respectively. This estimated critical concentration is the optimal value at which there is a balance in molecular interactions between the dilute and semi-dilute regime under the given conditions.

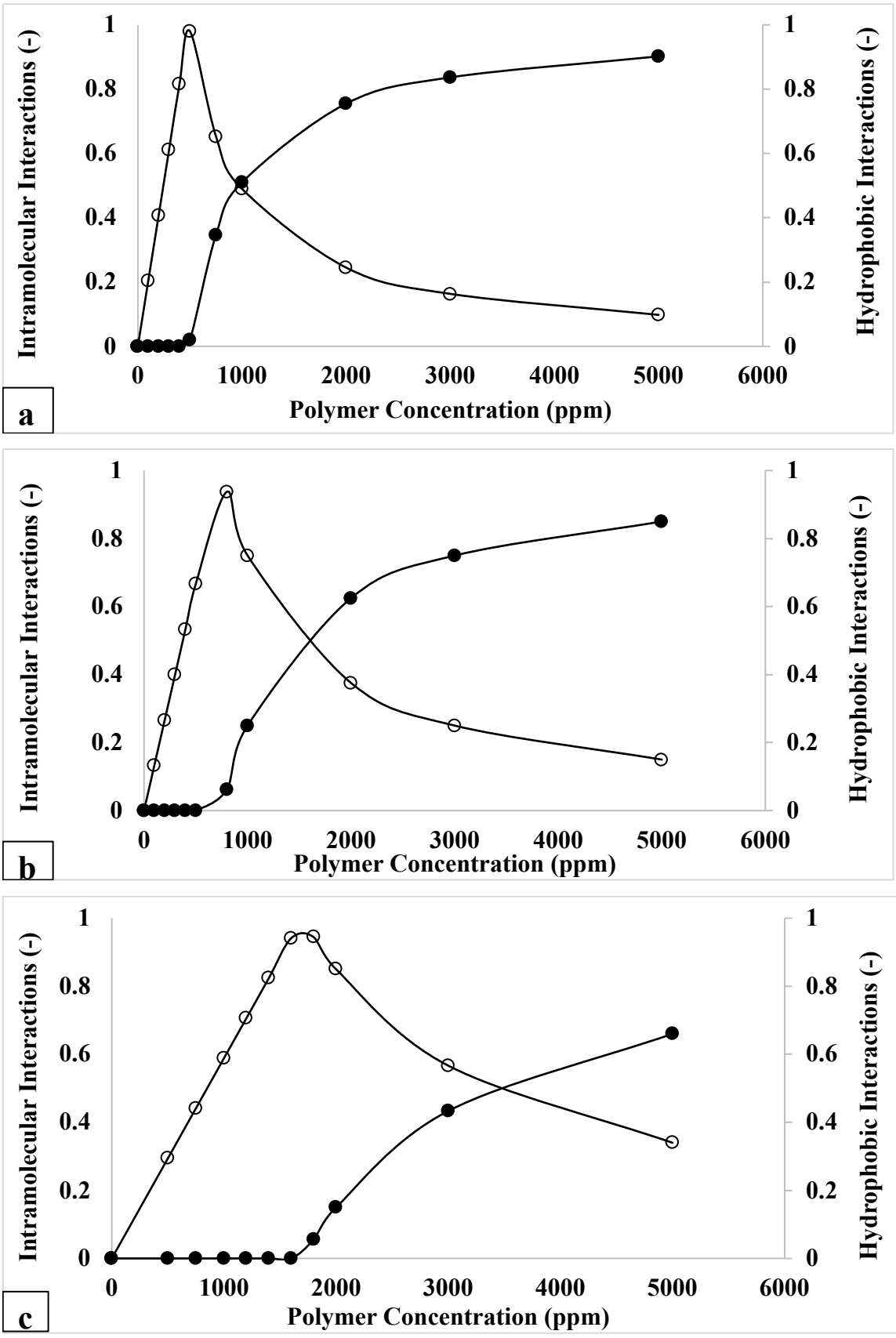

***Figure 6.6**: Plot of molecular interactions (intramolecular and hydrophobic interactions) against polymer concentration at 7.34/s and 4.9 %TDS **(a)** 25 ^{0}C **(b)** 50 ^{0}C **(c)** 75 ^{0}C.*

The increase in this critical concentration of the associative polymer required is evidence of the changing conditions of temperature as captured in Figure 6.6a – 6.6c. Furthermore, the hydrophobic interactions become the dominant interaction mechanism over the intramolecular interactions beyond this critical value. In other words, the critical value can be interpreted to characterise the onset of the *"Polymer Concentrated Regime"*. In this work, this critical concentration at which the concentrated regime commences was termed the "*Critical Separation Concentration,* $C_{sep,c}$". The significance of this novel approach is in the control and monitoring of hydrophobic interactions under different reservoir conditions, and this can be translated or adjusted for in the required polymer concentration. In addition, this approach would prevent the application of high polymer concentration with excessive hydrophobic interaction ($\mathrm{C_p} > C_{sep,c}$) dominant in the concentrated regime, which may affect transport in porous media and is further explained in the next section. It could be argued that the proportion of polymer chains lost from this hydrophobic interaction network could contribute to fluid-rock interaction effects such as adsorption or mechanical entrapment. However, for investigating the flow of hydrophobic interactions in porous media, these plots were employed in estimating the onset of the concentrated regime.

6.1.3. Significance of the Critical Separation Concentration

The significance of this novel approach in estimating the onset of the various concentration regimes lies in the control and monitoring of hydrophobic interactions under different reservoir conditions and how this can be adjusted for in the required polymer concentration. This importance can be summarized by considering three case scenarios. Firstly, polymer concentration less than the critical aggregation concentration and the critical separation concentration ($\mathrm{C_p} < \mathrm{C_{agg}} < \mathrm{C_{sep,c}}$). This scenario marks the absence of hydrophobic interactions among polymer chains in solution. The propagation of polymer solutions under these conditions would see polymer molecules interacting with the rock surface without sufficient viscosity for mobility control. Secondly, the scenario where polymer concentration is greater than the critical aggregation concentration but less than the critical separation concentration ($\mathrm{C_{sep,c}} > \mathrm{C_p} > \mathrm{C_{agg}}$). In this scenario, hydrophobic interactions exist between polymer molecules, and the propagation of these molecules would result in hydrophobic interactions lost to adsorption with the effect of entrapment minimal. Here, hydrophobic interactions could be sufficient to provide the needed mobility control during EOR. Thirdly, polymer concentration is higher than the critical aggregation concentration

and the critical separation concentration ($C_p > C_{sep,c} > C_{agg}$). Operating at these conditions would mean that there would be insufficient hydrophobic interactions propagated through the porous media. In addition, polymer molecules would be lost to dominant retention phenomena such as adsorption and entrapment mechanism. Therefore, the second scenario depicts that the application of associative polymers goes beyond operating above the critical aggregation concentration and ensuring that the injection concentration is below the critical separation concentration. This ensures that there are sufficient hydrophobic interactions for mobility control while minimizing the effect of polymer loss arising from different retention mechanisms.

6.2. Mapping of Concentration Regimes under Reservoir Conditions

Three different concentration regimes characterise the flow of polymers in porous media: dilute, semi-dilute, and concentrated. In this section, mapping of the various regimes was done using equations (3.1) to (3.6). In addition, plots were generated for the three regimes to show the effects of the various conditions and the transition/interactions that occur between the regimes

6.2.1. Thermal Degradation Effect

The thermal degradation of hydrophobic interactions is shown in Figure 6.7.

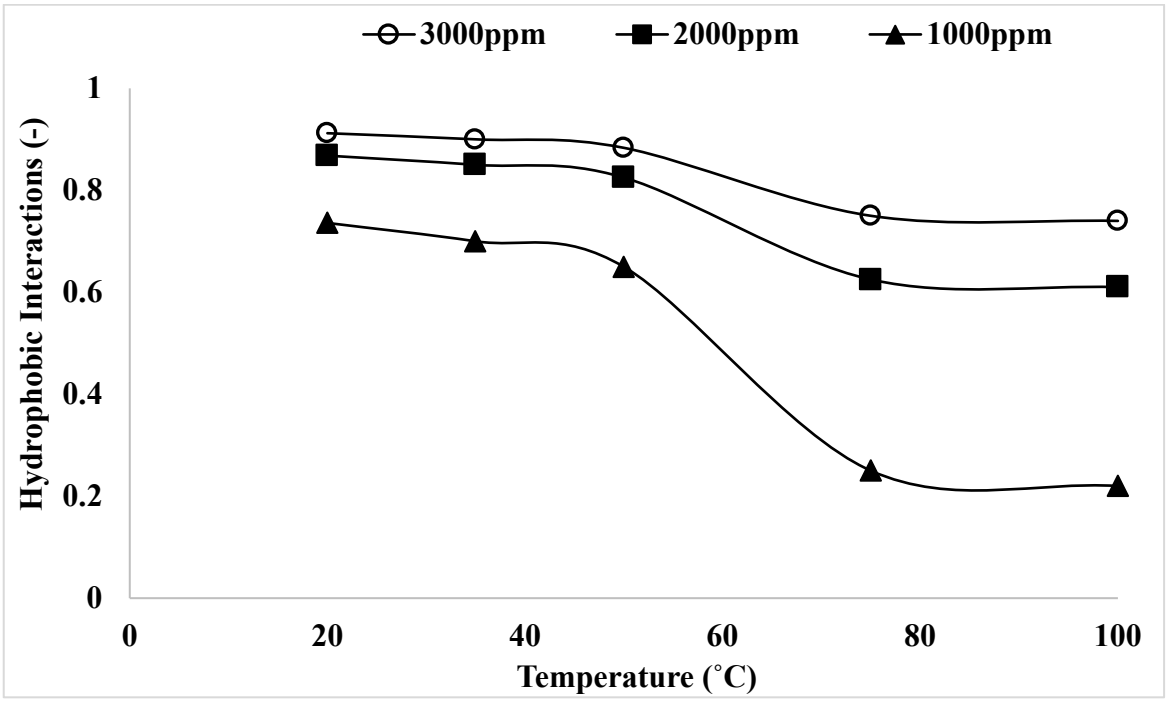

Figure 6.7*: Effect of temperature on computed hydrophobic interactions between associative polymer at different polymer concentrations and 4.9 %TDS.*

The degradation of hydrophobic interactions was observed to follow an *"entanglement – disentanglement"* phenomenon. The hydrophobic interactions show a two-stage degradation process for the various polymer concentrations, which can be labelled as entangled and disentangled stages. The entangled stage was maintained between the temperatures of 20 and 45 ℃. Here, the polymer chains remained relatively entangled, and the decrease in hydrophobic interactions was minimal. This *"entangled"* stage was maintained when the inputted thermal energy arising from heating was less than the cumulative interaction energy between the polymer chains. The effect of heating at this stage was manifested in the loss of solvent molecules (water molecules). However, between the temperatures of 45 and 75 ℃, the *"disentangled"* stage sets in. Here, the inputted thermal energy was greater than the cumulative interaction energy between polymer chains, and thus the chains can separate from each other in the hydrophobic interaction network. This disentanglement process marked the rapid decrease in hydrophobic interactions experienced. However, not all hydrophobic interactions between polymer chains at this stage would immediately be lost. This was due to the nature of the distribution of hydrophobic blocks on the polymer backbone. Beyond 75 ℃, the loss of hydrophobic interactions between the polymer chains again remains relatively constant. At this stage, hydrophobic interactions resulted from the largest polymer chains in solution and the loss of these interactions would require thermal energy inputted at even higher temperatures. Figure 6.8 shows the corresponding effect of this phenomenon on the concentration regimes at different polymer concentrations. At 3,000 ppm, it was observed that below 50 ℃, there were no significant changes in the associated concentration regimes. This stems from the high proportion of polymer molecules in solution and the relatively robust network of hydrophobic interactions between them. However, between 50 and 75 ℃, there were observed changes in the concentration regimes. The dilute regime increased with a corresponding decrease in the concentrated and semi-dilute regimes. But the concentrated remained dominant over the dilute regime, indicating that the polymer solution at that concentration would still have a significant level of viscosity (Figure 6.8a). The dominance of the concentrated reduced as the temperature increased to 100 ℃. At 2,000 ppm, the same pattern and trend observed at 3,000 ppm below 50 ℃ were observed. However, between 50 and 75 ℃, there was an increase in the dilute regime and a corresponding decrease in the concentrated (Figure 6.8b). Nevertheless, beyond 75 ℃, the dilute and semi-dilute regimes dominated over the concentrated regime.

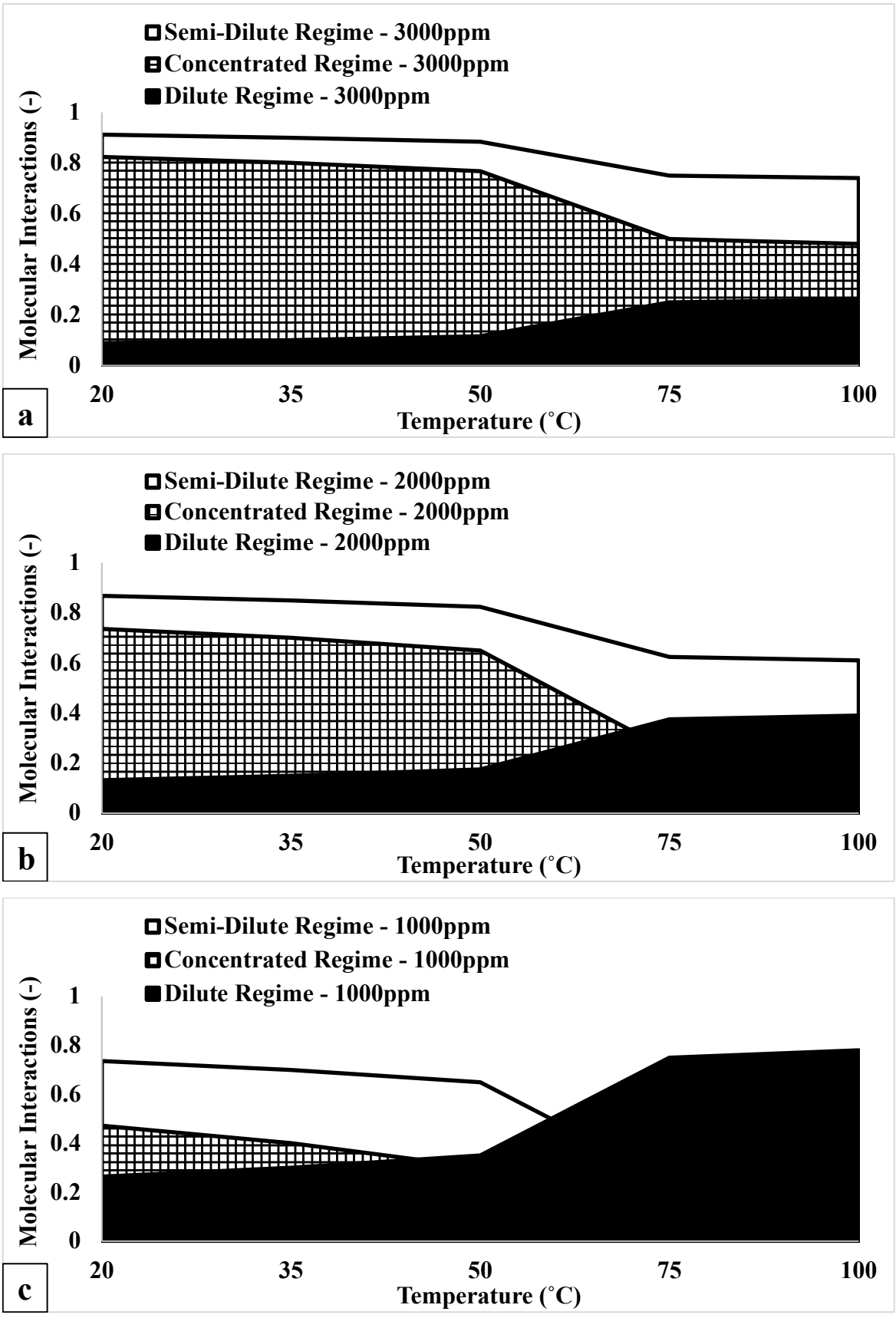

***Figure 6.8**: Effect of temperature on the concentration regimes of the associative polymer at 7.34/s and 4.9 %TDS (a) 3,000ppm (b) 2,000ppm (c) 1,000ppm.*

A similar trend observed at 2,000 ppm can be seen at 1,000 ppm, as shown in Figure 6.8c. The reversibility of the hydrophobic interactions is dependent on the degradation of the disentangled polymer molecules from the hydrophobic interaction network. Figure 6.9 shows that not all disentangled polymer chains reassociate to integrate back into the hydrophobic interaction network after heating to 100 ℃.

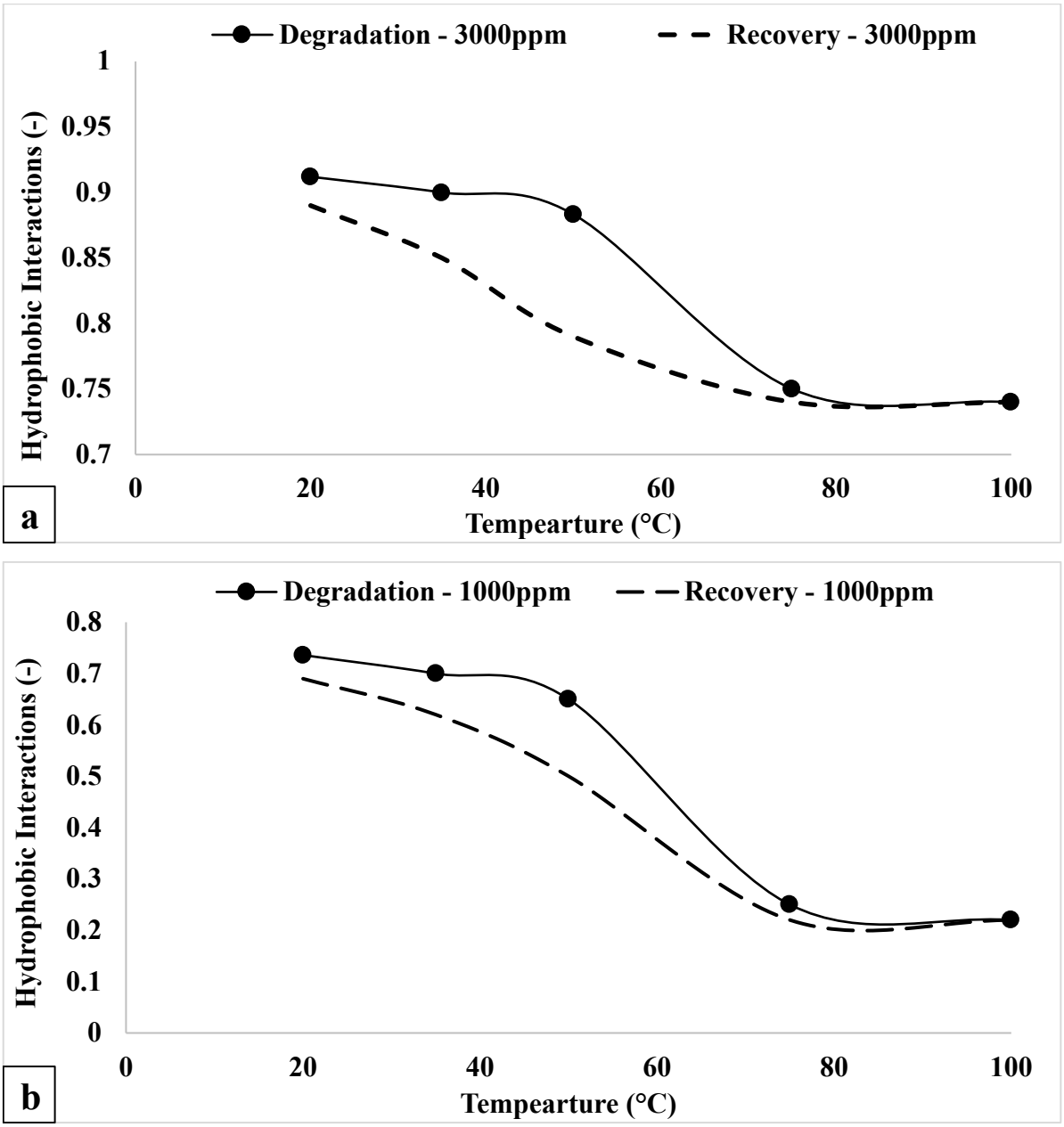

***Figure 6.9**: Thermal degradation study of hydrophobic interactions between polymer chains during heating and cooling at 4.9 %TDS and shear rate of 7.34/s (Radius of bob: 1.7245 cm and Radius of Rotor: 1.8415 cm). (a) 3000 ppm (b) 1000 ppm.*

This process of *"re-entanglement"* is due to the association of previously separated polymer chains from the hydrophobic interaction network. However, this recovery process of hydrophobic interactions during cooling from 100 to 20 ℃ show that the recovery path does

not follow the same path during the heating process, as shown in Figure 6.9. This shows that some of the polymer chains separated during the disentanglement stage were subject to thermal degradation. Degradation leads to the breakage of polymer chains, thereby reducing their tendency to interact with other chains in similar fashion before the breakage. The bounded area by the loss and recovery curves gives the fractional amount of polymer chains lost to chain scission or thermal degradation. Overall, this outcome has shown that the reversibility of hydrophobic interactions is dependent on the thermal degradation of the polymer molecules disentangled from the hydrophobic interaction network. The disentanglement of hydrophobic interactions is a recoverable process, while chain scission/degradation is an irreversible process. However, the recovery of hydrophobic interactions is not always a complete process due to polymer chains' mechanical degradation or scission. Furthermore, Figure 6.9 shows that the number of polymer chains lost to thermal degradation was higher at 3,000 ppm compared to 1,000 ppm. This was due to the large proportion of polymer molecules exposed to such conditions at 3,000 ppm compared to what is available at 1,000 ppm.

6.2.2. Chemical Degradation Effect

The effect of brine salinity on hydrophobic interactions can be classified as insignificant, as shown in Figure 6.10. Salinity–induced degradation of hydrophobic interactions was minimal due to the salt tolerance of the associative polymer. The screening effect caused by monovalent or divalent ions was not strong enough to penetrate the hydrophobic interactions between the polymer chains completely. The high molecular weight (16 MDa) of the studied polymer indicated that the polymer chains' hydrophobic block was relatively high, and the chains were also long enough to accommodate them. For shorter hydrophobic blocks on polymer chains, the screening effect caused by the monovalent and divalent ions effectively negated the hydrophobic interactions that existed between chains. However, where the hydrophobic blocks on the backbone of polymer chains were large, the screening effect caused by the ions in solutions may not be strong enough to negate the hydrophobic interactions between chains. Therefore, when the proportions of chains with large hydrophobic blocks were significant, the change in the critical aggregation concentration was minimal. This proposed mechanism explained the minimal difference in the hydrophobic interactions shown in Figure 6.10. Since the degradation of hydrophobic interactions was minimal, the recovery of hydrophobic interactions was fully attainable.

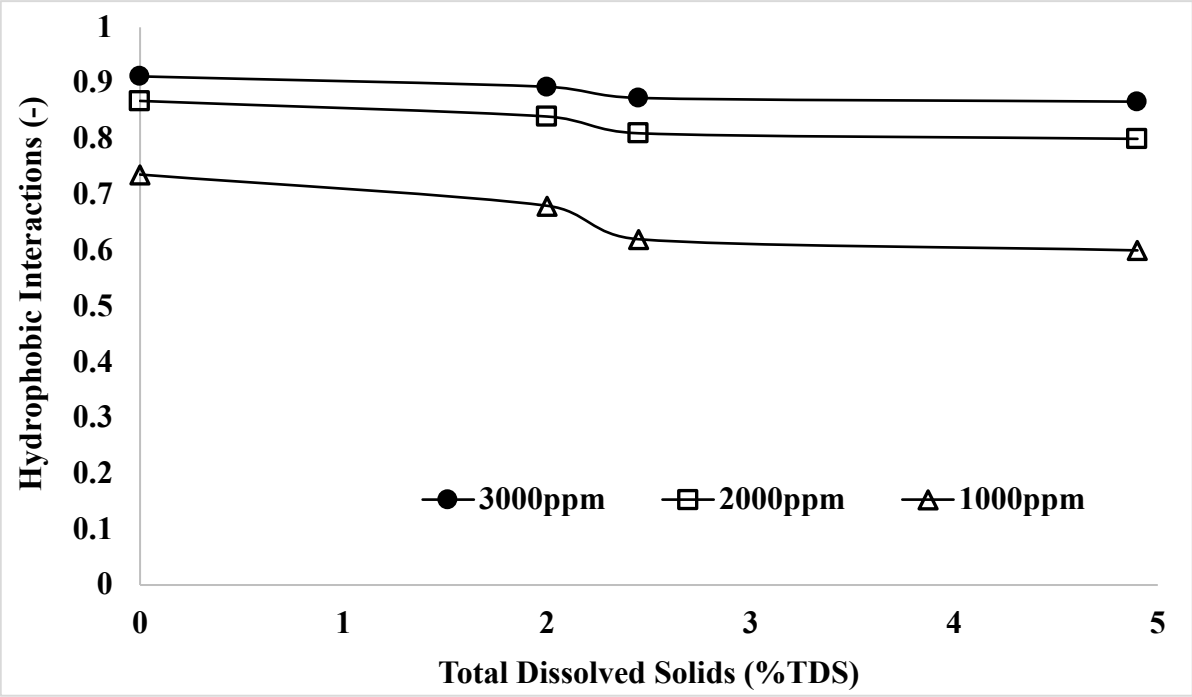

***Figure 6.10**: Effect of brine salinity and ion concentration on hydrophobic interactions for different polymer concentrations at 25 ℃ and shear rate of 7.34 /s.*

Figure 6.11 shows the corresponding effect of salinity conditions on the concentration regimes at different polymer concentrations. At 3,000 ppm, it was observed that between 0 and 2.45 %TDS, there was a minimal change associated with the concentration regimes. This stems from the high proportion of polymer molecules in solution and the relatively robust network of hydrophobic interactions between them, which counteracts the effects of the dissolved ions. Similarly, between 2.45 and 4.9 %TDS, there were no significant changes in the concentration regimes. The dilute regime remained relatively constant, likewise the concentrated and semi-dilute regimes. However, the concentrated remained dominant over the dilute regime, indicating that the polymer solution at this concentration would still have a significant level of viscosity (Figure 6.11a). At 2,000 ppm, the same pattern and trend observed at 3,000 ppm were observed. However, the concentrated remained dominant over the dilute regime, indicating that the polymer solution at this concentration still have a significant level of viscosity (Figure 6.11b). Nevertheless, beyond 2.45 %TDS, the concentrated regime remained dominant over the dilute and semi-dilute regime. However, at 1,000 ppm, as shown in Figure 6.11c, the dominance of the concentrated regime reduced entirely at 2 %TDS; this arises due to the smaller number of polymer molecules at 1,000 ppm compared with 2,000 and 3,000 ppm. The strength of hydrophobic interactions may be weaker compared to the screening effect.

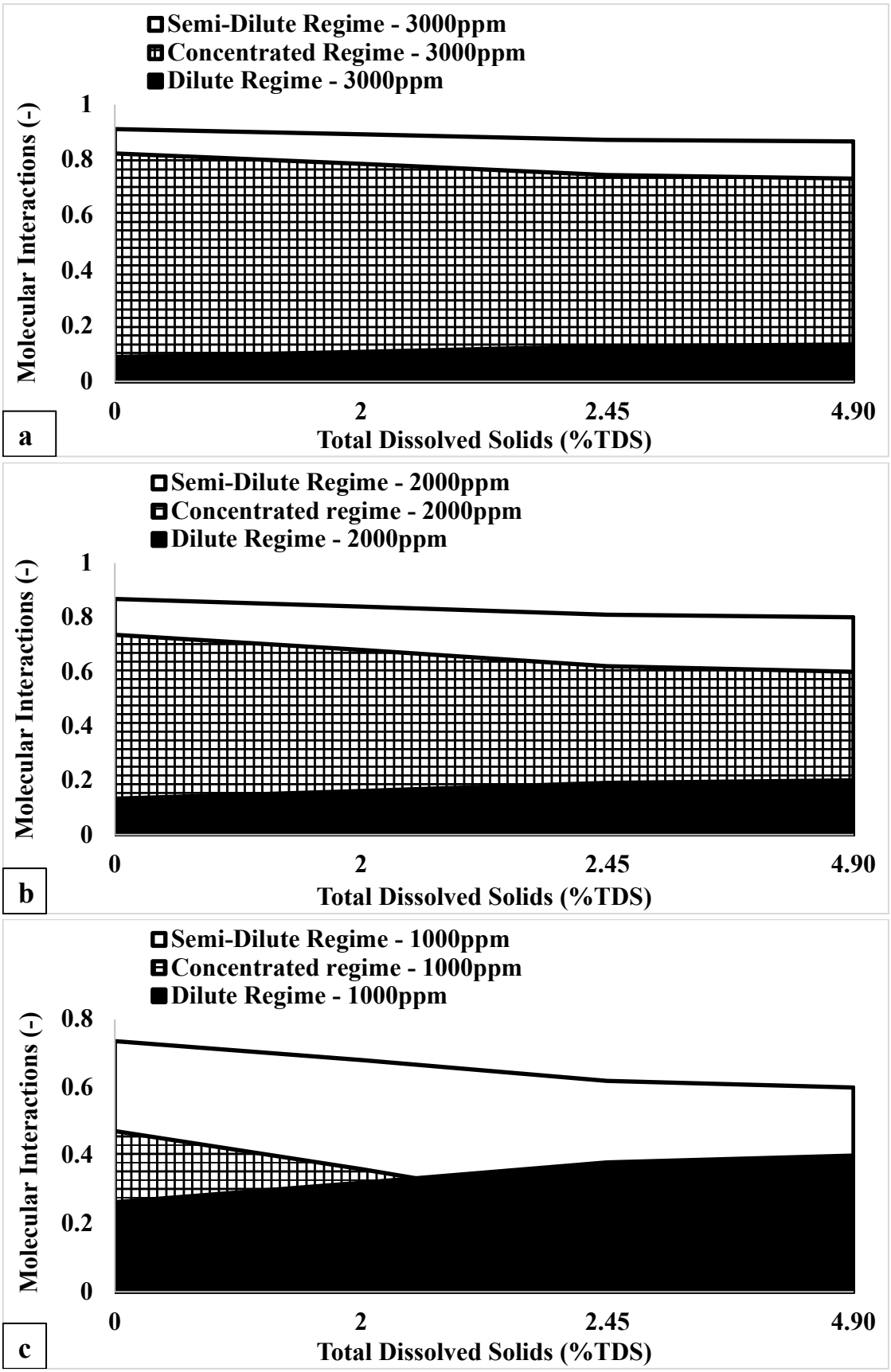

Figure 6.11*: Effect of salinity on the concentration regimes of the associative polymer at 7.34/s and 25*℃ *(a) 3,000 ppm (b) 2,000 ppm (c) 1,000 ppm.*

6.2.3. Shear Degradation Effect

The shear degradation of hydrophobic interactions is captured in Figure 6.12. The shear degradation of hydrophobic interactions followed the *"entanglement – disentanglement"* phenomenon described under the thermal degradation of hydrophobic interactions.

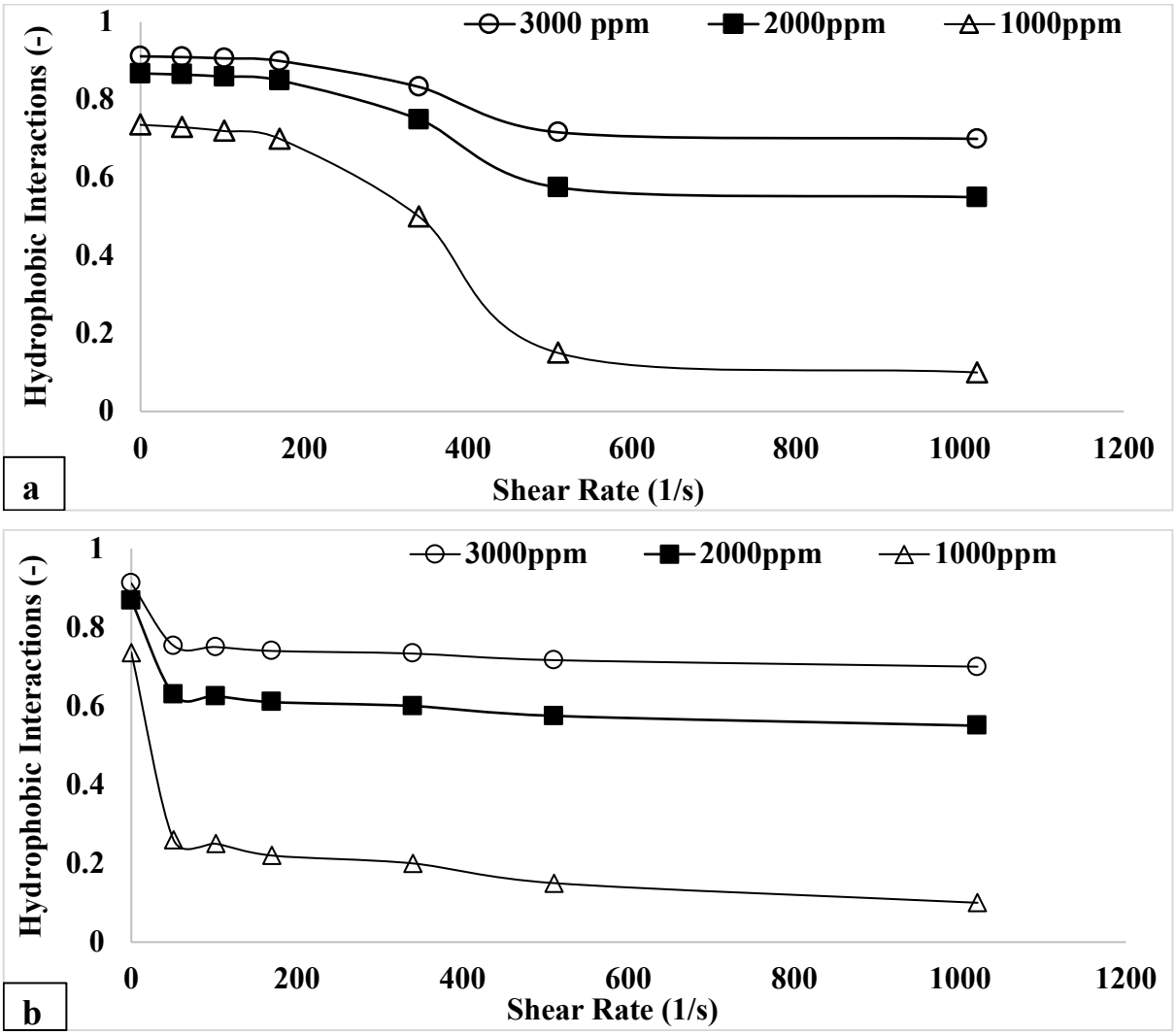

Figure 6.12*: Effect of shear rate on the hydrophobic interactions between associative polymers for different polymer concentrations (a) 25* ℃ *(b) 100* ℃*.*

The hydrophobic interactions follow a two-stage degradation process for the various polymer concentrations considered (1,000 – 3,000 ppm). Between 0 – 200 s^{-1}, the hydrophobic interactions between polymer chains were relatively constant. Here, the drag force arising from the application of flow conditions was insufficient to dissociate the polymer chains from the hydrophobic interaction network. This entanglement stage was the same irrespective of the polymer concentrations considered, as shown in Figure 6.12a. However, between 200 – 510 s^{-1}, the hydrophobic interactions undergo a rapid loss like that experienced under thermal degradation. At this stage, the drag force due to the applied

flow conditions has exceeded the strength of the hydrophobic interactions between polymer chains and, thus, disentangled from each other. Beyond 510 s^{-1}, the loss of hydrophobic interactions between the polymer chains again remains relatively constant in a similar manner to that experienced under thermal degradation. At this stage, hydrophobic interactions result from the largest polymer chains in solution and loss of these interactions required drag force at high flow conditions. However, when thermal and shear conditions were simultaneously considered, the loss mechanism does not follow the two-stage mechanism described, as shown in Figure 6.12b.

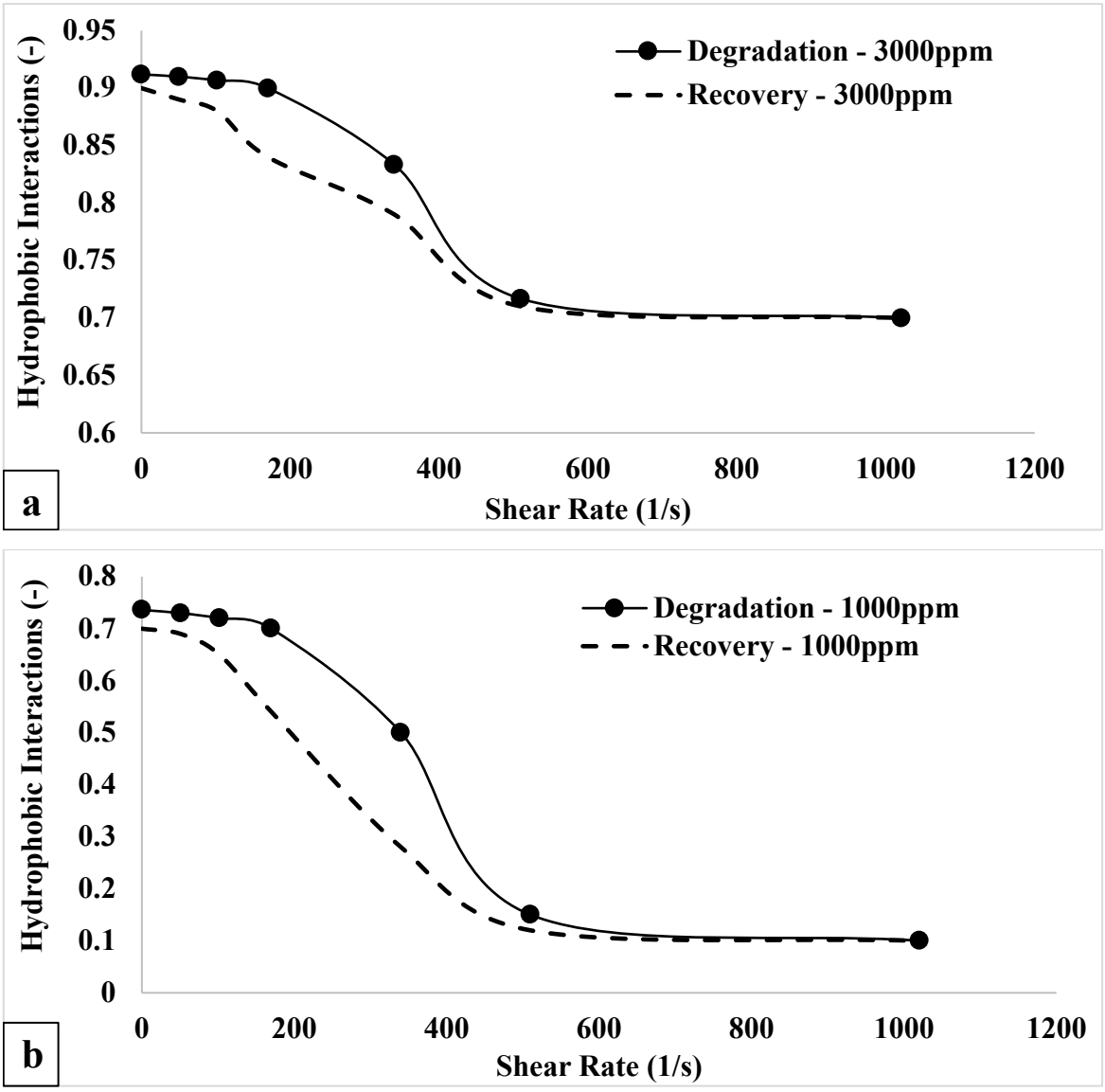

Figure 6.13*: Shear degradation and recovery of hydrophobic interactions at 25 °C and 4.9 %TDS for different polymer concentrations (a) 3,000 ppm (b) 1,000 ppm.*

Consideration of the interaction effect between temperature and shear rate on the hydrophobic interaction shows that the disentanglement process starts immediately and takes place between 0 – 51 s^{-1} and beyond this will result in a relatively constant

degradation process. Clearly, from Figure 6.12b, reservoir conditions on hydrophobic interactions occur through a factor interaction approach rather than a single factor approach. Figure 6.13 shows the recovery process of the polymer chains after the gradual removal of the applied shear rate.

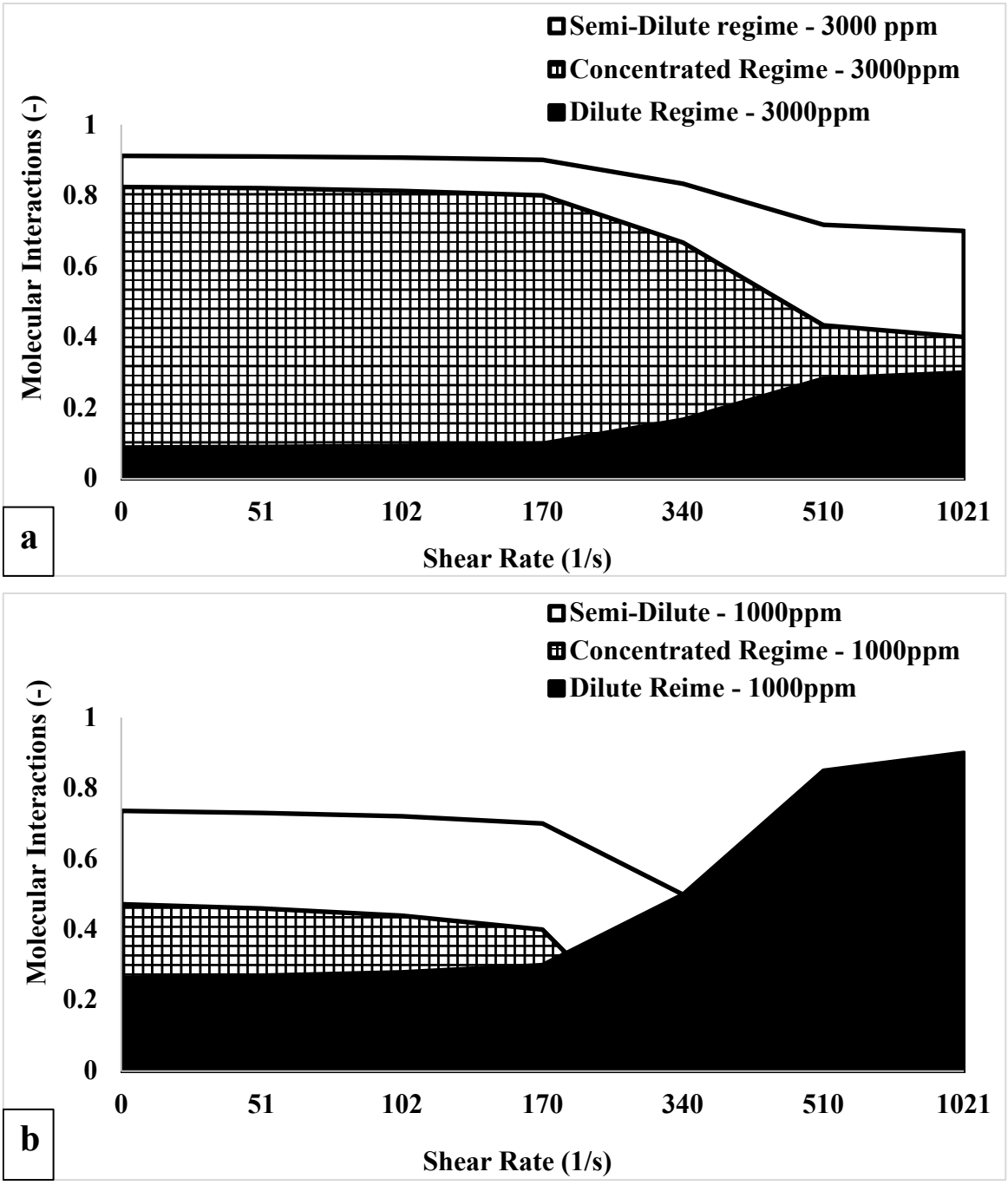

***Figure 6.14**: Effect of shear on the concentration regimes of the associative polymer at 4.9 %TDS and 25℃ (a) 3,000 ppm (b) 1,000 ppm.*

The recovery path of the polymer after the removal of the shear rate does not follow the same path as the degradation process. This indicates that some disentangled polymers from the hydrophobic interaction network do not associate back due to mechanical degradation

or chain scission. As such, the bounded area represents the fractional amount of polymer chains lost to scission or breakage. Figure 6.14 shows the corresponding effect of shear conditions on the polymer concentration regimes. At 3,000 ppm, it was observed that between 0 and 170 s^{-1} there was a minimal change associated with the concentration regimes. This stems from the high proportion of polymer molecules in solution and the relatively strong network of hydrophobic interactions between them, which counteracts the effects of the associated drag force on the network. However, between 170 and 510 s^{-1}, there were significant changes in the concentration regimes. Nevertheless, the proportion of polymer molecules in the semi-dilute regime was higher than the concentrated regimes indicating that molecules from the concentrated regime were lost to both the dilute and semi-dilute regime as shown in Figure 6.14a. Between 510 and 1021 s^{-1}, the concentration regimes maintained a relatively unchanged state. At 1,000 ppm, the pattern and trend observed were different from that obtainable at 3,000 ppm. Between 0 and 170 s^{-1}, the observed trend with concentration regimes reflected minimal changes indicating that the strength of the hydrophobic interactions was relatively greater than the applied drag force acting on the hydrophobic interaction network. However, between 170 and 1021 s^{-1}, there was a rapid transition from the concentrated regime to the semi-dilute to the dilute regimes. This arises from the fact that the strength of the applied force is greater than the strength of the hydrophobic interactions between molecules in the network. Furthermore, it can be observed that the molecules disentangled from the network were distributed between the dilute and semi-dilute regimes, with the dilute regime taking most of the disentangled molecules as the applied shear rates increased (Figure 6.14b). This shows that at improved flow conditions, the dilute regime becomes the dominant regime.

6.3. Experimental Validation of the Predictive Mapping of Conc. Regimes

6.3.1. Normalized Remaining Viscosity and Dimensionless Concentration

Equation (3.8) relates the normalized remaining viscosity, H_μ with the dimensionless concentration parameter, H_{C_p} used for characterising the hydrophobic interactions. Figure 6.15 shows the plot of H_μ against H_{C_p} for bulk rheological measurement using a viscometer. It would be observed that the normalized values for the viscosity at concentrations above the critical aggregation concentration directly matches the dimensionless concentration parameter.

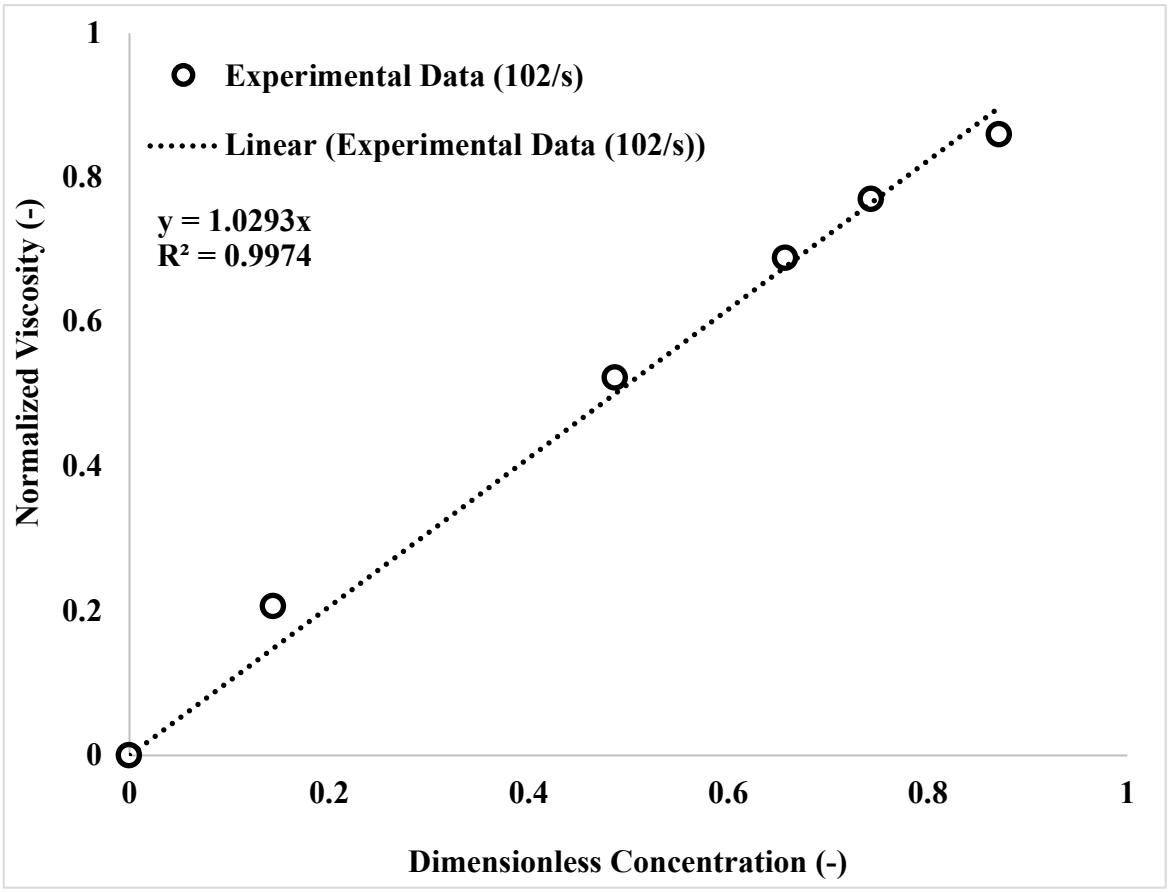

Figure 6.15*:Plot of normalized remaining viscosity against dimensionless concentration at 25℃, 4.9 %TDS and 102s^{-1}.*

The outcome represented in Figure 6.15 implies that the normalized remaining viscosity can be used to experimentally validate the mapping of the concentration regimes tracked in the previous section (Section 6.2). For experimental mapping of the hydrophobic interactions, equation (6.1) applied.

$$H_\mu = \frac{\mu_{ap} - \mu_{ag}}{\mu_0 - \mu_s} \quad (6.1)$$

Where μ_{ag} is the polymer viscosity at the critical aggregation concentration for the onset of hydrophobic interactions. However, Equation (6.1) takes into account both the semi-dilute and the concentrated regime. To distinguish semi-dilute from the concentrated regime, equation (6.2) was applied

$$H_\mu = \frac{\mu_{ap} - \mu_{sep,c}}{\mu_0 - \mu_s} \quad (6.2)$$

Where $\mu_{sep,c}$ is the polymer viscosity at the critical separation concentration for the onset of the concentrated regime. Thus, Equation (6.2) was used to distinguish the concentrated regime from the semi-dilute regime experimentally. In the case of the dilute regime, this was estimated simply as the deduction of the values of Equations (6.1) and (6.2) from one.

6.3.2. Polymer Concentration Regime Profile

Figure 6.16 shows the outcome of the normalized remaining viscosity at various temperature for 3,000 and 1,000 ppm.

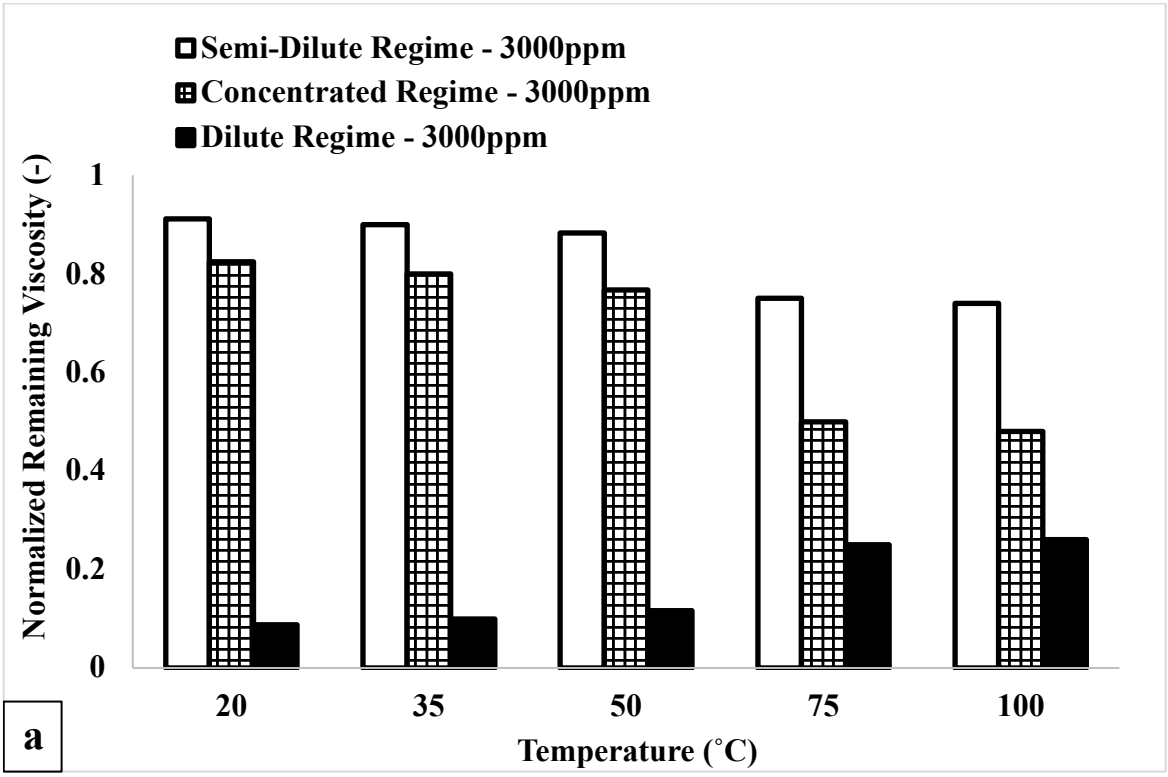

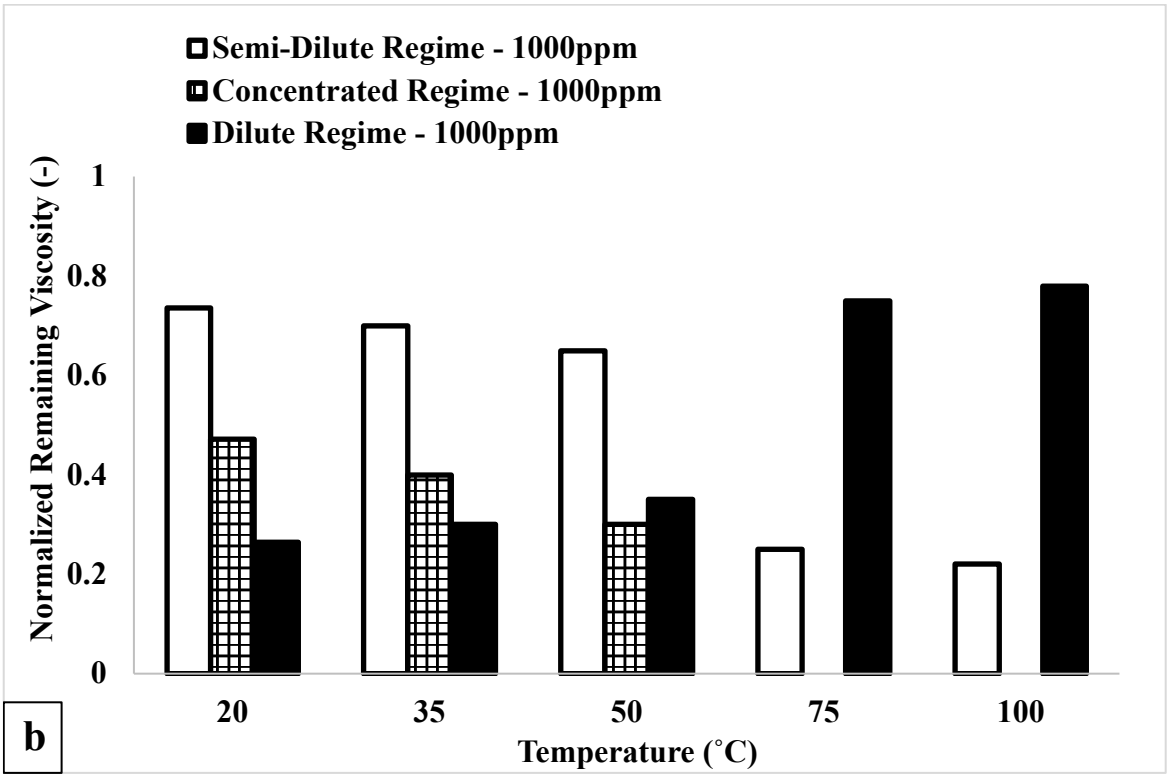

***Figure 6.16**:Plot of normalized remaining viscosity against temperature at 4.9 %TDS and 7.34 s^{-1}(a) 3,000 ppm (b) 1,000 ppm.*

The observed trends at 3,000 and 1,000 ppm were like what was predicted for the concentration regimes using the dimensionless concentration parameter for the quantitative characterisation of hydrophobic interactions. Similarly, Figure 6.17 shows the normalized remaining viscosity under different shear conditions.

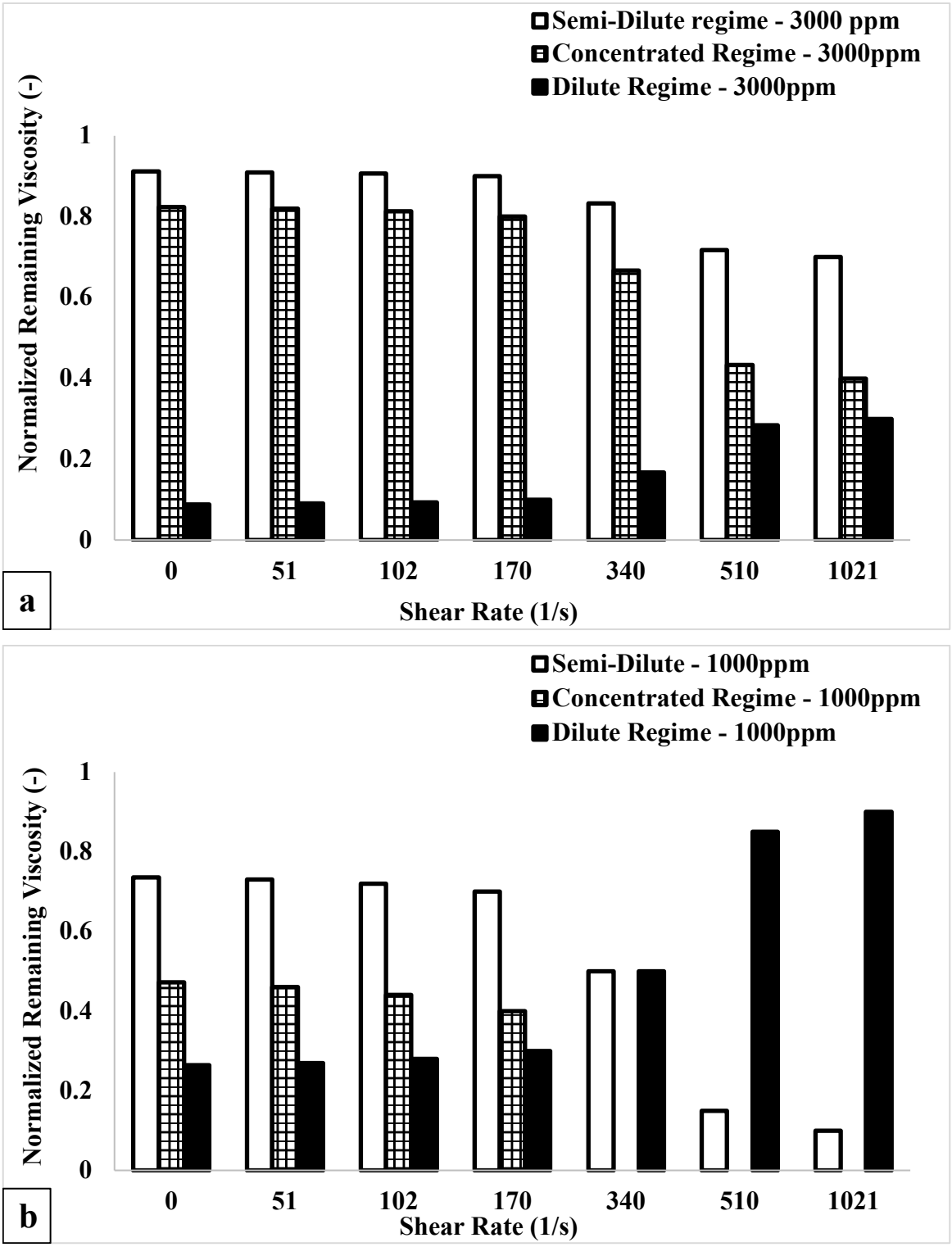

Figure 6.17*:Plot of normalized remaining viscosity against shear rates at 4.9 %TDS and 25 ℃(a) 3,000 ppm (b) 1,000 ppm.*

These observed trends under shear and temperature conditions were reflected under the predictive mapping of the concentration regimes.

6.4. Reversibility of Hydrophobic Interactions and Optimal Conditions

It was established from the preceding section that hydrophobic interactions between associative polymers are recoverable. However, the recovery process after subjecting it to thermal or shear degradation is not entirely complete. This incomplete recovery process results from the mechanical degradation or scission of some polymer chains after disentanglement from the hydrophobic interaction network. In this section, the effect of the various reservoir conditions studied on hydrophobic degradation was considered in the recovery of hydrophobic interactions. The goal of this section was to find the optimal reservoir conditions at which complete recovery of hydrophobic interactions would take place.

6.4.1. Optimal Themal Conditions for Hydrophobic Interaction Recovery

The recovery of hydrophobic interactions at different heating temperatures was captured in Figure 6.18.

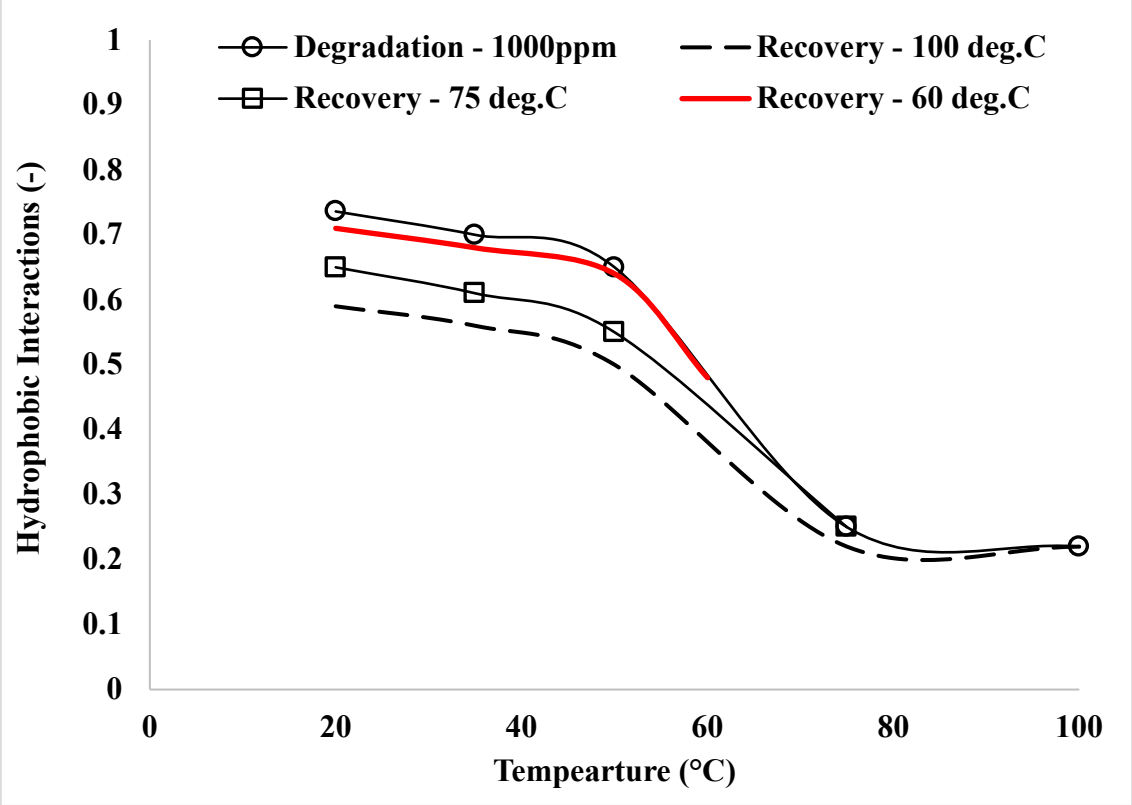

***Figure 6.18**: The recovery study of hydrophobic interactions (1,000 ppm, 7.34/s and 4.9 %TDS) after heating to temperatures 60, 75, and 100 ℃ respectively.*

The recovery paths after heating at 75 and 100 ℃ did not follow the degradation paths. The reason for this is, as explained earlier, stems from polymer chain breakage or scission. The breakage of polymer chains increases with the heating temperature. However, a careful study of the recovery of the hydrophobic interactions between polymer chains showed that at temperatures between 0 and 60 ℃, the thermally separated polymer chains from the interaction network experience complete recovery. However, for temperatures beyond 60 ℃, the recovery of the polymer chains back into the hydrophobic interaction network is not complete due to the degradation of some polymer chains. Therefore, an optimal temperature exists where the reversibility of associative polymers is maintained. However, this optimal temperature condition was determined while keeping other conditions such as salinity and shear rate constant.

6.4.2. Optimal Shear Conditions for Hydrophobic Interaction Recovery

Figure 6.19a shows the shear recovery of hydrophobic interactions after degradation at shear rates 340, 510, and 1021 s^{-1} respectively. The inability of hydrophobic interactions to be recovered along the degradation path after shearing at 510 and 1021 s^{-1} was due to chain scission or breakage. The mechanical degradation or scission of polymer chains ensures that the resulting smaller chains do not have sufficient hydrophobic blocks to initiate the strength of molecular interaction needed to re-associate with the hydrophobic interaction network. However, the recovery of hydrophobic interactions after shearing at 340 s^{-1} was almost on the same path as the shear degradation process. Therefore, the applied shear rate up to 340 s^{-1} allowed hydrophobic interactions to be sustained. In addition, the effect of shearing time on the sustainability of hydrophobic interactions was investigated. This was imperative as the propagation of associative polymers in porous media was done at a given shear rate and increasing shearing time. Figure 6.19b shows the time-dependent shear degradation of hydrophobic interactions at a constant rate of 100 s^{-1}(less than the optimal value of 340 s^{-1}). It can be observed that the propagation or shearing time significantly affects the recovery of hydrophobic interactions after the removal of shearing conditions. After prolonged shearing (9 hrs), the recovery of hydrophobic interactions indicated that polymer chains were still subjected to chain scission or mechanical degradation. This scission process was evident from the area bounded by the degradation and recovery curves in Figure 6.19b. The time-dependent scission of polymer chains occurred due to prolonged exposure of associating polymer network to shearing conditions. Although the applied flow conditions may not equate to the strength of

hydrophobic interactions between polymer chains, the constant application of the same flow conditions weakened the hydrophobic interactions over time.

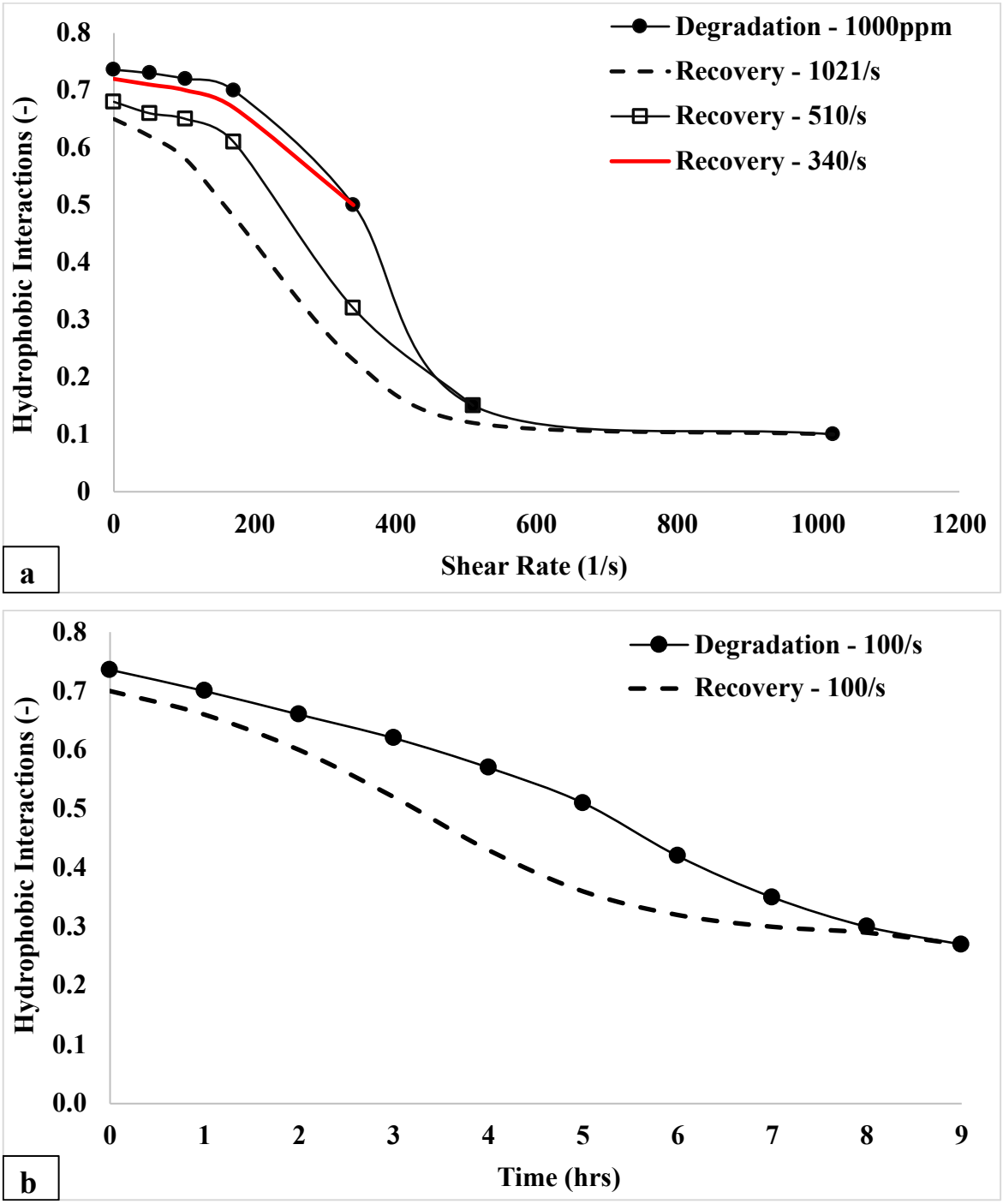

***Figure 6.19**: (a) The recovery study of hydrophobic interactions (1,000 ppm, 25 ℃ and 4.9 %TDS) after shearing at 340, 510, and 1021 s^{-1} respectively. (b) time-dependent study of the degradation and recovery of hydrophobic interactions at 25 ℃, 4.9 %TDS and shear rate of 100 s^{-1} for polymer concentration of 1,000 ppm.*

The weakening process of the hydrophobic interactions started from polymer chains with short hydrophobic blocks on its backbone and this progressively moved towards polymer chains with large hydrophobic blocks on its backbone. Figure 6.20 shows a plot indicating

a combination of the effect of polymer concentration, temperature, and shear rate on the associative interaction between polymer molecules. It can be observed that degradation effect is prominent at lower concentration due to less associative interactions as explained previously. This is indicated by the large area between the curves at 1,000 ppm compared to 3,000 ppm for both temperature and shear degradation.

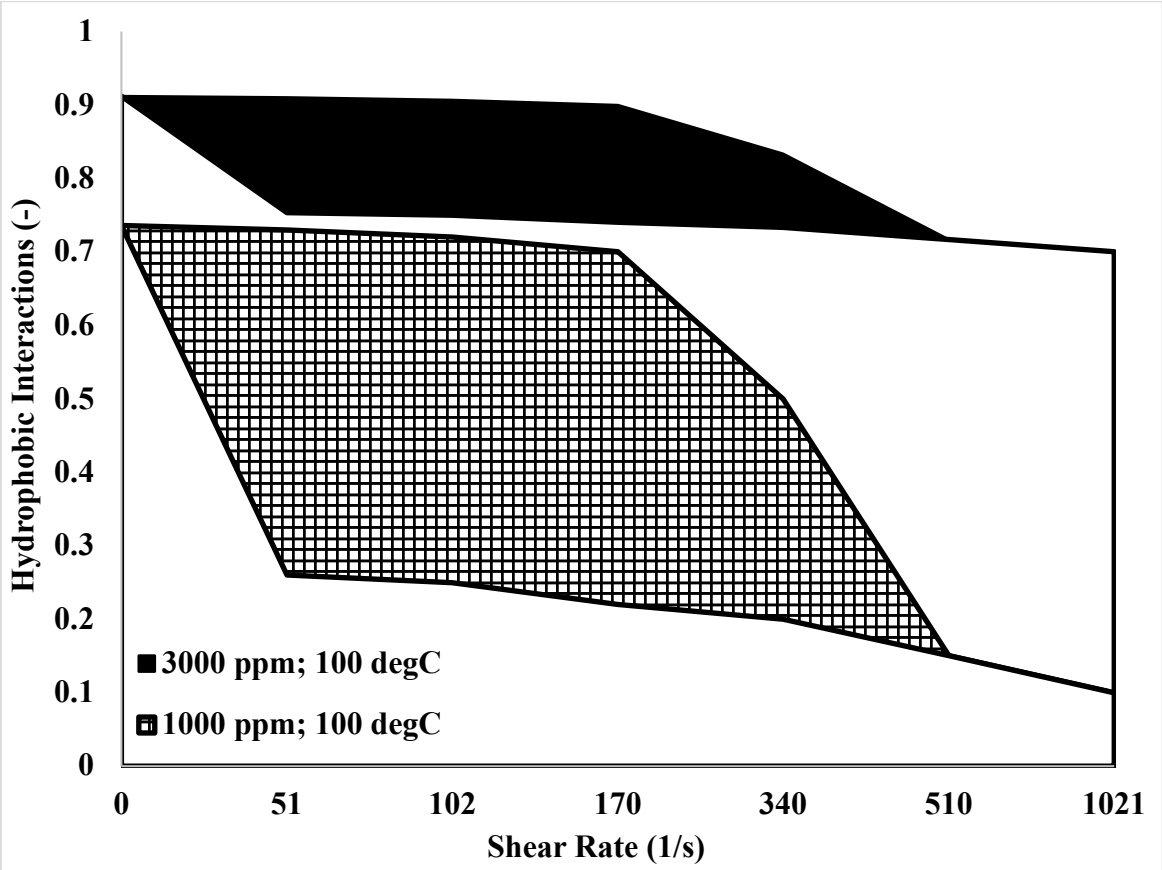

***Figure 6.20**: Plot showing the effect of the combination of polymer concentration, shear rate and temperature on the degradation of hydrophobic interactions between associative polymer molecules.*

6.5. Summary

Three concentrated regimes characterise polymer solutions. The dilute and semi-dilute regimes are well reported in the literature, with the concentrated regime less reported. The hydrophobic interactions between associative polymer chains were primarily a function of the balance between the molecular interactions arising from the hydrophobic effect in the semi-dilute regime and the intramolecular association dominant in the dilute regime. The effectiveness of these hydrophobic interactions was enhanced when operating above the critical aggregation concentration. The key finding reported in this chapter included the quantification of hydrophobic interactions in the semi-dilute regime and intramolecular

interactions in the dilute regime using dimensionless parameters defined based on suitable theoretical assumptions. This quantification procedure allowed for a clear numerical indication of the difference in the proportion of molecular interactions between the dilute and the semi-dilute regime. Also, a novel approach was developed for predicting the onset of the concentrated regime. This novel procedure ensured that the concentrated regime could be uniquely mapped out from the semi-dilute regime. This outcome of mapping out the concentrated regime gave two new insights into molecular interactions between associative polymers. Firstly, hydrophobic interactions were not the dominant molecular interactions under the semi-dilute regime. Beyond the critical aggregation concentration, there was an incremental growth in hydrophobic interactions; however, these interactions were less than the intramolecular interactions. Secondly, hydrophobic interactions were the dominant molecular interactions under the concentrated regime. Beyond the critical separation concentration, hydrophobic interactions dominate over the intramolecular interactions, and the proportion of these interactions was greater than the intramolecular interactions. The value of the critical separation concentration tends to vary with temperature, shear rate and brine salinity, like the critical aggregation concentration, which was evident in the mapping of the various concentration regimes. Consequently, the significance of this novel approach for the numerical description of the various concentration regimes is the control, monitoring and prediction of the sustainability of hydrophobic interactions under different reservoir conditions. This can be translated or adjusted for in the required polymer concentration for oil recovery operations.

CHAPTER SEVEN

7.0. Quantitative Mapping of Retention Mechanisms in a Porous Media

This chapter focussed on the outcome of the novel predictive approach developed for the quantitative mapping of the various retention mechanisms connected with associative polymers. Furthermore, a novel and modified experimental method for studying rate and concentration-dependent polymer retention in porous media were developed for validating the predictive approach. This was based on an accurate correlation of static to dynamic retention, which allowed for the corresponding mapping of the various retention mechanisms using well established trends in literature.

7.1. Predicting Polymer Retention Mechanisms

7.1.1. Transformation of Particle to Pore Size Distribution

The transformation of grain size to pore size distribution during packing was carried out using a modified form of the Kozeny-Carman equation for absolute permeability. The Kozeny-Carman equation is shown in equation (7.1)

$$k = \Phi_s^2 \frac{\phi^3 R_{gr}^2}{180(1-\phi)^2} \quad (7.1)$$

Where R_{gr} is the grain size of the disaggregated sand, k is the absolute permeability of the sand-packed media, Φ_s^2 is the sphericity (a measure of how close a particle resembles a perfect sphere) of the particles in the packed bed, which is 1 for spherical sand particles, ϕ is the porosity of the packed sand. The modified form of the Kozeny-Carman equation involved replacing the absolute permeability with the pore size, R_p as shown in equation (7.2). This assumed that flow through a porous medium can be represented by flow through a bundle of tubes of different radii. Within each tube, the flow rate is low enough that flow is laminar rather than turbulent (Skauge et al., 2018).

$$R_p^2 = \Phi_s^2 \frac{\phi^3 R_{gr}^2}{180(1-\phi)^2} \quad (7.2)$$

Figure 7.1 shows the plot of the corresponding pore size of the sand-pack media computed using equation (7.1) for the 40/60 and P230 silica sand. The distribution for the P230 silica sand is more skewed to the left, indicating tighter packing of the grain particles with more pore sizes in the lower value region. However, the 40/60 silica sand showed an approximate normal pore size distribution, as the pores were more centred around a higher value than the P230 sand. In like manner, the porosity values for both types of sand were 0.324 and

0.364 for the P230 and 40/60 silica sands respectively. This outcome for the porosity values followed a similar explanation.

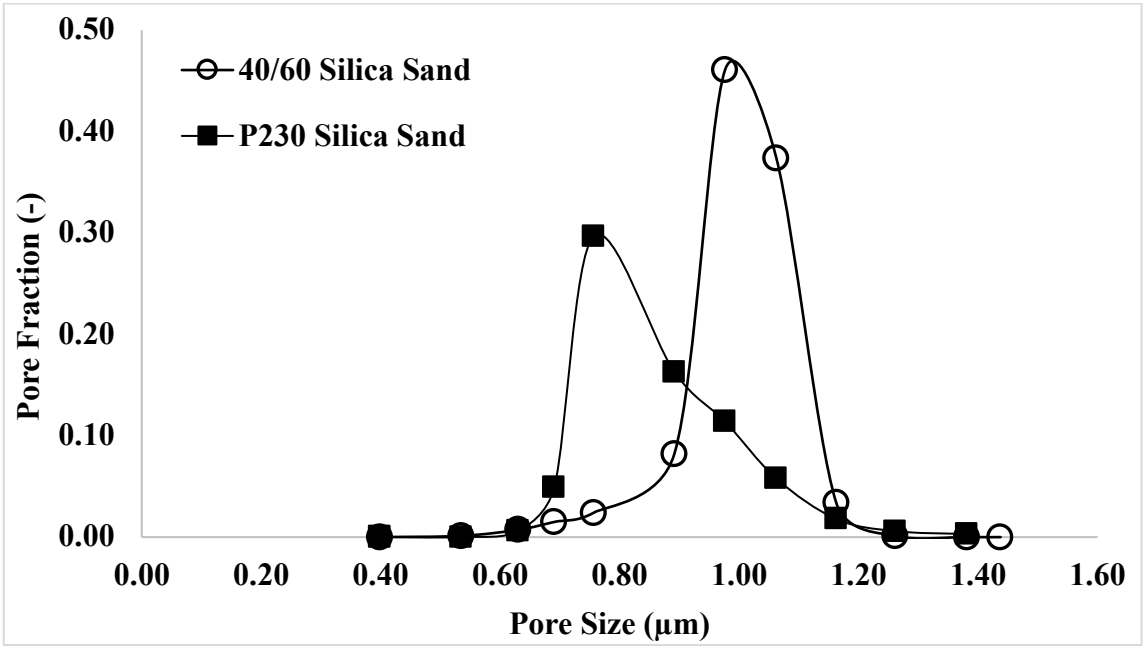

Figure 7.1*: Computed pore size distribution for the packed 40/60 and P230 silica sand*

7.1.2. Damaged Pore Volume (DPVor Γ_D) and Damaged Porosity, ϕ_d

The damaged pore volume, Γ_D represents the fraction of the pore volume damaged due to the various polymer retention mechanisms. These mechanisms, as stated earlier, include adsorption (monolayer or multilayer), entrapment of molecular aggregates and pore plugging. Figure 7.2 shows the plots of the damaged pore volume and damaged porosity against polymer concentration. From Figure 7.2, the DPV increased with polymer concentration while the porosity of the sand-pack media decreased, indicating an increase in the damaged porosity. The trend observed could be attributed to the presence of varied molecular interactions with polymer concentrations. The outcome of this was the multiplicity of various retention mechanisms as the concentration increased. From Figure 7.2a, the DPV maintained a relatively constant value up to about 236 ppm, beyond which there was a rapid rise in the DPV, and this trend could be explained in two parts. Firstly, the relatively constant value for the DPV up to 236 ppm was due to the presence of mainly adsorption. Secondly, the rapid rise in the DPV and damaged porosity beyond 236 ppm was due to a combination of adsorption and mechanical entrapment. This continued up to 750 ppm, beyond which the DPV was relatively constant. The relatively stable value of the DPV beyond 750 ppm indicates that mechanical entrapment starts to dominate the retention

mechanism. The dataset employed in the computation of the fractional damaged pore volume is contained in Appendix D.

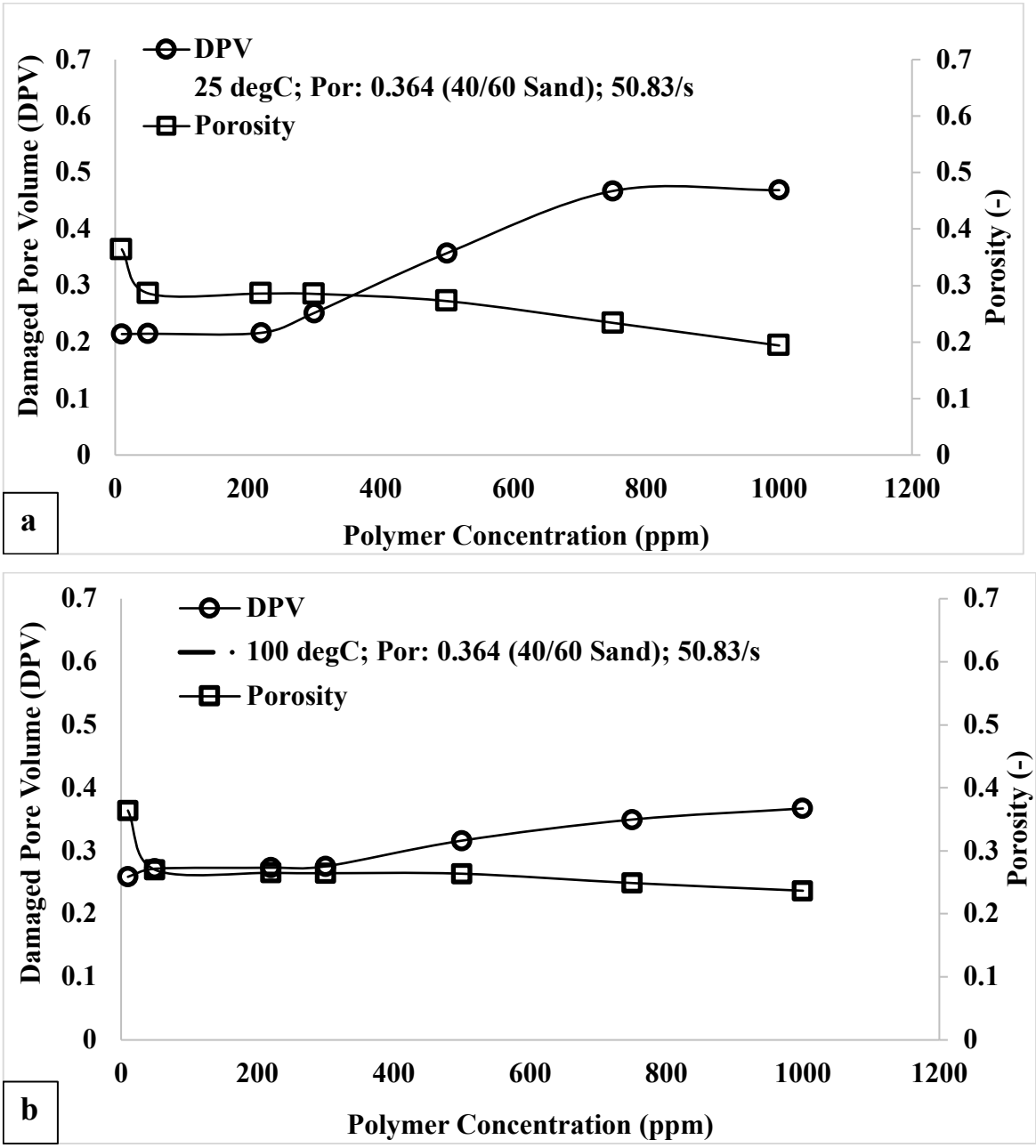

***Figure 7.2**: Plot of damaged pore volume and damaged porosity against polymer concentration at (a) 25 ℃ and (b) 100 ℃.*

Comparing Figures 7.2a and 7.2b shows the effect of temperature on the retention mechanisms observed with the retained polymer. The effect of temperature on the DPV at 100 ℃ was evident from Figure 7.2b, with the multiplicity of retention not observed until about 300 ppm compared to 236 ppm obtained at 25 ℃. In addition, the values for DPV and the damaged porosity increased gradually with concentration at 100 ℃, indicating the effect of thermal degradation on aggregates responsible for mechanical entrapment. Compared

with the conditions at 25 ℃; it could be inferred that adsorption dominated at higher temperatures with the effect of aggregates which brought about entrapment decreasing due to thermal degradation. Figure 7.3 shows the impact of different grain size (350 µm – 40/60 silica sand and 250 µm – P230 silica sand) on the predicted DPV and damaged porosity.

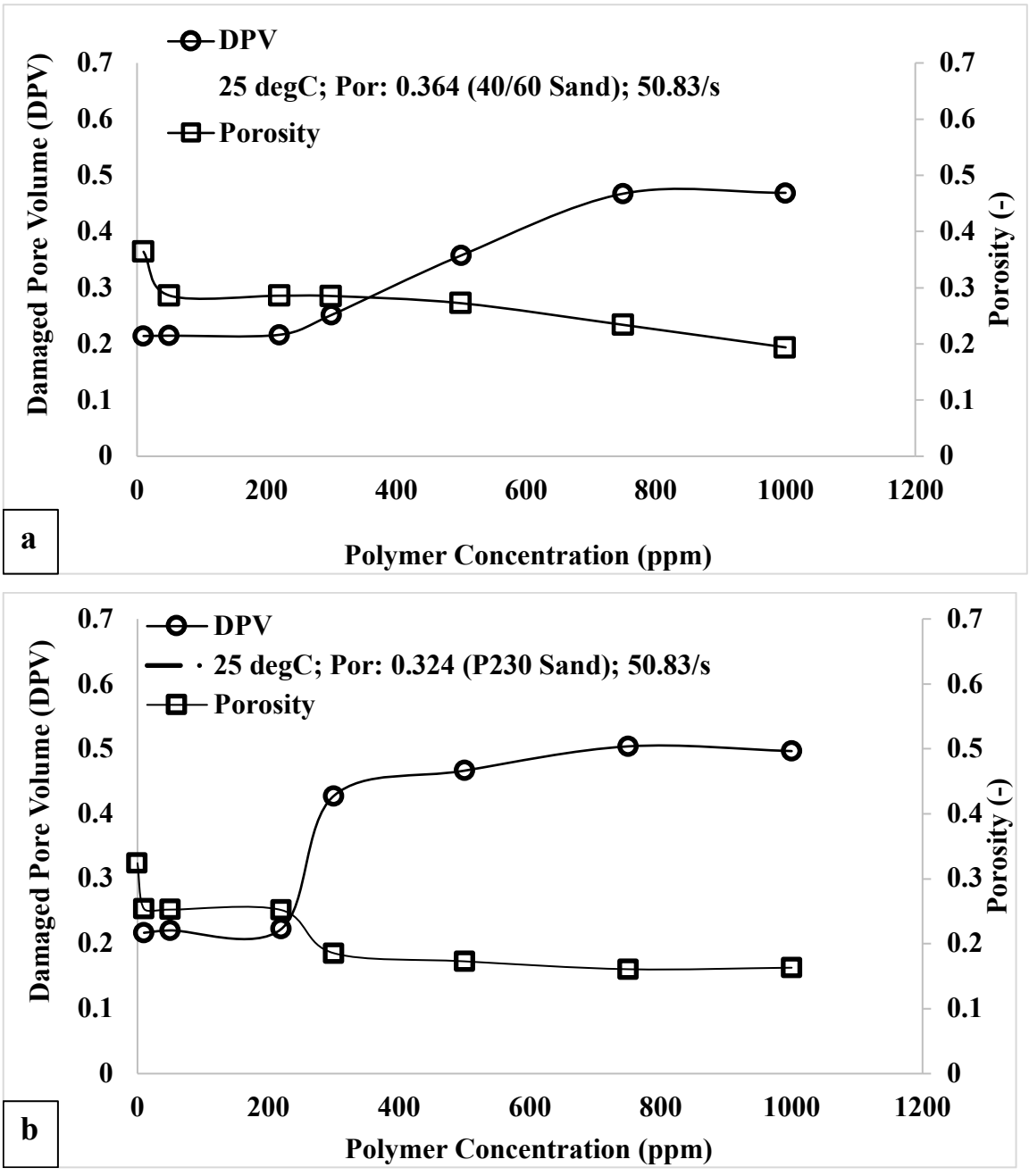

Figure 7.3*: Comparison between the predicted values for the DPV and damaged porosity against polymer concentration for different silica sands: (a) 40/60 and (b) P230.*

It was observed that the predicted values for DPV were higher for the P230 sand compared to the 40/60 sand. The low permeability of the P230 sand allows for more retention of polymer molecules at higher concentrations. For both types of sands, a significant rise in the DPV occurred around 236 ppm. However, there was a rapid rise in the DPV for the

P230 sand compared to the 40/60 sand, and this translated to the effect of significant polymer entrapment in the P230 sand.

7.1.3. Effect of Hydrophobic Interactions on DPV and Damaged Porosity

The associative or hydrophobic interaction between polymer molecules plays a vital role in the retention mechanisms during transport in porous media. Figure 7.4 shows a comparison between the predicted hydrophobic interactions between retained polymer molecules and the damaged pore volume at 25 and 100 ℃.

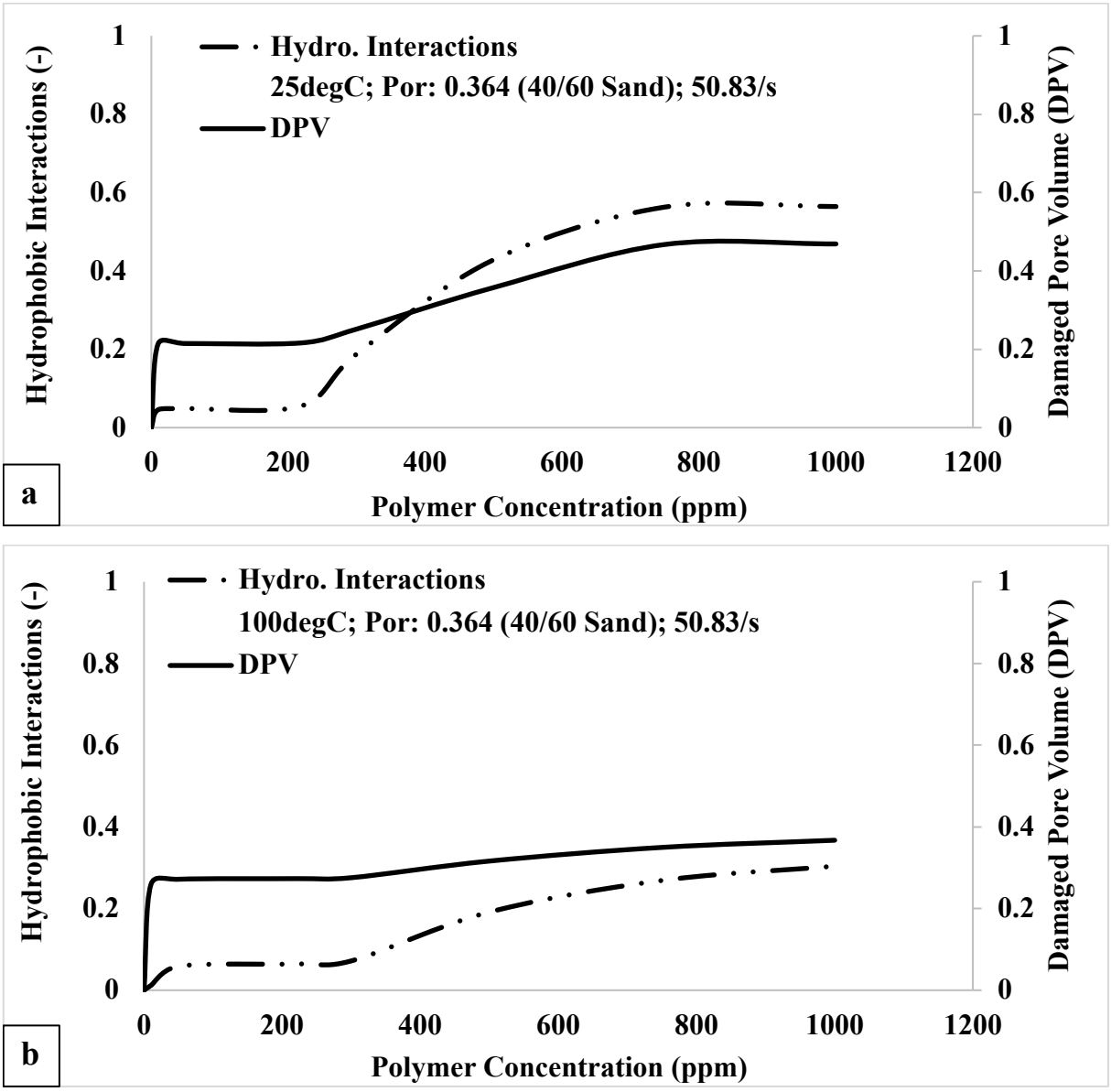

Figure 7.4*: Effect of predicted values of hydrophobic interactions among retained polymer molecules on the damaged pore volume at (a) 25* ℃ *and (b) 100* ℃.

The predicted values for the hydrophobic interactions, H_i were obtained using equation (3.91). Overall, a significant increase in the number of hydrophobic interactions as polymer

concentration increased led to a rise in the estimated damaged pore volume. This was the case irrespective of the temperature conditions at 25 or 100 ℃. However, the impaired pore volume increase was significantly slower at 100 ℃ (Figure 7.4b). This shows the effect of temperature conditions on the ability of retained polymer molecules to associate due to hydrophobic interaction. Similarly, the impact of the sand type on the predicted values for associative effect among the retained polymer molecules is shown in Figure 7.5.

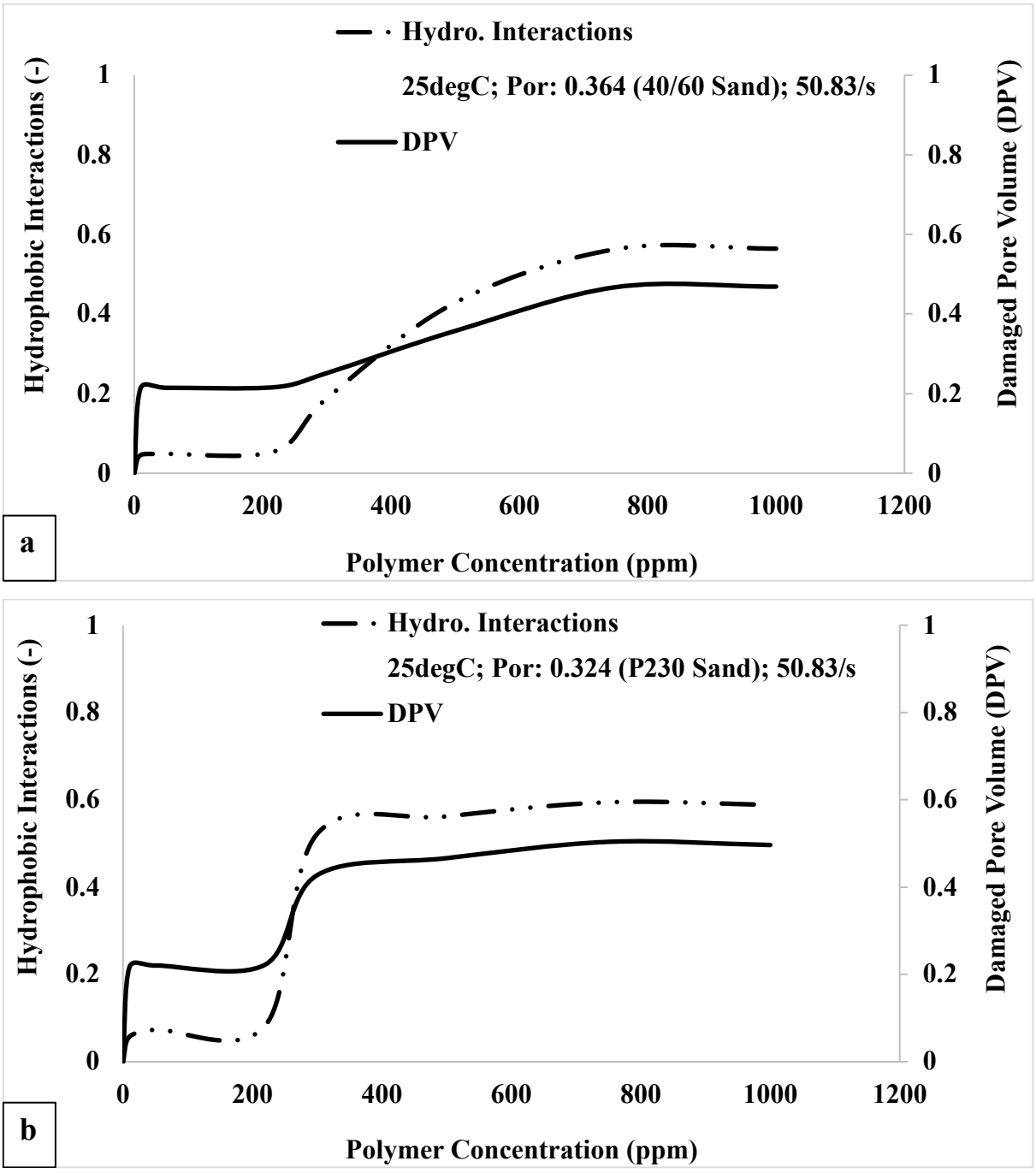

***Figure 7.5**: Predicted values for hydrophobic interactions between retained polymer molecules and the associated damaged pore volume for (a) 40/60 sand and (b) P230 sand.*

It can be observed that the predicted value for the hydrophobic interactions reaches a maximum rapidly for the P230 sand compared to the 40/60 sand. The low porosity of the P230 sand promoted rapid interactions among retained polymer molecules as concentration increased. For both types of sands, a significant rise in the DPV occurred around 236 ppm. However, there was a rapid rise in the DPV for the P230 sand compared to the 40/60 sand, and this translated to the effect of significant polymer entrapment in the P230 sand.

7.1.4. Mapping Retention Mechanisms: Adsorption, Entrapment & Plugging

The previous sections (7.1.2 and 7.1.3) gave a qualitative description of the contributory effect of the various mechanisms to the DPV and damaged porosity. The observed trends were based on the predicted effects of associative interactions among the retained polymer molecules. A quantitative description of the contributory effect of the various retention mechanisms puts a figure to their effect on the overall polymer retention in porous media. Figure 7.6 shows the two plots of the cumulative pore size distribution and the cumulative size distribution of the retained polymer molecules. For the cumulative pore size distribution, the area under the curve from 0.53 to 1.16 μm (as indicated by the thick arrowed line) describes the fractional pore sizes of the sand-pack media. For the second plot, the area under the curve from zero up to a size determined by the operating polymer concentration (represented by the different markers for the data points) describes the fractional size of the retained molecules. For example, the analysis of the retained polymer curve considered concentrations up to 1,000 ppm with the focus on 1,000 ppm, as indicated by the dashed arrowed line in Figure 7.6. The hydrodynamic size of the retained polymer molecules at 1,000 ppm was estimated using equations (3.93) and (3.94). Similar estimation was done for polymer concentrations less than 1,000 ppm. Figure 7.7 shows the relationship between the predicted size of the retained polymer molecules and the associated hydrophobic interactions against the corresponding polymer concentrations. The quantification of the different mechanisms was computed with a specific focus at 1,000 ppm as indicated by the dashed arrowed line. It would be observed that the dashed line encloses an area for the cumulative pore size distribution at 1,000 ppm. This enclosed area gives the inaccessible fractional pore (computed using equation 3.96) of the sand-pack, which arises due to the size of the retained polymer molecules ($R_{hi} \approx R_p$). Similarly, for the cumulative size distribution of the retained molecules at 1000 ppm, it was observed that the enclosed area computed under the pore size distribution was also enclosed under this curve. However, the enclosed space under the retained size distribution gave the fraction of the entrapped

molecules (computed equation 3.95) under the same condition ($R_{hi} \approx R_p$) rather than the inaccessible fractional pore.

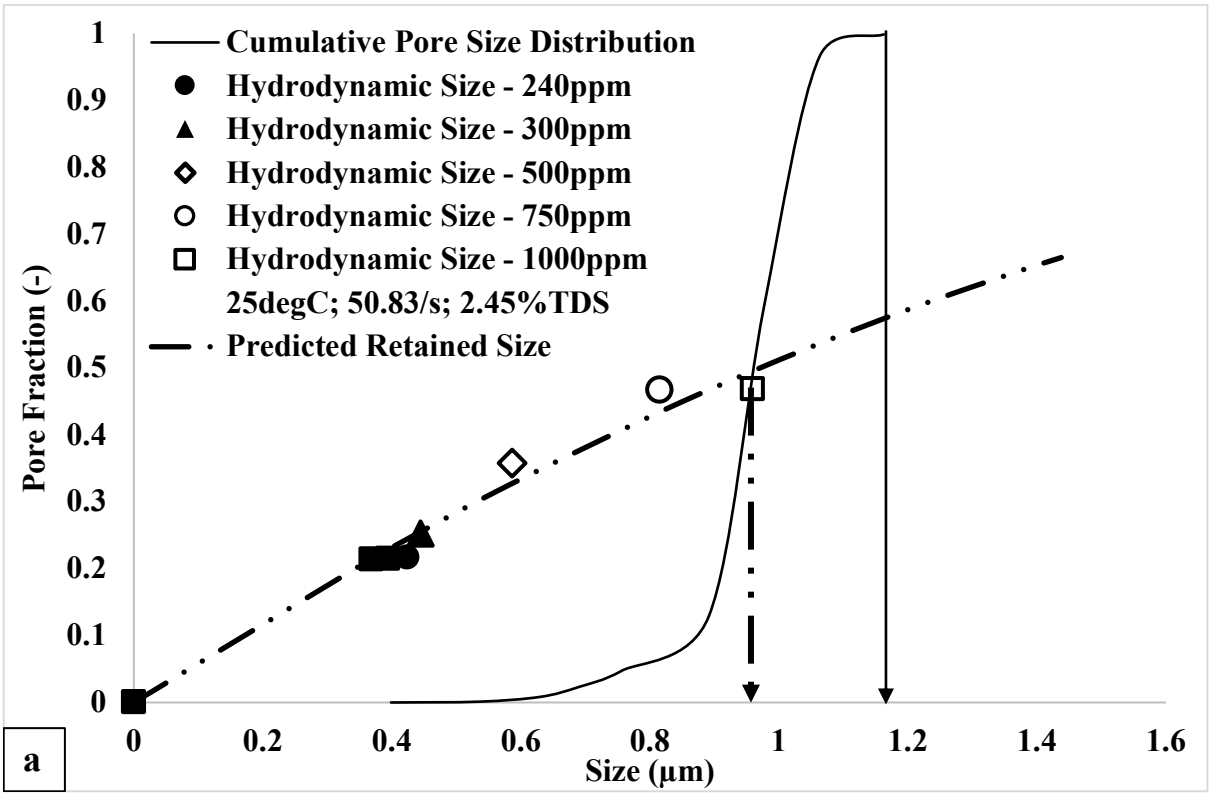

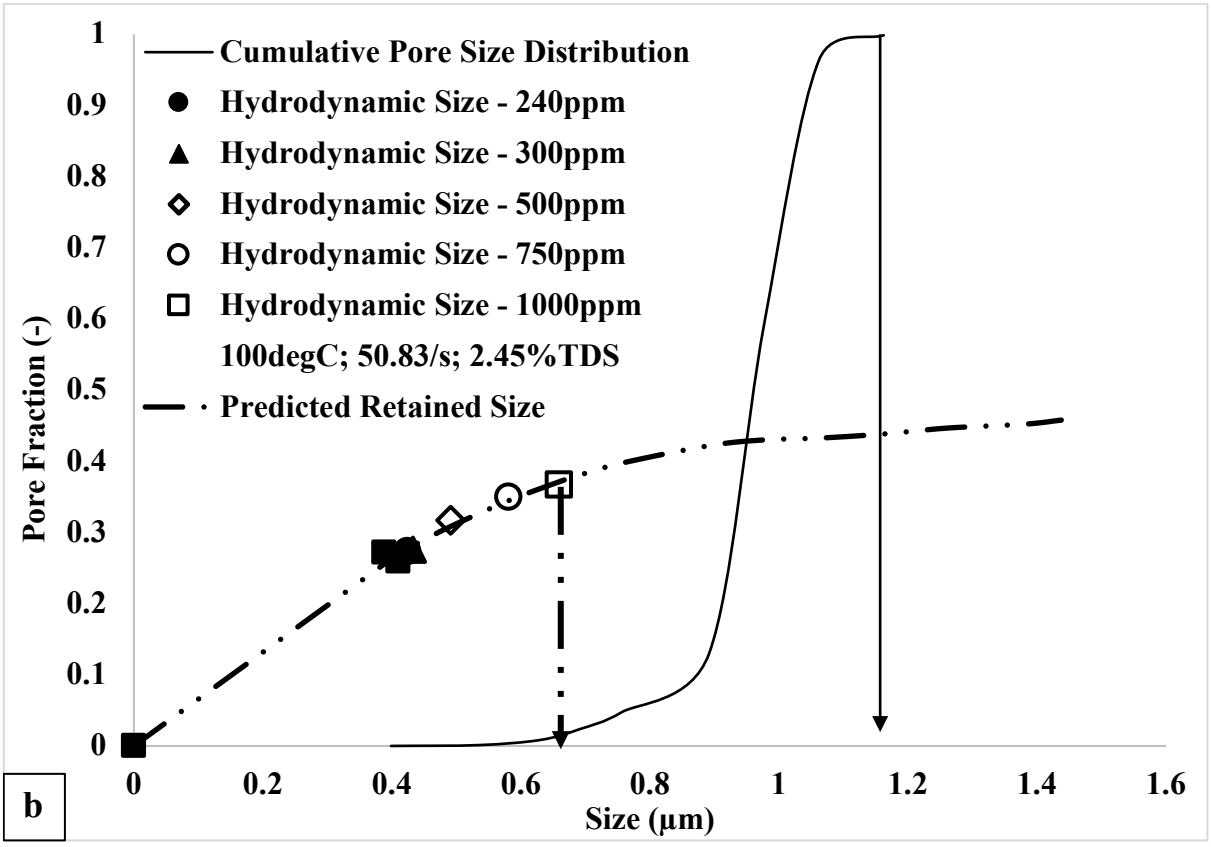

***Figure 7.6**: Prediction, quantification and mapping of the different retention mechanisms of associative polymers at different concentrations at (a) 25 ℃ and (b) 100 ℃.*

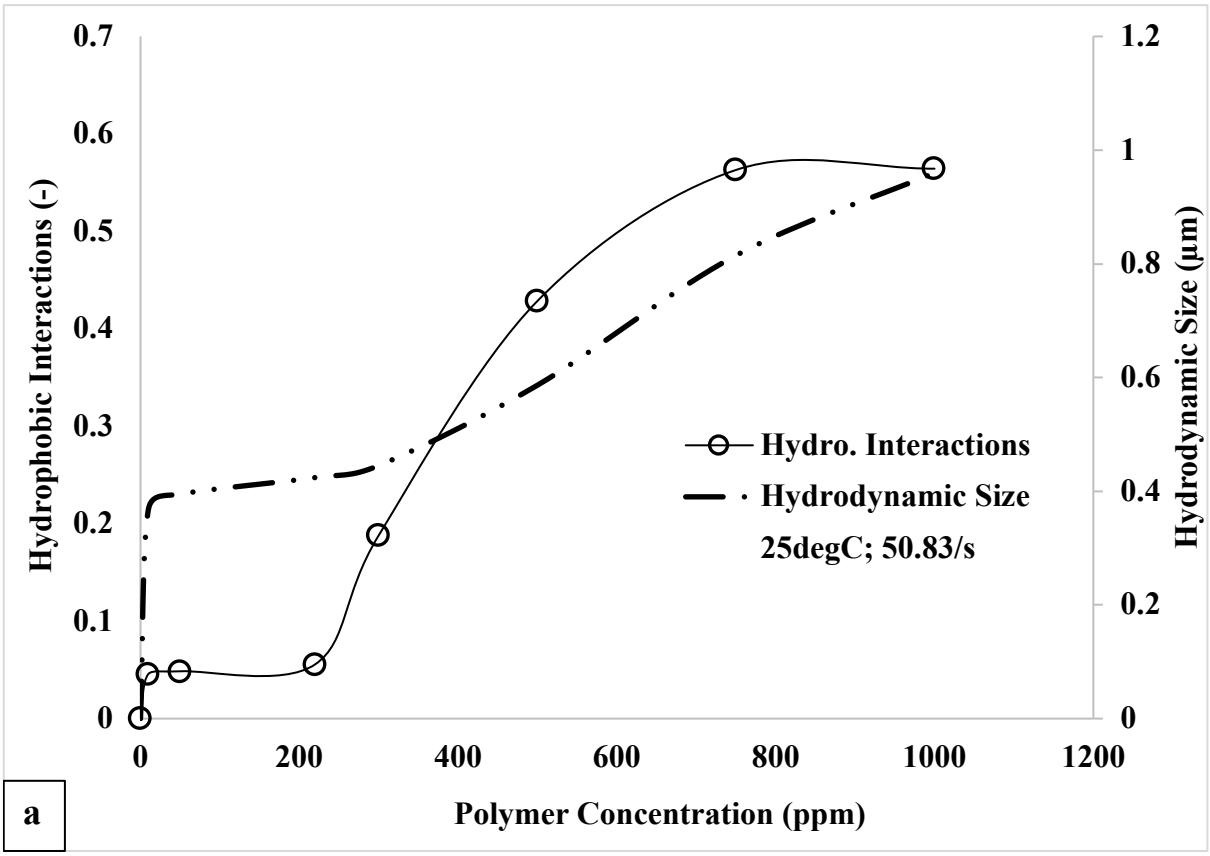

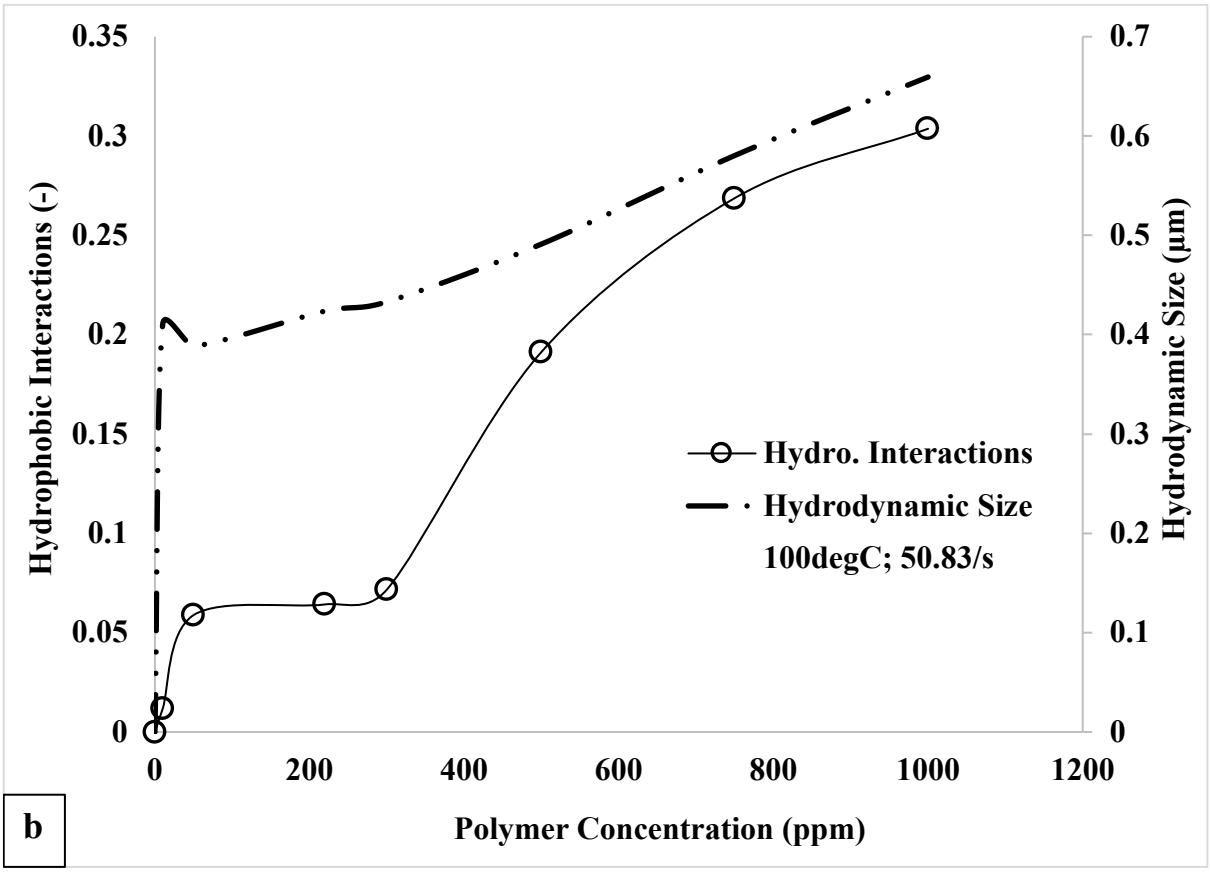

***Figure 7.7**: Plots of predicted hydrodynamic size of retained polymer molecules and the associated hydrophobic interactions against polymer concentrations at (a) 25 ℃ and (b) 100 ℃*

Table 7.1 shows a summary of the predicted values for entrapment and inaccessible pore. However, it would also be observed from Table 7.1 that the predicted values for the inaccessible fractional pore, I_{PV} is greater than the predicted values for entrapment, Γ_{ent}. It was concluded from this that the difference gives the pore fraction that is entirely accessible only to the brine solution, I_{PVo} and not to the polymer as described in equation (7.3)

Table 7.1*: Predicted values in terms of pore fraction for adsorption, entrapment and inaccessible pore volume at 25 and 100* ℃.

25 ℃; 50.83/s			
Concentration (ppm)	**Predicted IPV.**	**Predicted Entrapment**	**Predicted Adsorption**
300	0.006	0.001	0.999
500	0.038	0.015	0.985
750	0.155	0.085	0.915
1000	0.371	0.299	0.701

100 ℃; 50.83/s			
Concentration (ppm)	**Predicted IPV.**	**Predicted Entrapment**	**Predicted Adsorption**
300	0.0051	0.0041	0.996
500	0.0062	0.0043	0.996
750	0.0138	0.0122	0.988
1000	0.0213	0.0187	0.981

Table 7.2**:** *Predicted concentration values for the onset of entrapment and pore plugging at 25* ℃ *and 100* ℃.

Temperature (℃)	**C_{p-ent} (ppm)**	**C_{p-plug} (ppm)**
25	437.43	1574.54
100	710.28	2669.65

$$I_{PVo} = I_{PV} - \Gamma_{ent} \quad (7.3)$$

Pore plugging would occur when the predicted size of retained polymer molecules exceeds the upper limit of the pore size ($R_{hi} > 1.16$ μm). Similarly, computation of the pore fractions due to adsorption was done in like manner, as shown in Table 7.1. The computed hydrodynamic size of the pre-injection polymer was estimated using equation (3.84) as 0.43 μm ($R_h = 0.43$ μm). Therefore, the predicted sizes for the retained polymer molecules less than R_h indicated retention due only to monolayer adsorption. However, beyond R_h marked the onset of multilayer adsorption coupled with entrapment of molecular aggregates ($R_h < R_{hi} < R_p$). It would be observed that the effect of temperature resulted in the adsorption mechanism dominating over entrapment. Increased thermal effects resulted in loss of polymer aggregates, thereby minimizing the impact of molecular entrapment while expanding the influence of adsorption, as shown in Table 7.1. The onset of polymer entrapment was predicted using equation (3.98) and pore plugging with equation (3.99), as shown in Table 7.2. The observed trend with the predicted values for C_{p-ent} and C_{p-plug} were both increased with temperature with reasons due to the loss of molecular aggregates.

7.2. Experimental Validation of Predictive Approach

7.2.1. Correlating Static to Dynamic Retention Distribution

Correlation of the static to dynamic retention was carried out using the novel or modified experimental procedure described in Chapter 4.

7.2.1.1. Equivalent Injected Pore Volume (PV_{inj}) for Dynamic Retention

Under static adsorption in disaggregated sand, it is assumed that the only type of retention mechanism present is adsorption. The disaggregated sand used for the static retention study means that entrapment of polymer molecules was absent. Figure 7.8 shows the polymer adsorption profile against time for different polymer concentrations against time under static conditions. The adsorption of polymer molecules on the sand particles increased with concentration and time, as indicated. The rapid increase in polymer adsorption with concentration is due to the proportion of polymer molecules in solution. At low concentration, the number of molecules in solution is few and the surface coverage is less. As such, maximum adsorption is attained rapidly as represented in Figure 7.8 for concentration at 10 ppm. However, at 1,00 ppm, the number of molecules in solution is large with surface coverage greater than what is obtained at 10 ppm. The presence of more molecules in solution imply that it would take a longer time for solid surface coverage to be

attained. As such, the rate of adsorption is greater at 1,000 ppm compared to 10 ppm meaning more molecules is adsorbed as shown in Figure 7.8.

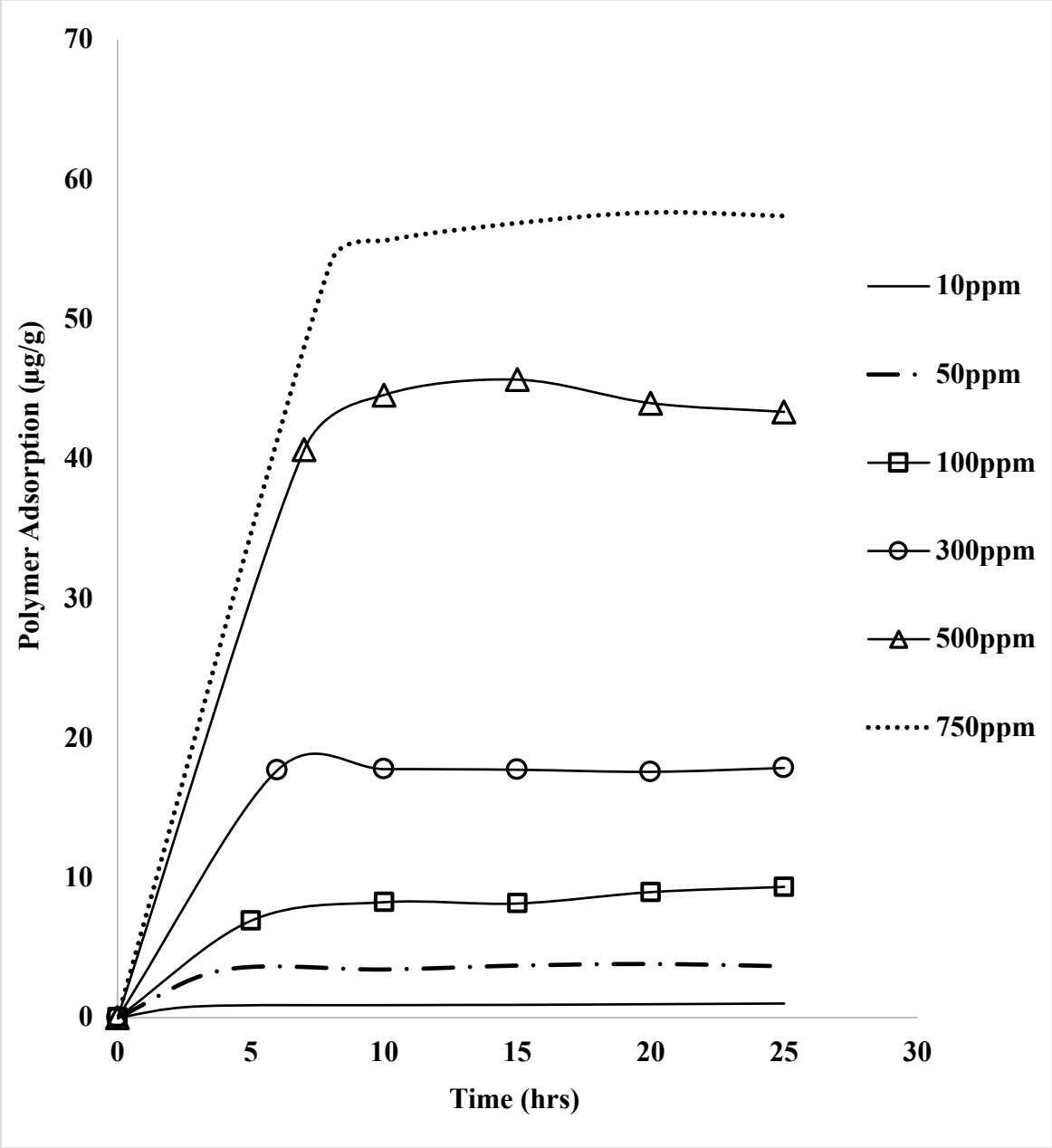

Figure 7.8*: Polymer adsorption against retention time under static conditions at 25 ℃, 2.5 %TDS and solid-liquid ratio of 0.1.*

Similarly, the time for the attainment of maximum retention increased with polymer concentration. The time for maximum polymer adsorption and the equivalent injected pore volume estimated from equation (4.18) is summarized in Table 7.3. The observed trend in the time for maximum retention can be related to the number of polymer molecules in the solution. At low polymer concentration, the number of molecules in solution are few as such fewer molecules diffused to the sand surface, and this process was swift.

***Table 7.3**: Computed equivalent injected pore volume, PV_{inj} for corelating static to dynamic retention at different polymer concentrations at 25 ℃, 2.5 %TDS and solid-liquid ratio of 0.1.*

Concentration (ppm)	Flowrate (ml/min)	Max. Ret. Time (hrs.)	PV_{inj}
100	1	5.1	3.11
	3	5.1	9.33
	6	5.1	18.6
300	1	6.5	4.04
	3	6.5	12.1
	6	6.5	24.2
500	1	7.0	4.35
	3	7.0	13.0
	6	7.0	26.1
750	1	8.2	4.97
	3	8.2	14.9
	6	8.2	29.8

However, at high polymer concentration, more molecules exist in the solution. The diffusion of these molecules to the sand surface is slower as molecules would compete to diffuse to the sand surface. Furthermore, more molecules in the solution mean that the adsorption may go beyond monolayer adsorption to multilayer adsorption, thereby increasing the time for the attainment of maximum adsorption. The equivalent injected pore volumes computed as shown in Table 7.3 were applied during the dynamic retention experiments as shown in the effluent concentration profiles for 500 ppm in Figure 7.9.

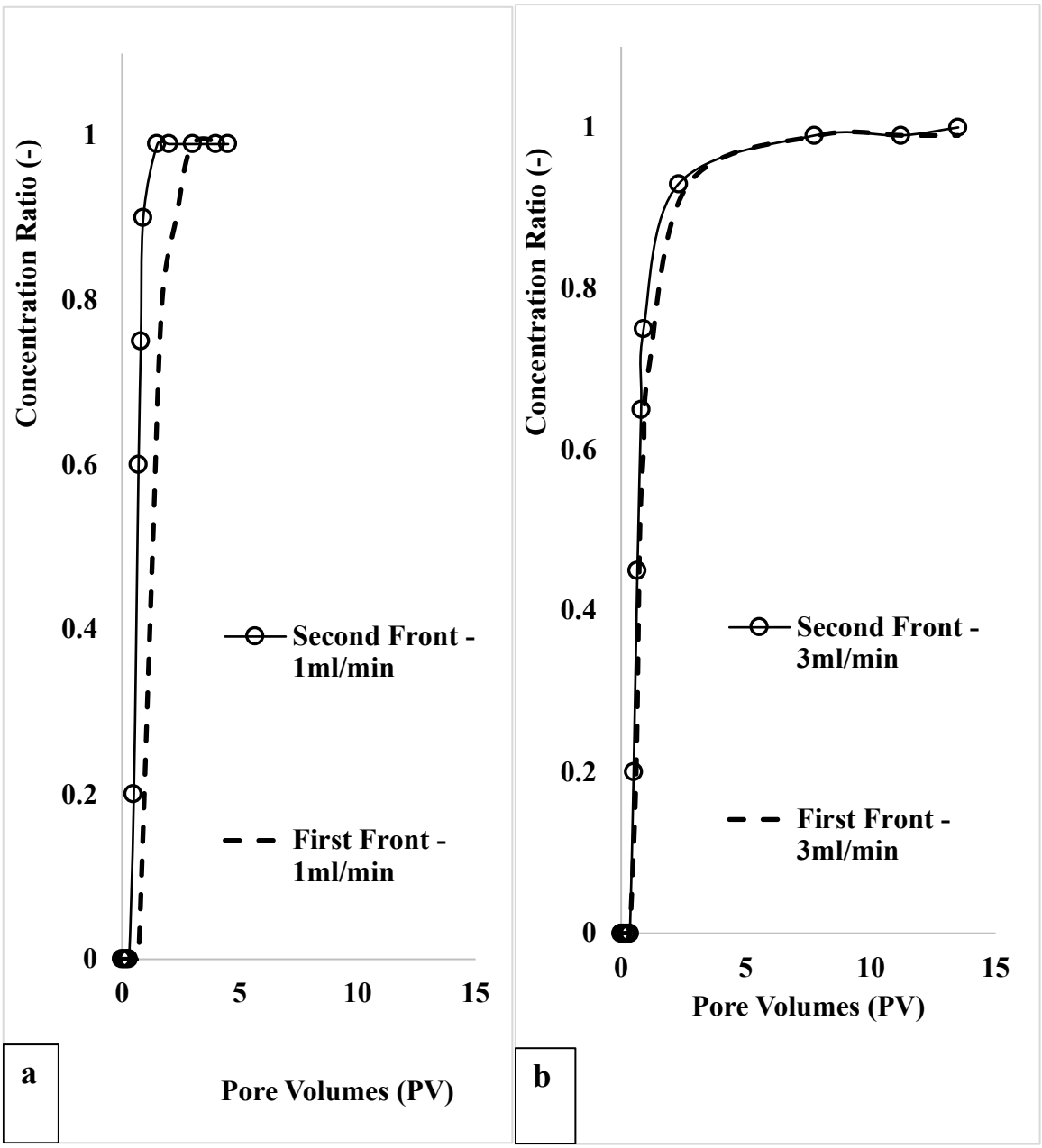

***Figure 7.9**: Effluent concentration profile for PVs up to equivalent PV_{inj} at 500 ppm (a) 1 mL/min (b) 3 mL/min.*

7.2.1.2. Solid to Liquid Ratio

The adsorption of the polymer molecules on the sand surface is a complex phenomenon that depends on the nature of the sand surface and its interactions with the polymer solution. In other words, the quantity of polymer solution and the availability of rock surface area dictate the extent of adsorption. Figure 7.10 show the effect of solid to liquid ratio on the adsorption of associative polymer molecules on the silica sand. Lower adsorption values were observed at low solid to liquid ratios. However, at high solid to liquid ratios, the adsorption values were higher.

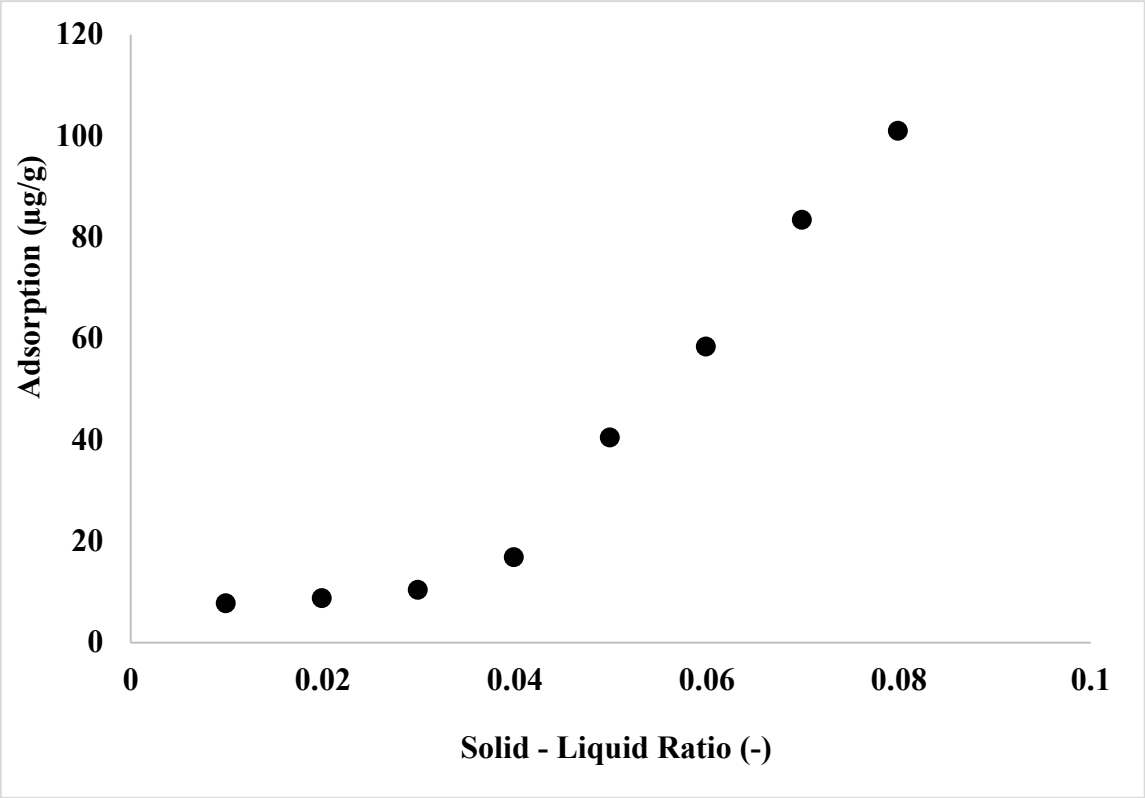

***Figure 7.10**: Effect of solid (specific surface area: 0.202m^2/g) on polymer adsorption for 1,000 ppm polymer solution at 25 ℃, 2.5 %TDS and pH of 7.18.*

This observed phenomenon is explained in terms of the grain surface area available. The available surface area is minimal at a low solid to liquid ratio, meaning that there is less area for polymer interactions with the sand particles. In addition, the steady values of polymer adsorption from 0.01 to 0.04 gives an insight into polymer interaction with the solid surface. At low solid to liquid ratios, the low adsorption values are due to the minimal surface area available for polymer molecules to interact with the solid surface. However, as the solid to liquid ratio increased beyond 0.04, the polymer adsorption increased rapidly. The increased adsorption suggests an increase in the surface area available for the polymer molecules to interact with the solid surface. This shows that the solid to liquid ratio is an essential parameter in the understanding of polymer-rock interaction.

7.2.2. Experimental Outcome on Mapping Polymer Retention Mechanisms

7.2.2.1. Effect of Flow Condition on Polymer Retention Mechanisms

Figure 7.11 shows the effect of flow conditions on the retention of associative polymers in the porous media using the novel experimental procedure. Operating at a low flowrate (Figure 7.11a), polymer adsorption was higher, and at a high flowrate (Figure 7.11b),

polymer adsorption was lower. The low adsorption isotherms under dynamic conditions arise due to the reduced contact time available for polymer molecules to interact with the sand surface.

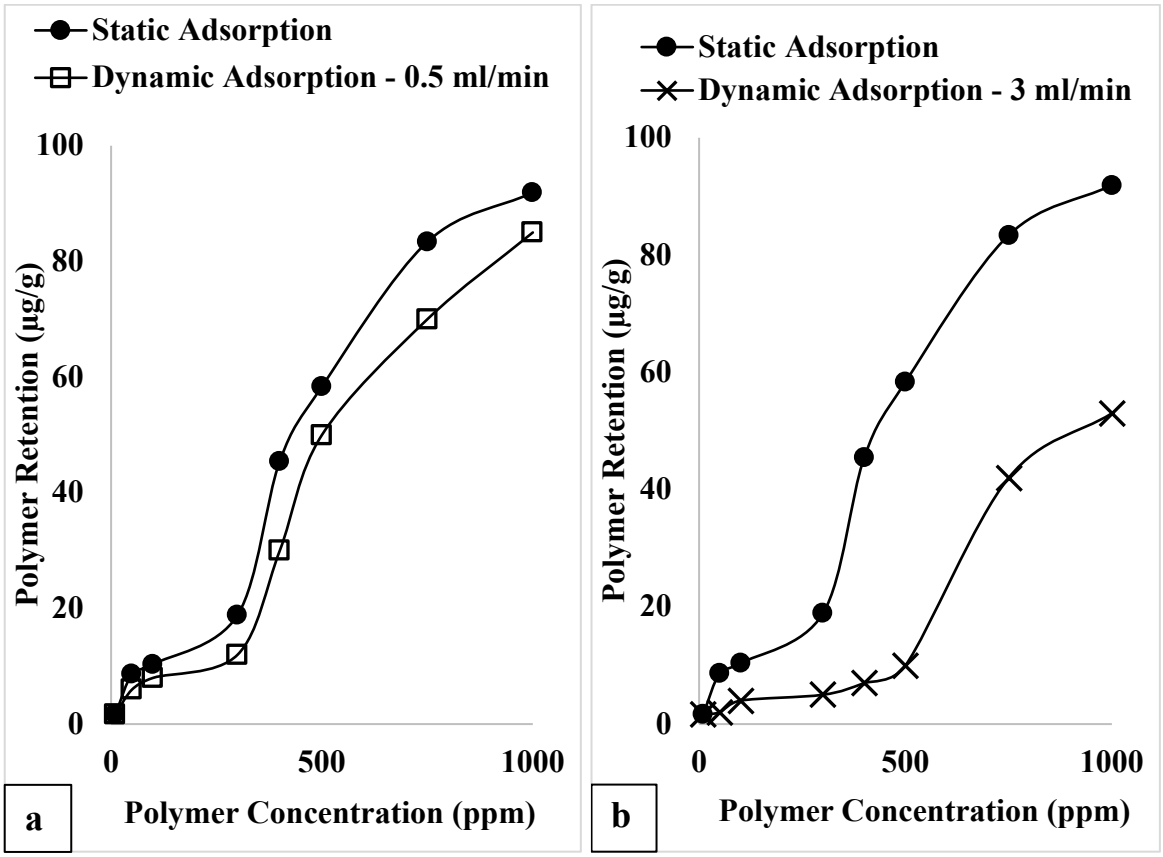

Figure 7.11*: Effect of flow conditions (flow rate) (a) 0.5 mL/min (b) 3 mL/min on the dynamic adsorption of associative polymer at 2.45 %TDS and 25* ℃.

The available contact time for polymer molecules increased with a reduced flow rate. However, dynamic adsorption in porous media is complex to understand compared with the static adsorption process. In addition, the disaggregated nature of the sand grains under the static adsorption test ensures that the exposed surface area per volume is higher than the compacted sand grains under dynamic conditions, which allows for a minimal exposed surface area per volume. Furthermore, the effect of inaccessible pore volume confirmed that the flow of polymer solution was accelerated in the porous media, thereby limiting the contact time and the proportion of molecules available to interact with the rock surface. The enclosed area by the adsorption isotherms in Figure 7.11 represents the amount of entrapped polymer molecules, as shown in Figure 7.12. Comparing Figure 7.12a and Figure 7.12b, the hydrodynamic retention arising from an increase in flow rate from 0.5 to 3 mL/min is computed as the difference in the enclosed area at 3 mL/min and 0.5 mL/min. The numerical value at each concentration was calculated using equation (4.21).

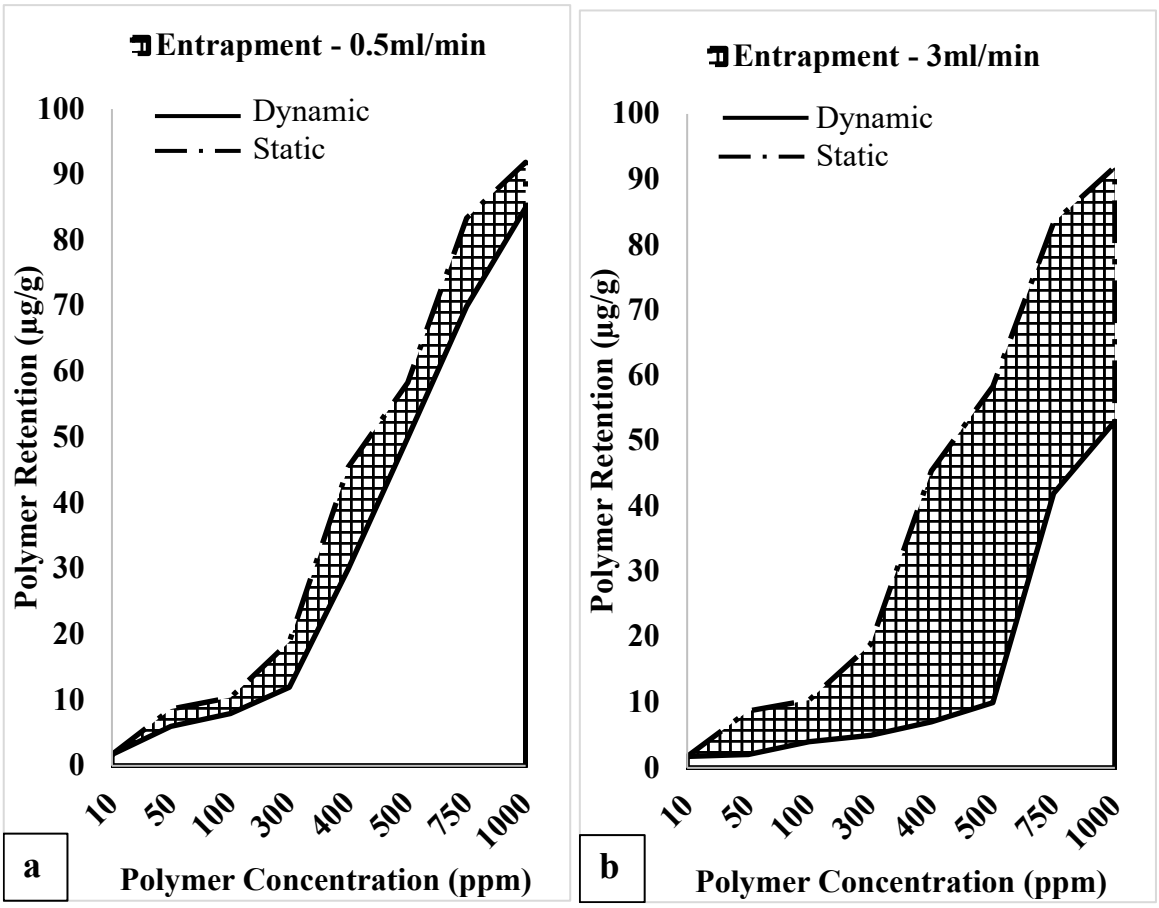

***Figure 7.12**: Effect of flow conditions (flow rate) (a) 0.5 mL/min (b) 3 mL/min on the entrapment of associative polymer at 2.45 %TDS and 25 ℃.*

Similar estimation was done using equation (4.21) at flowrates of 0.5 and 3 mL/min respectively. The trend from this outcome is that polymer entrapment increased with the flow rate at each polymer concentration. Entrapment was higher for each concentration at a higher flow rate, as shown in Figure 7.12b. The concentration dependency arises when multiple molecules in the form of aggregates arrive simultaneously at the pore throat large enough to admit one molecule, but not several molecular aggregates. From the above, the modified experimental approach provided more detailed information into the effect of flow condition on the adsorption and entrapment of polymer molecules.

7.2.2.2. Effect of Temperature on Polymer Retention Mechanisms

Figure 7.13a and Figure 7.13b shows the polymer adsorption isotherm at 1.5 mL/min for different temperatures of 25 and 100 ℃ respectively. It was observed that as the temperature increased from 25 to 100 ℃, the adsorption isotherm decreased. The increase in temperature results in an increase in the negative charge of the sand grains, and the outcome of this is

an increase in the charge repulsion between the exposed rock surface and the charged groups (carboxyl group, COO^-) on the remnant polymer molecules attached to the rock surface.

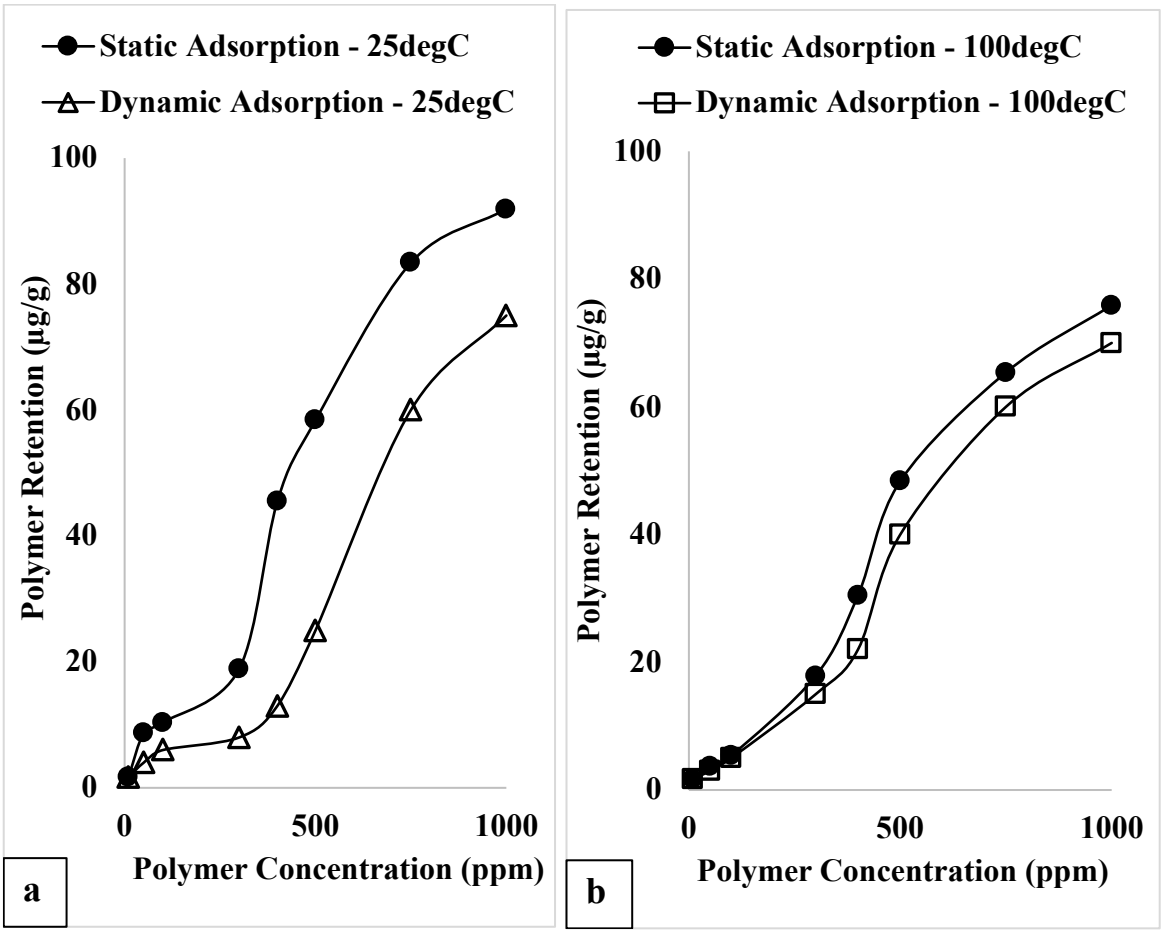

Figure 7.13*: Effect of temperature on the adsorption of associative polymer at a flowrate of 1.5 mL/min and 2.45 %TDS (a) 25* ℃ *and (b) 100* ℃*.*

This charge repulsion ensures that remnant polymer molecules on the rock surface are detached, reducing the adsorption isotherm. Similarly, the segment of polymer molecules attached to the rock surface via hydrogen bonding or van der Waals forces was lost due to thermal degradation, resulting in decreased adsorption. Figure 7.14a and Figure 7.14b shows the temperature effect on the entrapment of polymer molecules as estimated using equation (4.21). Polymer molecular aggregates are responsible for the entrapment mechanism in the porous media, and this arises when the size of the aggregate is about the size of the pore throat. However, increased temperature conditions allowed for the degradation of intermolecular interaction responsible for this, thereby reducing the size of the aggregates. This would allow for easy transport of the polymer molecules through the pore throat with reduced retention; however, the loss of the intermolecular interaction would have a significant effect on the mobility control mechanism of the polymer solution.

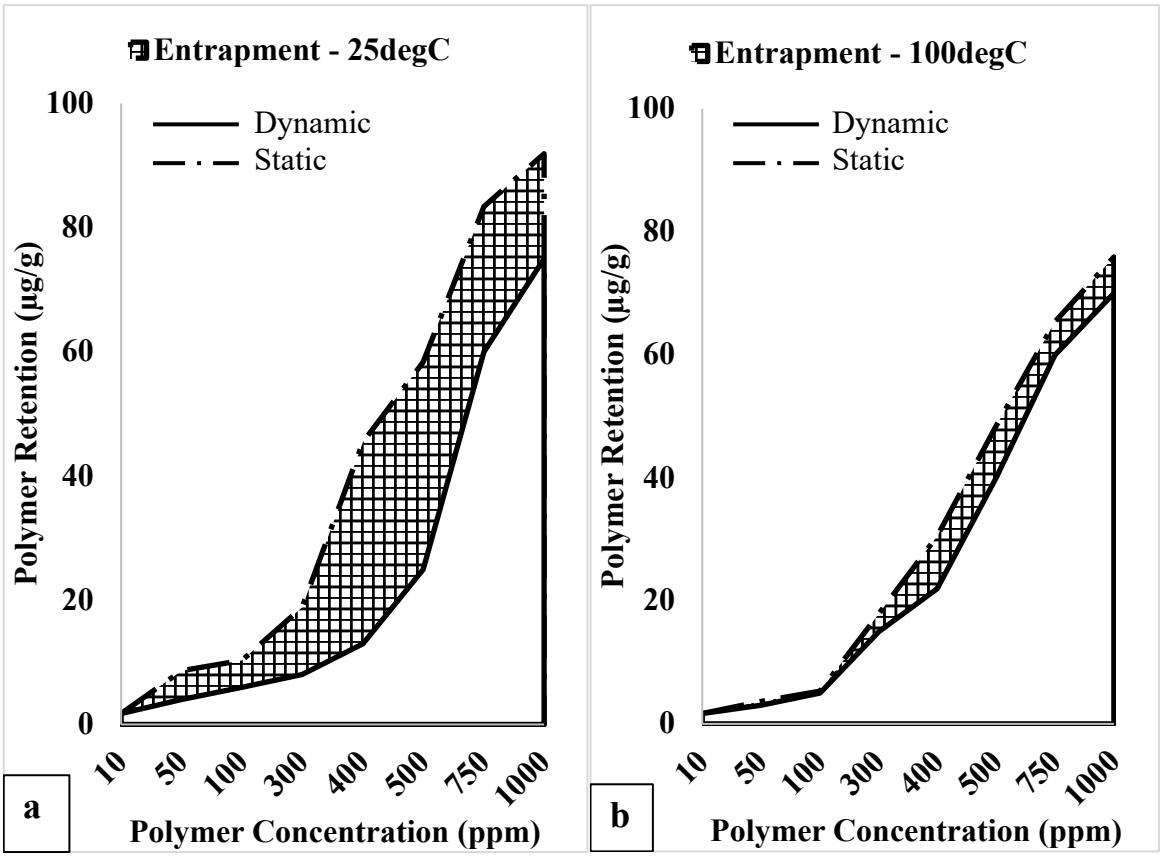

Figure 7.14*: Effect of temperature on the entrapment of polymer molecules on the 40/60 silica sand saturated with 2.45 %TDS brine solution and at a flowrate of 1.5 mL/min.*

7.2.2.3. Effect of Brine Salinity on Polymer Retention Mechanisms

From Figure 7.15, the adsorption of the polymer molecules increased with brine salinity from 2.5 to 4.9 %TDS with the ratio of monovalent sodium ions (Na^+) to divalent calcium ions (Ca^{2+}) kept at 10:1 irrespective of the concentration. Before contacting the sands with the polymer solutions, the sand grains were saturated with brine solutions with 2.5 to 4.9 %TDS concentrations. The increase in polymer adsorption with salinity is due to the increased presence of monovalent and divalent ions on the rock surface, reducing the charge repulsion between the negatively charged rock surface and the negatively charged carboxyl group on the polymer backbone. Furthermore, the increased ionic content on the rock surface ensures that the hydrodynamic volume of the adsorbed polymer molecule is reduced, thereby ensuring that there is an increased rock surface for more polymer molecules to attach to it. Figure 7.16 show the result of the experimental outcome on the effect of brine salinity on polymer entrapment. The brine salinity reduced the number of polymer molecules entrapped due to a reduction in the hydrodynamic size of the polymer molecules. Like the effect of salinity on adsorption, the presence of monovalent and divalent

ions reduced the charge repulsion between the negative carboxyl group on the polymer backbone.

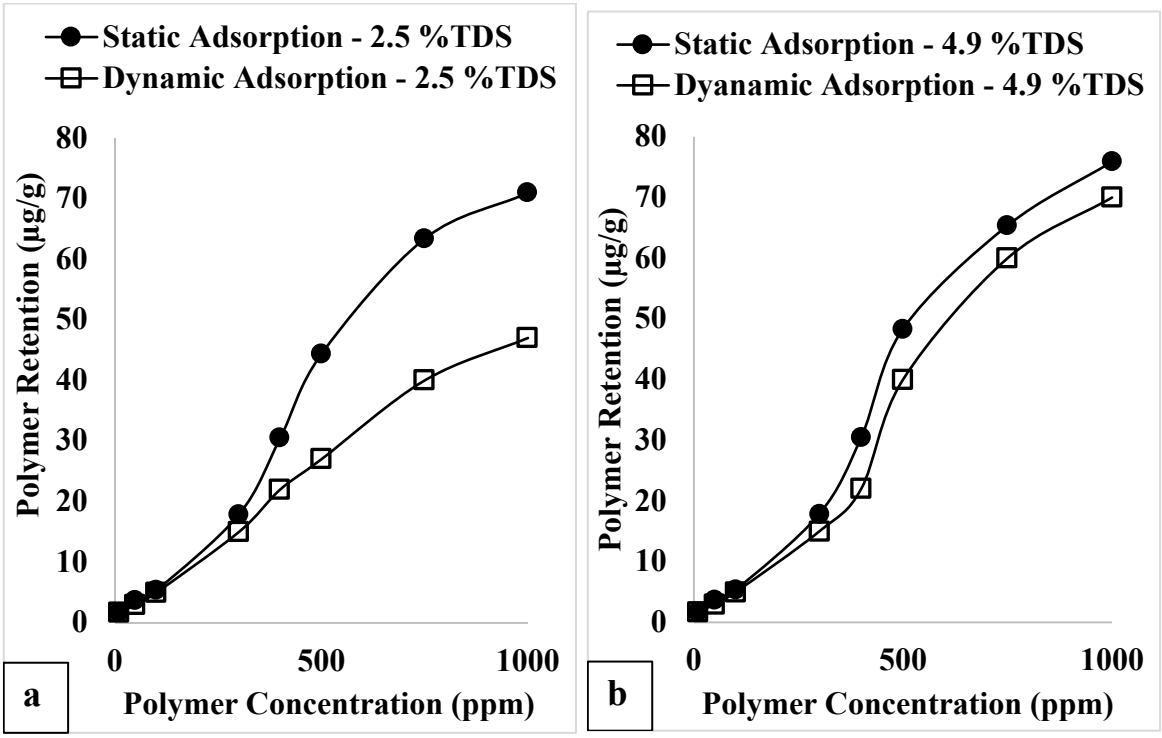

Figure 7.15*: Effect of brine salinity on the adsorption of associative polymer on the 40/60 silica sand at 25* ℃ *and 1.5 mL/min (a) 2.5 %TDS (b) 4.9 %TDS.*

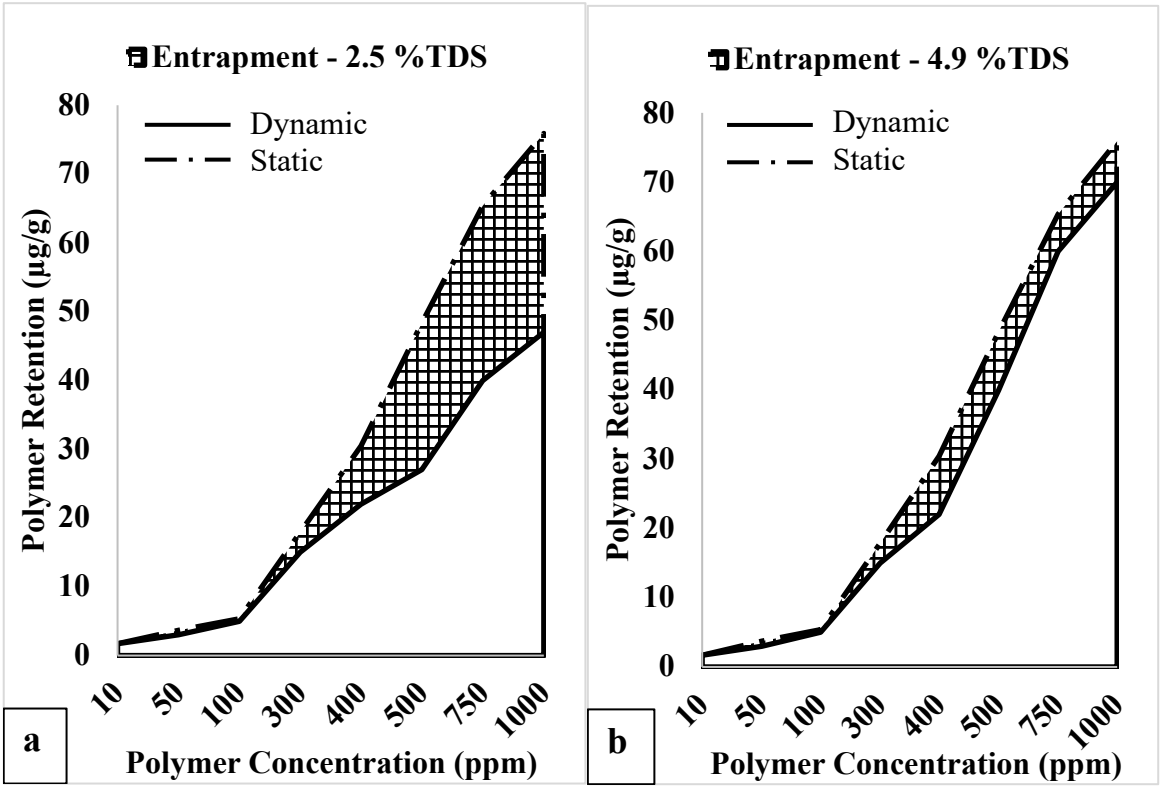

Figure 7.16*: Effect of brine salinity on the entrapment of associative polymer on the 40/60 silica sand at 25* ℃ *and flowrate of 1.5 mL/min (a) 2.5 %TDS (b) 4.9 %TDS.*

7.3. Comparison of Predictive and Experimental Outcomes

7.3.1. Polymer Adsorption

Table 7.4 shows a summary of the predicted and the experimental outcomes for the adsorption of the associative polymer. These outcomes were also plotted, as shown in Figure 7.17.

Table 7.4*: Predicted and experimental values of adsorption in terms of pore fraction at 25 and 100* ℃.

25 ℃; 50.83/s (0.5 mL/min)		
Concentration (ppm)	**Predicted Adsorption.**	**Experimental Adsorption.**
300	0.999	0.899
500	0.985	0.885
750	0.915	0.795
1000	0.701	0.852

100 ℃; 50.83/s (0.5 mL/min)		
Concentration (ppm)	**Predicted Adsorption**	**Experimental Adsorption.**
300	0.996	0.892
500	0.996	0.953
750	0.988	0.923
1000	0.981	0.933

To compare the effectiveness of the predictive approach in estimating the outcomes of the experimental procedure, the coefficient of determination, R^2 was applied in the correlation of the predicted outcome to the experimental outcome as plotted in Figure 7.17. At 25℃, the coefficient of determination, R^2 was 90.45% while at 100℃, the R^2 was 88.05%. The seemingly significant correlation between the predicted outcome and the experimental outcome shows that the developed experimental approach can be used for the quantitative mapping of the polymer adsorption distinctively from the other types of polymer retention mechanisms attributable to associative polymers.

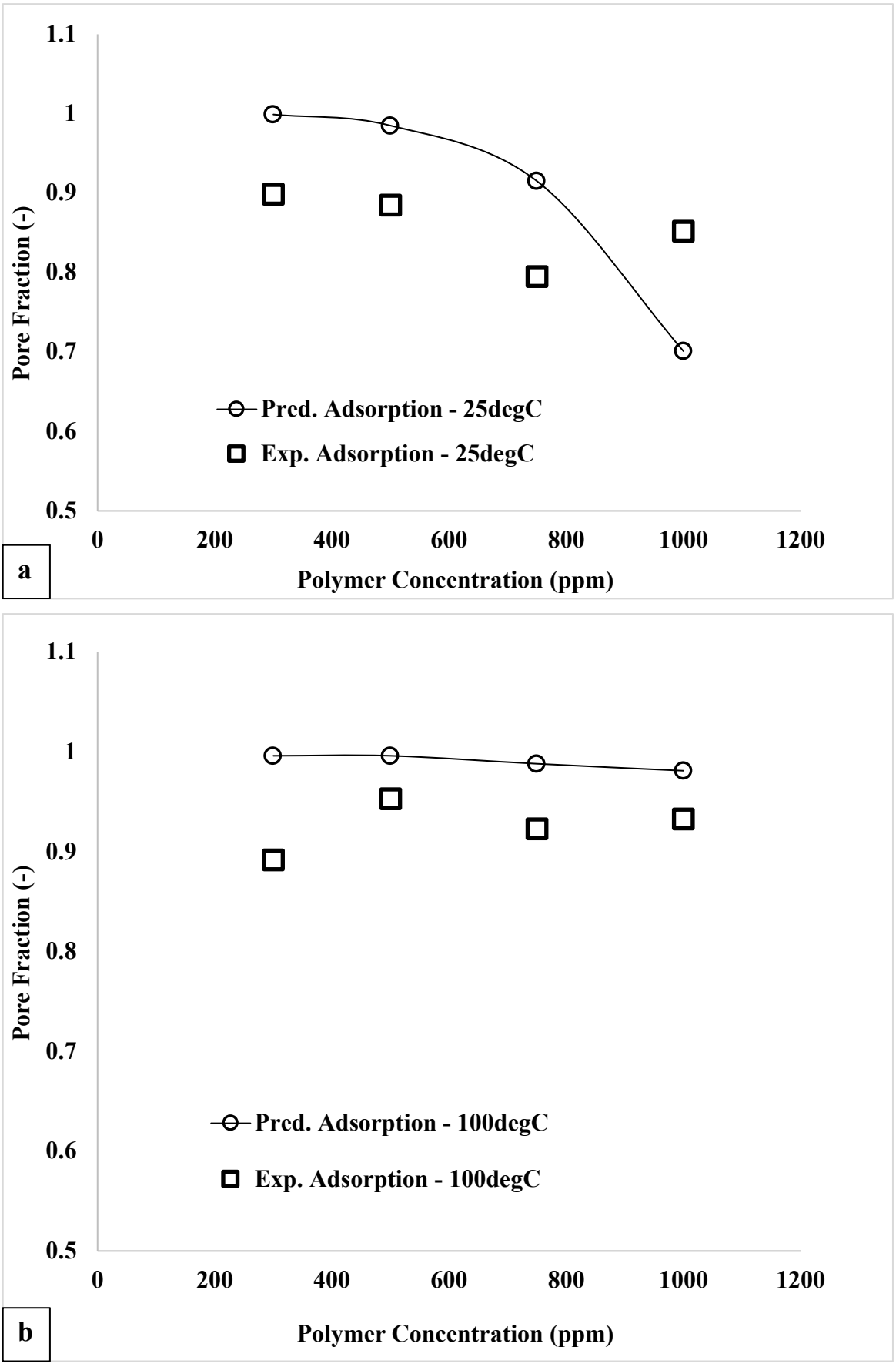

Figure 7.17*: Plot of the predicted and experimental outcomes for the mapping of polymer adsorption in terms of pore fraction at (a) 25* ℃ *and (b) 100* ℃.

7.3.2. Polymer Entrapment

Table 7.5 shows a summary of the predicted and the experimental outcomes for the entrapment of associative polymer in the sand-pack. These outcomes were also plotted as shown in Figure 7.18.

Table 7.5*: Predicted and experimental values of polymer entrapment in terms of pore fraction at 25* ℃ *and 100* ℃*.*

25 ℃**; 50.83/s (0.5 mL/min)**		
Concentration (ppm)	**Predicted Entrapment.**	**Experimental Entrapment.**
300	0.001	0.01
500	0.015	0.10
750	0.085	0.15
1000	0.299	0.21

100 ℃**; 50.83/s (0.5 mL/min)**		
Concentration (ppm)	**Predicted Entrapment.**	**Experimental Entrapment.**
300	0.0041	0.001
500	0.0043	0.012
750	0.0122	0.020
1000	0.0187	0.028

To compare the effectiveness of the predictive approach in estimating the outcomes of the experimental method, the coefficient of determination, R^2 was applied in the correlation of the predicted outcome to the experimental outcome as plotted in Figure 7.18. At 25 ℃, the coefficient of determination, R^2 was 87.43% while at 100 ℃, the R^2 was 87.05%. The seemingly significant correlation between the predicted outcome and the experimental outcome shows that the developed experimental approach can be used for the quantitative mapping of the polymer entrapment distinctively from the other types of polymer retention mechanisms attributable to associative polymers.

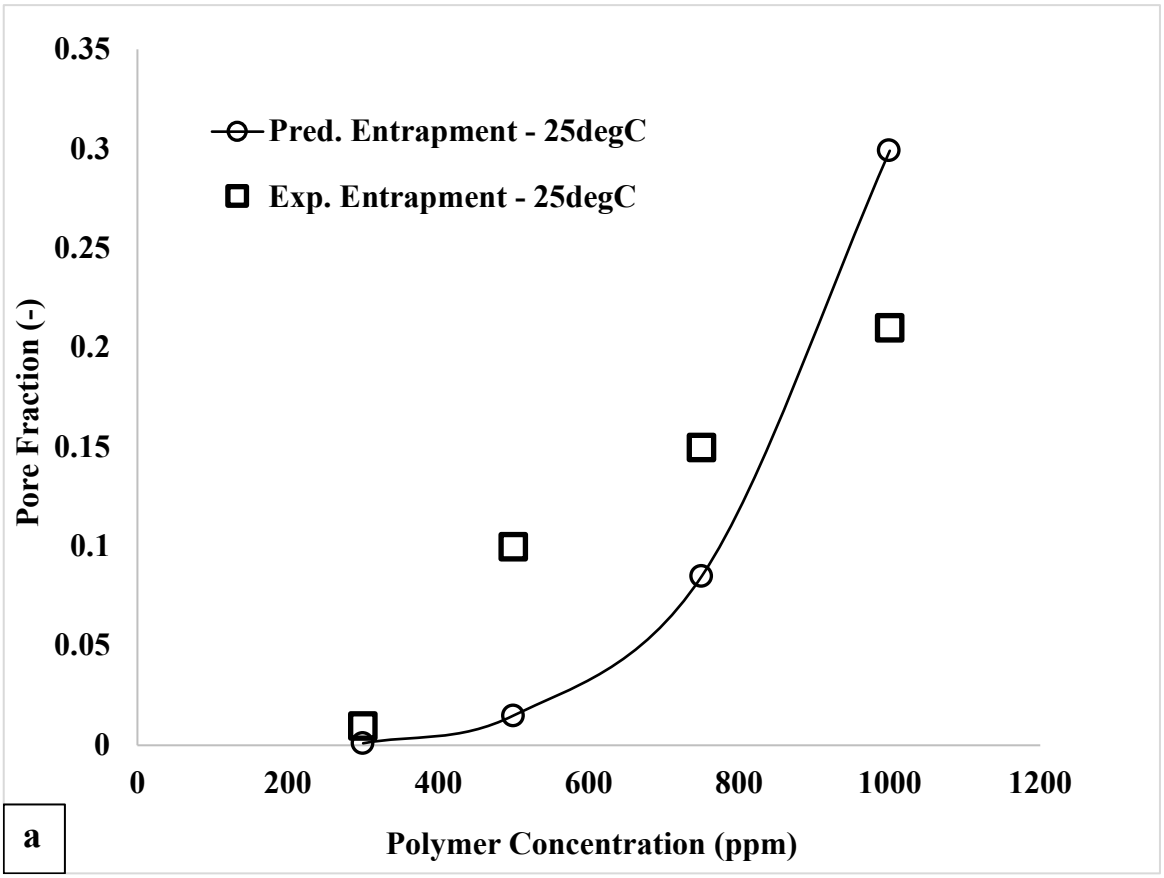

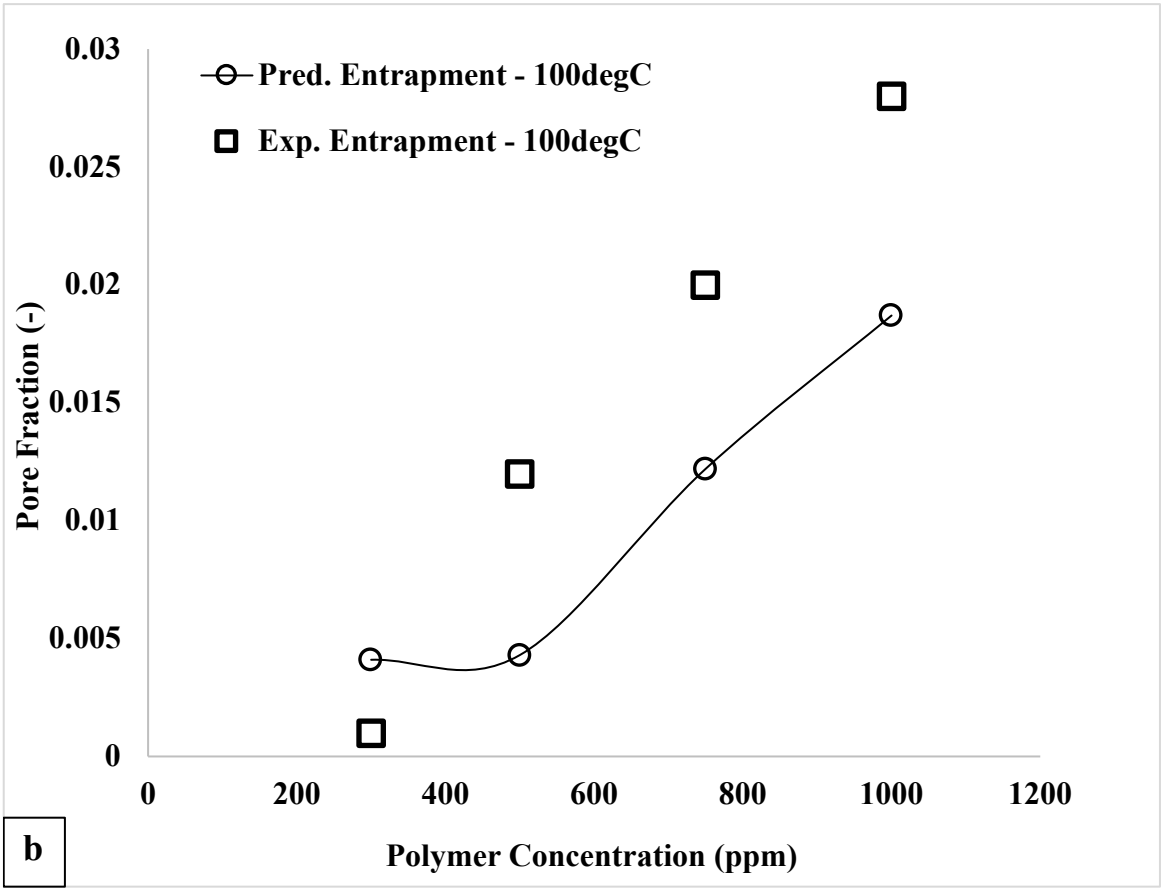

***Figure 7.18**: Plot of the predicted and experimental outcomes for the mapping of polymer entrapment in terms of pore fraction at (a) 25 ℃ and (b) 100 ℃.*

7.3.3. Inaccessible Pore Volume (IPV or I_{pv})

Validating the predictive approach developed in quantifying the inaccessible pore volume attributable to associative polymer involved experimental substantiation using a known experimental method. Figure 7.19 shows a comparison between the predicted and experimental values for the fractional pores inaccessible to the polymer molecules.

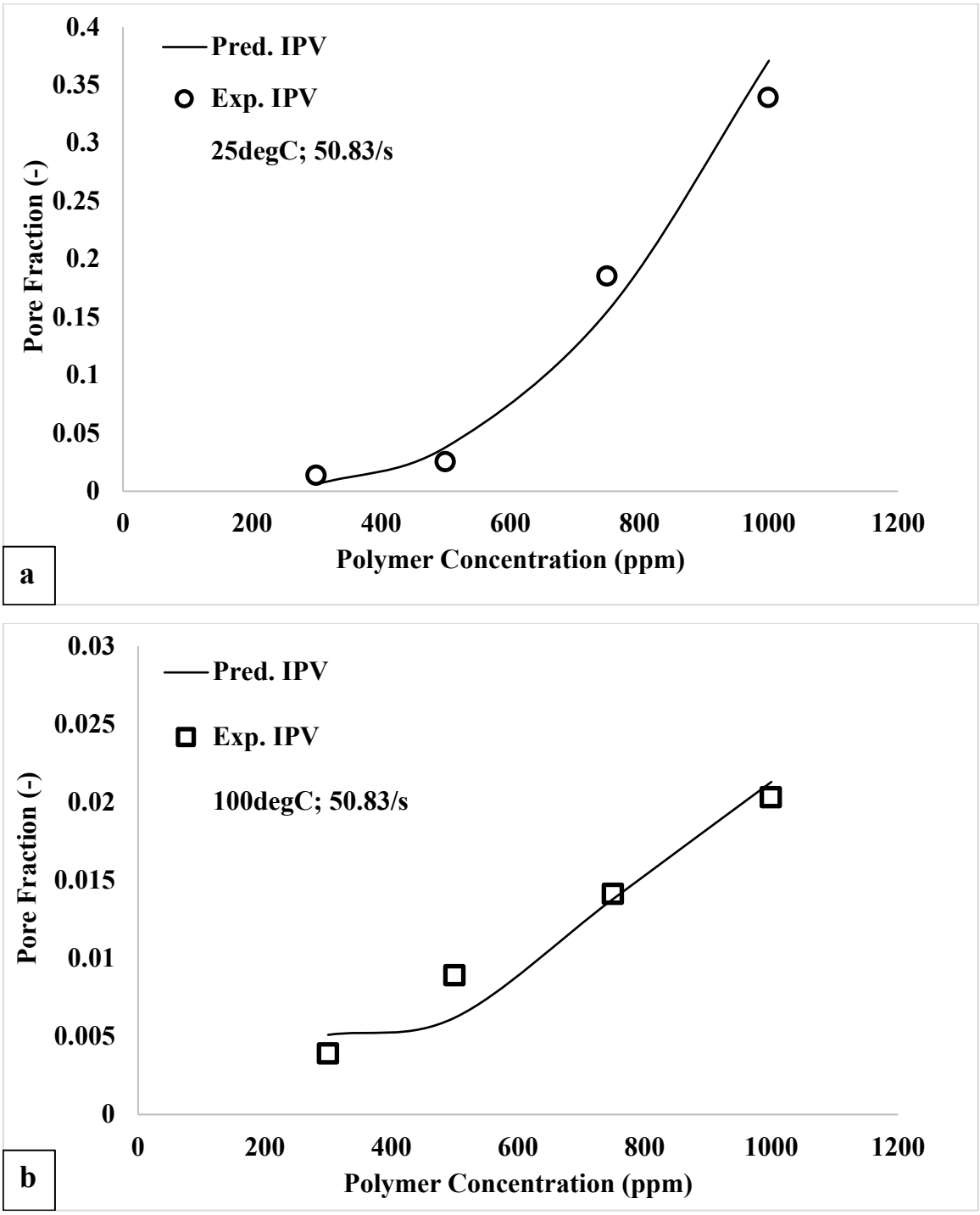

***Figure 7.19**: Comparison between the predicted and experimental values of the pore fraction inaccessible to polymer molecules at (a) 25 ℃ and (b) 100 ℃.*

7.4. Summary

The various types of retention mechanisms linked with associative polymers during transport in porous media were quantitatively described using a predictive and experimental approach. The uniqueness of the predictive approach is that it allowed for the determination of the critical concentration, which would mark the onset of the loss of molecular aggregates responsible for viscous polymer property to entrapment and plugging. All this was achieved by knowing the contributory effect of the associated hydrophobic interactions between the retained polymer molecules. Consequently, proper economic planning and computational forecasting of the performance of associative polymers can be made with the predictive approach. However, the predictive method for mapping the different retention types was developed using disaggregated sand. The use of disaggregated sand estimates the cumulative size distribution of the retained polymer molecules strictly via a predictive approach. Nonetheless, a novel experimental approach was developed to validate the predictive approach by correlating static to dynamic retention. This practical approach was based on an accurate correlation of static to dynamic retention, which allowed for the corresponding mapping of the various retention mechanisms using well-established trends in literature. The unique outcome of the modified experimental procedure was the appropriate quantification of polymer adsorption in addition to the entrapment. This is significant compared to using a dynamic retention test that does not uniquely define the various retention mechanisms but giving a generalized outcome. The result of the validation showed a significant correlation between the predictive and experimental result. However, an accurate representation of the experimental outcome could be achieved using consolidated porous media. The difference between the pre-distribution and post-distribution curves for the compact media would give the size distribution of retained polymer molecules in the compact porous media. This is an area of further works. Consequently, proper economic planning and experimental evaluation of computational forecasting of the performance of associative polymers during chemical enhanced oil recovery operations can be made with the developed approach.

CHAPTER EIGHT

8.0. Hydrophobic Interactions during Flow in a Porous Media

Understanding the flow of hydrophobic interactions in porous media was studied by injecting hydrophobically associating polymers in a sand-pack column. The flow of hydrophobic interactions was investigated by considering its corresponding effect on retention, shear thickening, degradation and the overall resistance (or pressure drop). However, the impact on polymer retention was covered in the previous chapter (Chapter Seven), and as such, the focus of this chapter was on the shear thickening, degradation and the overall resistance factor.

8.1. Mobility Control and Resistance Factor

The transport of polymer solutions in a porous media would result in various retention types and different flow regimes. The combined effect of polymer retention and flow regimes contribute to the overall pressure drop or resistance factor. However, this work was able to identify and quantify the distinct contribution of polymer retention and flow regimes to the overall resistance factor and pressure drop. The differential hydrophobic interactions were computed as the difference between the original value for hydrophobic interactions before injection and its apparent value due to polymer retention and flow regimes.

8.1.1. Effect of Polymer Concentration and Flowrate

Figure 8.1 shows the distinct contribution of polymer retention and shear thickening effect to the overall resistance factor. The effect of polymer concentration was captured in Figures 8.1a – 8.1c. At low polymer concentration (300 ppm), it was observed that the shear thickening effect contributes more to the resistance factor compared to the retention that arises from the transport in a porous media as captured by the differential values for the hydrophobic interactions. In other words, shear thickening was more prevalent at the low polymer concentration. However, as the polymer concentration increased from 300 to 500 and 1,000 ppm, the contributory effect of polymer retention to the resistance factor increased with retention dominant at 1,000 ppm (Figures 8.1b and 8.1c). This observed trend results from the significant number of hydrophobic interactions at high polymer concentrations. In addition, the trend indicates that most of the hydrophobic interactions are lost to various retention mechanisms at high concentration while the remaining few contribute to the desired shear thickening.

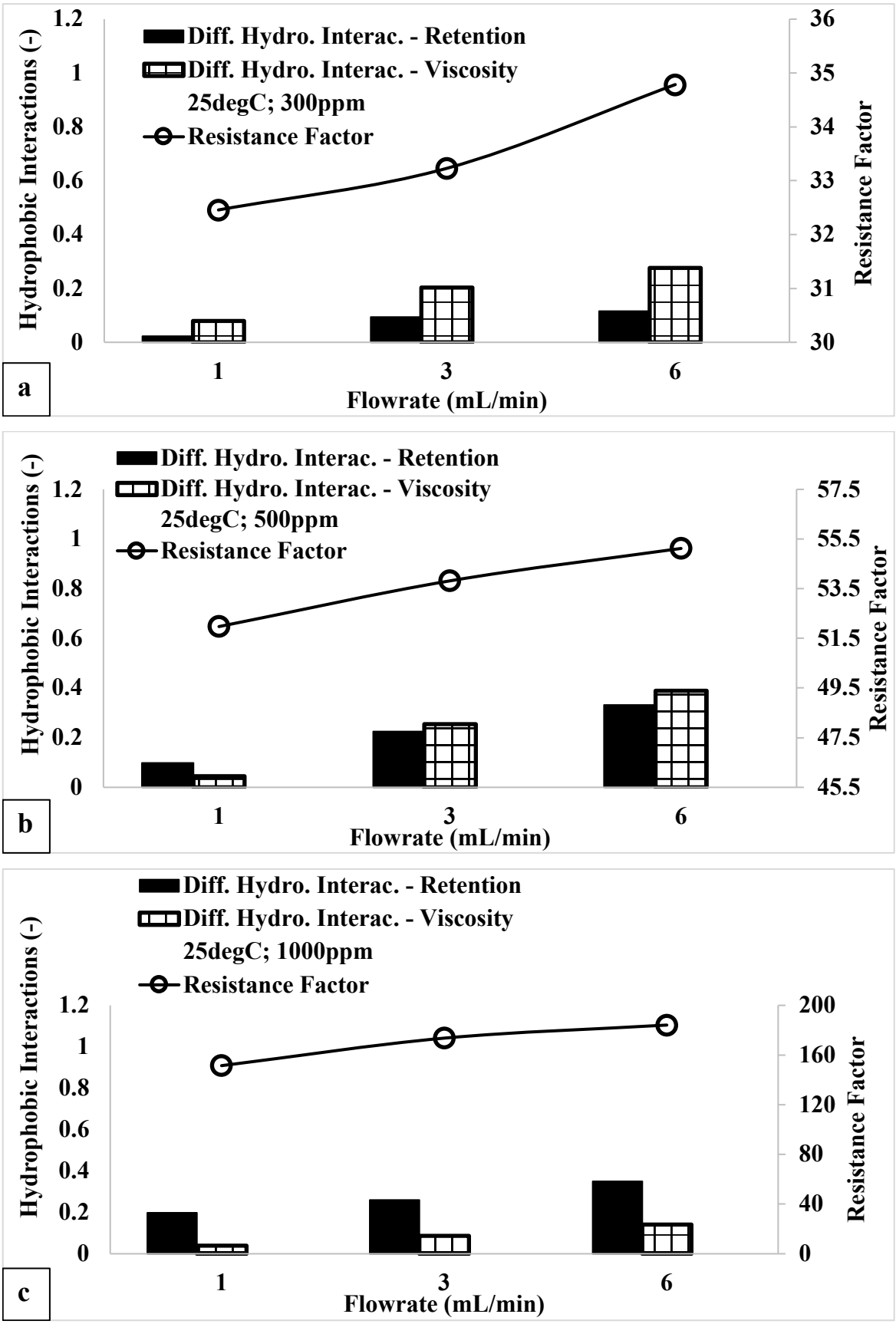

Figure 8.1*: Contributory effect of polymer retention and flow regimes on the resistance factor of associative polymer in a porous media at 25 ℃ (a) 300 ppm (b) 500 ppm (c)1,000 ppm*

The desired effect during polymer flooding is to see a significant level of polymer viscosity with minimal retention. From the observed trend, it was evident that low polymer concentration would provide the desired effect of low polymer retention; however, the corresponding viscosity effect may not meet the desired outcome for flooding operation. Therefore, a high polymer concentration would still be needed for sufficient viscosity effect. Optimizing the desired polymer concentration based on the knowledge of this phenomenon was discussed subsequently and not the focus in this section. Similarly, the impact of flow conditions was also evident on the contributory effect of polymer retention and shear thickening. At low polymer concentration (300 ppm), the impact of flowrate was noticeable in the increased polymer viscosity; however, retention also increased but not significant compared to the viscosity. Furthermore, as the polymer concentration increased (500 – 1,000 ppm), the effect of flowrate ensured that polymer retention became dominant over the shear thickening. As explained in the previous chapter, the flowrate increased the entrapment of polymer molecules in the porous media. This resulted in the reduction of the number of molecules available for viscous thickening. Overall, the hydrophobic interactions prevalent with associative polymers towards its mobility control mechanism reduced with an increase in the polymer concentration. However, this would change if other factors were considered, such as increased permeability, which minimizes polymer retention from entrapment. The pressure drop and, as such, the resistance factor is a summation of the effect of retention and flow regimes arising from the transport of associative polymers in a porous media.

8.1.2. Effect of Temperature

Figure 8.2 shows the effect of temperature on polymer retention and shear thickening arising from hydrophobic interactions to the resistance factor. Compared to Figure 8.1, the resistance factor at 100 ℃ was lower than at 25 ℃, and this was due to the thermal degradation of hydrophobic interactions. Although, the resistance factor still increased with concentration and flowrate following a similar trend explained earlier. However, the reduction in the resistance factor and the corresponding contributory effect of retention and viscous thickening can be explained in two ways. Firstly, the decrease in the retention effect with temperature arises from the increased negative charge of the sand grains, ensuring more repulsion between it and the negatively charged carboxyl group, thereby minimizing adsorption. Minimized entrapment was due to the degradation of hydrophobic interactions, thereby reducing the number of entrapped aggregates.

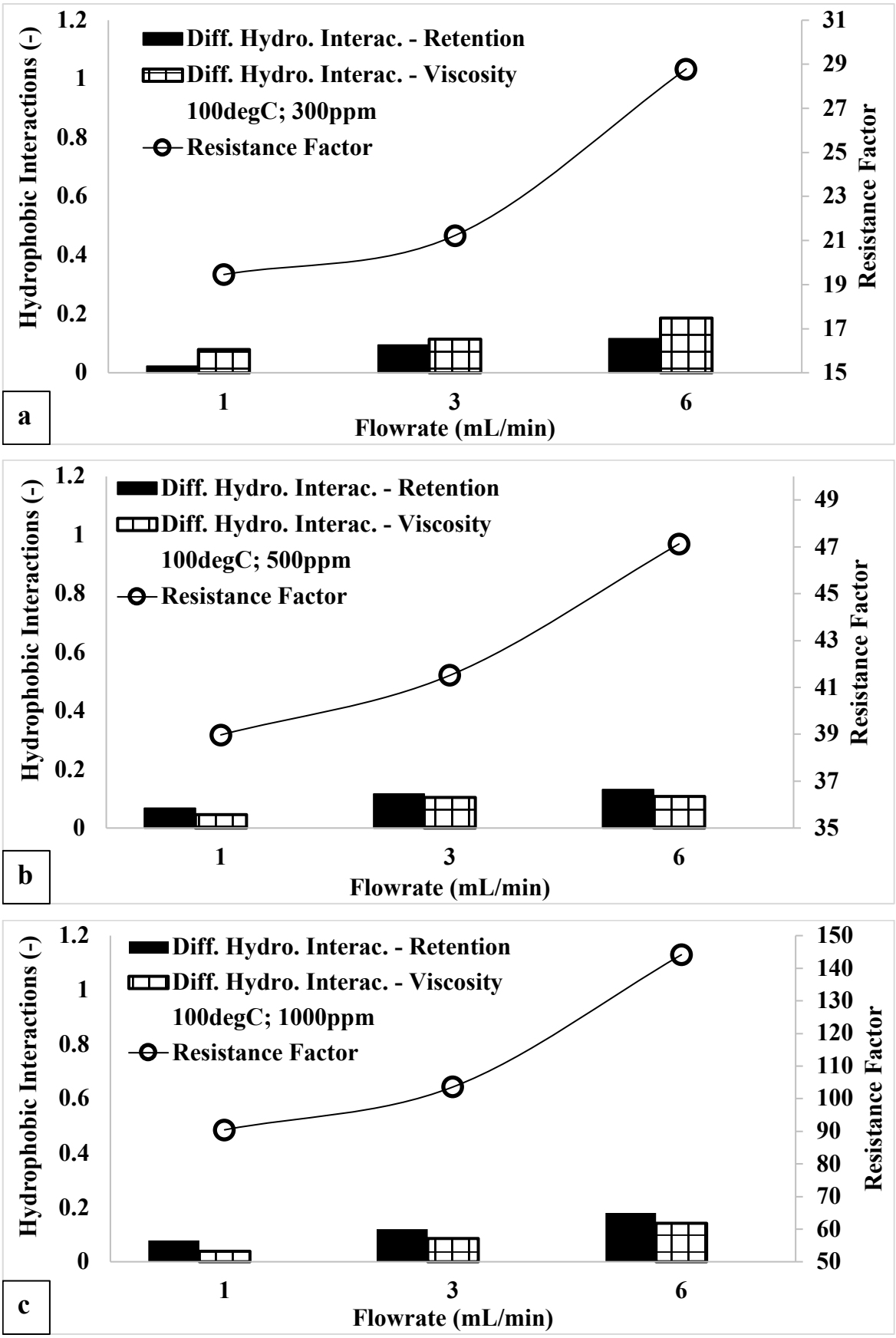

***Figure 8.2**: Contributory effect of polymer retention and flow regimes on the resistance factor of associative polymer in a porous media at 100 ℃ (a) 300 ppm (b) 500 ppm (c)1,000 ppm.*

Secondly, the reduction in the viscous thickening effect was solely due to the thermal degradation of the hydrophobic interactions, which exists between polymer molecules arising from the breakage of polymer chains (midpoint or random scission).

8.1.3. Proxy Modelling of Resistance Factor and Pressure Drop

The proxy modelling of the resistance factor was done to incorporate the contributory effects of polymer retention and viscous thickening. This was achieved using a statistical design of the experiment using the experimental data. The experimental data was divided into two parts. The first part was used in the development of the proxy model, while the second was applied in the validation of the model.

8.1.3.1. Regression Model

The statistical model obtained from regression analysis used in describing the resistance factor and pressure drop is given by the following non-linear equation, as shown in equation (8.1). The final expression in equation (8.1) was obtained after a Box-Cox Transformation of the response variable, $\left(\frac{\Delta P_p}{\Delta P_{wo}}\right)$.

$$\ln\left(\frac{\Delta P_p}{\Delta P_{wo}}\right) = 2.8007 - 0.662\left(\frac{Q}{Q_{dg}}\right) - 0.115\left(H_\mu\right) - 0.303\left(H_{C_p}\right) - 0.002276\left(C_p\right) \quad (8.1)$$

The obtained response model covered all terms as stated in Section 3.4. The coefficient of determination (R^2) for the obtained response model was 99.91 %. This indicates that the obtained statistical model was suitable for the design matrix since it was higher than 90 %. It indicated that the response model could account for 99.91 % variation in the response. This was also reflected in the difference between the R^2 value and the adjusted R^2 value (${R_{adj}}^2 = 99.81$ %) which was about 0.1 %. Similarly, the predicted R^2 value (${R_{pred}}^2 = 99.47$ %) was significantly close to the R^2 value, which indicates that the model is not overfitting. This implies that the terms in the model significantly contribute to the overall response (i.e., resistance factor and pressure drop). Furthermore, other statistical tools were used in addition to the R^2 value to determine the significance of the terms of the response surface model. The probability value (P-value) for the fitted model obtained in equation (8.1) was zero, which was less than 0.05 (5 % level of significance). This shows that the response surface model can confidently (> 95 %) investigate and predict the response variation in the experimental design matrix. The dataset for the proxy modelling is contained in Appendix E.

8.1.3.2. Fits and Diagnostic Plots of the Proxy Model

Diagnostic analysis of the model's predictive capability was carried out using the residual plot analysis. These plots consist of histogram plots of residuals, residual versus fits, residuals versus run order and the actual response versus predicted response. Figure 8.3 shows the histogram plot of the residuals, which was used to investigate the normality of the residuals and determine whether they were skewed or contain outliers.

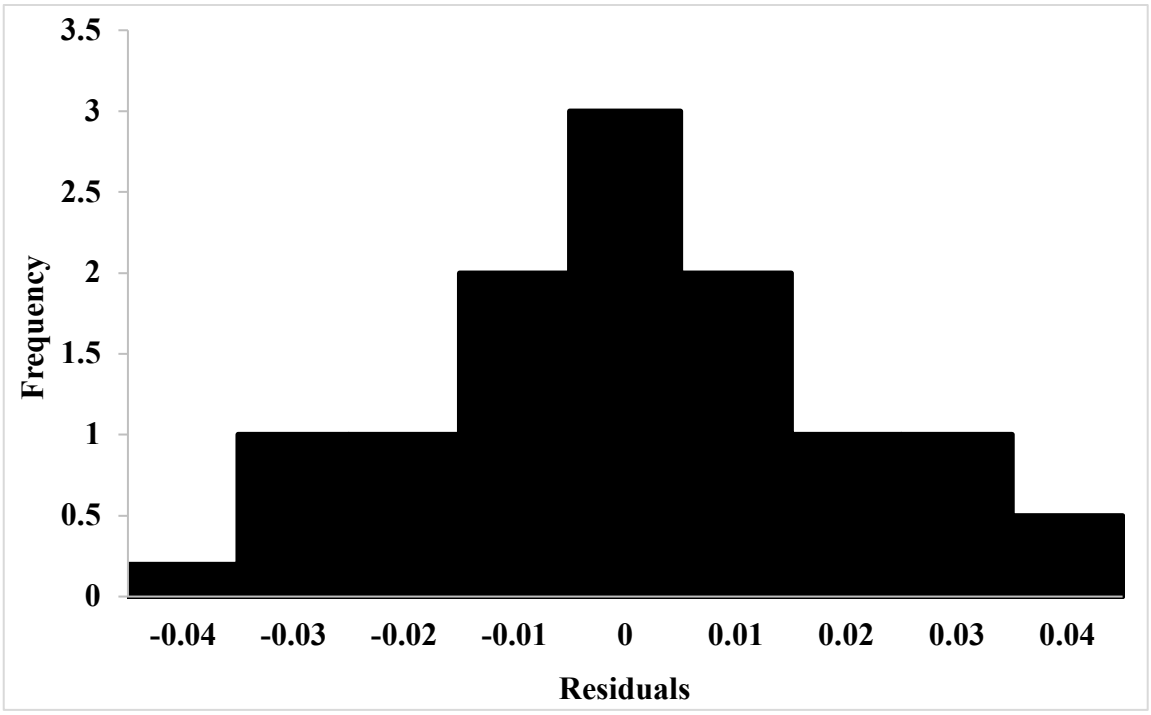

Figure 8.3*:Normality of the model residuals of equation (8.1) accessed using the Histogram plot analysis. The plot of the residuals follows approximately a normal distribution.*

The symmetrical distribution of the plot indicates a normal distribution of the residuals with no skewness (no long tails in any direction) or an outlier (a bar that is far from the other bars). Furthermore, the residual versus predicted fits and run order plot in Figure 8.4 was used to verify the assumption that the residuals from the equation (8.1) were randomly distributed and have a constant variance. The data points for the residuals can be observed to fall randomly on both sides of zero with no recognizable pattern in the data points. This shows that there was no outlier or missing higher-order terms in the model that may affect the model assumptions of normality. Similarly, the independence of the residuals from one another was investigated using the plot of the residuals versus experimental run order, as captured in Figure 8.4. A close observation of the residual plot shows that no trend or pattern was noticeable when displayed with run order. Also, the residuals fall randomly around the centreline of Figure 8.4, indicating no correlation between residuals.

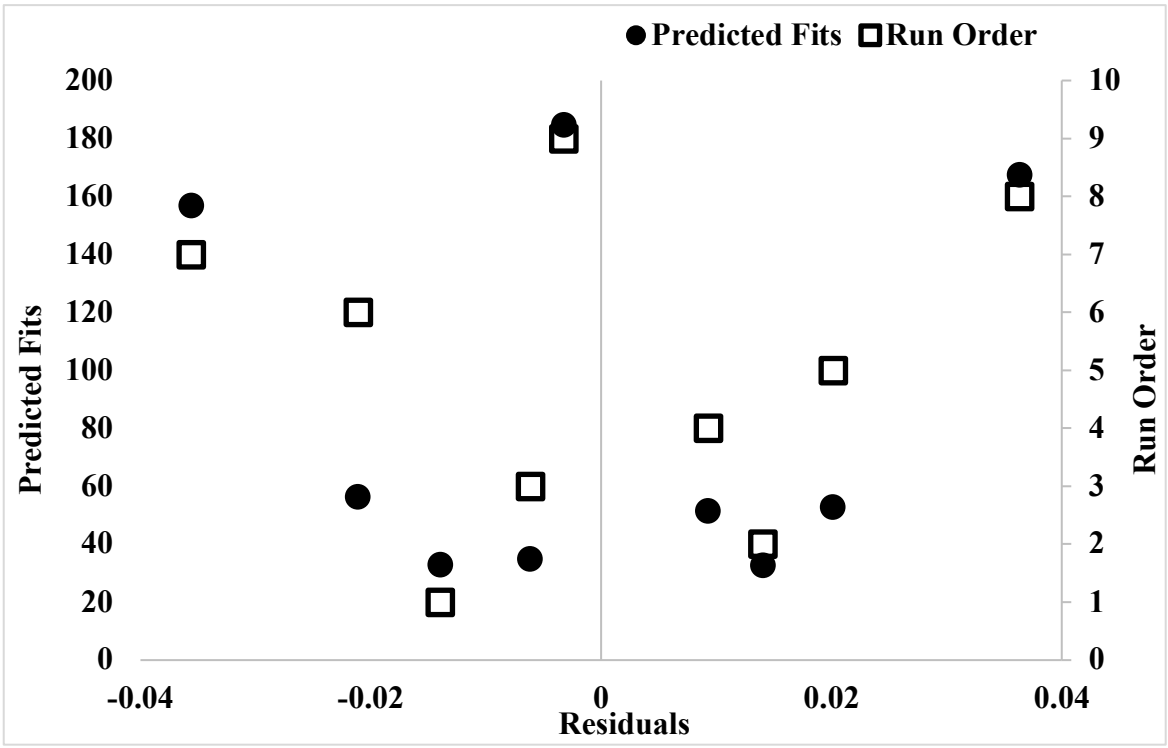

***Figure 8.4**: Diagnostic analysis of equation (8.1) using residual plot analysis.*

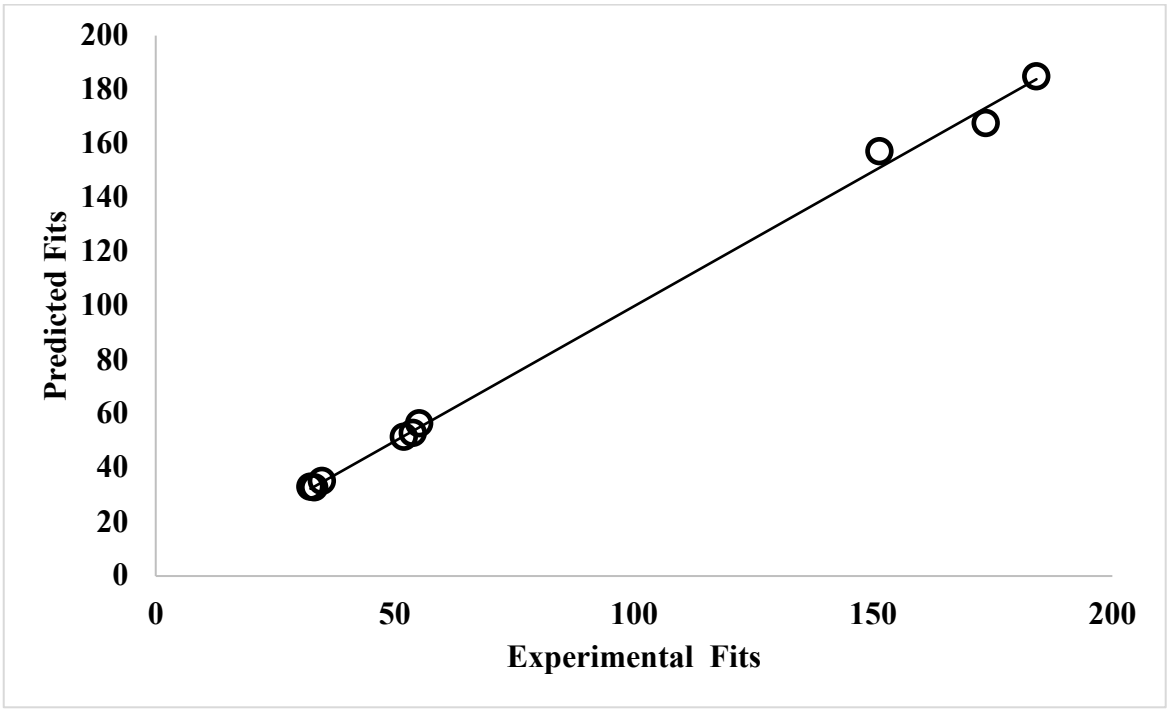

***Figure 8.5**: Diagnostic analysis of equation (8.1) using the plot of actual response against predicted response*

Figure 8.5 shows the scatter plot of the actual (observed) response against the predicted response. A 45° line was used to split the actual and predicted data points evenly. The distribution of the data points was observed to be close to the diagonal line indicating a strong correlation between the actual observation and the predicted response.

8.1.3.3. Statistical and Experimental Validation of Proxy Model

The statistical validation of the proxy model was carried out by analysing the confidence and prediction intervals as shown in Figure 8.6.

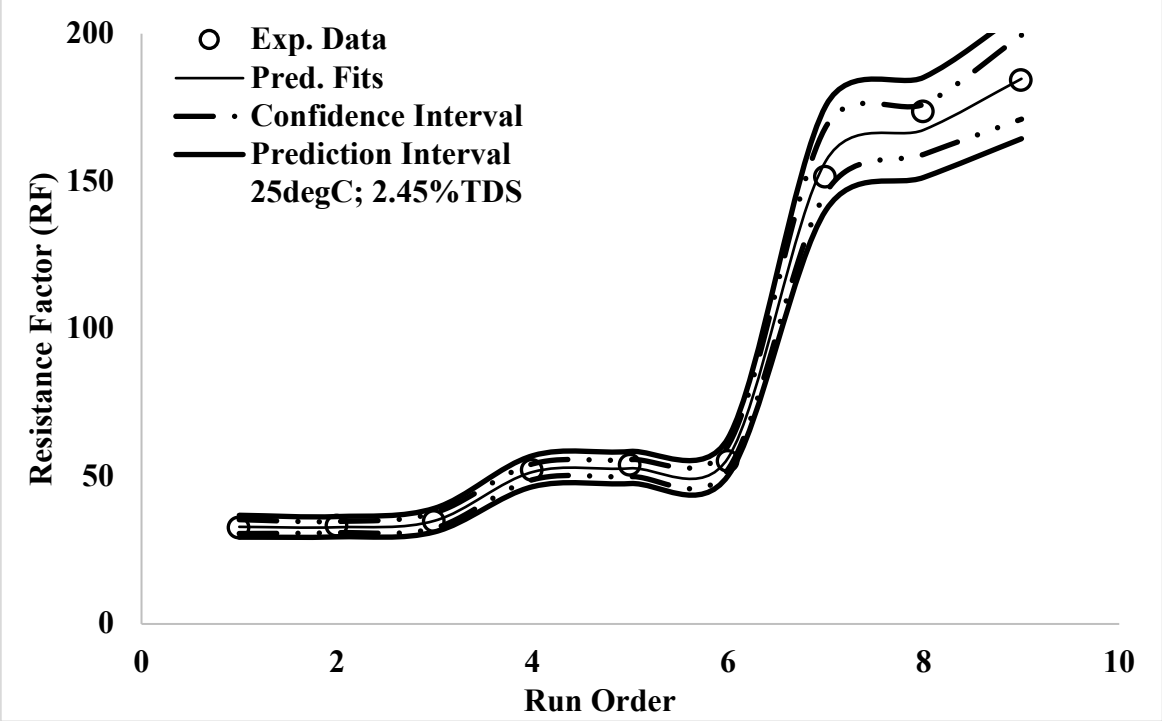

Figure 8.6*: Confidence interval and prediction interval for statistical validation of the developed model for in-situ prediction of pressure drop in porous media.*

Figure 8.6 shows the 95 % confidence and prediction interval for the resistance factor and pressure drop using equation (8.1). The tapered confidence interval connected with the generalized model is suggestive of the accuracy of the model in estimating the resistance factor and pressure drop for a definite set of the predictor variables. Furthermore, in accessing the applicability of the proposed model, the uncertainty of predicting the value of a single future observation or a fixed number of multiple future outcomes based on the distribution of previous outcomes was evaluated. This was done using the prediction interval, which was the range that is likely to contain a single future response for a selected combination of variable settings. Figure 8.6 shows the 95 % prediction interval for equation (8.1). There was a 95 % probability that future observations will be contained within the prediction interval. Furthermore, the narrowed gap of the prediction band indicates a reduced uncertainty in the prediction of future observations. Therefore, the proposed model can predict the resistance factor and the pressure drop for associative polymers in a porous media based on the statistical evaluation. Figure 8.7 shows a comparison between the experimental outcome and the predicted outcome using equation (8.1).

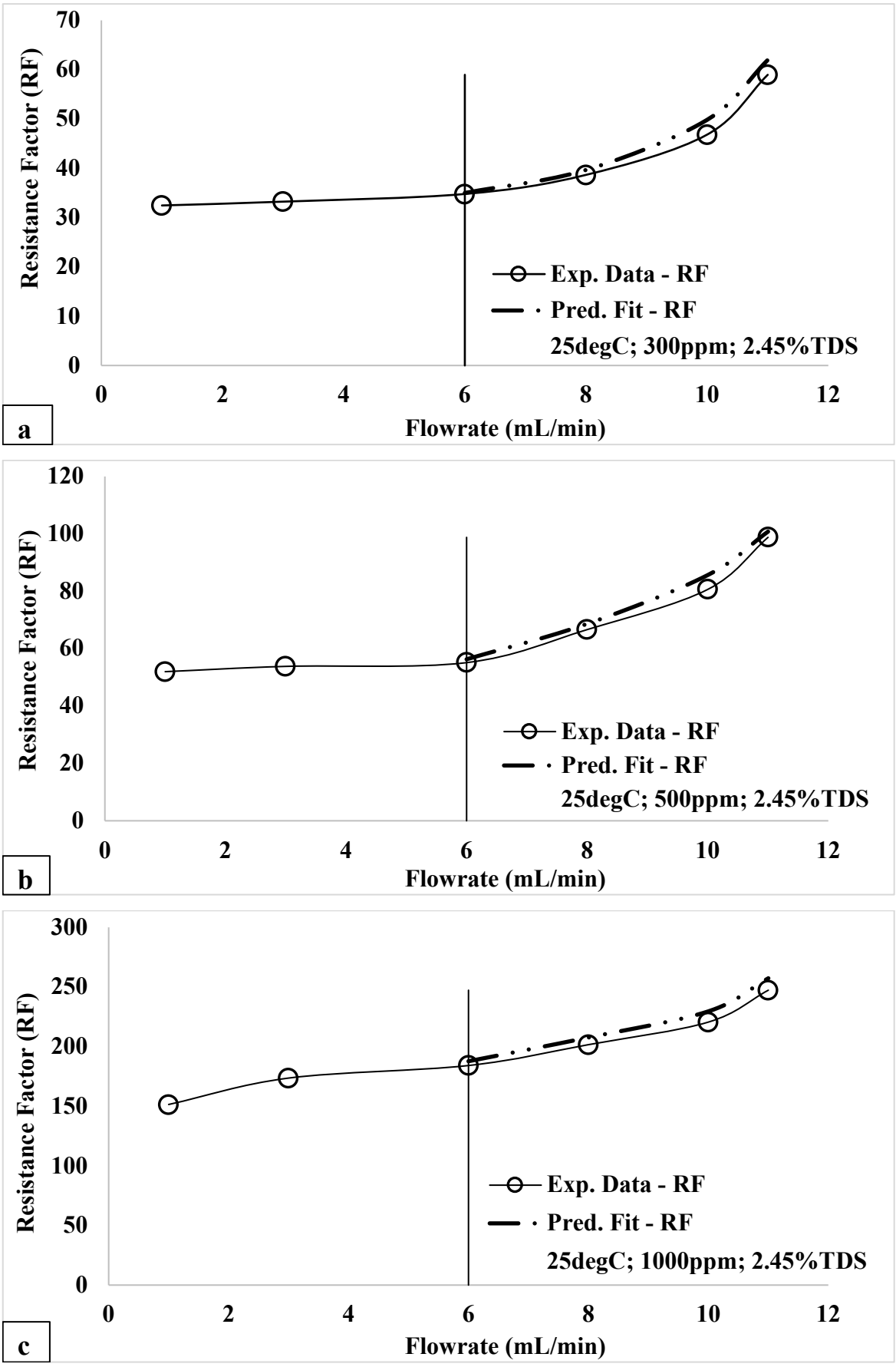

Figure 8.7*: Experimental validation of the developed model for resistance factor at 25 °C and 2.45 %TDS for polymer concentrations (a) 300 (b) 500 and (c) 1000 ppm.*

Experimental validation was done using data from the flowrates 6, 8, 10 and 11 mL/min. The R^2 values were estimated as 99.34, 99.46 and 99.65 % respectively, indicating a good correlation between the predicted and the experimental outcome (dataset contained in Appendix F).

8.2. Apparent Hydrophobic Interactions of the Polymer Propagation Front

The effective concentration of the polymer front, which travels in the direction of flow, is dependent on the level of hydrophobic interactions after the effects of polymer acceleration (inaccessible pore volume), retardation (polymer retention) and degradation (mechanical or thermal). Equation (3.72) was applied in predicting the effective concentration; however, this was normalized to reflect the dimensionless effluent concentration as shown in Equation (8.2).

$$\frac{C_{pe}}{C_{inj}} = \left[\frac{C_{ag}/C_{inj}}{\left(1-\left[\frac{H_o}{1+\beta_1\gamma_{sh}}+\frac{H_{max}\gamma_{el}}{\beta_2+\gamma_{el}}\right]\frac{1}{1+\beta_3\gamma_{deg}}\right)}\right]E_{PV} \qquad (8.2)$$

The ratio C_{ag}/C_{inj} reflects the normalized concentration for the onset of hydrophobic interactions while also using effluent concentration analysis in validating such predictions.

8.2.1. Effect of Concentration, Retention and Inaccessible Pore Volume

Figure 8.8a – Figure 8.8c shows the combined effect of polymer concentration, retention, and inaccessible pore volume on the onset of hydrophobic interactions between associative polymer molecules during propagation in the sand-pack media. The plots were constructed as follows:

a) The normalized effluent polymer concentration from the porous media was plotted against the number of injected pore volumes until the normalized effluent concentration was unity. This was the case for the second and first polymer front.
b) The normalized effective polymer concentration (equation 8.2) was plotted as a linear function from the origin up till it becomes tangential at the point where normalized effluent concentration is maximum.
c) The onset of hydrophobic interactions was predicted by estimating the normalized critical aggregation concentration (C_{ag}/C_{inj}) along the linear plot of the normalized effective concentration.
d) The plots of the normalized effluent concentration were also expressed in terms of the length of the porous media in addition to the number of pore volumes to determine the

distance along the porous media from the entry point for the onset of hydrophobic interactions.

The propagation of the polymer front into the porous media would initially result in an entry point disentanglement or degradation of the polymer molecules. Further propagation of the polymer front beyond the entry point would indicate a more negligible effect of the shear forces. The re-association of undegraded and disentangled polymer molecules would depend on the inaccessible pore volume, retention, and injected solution concentration. For the 500 ppm concentration in Figure 8.8a, the arrival of the polymer front after injecting 0.7 PV indicates an inaccessible pore volume of 0.3 PV. In the case of 750 and 1,000 ppm, the inaccessible pore volume corresponds to 0.5 and 0.65 PV respectively (Figure 8.8b and Figure 8.8c). Similarly, the amount of polymer retention was estimated to amount to 0.15, 0.25 and 0.40 PV respectively. The effect of those mentioned above on the onset of hydrophobic interactions shows that hydrophobic interactions did not start until 0.7, 0.5, and 0.3 PV have been injected for 500, 750 and 1000 ppm respectively.

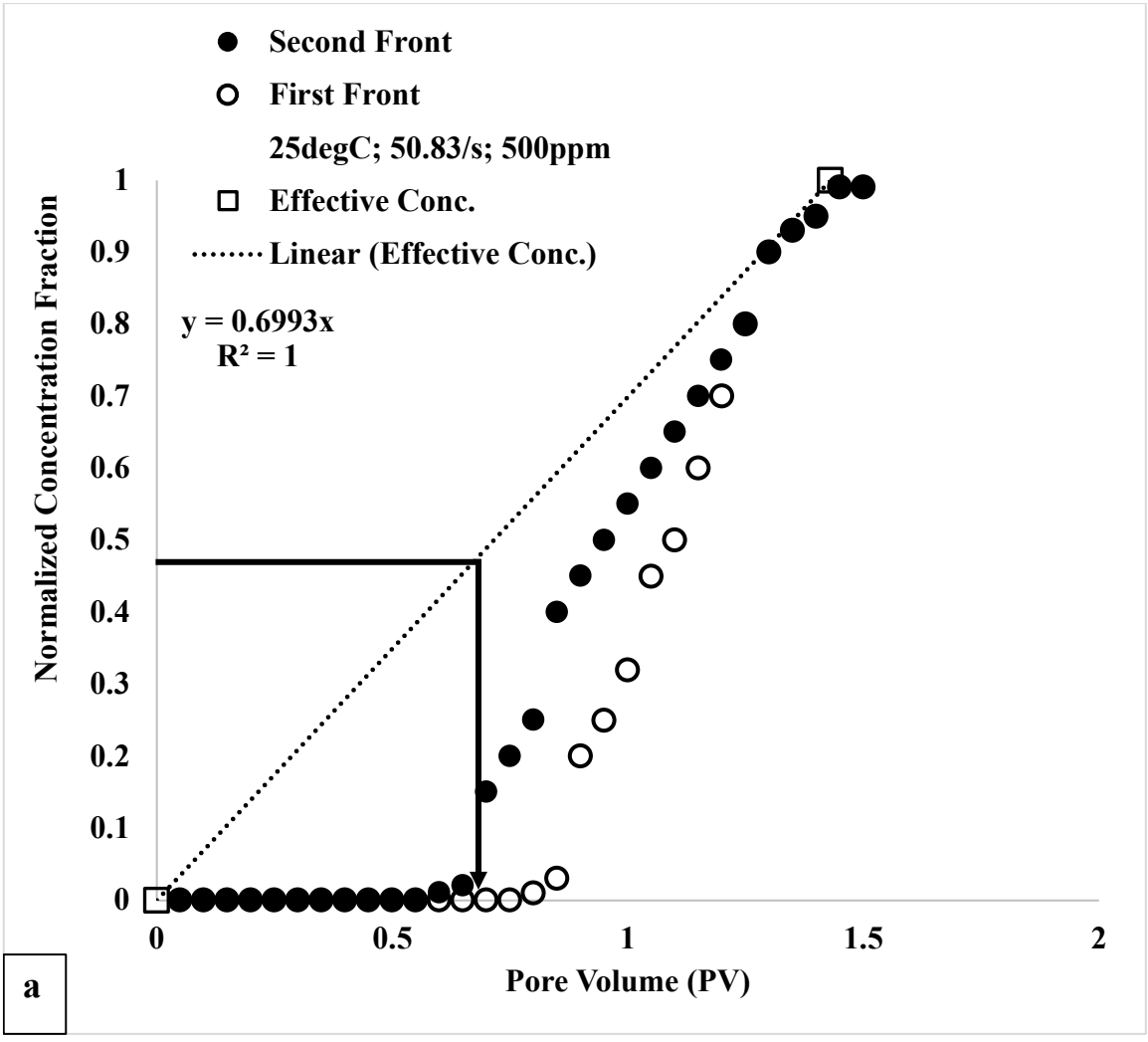

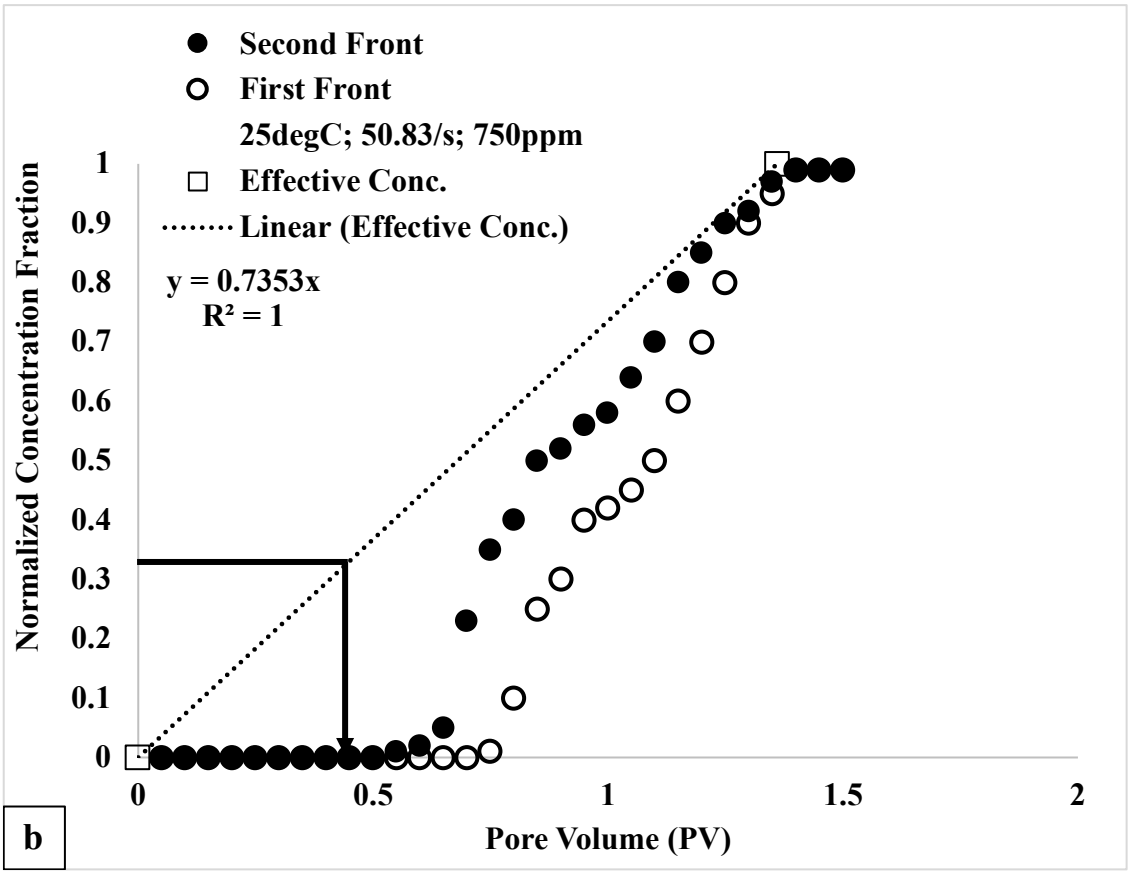

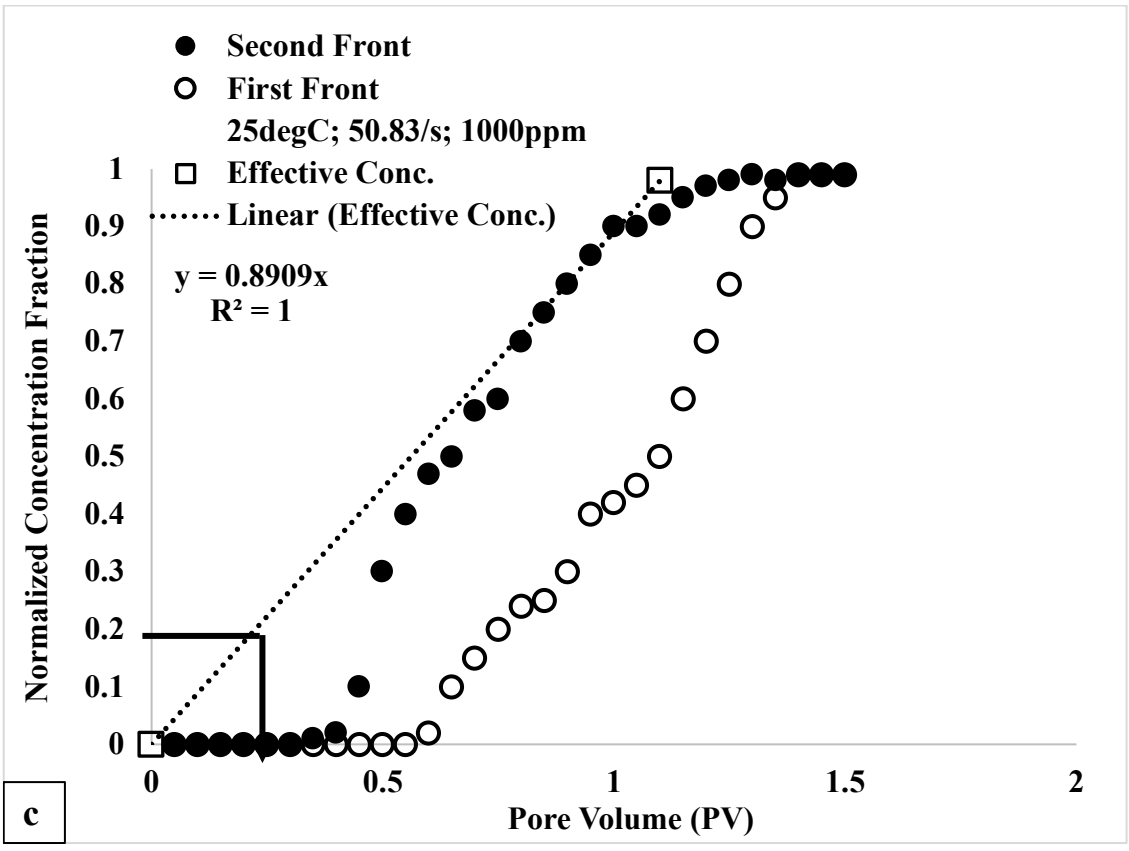

***Figure 8.8**:Polymer effluent analysis for the determination of the onset of hydrophobic interactions in the sand-pack media at 25 ℃ and 1mL/min (a) 500 ppm (b) 750 ppm (c) 1,000 ppm.*

The onset of hydrophobic interactions was estimated using the normalized ratio of C_{ag}/C_{inj} with C_{ag} equivalent to 236 ppm at 25 °C. The inaccessible pore volume computed here was the summation of the pore volume completely accessible to water/brine, and the pore volume lost to different retention mechanisms. Therefore, the inaccessible pore volume due to brine was computed as 0.15, 0.25 and 0.25 PV for 500, 750 and 1000 ppm respectively. As estimated above, the onset of hydrophobic interactions can be explained in terms of the proportion or amount of polymer molecules in the injected solution. At low concentration (300 ppm), the proportion of molecular aggregates arising from hydrophobic interactions was low. After the entry point degradation of these aggregates, the downward acceleration of molecules originating from the low inaccessible pore volume would indicate that molecules have time to spend apart due to the more insufficient mixing of molecules. More pore volumes would need to be injected before sufficient interactions begin between polymer molecules, which explains the high value of PV (0.7 PV) estimated for the onset of hydrophobic interactions at 300 ppm. However, at a high concentration (1,000 ppm), the proportion of molecular aggregates arising from hydrophobic interactions are high. Therefore, after the entry point degradation or disentanglement, there is an increased acceleration of molecules emerging from the high inaccessible pore volume (with polymer entrapment contributing to it as well), indicating that molecules would have less time to spend apart and thus associate rapidly, resulting in less injected pore volumes (0.3 PV) for the onset of hydrophobic interactions.

8.2.2. Effect of Flow Conditions

Flow conditions in porous media are tied to the applied flowrate, inducing the necessary shear conditions on the polymer solutions. The effect of applied flowrate on the propagation of hydrophobic interactions in the porous media was studied by considering the number of pore volumes required for the molecules in the propagating polymer front to re-associate for hydrophobic interactions. Figure 8.9 show the effect of applied flowrate on the onset of hydrophobic interactions between associative polymer molecules in the sand-pack media. After the conditions of retention have been satisfied in both cases, it was observed that the onset of hydrophobic interactions in the polymer front occurred after injecting 0.3 PV (at 1 mL/min) and 0.45 PV (at 6 mL/min).

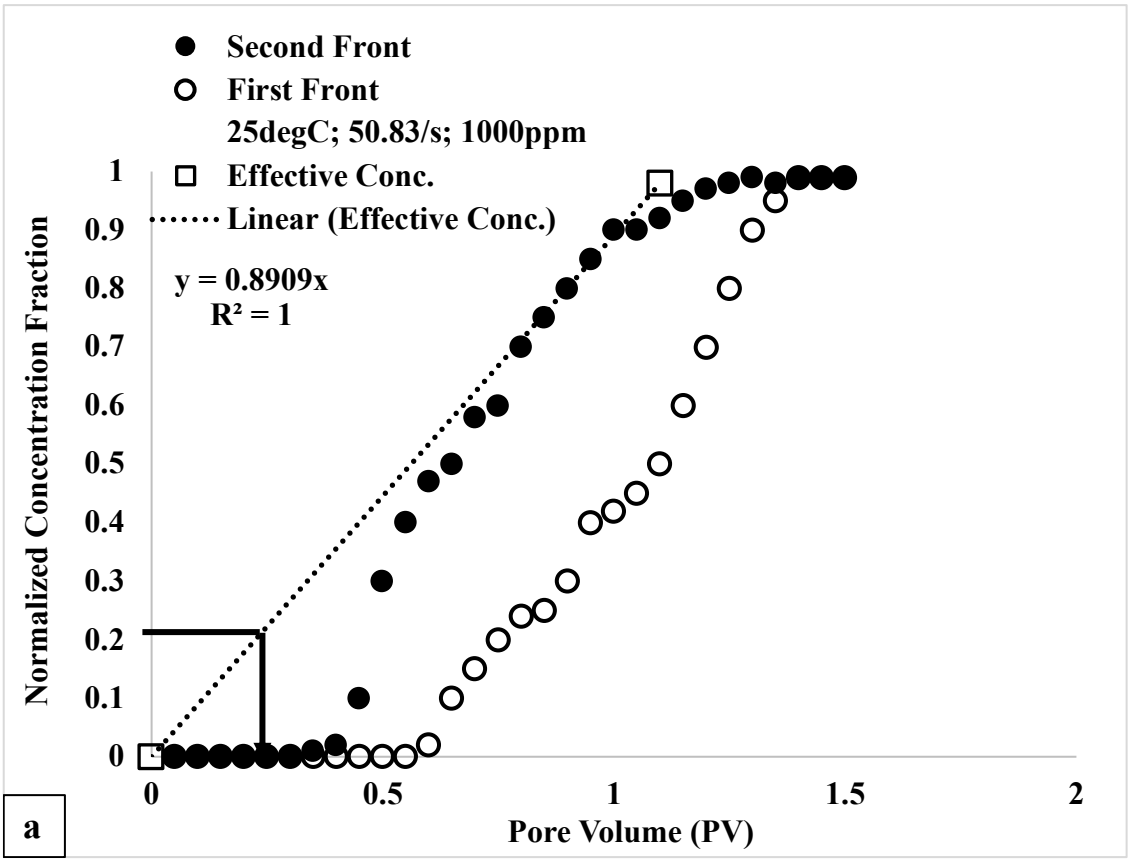

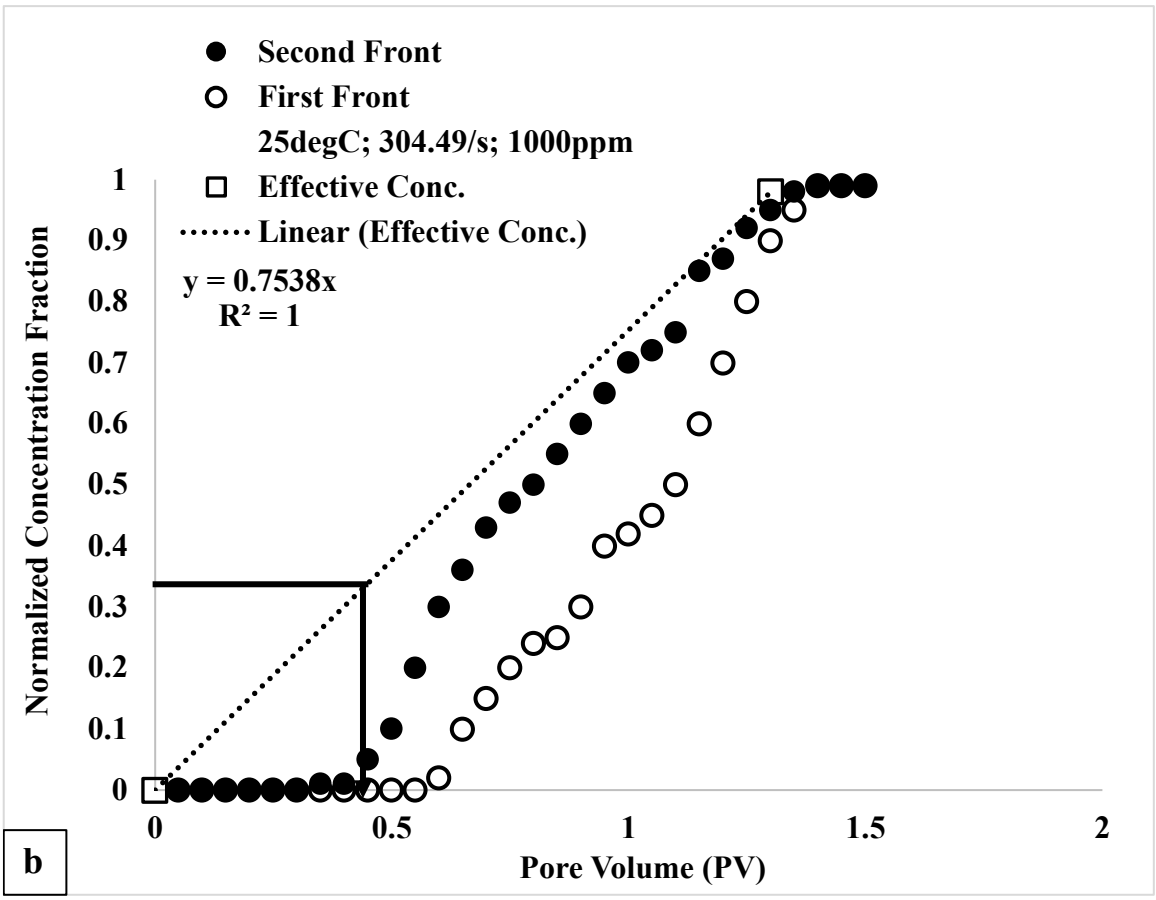

***Figure 8.9**: Polymer effluent analysis for the determination of the onset of hydrophobic interactions in the sand packed media at 1,000 ppm and 25 ℃ (a) 1 mL/min (b) 6 mL/min.*

The critical aggregation concentration changed with an increase in flow conditions, as explained in Chapter Six. The ratio of C_{ag}/C_{inj} was 0.35 with C_{ag} equivalent to 350 ppm at 25 ℃ and 6 mL/min. Generally, the effect of applied flow rate as captured in Figure 8.9 was manifested in the entry point degradation of the polymer molecules within the hydrophobic interaction aggregate leading to the disentanglement of polymer molecules or possible scission of polymer molecules. The rate of disentanglement or degradation increased with the injection rate. The increase in the polymer injection rate effectively increased the contact time disentangled polymer molecules must undergo associative interaction in the porous media. This specifically explains why the onset of hydrophobic interactions occurred at a lesser pore volume (0.3 PV) at 1 mL/min compared to the higher pore volume (0.45 PV) experienced at 6 mL/min. However, the excessive flowrate could induce a combination of polymer molecule disentanglement from the hydrophobic interaction network and mechanical scission of disentangled polymer molecules.

8.2.3. Degradation of the Polymer Propagation Front

Equation (3.54) was matched to experimental data for hydrophobic interactions obtained from the flow of different concentrations of associative polymers (300, 500 and 1000 ppm) in the sand-pack media as shown in Figure 8.10. The model developed for predicting in-situ hydrophobic interactions show a good match with the experimental data with R^2 values 0.96, 0.94 and 0.99 at polymer concentration of 300, 500 and 1000 ppm respectively. Similarly, the root mean square error (RMSE) was estimated at 0.081, 0.071 and 0.012 for polymer concentrations 300, 500 and 1000 ppm respectively. The decreasing value of the RMSE values with polymer concentration shows an increase in the model's predictive accuracy. It could be inferred from these estimates of the RMSE that the developed model in equation (3.54) was appropriate at higher polymer concentrations. A summary of the parameters of the fitted model for each polymer concentration is shown in Table 8.1.

Table 8.1*: Model parameters for equations 3.54, 3.56 and 3.62 obtained from regression analysis.*

Conc. (ppm)	H_o	β_2(1/s)	β_3(s)	γ_{c_deg} (1/s)	R^2	RMSE
300	0.20	275.93	0.00096	1038	0.96	0.081
500	0.43	645.37	0.00112	891	0.94	0.071
1,000	0.76	2425.1	0.00131	765	0.99	0.012

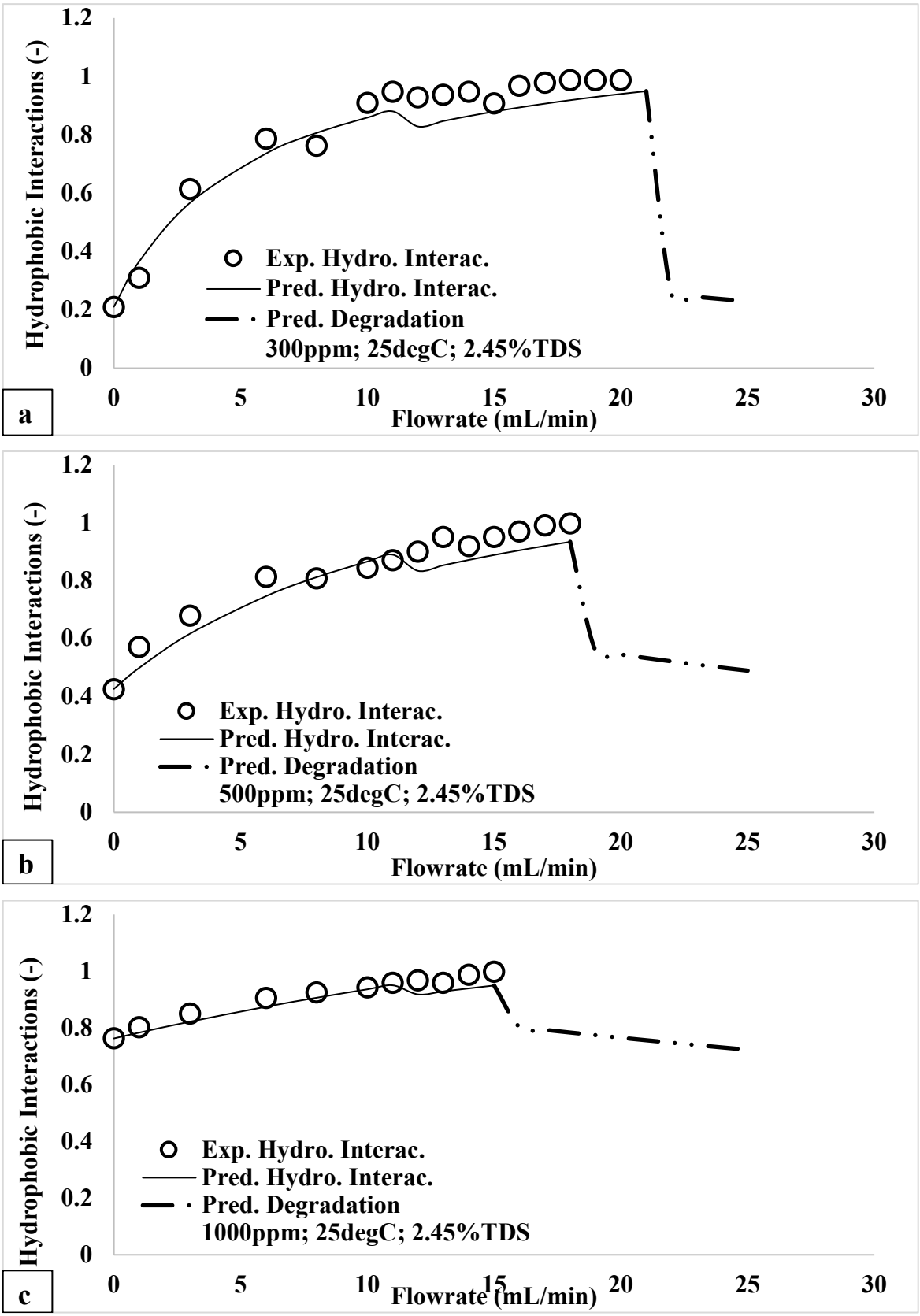

***Figure 8.10**: Experimental and predicted in-situ hydrophobic interactions during the flow of associative polymer (D118; 16MDa) in a sand-packed media ($\phi = 0.364$; $d_p = 350\mu m$) at 25 ℃ and 2.45 %TDS ($Na^+ : Ca^{2+}, Mg^{2+} = 10:1$) (a) 300 ppm (b) 500 ppm (c) 1000 ppm. Dataset is contained in Appendix F.*

The applied flow conditions divide the polymer behaviour into flow regimes in the porous media – shear thickening and degradation, as shown in Figure 8.10. The rate parameter β_2 obtained from the fitted model for the shear thickening regime was observed to increase with the polymer concentration (275.93/s, 645.37/s and 2425.1/s for 300, 500 and 1,000 ppm respectively). This rate parameter indicates the rate of hydrophobic association from the onset of these interactions until the start of degradation ($H_{app} = 1$). The low value for β_2 at 300 ppm indicates that the rate of hydrophobic association between polymer molecules in the sand-pack media was slow, and the associative effect would take place over an extensive range of flow conditions. Therefore, it would take a significant flow rate before mechanical degradation would set in. However, the considerable rate constant at 1,000 ppm ($\beta_2 = 2425.1/s$) indicates that the rate of hydrophobic interactions between polymer molecules was rapid, and the speedy extension and associative interaction of these molecules would ensure that degradations set in within the shortest possible flowrate compared to what was obtained at 300 ppm. From Table 8.1, the onset of polymer degradation was predicted to occur at 1038/s, 891/s and 765/s for 300, 500 and 1,000 ppm respectively. This was also reflected in the degradation flow regime in Figure 8.10. In addition, it was observed that the magnitude of the initial degradation decline from the peak value ($H_{app} = 1$) was minimal at 1,000 ppm compared to what was obtained at 300 ppm. Afterwards, the subsequent degradation was observed to follow a steady decline for each concentration; however, the subsequent decline was minimal at higher concentration. The number of polymer molecules available can explain this initial degradation decline during flow in the sand-pack media. Many molecules available at high concentration imply that the strength of the associative interaction is strong enough to withstand shear degradation conditions with minimal damage. However, this was not the case at a low concentration where the strength of the associative interactions was lower due to fewer polymer molecules in the solution. The model prediction of the onset of polymer degradation was experimentally validated by analysing the normalised effluent viscosity (N_{EV} from Equation 4.27) of the effluent polymer solution at each polymer concentration, as shown in Figure 8.11. The critical flow rate for the onset of polymer degradation was obtained by fitting equation 4.28 to N_{EV} profile for each concentration from which Q_{dg} was obtained. The equivalent shear rate value was obtained using equation 4.29. The experimentally obtained values for the onset of polymer degradation were 1088, 903 and 795/s for 300, 500 and

1,000 ppm respectively. These values compared very well with the predicted values for the onset of polymer degradation.

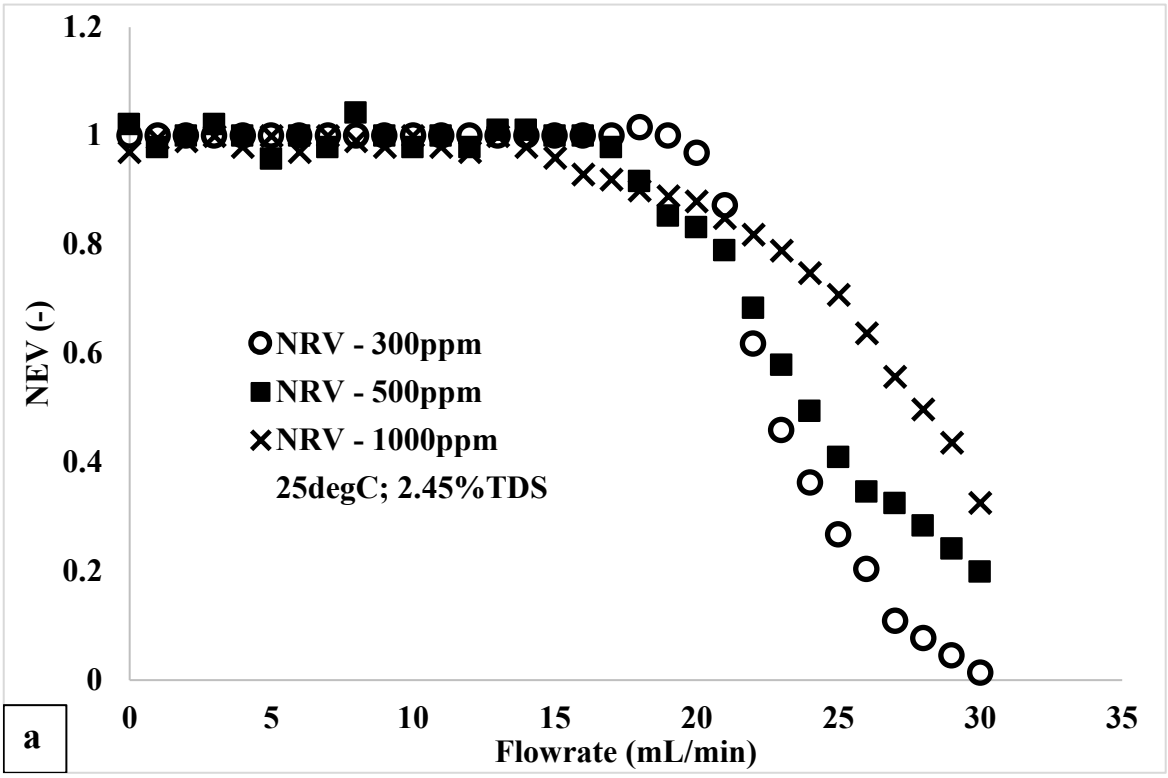

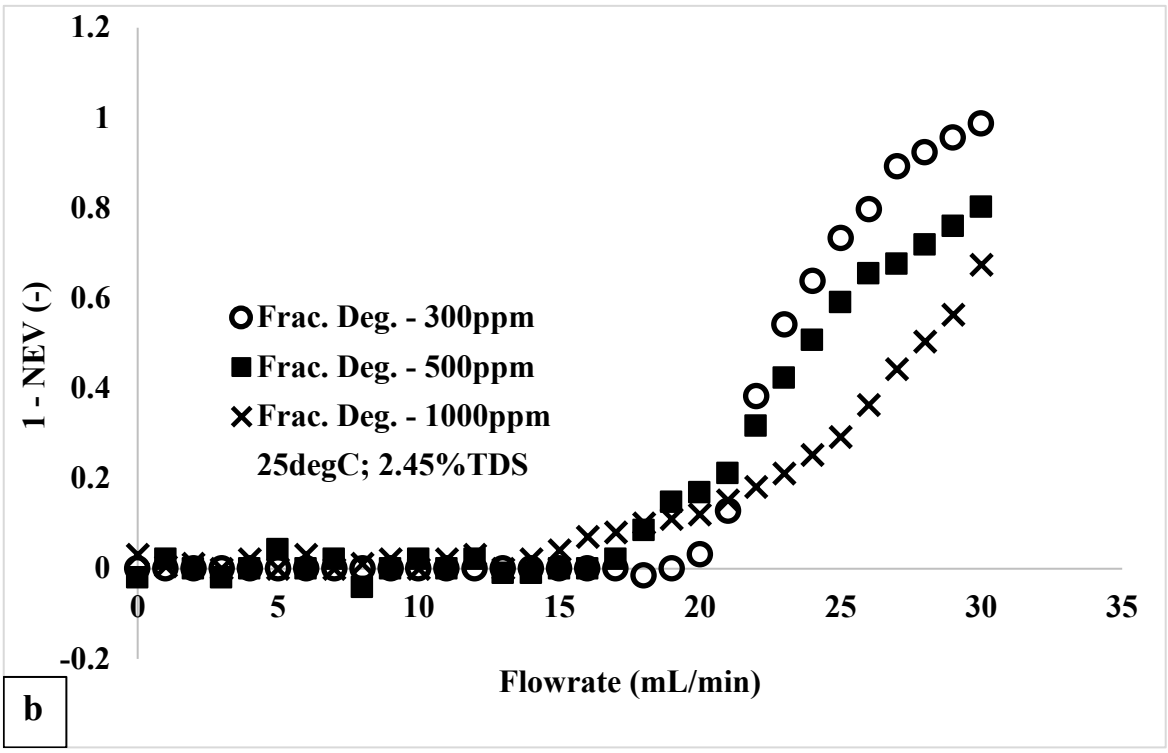

***Figure 8.11**: Effluent analysis for the experimental determination of the onset of polymer degradation at different concentrations at 25 ℃ and 2.45 %TDS (a) Normalized Effluent Viscosity (b) Fractional Degradation.*

8.3. Optimizing the Propagation of Associative Polymers

The optimized condition was to maintain and sustain the pre-injection level of hydrophobic interactions during propagation in a porous media, i.e., $\Delta H_{\mu} = \Delta H_{C_p}$ (Correction factor, $\omega_a = 1$). This condition implies that the proportion of hydrophobic interactions lost to different retention mechanisms is appropriately compensated with an equivalent increase in hydrophobic interactions arising from in-situ shear elongation effects.

8.3.1. Correction Factor

Figure 8.12 shows the trend for the correction factor from zero flow rate up to 6 mL/min.

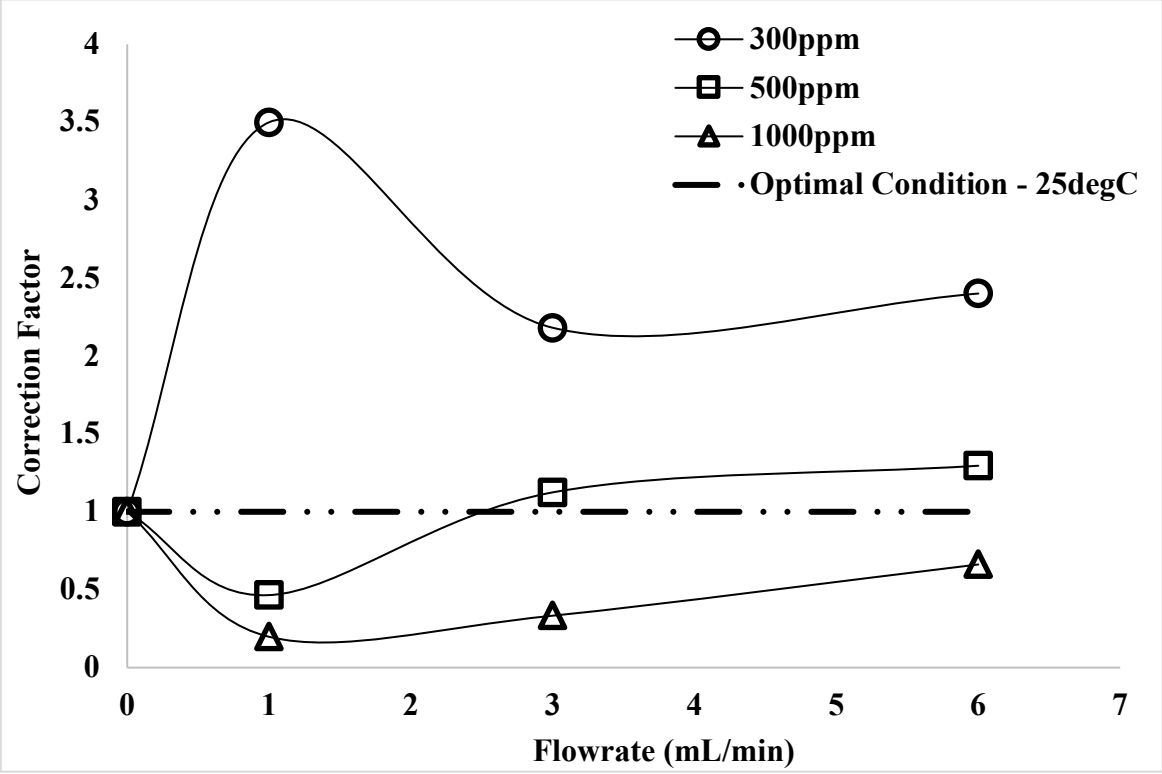

***Figure 8.12**: Plot of the correction factor against flowrate at different polymer concentrations. This was determined at a temperature of 25* ℃.

At a 1 mL/min flowrate, the correction factor was significantly greater than unity at 300 ppm. This indicates a substantial increase in hydrophobic interactions in the porous media compared to interactions lost to retention. However, this considerable increase in the hydrophobic interactions may not be sufficient to impact the necessary viscous thickening required for EOR. Typical oilfield polymer concentration values range between 1,000 to 2,500 ppm in the case of non-associative polymers. However, the correction factor at 500 and 1,000 ppm show values less than one at 1 mL/min. This outcome indicates that the effect of retention dominates over the viscous thickening arising from increased

hydrophobic interactions. Therefore, operating at a concentration between 1,000 and 2,500 ppm would imply a significant loss of hydrophobic interactions to polymer retention. Increased hydrophobic interactions due to elongation effects may not compensate for this loss. However, as the flow rates increased from 3 to 6 mL/min, the impact of incremental hydrophobic interactions from elongation effects gradually dominates over the loss of these interactions to retention. The implication of this is that the sustainability of hydrophobic interactions deep in a porous media is dependent on the polymer concentration, as explained earlier in Section 8.2.1. Similarly, the effect of temperature conditions on the correction factor was captured in Figure 8.13.

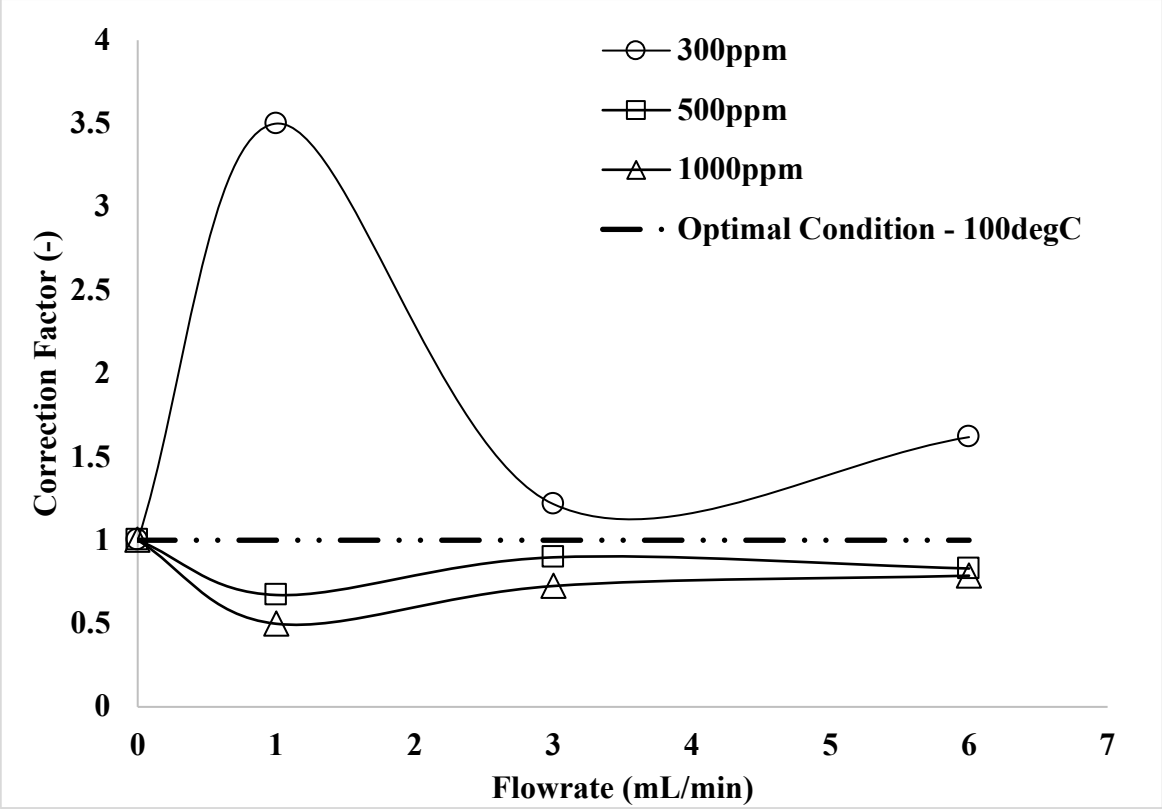

***Figure 8.13**: Plot of the correction factor against flowrate at different polymer concentrations. This was determined at a temperature of 100* ℃.

The overall temperature effect resulted in a simultaneous reduction in the incremental hydrophobic interactions for viscous thickening and polymer retention.

8.3.2. Optimal Settings for the Propagation of Hydrophobic Interactions

The determination of the optimal setting (optimal concentration) at which the pre-injection level of hydrophobic interactions can be sustained during propagation in a porous media was done by plotting the correction factor against the polymer concentration for different flow conditions in Figure 8.14. The optimal concentration was determined as the point at

which the optimal correction factor ($\omega_a = 1$) intersects the curves for each flowrate. These intersections marked the point at which the hydrophobic interactions lost to polymer retention is equally gained due to elongation effects in the porous media.

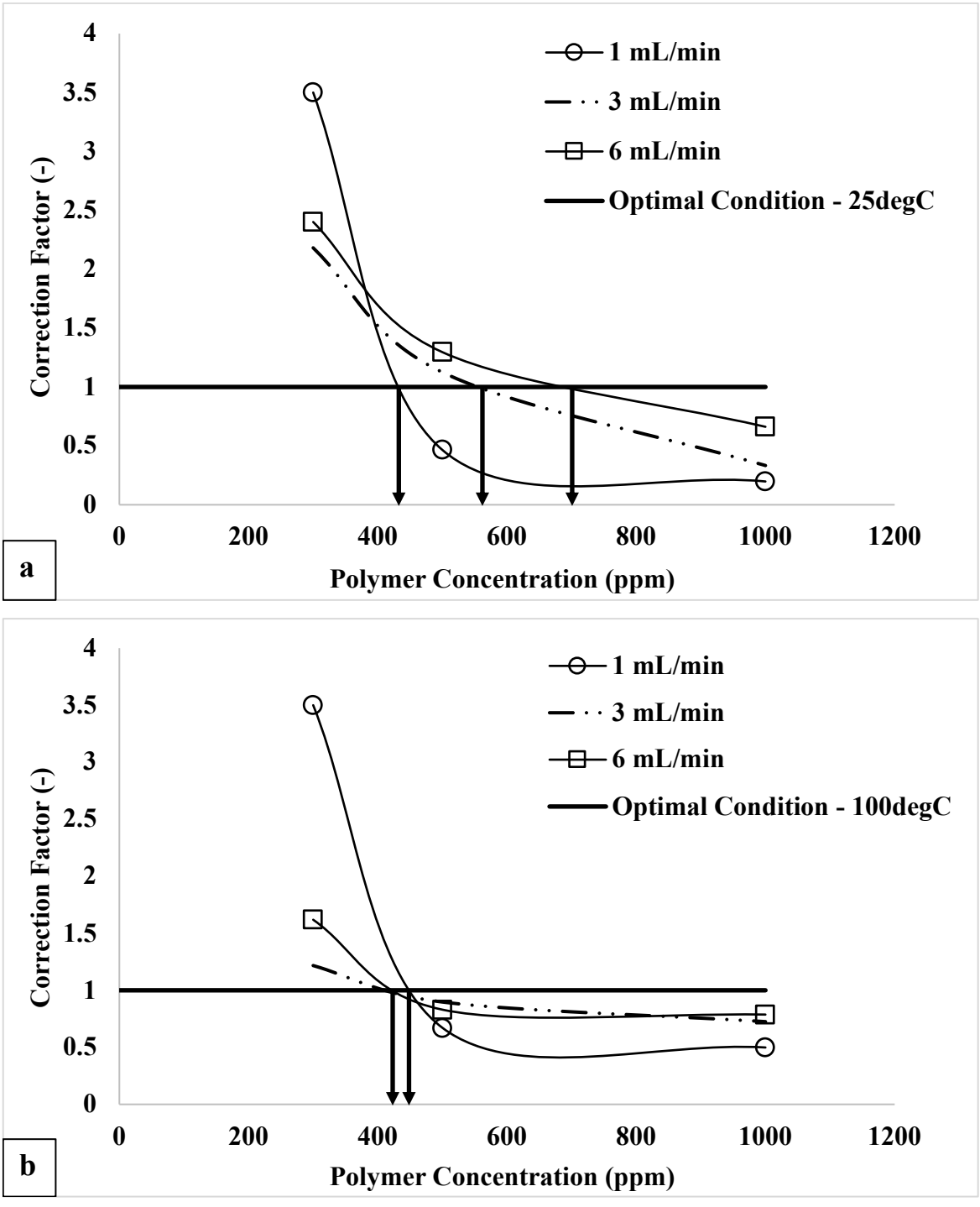

Figure 8.14*: Estimation of the optimal concentration at different flowrate at* $\omega_a = 1$ *(a) 25* ℃ *(b) 100* ℃.

At 25 ℃, the estimated optimal concentrations at 1, 3 and 6 mL/min were 420, 560 and 740 ppm respectively. However, at 100 ℃, the optimal concentrations at 1, 3 and 6 mL/min were 450, 430 and 430 ppm respectively. The effect of thermal degradation was evident in

the optimal concentrations as the temperature increased from 25 to 100 ℃. As mentioned earlier, the essence of developing the optimisation approach is to improve the injectivity of associative polymers by ensuring the hydrophobic interactions are sustained deep in the porous media. Figure 8.15 shows the outcome of polymer injection at the optimum concentration. It can be observed that the onset of hydrophobic interactions in the sand-packed media took place after injecting 0.8 PV with minimal loss of polymer aggregates to retention. This corresponds to 3.4 cm from the injection point for the onset of hydrophobic interactions in the porous media. The total length of the porous media is 12 cm indicating that the start of hydrophobic interactions takes place not far from the injection point and is sustained for a further distance of 8.6 cm into the porous media (Figure 8.15b). This outcome shows that hydrophobic interactions between associative polymers can be optimised for deep propagation in porous media. This optimisation approach is crucial as the loss of hydrophobic interactions close to the injection point would increase retention further into the porous media with a less viscous thickening effect. However, the reverse is the case with this approach as there is minimal loss of polymer aggregates arising from hydrophobic interactions to polymer retention after few pore volumes of injection.

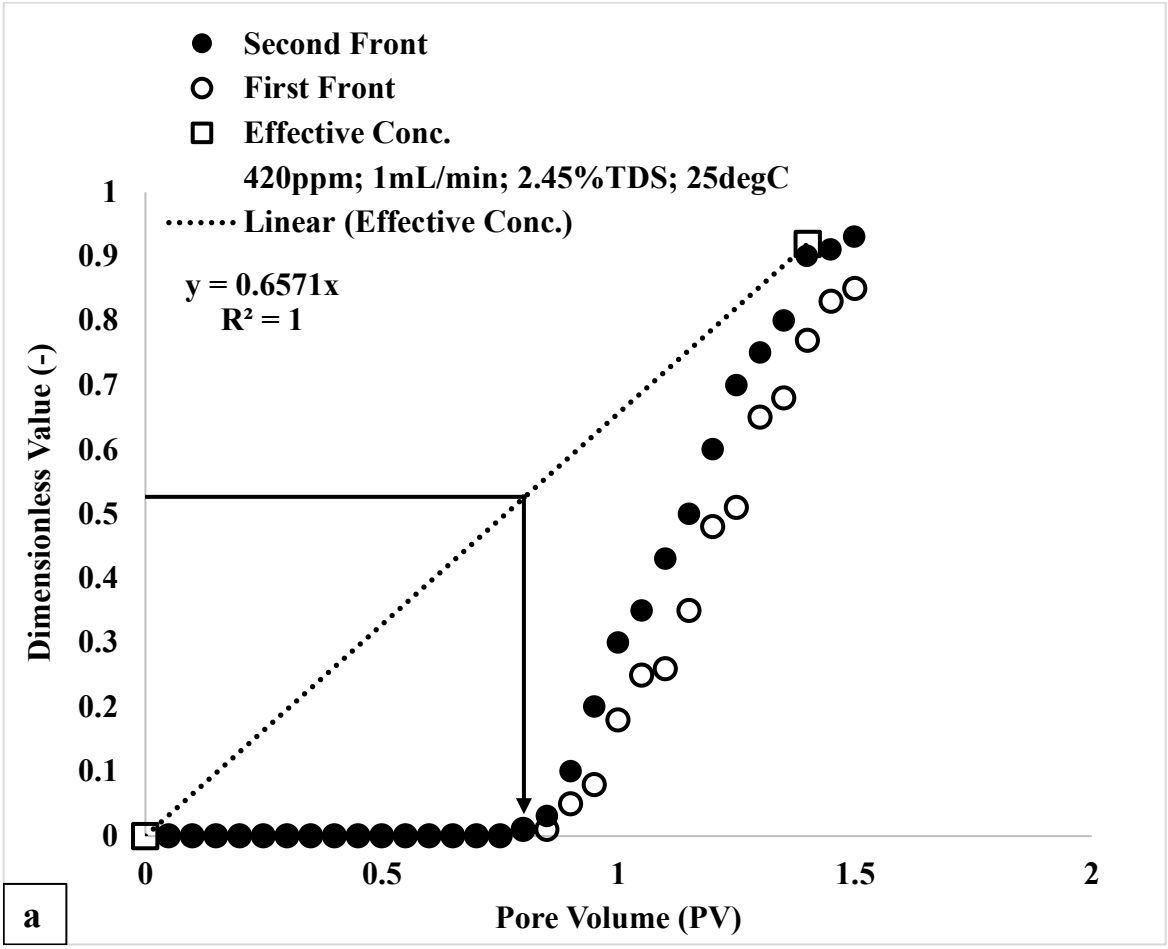

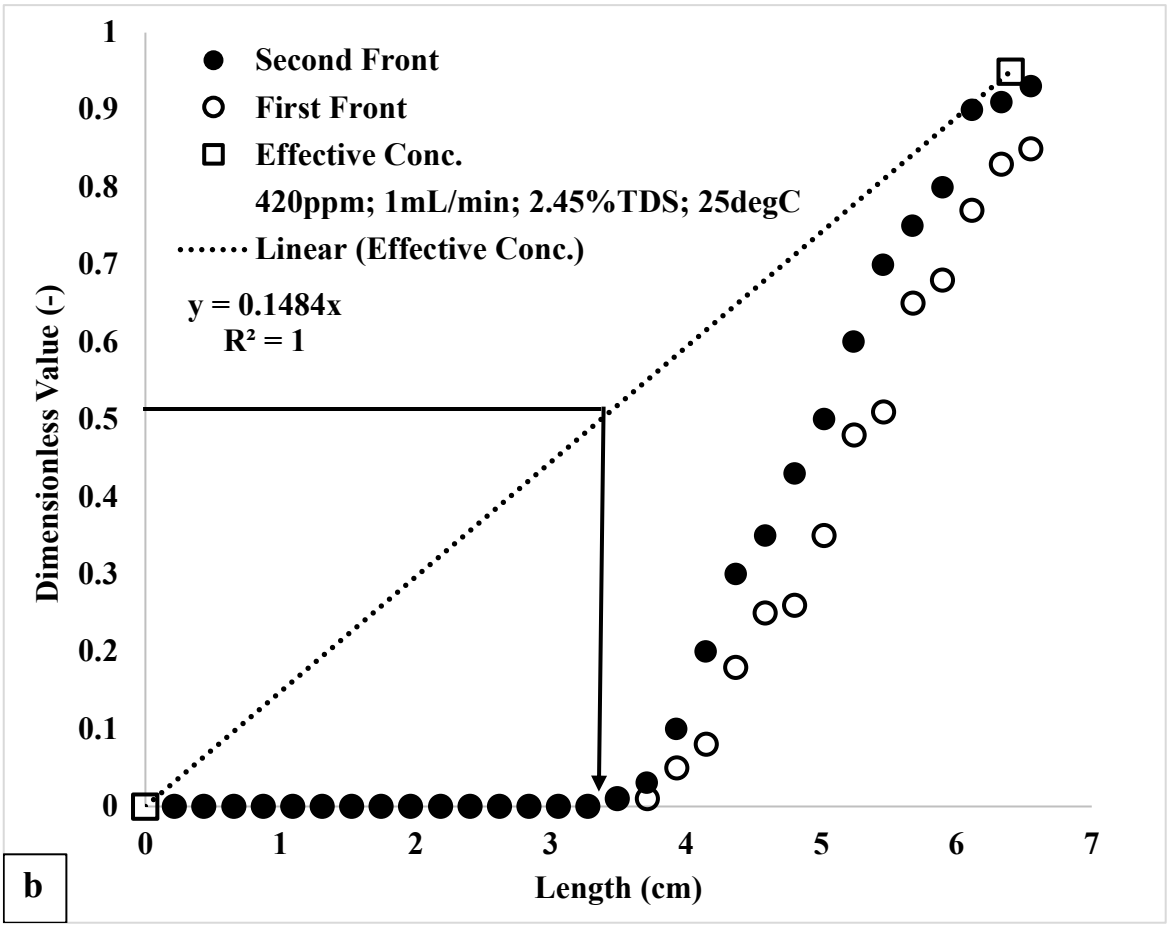

***Figure 8.15**: Polymer effluent analysis for the determination of the onset and sustainability of hydrophobic interactions in the sand packed media at the optimum concentration of 420 ppm (25 ℃ and 1 mL/min) in terms of (a) number of injected pore volume (b) distance from the injection point.*

8.4. Summary

The transport of the associative polymer in porous media was discussed, emphasising the propagation of hydrophobic interactions between the polymer molecules. It was established in this work that the high resistance factor experienced in the porous media was due in part to the incremental hydrophobic interactions arising from shear thickening and hydrophobic interactions lost to polymer retention contribute as well. However, a predictive model was developed which quantitatively captured the contributory effect of hydrophobic interactions lost to the retention and gained due to shear thickening to the overall pressure drop in the porous media. In addition, the impact of the proportion of hydrophobic interaction on the onset of polymer degradation was also reported with a high proportion leading to minimal degradation and low value for the critical rate for the start of degradation and vice versa. Similarly, a large proportion of hydrophobic interactions means that a significant amount of it is lost to polymer retention while also resulting in hydrophobic interactions occurring

after a few pore volumes have been injected. However, for a low proportion of these interactions at low polymer concentration, there is a minimal loss of these interactions to different retention mechanisms while ensuring that the onset of these interactions occurring after large pore volumes have been injected. The large pore volumes injected before the start of hydrophobic interactions at low concentration means that these interactions can be sustained deep in porous media. This necessitated the optimisation approach developed in defining the optimal setting for the injection concentration under different flow, salinity, and temperature conditions.

CHAPTER NINE

9.0. Conclusion and Recommendations

9.1. Research Findings and Conclusions

The hydrophobic interactions between associative polymers have resulted in two outcomes during transport in porous media. Firstly, these interactions resulted in the viscous thickening of the polymer solutions during propagation in porous media. Secondly, these interactions also resulted in the retention of polymer molecules in porous media. These two outcomes contributed to the overall pressure drop or resistance factor experienced during propagation. However, this work was able to quantitatively identify the contributions of hydrophobically induced polymer retention and viscous thickening to the pressure drop and resistance factor. These contributions were systematically studied from a predictive approach which was subsequently validated using the existing experimental method. But, where there was no current experimental procedure to validate the developed predictive system, novel experimental techniques were developed by modifying well defined experimental procedures laid out in the American Petroleum Institute (API) specification for the analysis of polymers for enhanced oil recovery. The key findings of this research work can be summarised as follows:

a) Hydrophobic interactions can be quantified on a mass or volume proportion depending on the units of the polymer concentration. This parameter accounted for the proportion of molecular interactions and not the strength of these interactions. This novel parameter was defined based on the knowledge of the critical aggregation concentration for the onset of hydrophobic interactions. Furthermore, another critical concentration (known as the critical separation concentration) was identified, beyond which hydrophobic interactions between the polymer molecules become dominant over intramolecular interactions consistent with the dilute regime.
b) The defined parameter in (a) allowed for the accurate mapping of the various polymer concentration regimes and the novel critical separation concentration parameter identified for the onset of the concentrated regime. It was concluded from this work that the critical separation concentration which marked the start of the concentrated regime was approximately twice the critical aggregation concentration, i.e. $C_c \approx 2C_{ag}$. In other words, the aggregation concentration distinguished the dilute from the semi-dilute

regime, while the critical separation concentration separated the semi-dilute from the concentrated regime.

c) The hydrophobic interactions lost from the polymer enriched phase flowing at the centre of the pores to different retention mechanisms play a significant role in pore damage. The proportion of hydrophobic interactions lost to polymer retention at 25 ℃ was estimated using the developed model for H_{C_p} in equation (3.91) and this varied from 0.04 to 0.56 for polymer concentrations from 50 to 1,000 ppm. The lost hydrophobic interactions amounted to an estimated damaged pore volume ranging from 0.21 to 0.46 PV and a porosity reduction from 0.364 to 0.19. Similar estimations were obtained at 100 ℃ with hydrophobic interactions ranging from 0.05 at 50 ppm to 0.30 at 1,000 ppm. The damaged pore volume ranged from 0.20 to 0.36 PV, and porosity reduction ranged from 0.364 to 0.236 for 50 – 1,000 ppm respectively.

d) The predictive approach for mapping the various types of retention mechanisms based on the knowledge of the hydrophobic interactions lost showed that adsorption dominated over entrapment for a given damaged pore volume at low polymer concentrations. However, as the concentration increased, the effect of adsorption reached a maximum and entrapment dominated at higher polymer concentrations. At 25 ℃, the quantitatively mapped adsorption accounted for 99.9, 98.5 and 91.5 % of the total damaged pore volume for 300, 500 and 750 ppm respectively, while entrapment amounted to 0.1, 1.5 and 8.5 % of the damaged pore volume. However, beyond 750 ppm, the fractional amount attributed to entrapment increased to a value of 29.9 % at 1,000 ppm, while the equivalent value for adsorption was 70.1 %; however, at 100 ℃, the quantitatively mapped adsorption dominated over entrapment. This accounted for 99.6, 99.6, 98.8 and 98.1 % of the total damaged pore volume for 300, 500, 750 and 1,000 ppm respectively, while entrapment amounted to 0.4, 0.4, 1.2 and 1.9 % of the damaged pore volume.

e) A novel experimental procedure was developed to validate the predictive approach for mapping the different hydrophobically-induced polymer retention mechanisms. This was achieved by combining existing techniques defined for static and dynamic retention in the API Specification 63. In other words, the static retention procedure was experimentally mapped to the dynamic retention, and both retention outputs were compared for adsorption and entrapment respectively. At 25 ℃, the experimentally mapped adsorption accounted for 89.8, 88.5, 79.5 and 85.2 % of the total damaged pore

volume for 300, 500, 750 and 1,000 ppm respectively compared to the predicted outcome of 99.9, 98.5, 91.5 and 70.1 %. The level of correlation, R^2 between the predicted and the experimental outcome was 90.45 %. The experimentally mapped entrapment amounted to 1, 10, 15 and 21 % for 300, 500, 750 and 1,000 ppm respectively, compared to the predicted outcome of 0.1, 1.5, 8.5 and 29.9 %. The level of correlation, R^2 between the predicted and the experimental outcome was 87.43 %.

f) The observed high resistance factor for the polymer flow in the sand-pack media was due to both retention and viscous thickening with hydrophobic interactions significantly contributing to both cases. At 300 ppm, the net hydrophobic interactions lost to polymer retention were 0.02, 0.09 and 0.11 at flowrates of 1, 3 and 6 mL/min. But the net hydrophobic interactions gained due to shear elongation effects (viscous thickening) were 0.07, 0.20 and 0.28 at flowrates of 1, 3 and 6 mL/min. This outcome indicated that at this concentration (300 ppm), the viscous thickening effect contributed more to the resistance factor and the pressure drop. However, at a high concentration of 1,000 ppm, the net hydrophobic interactions lost to polymer retention were 0.19, 0.25 and 0.35 at flowrates of 1, 3 and 6 mL/min. But the net hydrophobic interactions gained due to shear elongation effects (viscous thickening) were 0.04, 0.08 and 0.14 at flow rates of 1, 3 and 6 mL/min respectively, indicating that polymer retention contributed more to the resistance factor/pressure-drop.

g) The sustainability of the hydrophobic interactions deep into a porous media was discovered to depend on the onset of hydrophobic interactions in the porous media. This was in addition to the previously observed effects of retention and shear elongation. A modified polymer effluent analysis was developed and correlated to the set equation in (8.2) to estimate the onset of hydrophobic interactions in the porous media. At a flow rate of 1 mL/min, in-situ hydrophobic interactions did not start until 0.7, 0.5 and 0.3 PVs were injected for 500, 750 and 1000 ppm respectively. However, an increase in the flow rate to 6 mL/min saw the onset of hydrophobic interactions commenced after injecting a higher number of pore volumes (0.45 PV) for 1,000 ppm. In both cases from the onset of hydrophobic interactions, these associative effects were sustained in the range of parameters studied (i.e., temperature, flow rate and salinity). The observed outcomes showed that the sustainability of hydrophobic interactions in porous media decreased with polymer concentration since the PV for the onset of these interactions decreased with concentration. However, the PV for the start of hydrophobic interactions

increased with flowrate, indicating that these interactions deep in the porous media increased with flowrate.

h) An optimisation approach was developed to improve further the sustainability of hydrophobic interactions in porous media. The optimised condition was obtained when the correction factor that related the net hydrophobic interactions lost to polymer retention and the net hydrophobic interactions gained from elongation effects was unity ($\omega_a = 1$). The optimised polymer concentrations at 25 ℃ for 1, 3, and 6 mL/min were 420, 560 and 740 ppm. However, at 100 ℃, the optimal concentrations at 1, 3 and 6 mL/min were 450, 430 and 430 ppm. The effect of thermal degradation was evident in the optimal concentrations as the temperature increased from 25 to 100 ℃.

Based on these findings highlighted above, this work has been able to achieve the objectives which was set out in chapter one. These achievements include:

a) a dimensionless parameter to quantify the proportion of hydrophobic interactions.
b) a model for predicting in-situ pressure drop based on the effect of in-situ hydrophobic interactions on the different polymer retention mechanisms and polymer flow regimes.
c) A novel experimental procedure for validating the predictions of the developed model for mapping the various retention mechanisms in a porous media.
d) An optimisation approach for maximising the propagation of hydrophobic interactions between associative polymers in a porous media

9.2. Research Contributions to Knowledge

This research work has given new insights into the transport of hydrophobically associating polymers in porous media. Furthermore, these insights were significant for optimising and maximising hydrophobic interactions between polymer chains during transport in porous media. The substantial and impactful contributions of this research work to the body of knowledge include the following:

a) Identifying a unique and measurable parameter for quantifying the proportion of hydrophobic interactions between associative polymer molecules during flow in porous media. Also, the total ratio of molecular interactions in terms of associative and non-associative was computed as unity. Therefore, for a given estimation of associative hydrophobic interactions, the corresponding balance of non-associative interactions can also be calculated. However, this parameter does not indicate the magnitude or strength of the interaction between the polymer molecules.

b) Develop a novel experimental approach for estimating fractional damaged pore volume based on accurate mapping of static polymer retention to dynamic polymer retention. The mapping of static retention to dynamic retention involves using the same solid to liquid ratio and retention time. The dynamic retention time was calculated using Pore Volume (PV) in relation to the total static retention time for maximum retention to the flow conditions under dynamic conditions.

c) Based on the unique predictive approach for estimating fractional damaged pore volume, a novel method was developed to map the various types of polymer retention mechanisms (monolayer and multilayer adsorption, polymer mechanical entrapment and polymer pore plugging) using the distribution of hydrophobic interactions between retained polymer molecules. Besides, a new equation was also developed to predict the onset of mechanical entrapment and the onset of pore plugging. This was achieved with the knowledge of the associative interactions that exist between the retained polymer molecules There is no reported expression in literature which predicts the onset of polymer entrapment and plugging. This makes the expression developed in this work stand out and can act as the basis future modelling works in polymer retention studies.

d) The development of a new model for predicting hydrophobic interactions between associative polymers under different flow regimes (shear thinning, shear thickening and degradation) during transport in a porous media with minimal fitting parameters. The relevant parameters incorporate primary reservoir conditions and polymer properties known to affect the performance of associative polymers. The knowledge of the amount of in-situ hydrophobic interactions allowed for the computation of the effective polymer concentration during transport in a porous media.

e) A novel approach for predicting the onset of shear thickening and the onset of shear degradation. Predicting the onset of shear degradation was based on the proportion of hydrophobic interactions as defined by the identified dimensionless parameter from (a). However, the onset of shear thickening was based on the ratio of the characteristic times, which represents the fitting parameters in the developed model for flow regimes in (d). This shows that the onset of shear thickening was independent of the proportion of hydrophobic interactions.

f) An optimisation approach for maximising the propagation of associative interactions based on the identified contributory effect to polymer retention and effective viscosity. Optimal conditions were defined based on the point at which the impact on polymer retention on hydrophobic interactions cancel out the corresponding effect of flow

regimes on the hydrophobic interactions, thereby ensuring that propagation of associative interactions was significantly maintained at the pre-injection estimate of the interactions.

9.3. Recommendations and Proposals for Further Works

The recommendations suggested for further works were based on the identified limitations of this research work and are as follows:

a) Determination of the size distribution of the retained polymer molecules using a consolidated core sample. This can be achieved by comparing the pore size distribution before and after the polymer injection. This would further reduce the uncertainty surrounding the developed predictive model related to the estimation of the size distribution of retained polymer molecules. In this research work, the pore size distribution of the unconsolidated sand-pack media was estimated using the Kozeny-Carman equation, and this may further explain the added uncertainty manifested in the difference in the coefficient of determination values for the predictive and experimental approach used in mapping the various retention mechanisms in the unconsolidated sand-pack media.
b) Comparison of the developed optimisation approach to determine an optimal polymer concentration with other established procedures employed in the industry for a similar purpose. Furthermore, the optimisation approach was developed using demonstrated knowledge for hydrophobic interactions in associative polymers. This can also be employed to determine an optimal concentration for non-associative polymers such as hydrolysed polyacrylamide. This is thought to be achievable because non-associative polymers exhibit intermolecular interactions beyond the critical overlap concentration. This is synonymous with the critical aggregation concentration observed with associative polymers. However, the critical aggregation concentration is always less than the critical overlap concentration indicating that hydrophobic interactions in associative polymers are always stronger than the intermolecular interactions present among non-associative polymers. Finally, an experimental evaluation of the optimal concentration for the purpose of oil recovery would be required.

9.4. Research Output and Publications

The following research publications represent some of the significant output of this work:

a) **Afolabi, R. O.**, Oluyemi, G. O., Officer, S., & Ugwu, J. O. (2019). Hydrophobically Associating Polymers for Enhanced Oil Recovery – Part A: A Review on the Effects of Some Key Reservoir Conditions. *Journal of Petroleum Science and Engineering, 180*, 681-698.

b) **Afolabi, R. O.**, Oluyemi, G. O., Officer, S., & Ugwu, J. O. (2019). Hydrophobically Associating Polymers for Enhanced Oil Recovery – Part B: A Review of Modelling Approach to Flow in Porous Media. *Journal of Molecular Liquids, 293*, 111495.

c) **Afolabi, R. O.**, Oluyemi, G. O., Officer, S., & Ugwu, J. O. (2020). Determination of a Critical Separation Concentration for Associative Polymers in Porous Media Based on Quantification of Dilute and Semi-Dilute Concentration Regimes. *Journal of Molecular Liquids, 317*, 114142.

d) **Afolabi, R. O.**, Oluyemi, G. O., Officer, S., & Ugwu, J. O. (2021). A New Approach for Quantitative Mapping of Retention Mechanisms of Associative Polymers in Porous Media. *Journal of Molecular Liquids, 343,* 117385.

References

Abbas, S., Sanders, A. W., & Donovan , J. C. (2013). Applicability of hydroxyethylcellulose polymers for chemical EOR. *SPE Enhanced Oil Recovery Conference.* Kuala Lumpur: Society of Petroleum Engineers.

Abidin, A. Z., Puspasari, T., & Nugroho, W. A. (2012). Polymers for enhanced oil recovery technology. *Procedia Chemistry, 4*, 11-16.

Afolabi, R. O. (2015). Effect of surfactant and hydrophobe content on the rheology of poly(acrylamide-co-N-doedecylacrylamide) for potential enhanced oil recovery application. *American Journal of Polymer Science, 5*(2), 41-46.

Afolabi, R. O., Oluyemi, G. O., Officer, S., & Ugwu, J. O. (2019). Hydrophobically associating polymers for enhanced oil recovery – Part A: A review on the effects of some key reservoir conditions. *Journal of Petroleum Science and Engineering, 180*, 681-698.

Ahmed, S., Elraies, K. A., Tan, I. M., & Hashmet, M. R. (2017). Experimental investigation of associative polymer performance for CO2 foam enhanced oil recovery. *Journal of Petroleum Science and Engineering, 157*, 971-979.

Akbari, S., Mahmood, S. M., Tan, I. M., Bharadwaj, A. M., & Hematpour, H. (2017). Experimental investigation of the effect of different process variables on the viscosity of sulfonated polyacrylamide copolymers. *Journal of Petroleum Exploration and Production Technology, 7*, 87–101.

Akbulut, M., & Temizel, C. (2017). Technology update: Adjustable, supramolecular viscosity modifiers as displacement fluids in EOR. *Journal of Petroleum Technology, 69*(4), 1-3.

Algi, M. P., & Okay, O. (2014). Highly Stretchable Self-Healing Poly(N,N-dimethylacrylamide) hydrogels. *European Polymer Journal, 59*, 113-121.

Alquraishi, A. A., & Alsewailem, F. D. (2012). Xanthan and guar polymer solutions for water shutoff in high-salinity reservoirs. *Carbohydrate Polymers, 88*(3), 859-863.

Al-Hajri, S., Mahmood, S. M., Abdulehah, H., & Akbari, S. (2018). An overview on polymer retention on porous media. *Energies, 11*(10), 2751

Al-Sabagh, A. M., Kandile, N. G., El-Ghazawy, R. A., Noor El-Din, M. R., & El-Sharaky, E. A. (2016). Solution properties of hydrophobically modified polyacrylamides and their potential use for polymer flooding application. *Egyptian Journal of Petroleum, 25*, 433-444.

Al-Shakry, B., Skauge, T., Shiran, B. S., & Skauge, A. (2019). Polymer injectivity: investigation of mechanical degradation of enhanced oil recovery polymers using in-situ rheology. *Energies, 12*, 49-74.

Amirian, E., Dejam, M., & Chen, Z. (2018). Performance forecasting for polymer flooding in heavy oil reservoirs. *Fuel, 216*, 83-100.

Arinkoola, A. O., Olalekan, S. T., Salam, K. K., Omoloa, J. M., & Gafar, A. O. (2018). Potential evaluation and optimization of natural biopolymers in water-based Drilling mud. *Journal of Chemical and Petroleum Engineering, 52*(1), 1-12.

Austad, T., Ekrann, S., Fjelde, I., & Taugbol, K. (1997). Chemical flooding of oil reserviors Part 9. Dynamic adsorption of surfactant onto sandstone cores from injection water with and without polymer present. *Colloids and Surfaces A: Physiochemical and Engineering Aspects, 127*(1), 69-82.

Azad, M. S., & Trivedi, J. J. (2017). Injectivity behaviour of copolymer and associative polymers decoded using extensional viscosity characterization: Effect of hydrophobic association. *SPE Western Regional Meeting.* California: Society of Petroleum Engineers.

Badi, N. (2017). Non-linear PEG-based thermoresponsive polymer systems. *Progress in Polymer Science, 54-79*, 66.

Bai, Y., Shang, X., Wang, Z., & Zhao, X. (2018). Experimental study on hydrophobically associating hydroxyethyl cellulose flooding system for enhanced oil recovery. *Energy and Fuels, 32*, 6713-6725.

Bains, G., Patel, A. B., & Narayanaswami, V. (2011). Pyrene: A probe to study protein conformation and conformational changes. *Molecules, 16*, 7909-7935.

Bang, F., Cech, T., & Gebert, S. (2017). Poly(methacrylic Acid-co-Ethyl Acrylate): comparing three different grades in regard to preparation and functionality features in enteric release film-coating applications. *2nd European Conference on Pharmaceutics.* Krakow, Poland: Pharma Solutions Sales Europe.

Barker, I. C., Cowie, J. M., Huckerby, T. N., Shaw, D. A., Soutar, I., & Swanson, L. (2003). Studies of the “smart” thermoresponsive behavior of copolymers of N-Isopropylacrylamide and N,N-Dimethylacrylamide in dilute aqueous solution. *Macromolecules, 36*(20), 7765–7770.

Barmar, M., Kaffashi, B., & Barikani, M. (2010). Investigating the Uni-HEUR Thickener Performance considering Hydrophilic Segment Lenght. *Colloids and Surfaces A: Physicochemical and Engineering Aspects, 364*, 105-108.

Branham, K. D., Snowden, H. S., & McCormick, C. L. (1996). Water soluble copolymers. 64. effects of ph and composition on associative properties of amphiphilic acrylamide/acrylic acid terpolymers. *Macromolecules, 29*, 254-262.

Brassinne, J., Bourgeois, J.-P., Fustin, C. A., & Gohy, J. F. (2014). Thermo-responsive properties of metallo-supramolecular block copolymer micellar hydrogels. *Soft Matter, 10*, 3086-3092 .

Candau, F., & Selb, J. (1999). Hydrophobically-modified polyacrylamides prepared by micellar polymerization. *Advances in Colloid and Interface Science, 79*(2-3), 149-172.

Candau, F., Biggs, S., Hill, A., & Selb, J. (1994). Synthesis, structure and properties of hydrophobically associating polymers. *Progress in Organic Coatings, 24*(1-4), 11-19.

Çavuş, S. (2010). Poly(methacrylamide-co-2-acrylamido-2-methyl-1-propanesulfonic acid) hydrogels: Investigation of pH- and temperature-dependent swelling characteristics and their characterization. *Journal of Polymer Science Part B: Polymer Physics, 48*(23), 2497-2508.

Chen, H., Ye, Z., Han, L., & Luo, P. (2012). Studies on the self-assembly behavior of the hydrophobically associating polyacrylamide. *Journal of Applied Polymer Science, 123*(4), 2397-2405.

Chen, T., Song, Z., Fan, Y., Hu, C., Qiu, L., & Tang, J. (1998). A pilot test of polymer flooding in an elevated temperature reservior. *SPE Reservior Evaluation and Engineering , 1*(1), 24-29.

Chen, T., Song, Z., Fan, Y., Hu, C., Qiu, L., & Tang, J. (1998). A pilot test of polymer flooding in an elevated-temperature reservoir . *SPE Reservoir Evaluation & Engineering, 1*(1), 24-29.

Chen, Z. (2016). *Polyacrylamide and its derivatives for oil recovery.* Thesis, Department of Chemistry. Missouri: Missouri University of Science and Technology.

Choi, B., Jeong, M. S., & Lee, K. S. (2014). Temperature-dependent viscosity model of HPAM polymer through high-temperature reservoirs. *Polymer Degradation and Stability, 110*, 225-231.

Choi, J., Ka, D., Chung, T., Jung, J., Koo, G., Uhm, T., & Jung, H. (2015). Evaluation of highly stable ultrahigh-molecular-weight partially hydrolyzed polyacrylamide for enhanced oil recovery. *Molecular Research, 23*(6), 518-524.

Cilurzo, F., Selmin, F., Gennari, C., Montanari, L., & Minghetti, P. (2014). Application of methyl methacrylate copolymers to the development of transdermal or loco-regional drug delivery systems. *Expert Opinion on Drug Delivery , 11*(7), 1033-1045.

Cui, Q., Zhang, J., Xue, T., & Zhang, J. (2016). Study on synthesis and application performance of hydrophobic associated polymer drag reducing agent. *Journal of Residuals Science & Technology, 13*(6), 1-10.

Dai, C., Xu, Z., Wu, Y., Zou, C., Wu, X., Wang, T., & Zhao, M. (2017). Design and study of a novel thermal-resistant and shear-stable amphoteric polyacrylamide in high-salinity solution. *Polymers, 9*(7), 1-12.

Dai, Y., Wu, F., Li, M., & Wang, E. (2008). Properties and influence of hydrophobically associating polyacrylamide modified with 2-phenoxylethylacrylate. *Frontiers of Material Science in China, 2*(1), 113–118.

Das, B. M., Gogoi, S. B., & Mech, D. (2017). Micellar-polymer for enhanced oil recovery for Upper Assam Basin. *Resource Efficient Technologies, 3*, 82-87.

Data, M. J., Milanesio, J. M., Martini, R., & Strumia, M. (2018). Synthesis techniques for polymers applied to enhanced oil recovery. *MOJ Polymer Science, 2*(1), 17-20.

Deen, G. R. (2012). Solution properties of water-soluble “smart” poly(n-acryloyl-n′-ethyl piperazine-co-methyl methacrylate). *Polymers, 4*, 32-45.

Delamaide, E., Zaitoun , A., & Renard , G. (2013). Pelican lake field: first successful application of polymer flooding in a heavy oil reservoir. *SPE Enhanced Oil Recovery Conference* (pp. 1-22). Kuala Lumpur: Society of Petroleum Engineers.

Deng, Q., Li, H., Li, Y., Cao, X., Yang, Y., & Song, X. (2014). Rheological properties and salt resistance of a hydrophobically associating polyacrylamide. *Australian Journal of Chemistry, 67*(10), 1396–1402.

Deng, S. B., Bai, R. B., Chen, J. P., Yu, G., Jiang, Z., & Zhou, F. (2002). Effects of alkaline/surfactant/polymer on stability of oil droplets in produced water from ASP flooding. *Colloids and Surfaces A: Physicochemical and Engineering Aspects, 211*(2-3), 275-284.

Duhamel, J. (2012). Internal dynamics of dendritic molecules probed by pyrene excimer formation. *Polymers, 4*(1), 211-239.

Dupas, A., Heanaut, I., Rousseau, D., Poulain, P., Tabary, R., Argillier, J. F., & Aubry, T. (2013). Impact of polymer mechanical degradation on shear and extensional viscosities: toward better injectivity forecasts in polymer flooding operations. *SPE*

International Symposium on Oilfield Chemistry. Texas: Society of Petroleum Engineers.

Dupuis, G., Rousseau, D., Tabary, R., & Grassi, B. (2010). How to get the best out of hydrophobically associating polymersfor ior? new experimental insights. *SPE Improved Oil Recovery Symposium.* Oklahoma, USA.

Dupuis, G., Rousseau, D., Tabary, R., & Grassi, B. (2011). Flow of hydrophobically modified water-soluble polymer solutons in porous media: new experimental insights in the diluted regime. *SPE Journal, 16*(1), 43-54.

El-Hoshoudy, A. N., Desouky, S. E., Al-Sabagh, A. M., Betiha, M. A., El-Kady, M. Y., & Mahmoud, S. (2017). Evaluation of solution and rheological properties for hydrophobically associated polyacrylamide copolymer as a promised enhanced oil recovery candidate. *Egyptian Journal of Petroleum, 26*, 779-785.

El-Hoshoudy, A., Desouky, S., Al-sabagh, A., El-kady, M., Betiha, M., & Mahmoud, S. (2015). Synthesis and characterization of polyacrylamide crosslinked copolymer for enhanced oil recovery and rock wettability alteration. *International Journal of Oil, Gas and Coal Engineering, 3*(4), 47-59.

Fang, C., Jing, Y., Zong, Y., & Lin, Z. (2016). Effect of N,N-dimethylacrylamide (DMA) on the comprehensive properties of acrylic latex pressure sensitive adhesives. *International Journal of Adhesion and Adhesives, 71*, 105-111.

Feng, H., Lu, X., Wang, W., Kang, N., & Mays, J. W. (2017). Block copolymers: synthesis, sel-assembly and applications. *Polymers, 9*, 1-31.

Feng, Y. J., Billon, L., Grassl, B., Bastiat, G., Borisov, O., & Francois, J. (2005). Hydrophobically associating polyacrylamides and their partially hydrolyzed derivaties prepared by post-modification. 2. properties of non-hydrolyzed polymers in pure water and brine. *Polymer, 46*(22), 9283-9295.

Fernyhough, C., Ryan, A. J., & Battaglia, G. (2009). pH controlled assembly of a polybutadiene–poly(methacrylic acid) copolymer in water: packing considerations and kinetic limitations . *Soft Matter, 5*(8), 1674-1682 .

Gao, C. H. (2011). Scientific research and field applications of polymer flooding in heavy oil recovery. *Journal of Petroleum Exploration and Production Technology, 1*, 65-70.

Gao, C. H. (2014). Experiences of polymer flooding projects at shengli oilfield. *SPE EOR Conference at Oil and Gas West Asia.* Muscat: Society of Petroleum Engineers.

Garcia-Ochoa, F., Santos, V. E., Casas, J. A., & Gomez, E. (2000). Xanthan Gum: production, recovery, and properties. *Biotechnology Advances, 18*, 549-579.

Giz, A., Cüatalgil-Giz, H., Alb, A., Brousseau, J., & Reed, W. F. (2001). Kinetics and mechanisms of acrylamide polymerization from absolute, online monitoring of polymerization reaction. *Macromolecules, 34*, 1180-1191.

Gong, H. J., Zhang, H., Xu, L., Li, K. N., Yu, L., San, Q., & Dong, M. (2017). The synergistic effect of branched preformed particle gel and hydrolyzed polyacrylamide on further enhanced oil recovery after polymer flooding. *Energy and Fuels, 31*, 7904-7910.

Gong, H., Xu, G., Zhu, Y., Wang, Y., Wu, D., Nui, M., & Wang, H. (2008). Influencing factors on the properties of complex systems consisting of hydrolyzed polyacrylamide/triton x-100/cetyl trimethylammonium bromide: viscosity and dynamic interfacial tension studies. *Energy and Fuels, 23*(1), 300-305.

Gong, L. X., & Zhang, X. F. (2009). A new approach to the synthesis of hydrophobically associating polyacrylamide via the inverse miniemulsion polymerization in the presence of template. *Express Polymer Letters, 3*(12), 778–787.

Gou, S., Luo, S., Liu, T., Zhao, P., He, Y., Pan, Q., & Guo, Q. (2015). A novel water-soluble hydrophobically associating polyacrylamide based on oleic imidazoline and sulfonate for enhanced oil recovery. *New Journal of Chemistry, 39*, 7805-7815.

Guo, Y. J., Hu, J., & Zhang, X. M. (2016). Flow behavior through porous media and microdisplacement performance of hydrophobically modified partially hydrolyzed plyacrylamide. *SPE Journal, 21*(3), 688-705.

Guo, Y. J., Liu, J.-x., Zhang, X., Feng, R., Li, H., Zhang, J., & Luo, P. (2012). Solution property investigation of combination flooding systems consisting of gemini–non-ionic mixed surfactant and hydrophobically associating polyacrylamide for enhanced oil recovery. *Energy and Fuels, 26*(4), 2116–2123.

Guo, Y., Zhang, J., Zhang, X., Hu, J., Wang, W., & Liang, Y. (2018). Investigation and application of an associative polymer-surfactant binary system for a successful flooding pilot in a high temperature, high salinity ordinary heavy oil reservior. *SPE EOR Conference at Oil and Gas West Asia.* Muscat, Oman.

Habibi, H., & Khosravi-Darani, K. (2017). Effective variables on production and structure of xanthan gum and its food applications: A review. *Biocatalysis and Agricultural Biotechnology, 10*, 130-140.

Han, F. Q., Shao, B., Wang, Q. W., Guo, C. G., & Liu, Y. X. (2010). Synthesis and characterization of carboxymethylcellulose and methyl methacrylate graft copolymers. *Pigment & Resin Technology, 39*(3), 156-162.

Han, F., Xiong, D., Wang, Q., Shao, B., & Chen, M. (2013). Thermal properties of carboxymethylcellulose and methyl methacrylate graft copolymers. *Journal of Macromolecular Science Part B: Physics, 52*(9), 1242-1249.

Han, M., Xiang, W., Zhang, J., Jiang, W., & Sun, F. (2006). Application of EOR Technology by means of polymer flooding in bohai oil fields. *SPE International Oil and Gas Conference and Exhibition.* Beijing, China.

Hashmet, M. R., AlSumaiti, A. M., Qaiser, Y., & AlAmeri, W. S. (2017). Laboratory investigation and simulation modeling of polymer flooding in high-temperature, high-salinity carbonate reservoirs. *Energy and Fuels, 31*, 13454−13465.

Hashmet, M. R., Onur, M., & Tan, I. M. (2014). Empirical correlations for viscosity of polyacrylamide solutions with the effects of concentration, molecular weight and degree of hydrolysis of polymer . *Journal of Applied Sciences, 14*, 1000-1007.

Hayahara, T., & Takao, S. (1968). Relationship between polymer concentration and molecular weight in the viscosity behavior of concentrated solutions. *Kolloid-Zeitschrift und Zeitschrift für Polymere, 225*(2), 106-111.

Henaut, I., Pasquier, D., Rovinetti, S., & Espagne, B. (2015). HP-HT drilling mud based on environmently-friendly fluorinated chemicals. *Oil & Gas Science and Technology – Rev. IFP Energies nouvelles, 70*(6), 917-930.

Hood, M. A., Mari, M., & Muñoz-Espí, R. (2014). Synthetic strategies in the preparation of polymer/inorganic hybrid nanoparticles. *Materials, 7*, 4057-4087.

Hourdet, D., Gadgil, J., Podhajecka, K., Badiger, M., Brulet, A., & Wadgaonkar, P. (2005). Thermoreversible behavior of associating polymer solutions: thermothinning versus thermothickening. *Macromolecules, 38*, 8512-8521.

Huaiping, Z., Xu, K., Ai, H., Chen, D., Xv, L., & Chen, M. (2008). Synthesis, characterization and solution properties of hydrophobically modified polyelectrolyte poly(AA-co-TMSPMA). *Journal of Solution Chemistry, 37*, 1137-1148.

Huh, Z., Haruna, M., Gao, H., Nourafkan, E., & Wen, D. (2017). Rheological properties of partially hydrolyzed polyacrylamide seeded by nanoparticles. *Industrial and Engineering Chemistry Research, 56*, 3456−3463.

Huifen, X., Ye, J., Kong , F., & Wu, J. (2004). Effect of elastic behavior of HPAM Solutions on displacement efficiency under mixed wettability conditions. *SPE Annual Technical Conference and Exhibition.* Texas: Society of Petroleum Engineers.

Idahosa, P. E. G., Oluyemi, G. F., Oyeneyin, M. B. & Prabhu, R. (2016). Rate-Dependent Polymer Adsorption in Porous Media. *Journal of Petroleum Science and Engineerin*g. *143*, 65-71

Ihara, T., Nishioka, T., Kamitani, H., & Kitsuki, T. (2004). Solution properties of novel polysaccharide derivative. *Chemical Letters, 33*, 1094-1095.

Jang, H. Y., Zhang, K., Chon, B. H., & Choi, H. J. (2015). Enhanced oil recovery performance and viscosity characteristics of polysaccharide xanthan gum solution. *Journal of Industrial and Engineering Chemistry, 21*, 741-745.

Jincheng, M., Tan, H., Yang, B., Zhang, W., Yang, X., Zhang, Y., & Zhang, H. (2018). Novel hydrophobic associating polymer with good salt tolerance. *Polymers, 10*(8), 1-19.

Jordan, J. H., & Gibb, B. C. (2015). Molecular containers assembled through the hydrophobic effect. *Chemical Society Reviews, 44*(2), 547-585 .

Kajjumba, G. W., Emik, S., Ongen, A., Ozkan, H. K., & Aydin, S. (2018). Modelling of Adsorption Kinetic Processes - Errors, Theory and Application, Advanced Sorption Process Applications, Serpil Edebali, IntechOpen, DOI: 10.5772/intechopen.80495

Kamal, M. S., Sultan, A. S., Al-Mubaiyedh, U. A., & Hussein, I. A. (2015). Review on polymer flooding: Rheology, adsorption, stability, and field applications of various polymer systems. *Polymer Reviews*, 1-40.

Kang, K. W., Hwang, C. W., & Hwang, T. S. (2015). Synthesis and properties of sodium vinylbenzene sulfonate-grafted poly(vinylidene fluoride) cation exchange membranes for membrane capacitive deionization process. *Macromolecular Research, 23*(12), 1126–1133.

Kang, P. S., Lim, J. S., & Huh, C. (2016). Screening criteria and considerations of offshore enhanced oil recovery. *Energies, 9*(44), 1-18.

Kastner, U., Hoffmann, H., Donges, R., & Ehrler, R. (1996). Interactions between modified hydroxyethyl cellulose (HEC) and surfactants. *Colloids and Surfaces A: Physicochemical and Engineering Aspects, 112*, 209-225.

Katzbauer, B. (1998). Properties and applications of xanthan gum. *Polymer Degradation and Stability, 59*(1-3), 81-84.

Kawakami, K., Ihara, T., Nishioka, T., Kitsuki, T., & Suzuki, Y. (2006). Salt tolerance of an aqueous solution of a novel amphiphilic polysaccharide derivative. *Langmuir, 22*, 3337-3343.

Khromiak, U., Levytskyi, V., Stepova, K., & Tarnawsky, A. (2018). Synthesis and properties of adhesive polymer-methylmethacrylate materials. *International Journal of Polymer Science, 2018*, 1-9.

Kjoniksen, A. L., Beheshti, N., Kotlar, H. K., Zhu, K. Z., & Nystrom, B. (2008). Modified polysaccharides for use in enhanced oil recovery. *European Polymer Journal, 44*, 959-967.

Kornberger, M., Gumpenberger, T., Deckers, M., Zechner, M., & Clemens, T. (2013). Polymer Solution injection-near wellbore dynamics and displacement efficiency: Pilot test results, matzen field, austria. *EAGE Annual Conference & Exhibition incorporating SPE Europec.* London: Society of Petroleum Engineers.

Kundakci, S., Karadağ, E., & Üzüm , O. B. (2011). Investigation of swelling/sorption characteristics of highly swollen AAm/AMPS hydrogels and semi IPNs with PEG as biopotential sorbent . *Journal of Encapsulation and Adsorption Sciences, 1*, 7-22.

Lacey, M., Hollis, C., Oostrom, M., & Shokri, N. (2017). Effects of pore and grain size on water and polymer flooding in micromodels. *Energy and Fuels, 31*, 9026−9034.

Lai, N., Dong, W., Ye, Z., Dong, J., Qin, X., Chen, W., & Chen, K. (2013). A water soluble acrylamide hydrophobically associating polymer: Synthesis, characterization and properties as EOR chemical. *Journal of Applied Polymer Science, 129*(4), 1888-1896.

Lai, N., Dong, W., Ye, Z., Dong, J., Qin, X., Chen, W., & Chen, K. (2013). A water-soluble acrylamide hydrophobically associating polymer: Synthesis, characterization, and properties as EOR chemical. *Journal of Applied Polymer Science, 129*, 1888-1896.

Lee, R. S., Wang, S. W., Li, Y. C., & Fang, J. Y. (2015). Synthesis and characterization of thermo-responsive and photo-cleavable block copolymers as nanocarriers. *RSC Advances, 5*, 497-512.

Levitt, D. B., & Pope, G. A. (2008). Selection and screening of polymers for enhanced oil recovery. *SPE/DOE Improved Oil Recovery Symposium* (pp. 1-18). Oklahoma: Society of Petroleum Engineers.

Li, K., Jing, X., He, S., & Wei, B. (2016). Static adsorption and retention of viscoelastic surfactant in porous media: EOR implication. *Energy and Fuels, 30*, 9089–9096.

Li, Q., Pu, W., Wei, B., Jin, F., & Li, K. (2016). Static adsorption and dynamic retention of an anti-salinity polymer in low permeability sandstone core. *Journal of Applied Polymer Science, 134*(8), 44487-44494.

Li, X., Shu, Z., Luo, P., & Ye, Z. (2018). Associating polymer networks based on cyclodextrin inclusion compounds for heavy oil recovery. *Journal of Chemistry, 2018*, 1-9.

Li, X., Xu, Z., Yin, H., Feng, Y., & Quan, H. (2017). Comparative studies on enhanced oil recovery: Thermoviscosifying polymer versus polyacrylamide. *Energy and Fuels, 31*, 2479−2487.

Liao, G. Z., Wang, Q., Wang, H. Z., Liu, W. D., & Wang, Z. (2017). Chemical flooding development status and prospect. *Acta Petrolei Sinica, 38*(2), 196-207.

Li-Bin, D., Dong-Qing, Z., Shou-Ping, L., & Yun-Xiang, Z. (2010). Effects of ethylene oxide spacer length on solution properties of water-soluble fluorocarbon-containing hydrophobically associating poly (Acrylic Acid-co-Rf-PEG Macromonomer). *Chinese Journal of Chemistry, 21*(6), 698-705.

Liu, B., Sun, X. S., Wang, K., Xu, H., Liu, Q., Liu, X., & Song, S. (2007). Flooded by high concentration polymer doubled oil recovery of common polymer on field test with 20% closed to the result of lab testing in Daqing. *International Oil Conference and Exhibition.* Mexico City: Society of Petroleum Engineers.

Liu, X. J., Jiang, W. C., Gou, S. H., Ye, Z. B., & Xie, X. D. (2012). Synthesis and evaluation of water soluble acrylamide binary sulfonates copolymer on MMT crystalline interspace and EOR. *Journal of Polymer Science, 125*(2), 1252-1260.

Liu, X., Jiang, W., Gou, S., Ye, Z., Feng, M., Lai, N., & Liang, L. (2013). Synthesis and evaluation of novel water soluble copolymers based on acrylamide and modular beta-cyclodextrin. *Carbohydrate Polymers, 96*(1), 47-56.

Lohne, A., Nodland, O., Stavland, A., & Hiorth, A. (2017). A model for non-Newtonian flow in porous media at different flow regimes. *Computational Geosciences, 21*, 1289-1312.

Lu, H., Huang, Z., & Feng, Y. (2010). Solution association characterization of hydrophobically associating polyacrylamide obtained from produced fluids. *Journal of Macromolecular Science, Part A: Pure and Applied Chemistry, 47*, 423-428.

Mahmoud, M., Elkatatny, S., & Abdelgawad, K. Z. (2017). Using high- and low-salinity seawater injection to maintain the oil reservoir pressure without damage. *Journal of Petroleum Exploration and Production Technology, 7*, 589–596.

Maia, A. M., Costa, M., Borsali, R., & Garcia, R. B. (2005). Rheological behavior and scattering studies of acrylamide based copolymer solutions. *Macromolecular Symposia, 229*(1), 217-227.

Mei, Y., Bai, Y., & Wang, L. (2016). Effect of pH on binding of pyrene to hydrophobic fractions of dissolved organic matter (DOM) isolated from lake water. *Acta Geotechnica, 35*(3), 288–293 .

Meiqin, L., Chunling, Z., Hua, Z., Mingyuan, L., Hongbo, F., & Jixiang, G. (2008). Influence of polymers on the stability of gudao crude oil emulsions. *Petroleum Science, 5*, 159-162.

Meyers, J. J., Pitts, M. J., & Wyatt , K. (1992). Alkaline-Surfactant-Polymer flood of the West Kiehl, Minnelusa Unit. *SPE/DOE Enhanced Oil Recovery Symposium.* Oklahoma: Society of Petroleum Engineers.

Mogollon, J. L., & Lokhandwala, T. (2013). Rejuvenating viscous oil reservoirs by polymer injection: Lessons learned in the field. *SPE Enhanced Oil Recovery Conference.* Kuala Lumpur: Society of Petroleum Engineers.

Mori, H., Kudo, E., Saito, Y., Onuma, A., & Morishima, M. (2010). RAFT polymerization of vinyl sulfonate esters for the controlled synthesis of poly(lithium vinyl sulfonate) and sulfonated block copolymers. *Macromolecules, 43*(17), 7021–7032.

Mori, H., Saito, Y., Takahashi, E., Nakabayashi, K., Onuma, A., & Morishima, M. (2012). Controlled synthesis of sulfonated block copolymers having thermoresponsive property by RAFT polymerization of vinyl sulfonate esters. *Polymer, 53*(18), 3861-3877.

Nee, S. L., Khalil , M., Jan, B. M., & Ali, B. S. (2016). Novel lightweight biopolymer drilling fluid for underbalanced drilling. *Offshore Technology Conference Asia.* Kuala Lumpur: Offshore Technology Conference.

Nesrinne, S., & Djamel, A. (2017). Synthesis, characterization and rheological behavior of pH sensitive poly(acrylamide-co-acrylic acid) hydrogels. *Arabian Journl of Chemistry, 10*(4), 539-547.

Niskanen, J., & Tenhu, H. (2017). How to manipulate the upper critical solution temperature (UCST)? *Polymer Chemistry, 8*, 220-232.

Oh, S. Y., Kim, H. J., & Bae, Y. C. (2013). Molecular thermodynamic analysis for phase transitions of linear and cross-linked poly(N-isopropylacrylamide) in water/2-propanol mixtures. *Polymer, 54*, 6776-6784.

Oruwori, A. E., & Ikiensikimama , S. S. (2010). Determination of water salinities in hydrocarbon bearing reservoirs of some Niger Delta fields - Nigeria. *Nigeria Annual International Conference and Exhibition* (pp. 1-10). Calabar: Society of Petroleum Engineers.

Page, M., Lecourtier, J., Noik, C., & Foissy, A. (1993). Adsorption of polyacrylamides and polysaccharides on siliceous materials and kaolinite: Influence of temperature. *Journal of Colloid and Interface Science, 161*(2), 450-454.

Palaniraj, A., & Jayaraman, V. (2011). Production, recovery and applications of xanthan gum by xanthomonas campestris. *Journal of Food Engineering, 106*, 1-12.

Pancharoen, M. (2009). *Physical properties of associative polymer solutions.* Stanford University, Department of Energy Resources Engineering. Stanford: Stanford University.

Pancharoen, M., Thiele, M. R., & Kovscek, A. R. (2010). Inaccessible pore volume of associative polymer floods. *SPE Improved Oil Recovery Symposium.* Oklahoma: Society of Petroleum Engineers.

Pandey, S., Redden, R. A., Hendricks, A. E., Flectcher, K. A., & Palmer, C. P. (2003). Characterization of the solvation environment provided by dilute aqueous solutions of novel siloxane polysoaps using the fluorescence probe pyrene. *Journal Coolid Interface Science, 262*(2), 579-587.

Panthi, K., Mohanty, K., & Sharma, H. (2013). ASP flood of a viscous oil in a carbonate rock. *SPE Annual Technical Conference and Exhibition.* New Orleans: Society of Petroleum Engineers.

Patokina, O. Y. (2015). Polymer flooding by hydrophobically associating polyacrylamide (technology of preparation. the study of the process stability and degradation). *SPE Russian Petroleum TechnologyConference.* Moscow, Russia.

Pavlov, G. M., Dommes, O. A., Gosteva, A. A., Okatova, O. V., Gavrilova, I. I., & Panarin, E. F. (2018). Sizes of macromolecules of copolymers of N-Methyl-N-vinylacetamide and N-Methyl-N-vinylamine hydrochloride with low charge linear density. *Polymer Science, Series A, 60*(2), 172–178.

Pei, Y., Zhao, L., Du, G., Li, N., Xu, K., & Yang, H. (2016). Investigation of the degradation and stability of acrylamide-based polymers in acid solution: Functional monomer modified polyacrylamide. *Petroleum, 2*(4), 399-407.

Pitts, M. J., Wyatt, K., & Surkalo, H. (2004). Alkaline-polymer flooding of the David pool, Lloydminster Alberta. *SPE/DOE Symposium on Improved Oil Recovery.* Oklahoma: Society of Petroleum Engineers.

Pitts, M., Dowling, P., Wyatt, K., Surkalo, H., & Adams , K. C. (2006). Alkaline-Surfactant-Polymer flood of the Tanner Field. *SPE/DOE Symposium on Improved Oil Recovery.* Oklahoma: Society of Petroleum Engineers.

Pratap, M., & Gauma, M. S. (2004). Field implementation of Alkaline-Surfactant-Polymer (ASP) flooding : A maiden effort in India. *SPE Asia Pacific Oil and Gas Conference and Exhibition.* Perth: Society of Petroleum Engineers.

Prazeres, T. J., Beingessner, R., & Duhamel, J. (2001). Characterization of the association level of pyrene-labeled HASEs by fluorescence. *Macromolecules, 34*(22), 7876–7884.

Principi, T., Ester-Goh, C. C., Liu, R. C., & Winnik, F. M. (2000). Solution properties of hydrophobically modified copolymers of N-Isopropylacrylamide and N-Glycine acrylamide: A study by microcalorimetry and fluorescence spectroscopy. *Macromolecules, 33*(8), 2958–2966.

Pu, H., & Xu, Q. (2009). An update and perspective on field-scale chemical floods in Daqing oilfield. *SPE Middle East Oil and Gas Show and Conference.* Manama: Society of Petroleum Engineers.

Qavi, S., Pourmahdian, S., & Eslami, H. (2014). Acrylamide hydrogels preparation via free radical crosslinking copolymerization: Kinetic study and morphological investigation. *Journal of Macromolecular Science, Part A: Pure and Applied Chemistry, 51*(10), 842–848.

Quan, H., Li, Z., & Huang, Z. (2016). Self-assembly properties of a temperature and salt tolerant amphoteric hydrophobically associating polyacrylamide. *RSC Advances, 6*, 49281-49288.

Quan, H., Lu, Q., Chen, Z., Huang, Z., & Jiang, Q. (2019). Adsorption-desorption behavior of the hydrophobically associating copolymer AM/APEG/C-18/SSS. *RSC Advances, 9*, 12300-12309.

Rabiee, A., Zeynali, M. E., & Baharvand, H. (2005). Synthesis of high molecular weight partially hydrolyzed polyacrylamide and investigation on its properties. *Iranian Polymer Journal, 14*(7), 603-608.

Raffa, P., Broekhuis, A. A., & Picchioni, F. (2016). Polymeric surfactants for enhanced oil recovery: A review. *Journal of Petroleum Science and Engineering, 145*, 723–733.

Rashidi, M., Blokhus, A. M., & Skauge, A. (2010). Viscosity study of salt tolerant polymers. *Journal of Applied Polymer Science, 117*, 1551–1557 .

Rashidi, M., Sandvik, S., Blokhus, A., & Skauge, A. (2009). Static and dynamic adsorption of salt tolerant polymers. *15th European Symposium on Improved Oil Recovery.* Paris: Society of Petroleum Engineers.

Reichenbach-Klinke, R., Stavland, A., Strand, D., Langlotz, B., & Brodt, G. (2016). Can associative polymers reduce the residual oil saturation. *SPE EOR Conference at Oil and Gas West Asia.* Muscat: Society of Petroleum Engineers.

Riahinezhad, M., Romero-Zerón, L., McManus, N., & Penlidis, A. (2017). Design of tailor-made water-soluble copolymers for enhanced oil recovery polymer flooding applications. *Macromolecular Reaction Engineering, 11*, 1-9.

Rintoul, I. (2017). Kinetic control of aqueous polymerization using radicals generated in different spin states. *Processes, 5*(2), 1-12.

Rottava, I., Batesini, G., Silva, M. F., Lerin, L., Oliveira, D., Padilha, F. F., & Treichel, H. (2009). Xanthan gum production and rheological behavior using different strains of Xanthomonas sp. *Carbohydrate Polymers, 77*, 65-71.

Sabhapondit, A., Borthakur, A., & Haque, I. (2003). Characterization of acrylamide polymers for enhanced oil recovery. *Journal of Applied Polymer Science, 87*, 1869–1878.

Sabhapondit, A., Borthakur, A., & Haque, I. (2003). Water soluble acrylamidomethyl propane sulfonate (AMPS) Copolymer as an Enhanced Oil Recovery Chemical . *Energy and Fuels, 17*(3), 683-688.

Saeed, A., Mahmood, S. M., Tan, I. M., Ghaedi, H., & Ling, O. L. (2017). Assessment of polyacrylamide based co-polymers enhanced by functional group modifications with regards to salinity and hardness. *Polymers, 9*, 1-16.

Santis, S. D., Mesa, C., & Masci, G. (2017). On the upper critical solution temperature of pnipaam in an ionic liquid: effect of molecular weight, tacticity and water. *Polymer, 120*, 52-58.

Sarsenbekuly, B., Kang, W., Fan, H., Yang, H., Dai, C., Zhao, B., & Aidarova, S. B. (2017). Study of salt tolerance and temperature resistance of a hydrophobically modified polyacrylamide based novel functional polymer for EOR. *Colloids and Surfaces A: Physicochemical and Engineering Aspects, 514*, 91-97.

Seright, R. S., Fan, T., Wavrik, K., Wan, H., Galliard, N., & Favero, C. (2011). Rheology of a new sulfonic associative polymer in porous media. *SPE Reservior Evaluation and Evaluation, 14*(6), 726-734.

Sharafi, M. S., Jamialahmadi, M., & Hoseinpour, S.-A. (2018). Modeling of viscoelastic polymer flooding in core-scale for prediction of oil recovery using numerical approach. *Journal of Molecular Liquids, 250*, 295-306.

Shatat, R. S., & Niazi, S. K. (2018). Using free radical polymerization and mannich reaction, synthesis and characterization of cationic polyacrylamides having similar molecular weight but different charge densities. *European Journal of Chemistry, 9*(2), 79-83.

Shemper, B. S., Acar, A. E., & Mathias, L. J. (2002). Synthesis of linear and starlike polymers from poly(propylene glycol) methacrylate using controlled radical polymerization. *Journal of Polymer Science Part A: Polymer Chemistry, 40*(3), 334-343.

Silva, I. P., Aguiar, A. A., Rezende, V. P., Monsores, A. L., & Lucas, E. F. (2018). A polymer flooding mechanism for mature oil fields: Laboratory measurements and field results interpretation. *Journal of Petroleum Science and Engineering, 161*, 468-475.

Siu, H., & Duhamel, J. (2008). Molar absorption coefficient of pyrene aggregates in water. *Journal of Physical Chemistry B, 112*(48), 15301–15312.

Skauge, A., Zamani, N., Jacobsen, J. G., Shiran, B. S., Al-Shakry, B., & Skauge, T. (2018). Polymer flow in porous media: Relevance to enhanced oil recovery. *Cooloids and Interfaces, 2*(3), 1-27.

Smith, G. L., & McCormick, C. L. (2001). Water soluble polymers. 80. Rheological and photophysical studies of pH responsive terpolymers containing hydrophobic twin-tailed acrylamide monomers. *Macromolecules, 34*, 5579-5586.

Sochi, T. (2010). Non-newtonian flow in porous media. *Polymer, 51*, 5007-5023.

Sun, J., Du, W., Pu, X., Zou, Z. Z., & Zhu, B. B. (2015). Synthesis and evaluation of a novel hydrophobically associating polymer based on acrylamide for enhanced oil recovery. *Chemical Papers, 69*(12), 1598-1607.

Sveistrup, M., Mastrigt, F. v., Norrman, J., Picchioni, F., & Paso, K. (2016). Viability of biopolymers for enhanced oil recovery. *Journal of Dispersion Science and Technology, 37*, 1160–1169.

Szymański, J. K., Abul-Haija, Y. M., & Cronin, L. (2018). Exploring strategies to bias sequence in natural and synthetic oligomers and polymers. *Accounts of Chemical Research, 51*, 649-658.

Taghizadeh, M. T., & Foroutan, M. (2004). Water-soluble copolymers of N-vinylpyrrolidone and vinyl acetate: Synthesis, characterization, and monomer reactivity at high conversions. *Journal of Polymer Research, 11*(3), 203–209.

Taheri-Shakib, J., Rajabi-Kochi, M., Kazemzadeh, E., Naderi, H., Salimidelshad, Y., & Esfahani, M. (2018). A comprehensive study of asphaltene fractionation based on adsorption onto calcite, dolomite and sandstone. *Journal of Petroleum Science and Engineering, 171*, 863-878.

Tam, K. C., Jenkins, R. D., Winnick, M. A., & Bassett, D. R. (1998). A structural model of hydrophobically modified urethane-ethoxylate (HEUR) associative polymers in shear flows. *Macromolecules, 31*, 4149-4159.

Tang, Y., Liu, S. Y., Armes, S. P., & Billingham, N. C. (2003). Solubilization and controlled release of a hydrophobic drug using novel micelle-forming ABC triblock copolymers. *Biomacromolecules, 4*, 1636-1645.

Taylor, K. C., & Nasr El-Din, H. A. (1998). Water soluble hydrophobically associating polymers for improved oil recovery: A literature review. *Journal of Petroleum Science and Engineering, 19*, 265-280.

Tiwari, D., Marathe, R., Patel, N., Ramachandran, K., Maurya, C., & Tewari, P. (2008). Performance of polymer flood in Sanand Field, India - A case study. *SPE Asia Pacific Oil and Gas Conference and Exhibition.* Perth: Society of Petroleum Engineers.

Torrealba, V. A., & Hoteit, H. (2019). Improved polymer flooding injectivity and displacement by considering compositionally-tuned slugs. *Journal of Petroleum Science and Engineering, 178*, 14-26.

Tovar, F., Barrufet, M., & Schechter, D. (2014). Long term stability of acrylamide based polymers during chemically assisted CO2 WAG EOR. *SPE Improved Oil Recovery Symposium* (pp. 1-9). Oklahoma: Society of Petroleum Engineers.

Uranta, K., Gomari, S. R., Russell, P., & Hamad, F. (2018). Determining safe maximum temperature point (SMTP) for polyacrylamide polymer (PAM) in saline solutions. *Journal of Oil, Gas and Petrochemical Sciences, 1*(1), 1-8.

Vargo, J., Turner, J., Bob, V., Pitts, M., Wyatt, K., Surkalo , H., & Patterson , D. (2000). Alkaline-Surfactant-Polymer flooding of the Cambridge Minnelusa Field. *SPE Reservoir Evaluation & Engineering, 3*(6), 1-7.

Victor, R., Woisel, P., & Hoogenboom, R. (2016). Supramolecular control over thermoresponsive polymers. *Materials Today, 19*(1), 44-55.

Volpert., E., Selb, J., & Candau, F. (1998). Adsorption of hydrophobically associating polyacrylamides on clay. *Langmuir, 14*(7), 1870–1879.

Wan, W., Pickett, P. D., Savin, D. A., & McCormick, C. L. (2014). Structurally controlled "polysoaps" via RAFT copolymerization of AMPS and n-dodecylacrylamide for environmental remediation. *Polymer Chemistry, 5*, 819-827.

Wang, F., Peng, J., Dong, R., Chang, X., Ren, B., & Tong, Z. (2016). Highly efficient hydrophobically modified ethoxylated urethanes(HEURs) end-functionalized by two-tail dendritic hydrophobes: Synthesis, solution rheological behavior and thickening in latex. *Colloids and Surfaces A: Physicochemical and Engineering Aspects, 502*, 114-120.

Wassmuth, F., Green, K., & Bai, J. (2012). Associative polymers outperform regular polymers displacing heavy oil in heterogenous systems. *SPE Heavy Oil Conference* . Alberta, Canada.

Wei, Z., Jian, Z., Ming, H., Wentao, X., Guozhi, F., Wei, J., & Shouwei, Z. (2007). Application of hydrophobically associating water soluble polymer for polymer flooding in China offshore heavy oilfield. *International Petroleum Technology Conference* (pp. 1-5). Dubai: Society of Petroleum Engineers.

Wever, D. A., Picchioni, F., & Broekhuis, A. A. (2011). Polymers for enhanced oil recovery: A paradigm for structure-property relationship in aqueous solution. *Progress in Polymer Science, 36*, 1558-1628.

Wever, D. A., Picchioni, F., & Broekhuis, A. A. (2013). Comblike polyacrylamides as flooding agent in enhanced oil recovery. *Industrial and Engineering Chemistry Research, 52*, 16352-16363.

Willersinn, J., & Schmidt, B. V. (2017). Self-assembly of double hydrophilic poly(2-ethyl-2-oxazoline)-b-poly(N-vinylpyrrolidone) block copolymers in aqueous solution. *Polymers, 9*(7), 1-15.

Wyatt, N. B., Gunther, C. M., & Liberatore, M. W. (2011). Increasing viscosity in entangled polyelectrolyte solutions by the addition of salt. *Polymer, 52*(11), 2437-2444.

Xie, K., Lu, X., Li, Q., Jiang, W., & Yu, Q. (2016). Analysis of reservoir applicability of hydrophobically associating polymer. *SPE Journal, 21*(1), 1-9.

Xiong, B., Loss, R. D., Sheilds, D., Pawlik, T., Hochreiter, R., Zydney, A. L., & Kumar, M. (2018). Polyacrylamide degradation and its implications in environmental systems. *npj Clean Water, 1*(17), 1-9.

Xu, B., Yekta, A., Li, L., Masoumi, Z., & Winnik, M. A. (1996). The functionality of associative polymer network: the association behavior of hydrophobically modified urethane-ethoxylate (HEUR) associative polymers in aqueous solution. *Colloids and Surfaces A: Physicochemical and Engineering Aspects, 112*, 239-250.

Xu, L., Xu, G., Liu, T., Chen, Y., & Gong, H. (2013). The comparison of rheological properties of aqueous welan gum and xanthan gum solutions. *Carbohydrate Polymers, 92*, 516-522.

Xu, X., Saeedi, A., & Liu, K. (2016). Laboratory studies on CO2 foam flooding enhanced by a novel amphiphilic ter-polymer. *Journal of Petroleum Science and Engineering, 138*, 153-159.

Yabin, N., Jian, O., Zhuoyan, Z., Guijiang, W., Guanghua, S., & Lijun, S. (2001). Research on hydrophobically associating water-soluble polymer used for EOR. *SPE International Symposium on Oilfield Chemistry* (pp. 1-4). Houston: Society of Petroleum Engineers.

Yamamoto, S., Miyashita, T., & Mitsuishi, M. (2017). Amphiphilic acrylamide block copolymer: RAFT block copolymerization and monolayer behaviour. *RSC Advances, 7*, 44954–44960.

Yan, H., & Row, K. H. (2006). Characteristic and synthetic approach of molecularly imprinted polymer. *International Journal of Molecular Sciences, 7*, 155-178.

Yang, F., Wang, D., Wang, G., Sui, X., Liu, W., & Kan, C. (2006). Study on high concentration polymer flooding to further enhance oil recovery. *SPE Annual Technical Conference and Exhibition.* Texas: Society of Petroleum Engineers.

Yang, X., Liu, J., Li, P., & Liu, C. (2015). Self-assembly properties of hydrophobically associating perfluorinated polyacrylamide in dilute and semi-dilute solutions. *Journal of Polymer Research, 22*(103), 1-7.

Ye, Z., Feng, M., Gou, S., Liu, M., Huang, Z., & Liu, T. (2013). Hydrophobically associating acrylamide-based copolymer for chemically enhanced oil recovery. *Journal of Applied Polymer Science, 130*(4), 2901-2911.

Ye, Z., Gou, G., Gou, S., Jiang, W., & Lui, T. (2013). Synthesis and characterization of a water soluble sufonates copolymer of acrylamide and N-allybenzamide as enhanced oil recovery chemical. *Journal of Applied Polymer Science, 128*(3), 2003-2011.

Yin, H., Wang, D., & Zhong, H. (2006). Study on flow behavior of viscoelastic polymer solution in micropore with dead end. *SPE Annual Technical Conference and Exhibition* (pp. 1-10). Texas: Society of Petroleum Engineers.

Yun, W. (2014). *Micro visual investigation of polymer retention in a micromodel.* Thesis, Stanford: Stanford University.

Zamani, N., Bondino, I., Kaufmann, R., & Skauge, A. (2015). Effect of porous media properties on the onset of polymer extensional viscosity. *Journal of Petroleum Science and Engineering, 133*, 483-495.

Zeng, F., Yang, M., Zhang, J., & Varshney, S. K. (2002). Synthesis and characterization of block copolymers from 2-vinylnaphthalene by anionic polymerization. *Journal of Polymer Science Part A: Polymer Chemistry, 40*(24), 4387-4397.

Zeynali, M. E., & Rabbii, A. (2002). Alkaline hydrolysis of polyacrylamide and study on poly(acrylamide-co-sodium acrylate) properties. *Iranian Polymer Journal, 11*(4), 269-275.

Zeynali, M. E., Rabii, A., & Baharvand, H. (2004). Synthesis of partially hydrolyzed polyacrylamide and investigation of solution properties (viscosity behaviour). *Iranian Polymer Journal, 13*(6), 479-484.

Zhang, J., Wang, K., He, F., & Zhang, F. (1999). Ultimate evaluation of the alkali/polymer combination flooding pilot test in XingLongTai oil field. *SPE Asia Pacific Improved Oil Recovery Conference.* Kuala Lumpur: Society of Petroleum Engineers.

Zhang, L. J., Yue, X. A., & Guo, F. (2008). Micro-mechanisms of residual oil mobilization by viscoelastic fluids. *Petroleum Science, 5*, 56-61.

Zhang, Q., & Hoogenboom, R. (2015). Polymers with upper critical solution temperature behavior in alcohol/water solvent mixtures. *Progress in Polymer Science, 48*, 122-142.

Zhang, X., Jiang, G., Xuan, Y., Wang, L., & Huang, X. (2017). Associating copolymer acrylamide/diallyldimethylammonium chloride/butyl acrylate/2-acrylamido-2-methylpropanesulfonic acid as a tackifier in clay-free and water-based drilling fluids. *Energy and Fuels, 31*, 4655−4662.

Zhang, Y., Wang, Y., Xue, F., Wang, Y., Ren, B., Zhang, L., & Ren, S. (2015). CO2 foam flooding for improved oil recovery: reservior simulation models and influencing factors. *Journal of Petroleum Science and Engineering, 133*, 838-850.

Zhao, G. Q., & Chen, S. B. (2007). Nonlinear rheology of aqueous solutions of hydrophobically modified hydroxyethyl cellulose with nonionic surfactant. *Journal of Colloid Interface Science, 316*, 858-866.

Zhao, J., Fan, H., You, Q., & Jia, Y. (2017). Distribution and presence of polymers in porous media. *Energies, 10*, 2118-2131.

Zhijian, Q., Yigen, Z., Zhang , X., & Jialin, D. (1998). A successful ASP flooding Pilot in Gudong oil field. *SPE/DOE Improved Oil Recovery Symposium.* Oklahoma: Society of Petroleum Engineers.

Zhong, C., Zhang, H., & Feng, L. (2014). Solution behavior and associating structures of a salt-tolerant tetra-polymer containing an allyl-capped macromonomer. *Journal of Polymer Research, 21*, 1-9.

Zhong, H., Zhang, W., Yin, H., & Liu, H. (2017). Study on the mechansim of viscoelastic polymer transient flow in porous media. *Geofluids, 2017*, 1-8.

Zhou, H., Song, G.-Q., Zhang, Y.-X., Chen, J., Jiang, M., Hogen-Esch, T. E., & Haeussling, L. (2001). Hydrophobically modified polyelectrolytes, 4, Synthesis and solution properties of fluorocarbon containing poly(acrylic acid). *Macromolecular Chemistry and Physics, 202*, 3057-3064.

Zhou, S. N., & Lai, E. P. (2004). N-phenylacrylamide functional polymer with high affinity for Ochratoxin A. *Reactive and Functional Polymers, 58*(1), 35-42.

Zhou, W., Zhang, J., Feng, G., Jiang, W., Sun, F., Zhou, S., & Liu, Y. (2008). Key technologies of polymer flooding in offshore oilfield of Bohai Bay. *SPE Asia Pacific Oil and Gas Conference and Exhibition* (pp. 1-5). Perth: Society of Petroleum Engineers.

Zhu, D., Han, Y., Zhang, J., Li, X., & Feng, Y. (2014). Enhancing rheological properties of hydrophobically associative polyacrylamide aqueous solutions by hybriding with silica nanoparticles. *Journal of Applied Polymer Science, 131*(19), 1-8.

Zhu, J., Xiao, W. F., Dong, L. T., & Teng, F. (2012). Research on the influence of stiffness of copolymer(N-Tert-octylacrylamide/Acrylic acid/methyl methacrylate/butylaminoethyl methacrylate/Hydroxypropyl methacrylate) by methyl methacrylate and N-tert-octylacrylamide. *Advanced Materials Research, 557-559*, 968-972.

Zhuang, D. Q., Da, J. C., Zhang, Y., Dieing, R., Ma, L., & Haeussling, L. (2001). Hydrophobically modified polyelectrolytes II: Synthesis and characterization of poly(acrylic Acid-co-Alkyl Acrylate). *Polymers for Advanced Technologies, 12*, 616-625.

Zou, C., Zhao, P., Hu, X., Yan, X., Zhang, Y., Wang, X., & Luo, P. (2013). Beta-cyclodextrin-functionalized hydrophobically associating acrylamide copolymer for enhanced oil recovery. *Energy and Fuels, 27*, 2827-2834.

APPENDIX A: Dataset for Size Distribution Analysis of Silica Sand

The dataset below were obtained during the sieve analysis of the 40/60 and P230 silica sands.

A.1. 40/60 Silica Sand

Table A.1*: Results obtained from the sieve analysis of the 40/60 silica sand using a mechanical shaker at room temperature (20 ℃).*

40/60 Silica Sand Sieve Analysis						
Sieve Size (μm)	**Initial Weight of Pan (g)**	**Final Weight of Pan (g)**	**Mass Retained (g)**	**Fractional Mass Retained**	**Percent Mass Retained (%)**	**Cumulative Retained (%)**
650	352.8	352.8	0.0	0	0	0
600	352.8	352.9	0.1	0.00012276	0.012275964	0.012275964
500	321.6	322.8	1.2	0.001473116	0.147311564	0.147311564
425	325.4	353.2	27.8	0.034127179	3.412717898	3.560029462
355	335.2	639.6	304.4	0.373680334	37.36803339	40.92806285
300	325.0	700.6	375.6	0.461085195	46.10851952	87.03658237
250	328.6	395.4	66.8	0.082003437	8.200343727	95.2369261
180	279.0	298.6	19.6	0.024060889	2.406088878	97.64301498
150	310.6	322.8	12.2	0.014976676	1.497667567	99.14068254
125	301.6	307.5	5.9	0.007242819	0.724281856	99.8649644
90	290.4	291.4	1.0	0.001227596	0.122759637	99.98772404
50	363.8	363.8	0.0	0	0	99.98772404

A.2. P230 Silica Sand

Table A.2: *Results obtained from the sieve analysis of the P230 silica sand using a mechanical shaker at room temperature (20 ℃).*

P230 Silica Sand Sieve Analysis						
Sieve Size (μm)	**Initial Weight of Pan (g)**	**Final Weight of Pan (g)**	**Mass Retained (g)**	**Fractional Mass Retained**	**Percent Mass Retained (%)**	**Cumulative Retained (%)**
600	352.8	355.2	2.4	0.002946231	0.294623128	0.294623128
500	321.6	326.4	4.8	0.005892463	0.589246256	0.589246256
425	325.4	340	14.6	0.017922907	1.792290695	2.086913823
355	335.2	382.2	47	0.057697029	5.769702922	7.856616744
300	325	417.8	92.8	0.113920943	11.39209428	19.24871102
250	328.6	461.4	132.8	0.163024797	16.30247974	35.55119077
180	279	520.8	241.8	0.296832801	29.68328014	65.23447091
150	310.6	350.6	40	0.049103855	4.910385465	70.14485637
125	301.6	306.6	5	0.006137982	0.613798183	70.75865455
90	290.4	290.4	0	0	0	70.75865455
50	363.8	364	0.2	0.000245519	0.024551927	70.78320648
50	363.8	363.8	0	0	0	70.78320648

APPENDIX B: Dataset for Molecular Weight Determination of Polymer Sample.

The molecular weight of the polymer samples D118 and C1205 were obtained using viscometry analysis.

B.1. D118 Associative Polymer

Table B.1*: Viscometry data (using a glass viscometer) for the determination of the molecular weight of associative polymer (D118) at room temperature (20 ℃)*

Polymer Concentration (C, g/dL)	Solution Time1 (s)	Solution Time2 (s)	Average Solution Time (s)	Solvent Time (s)	Specific Viscosity (ηsp)	Relative Viscosity (ηrel)	ηsp/C (dL/g)	In(ηrel)	In(ηrel)/C (dL/g)
0.005	39	41	40	33	0.212121212	1.212121212	42.42424242	0.192371893	38.47437853
0.010	43	41	42	33	0.272727273	1.272727273	27.27272727	0.241162057	24.11620568
0.015	46	46	46	33	0.393939394	1.393939394	26.26262626	0.332133835	22.14225567
0.020	46	46	46	33	0.393939394	1.393939394	19.6969697	0.332133835	16.60669175

B.2. C1205 Associative Polymer

Table B.2*: Viscometry data (using a glass viscometer) for the determination of the molecular weight of associative polymer (C1205) at room temperature (20 ℃)*

Polymer Concentration (C, g/dL)	Solution Time1 (s)	Solution Time2 (s)	Average Solution Time (s)	Solvent Time (s)	Specific Viscosity (ηsp)	Relative Viscosity (ηrel)	ηsp/C (dL/g)	In(ηrel)	In(ηrel)/C (dL/g)
0.005	39	37	38	33	0.151515152	1.151515152	30.3030303	0.141078598	28.21571965
0.010	42	42	42	33	0.272727273	1.272727273	27.27272727	0.241162057	24.11620568
0.015	47	47	47	33	0.424242424	1.424242424	28.28282828	0.35364004	23.57600268
0.020	51	51	51	33	0.545454545	1.545454545	27.27272727	0.435318071	21.76590356

APPENDIX C: Dataset for Bulk Polymer Rheology and Predictive Modelling

C.1. Polymer Bulk Viscosity

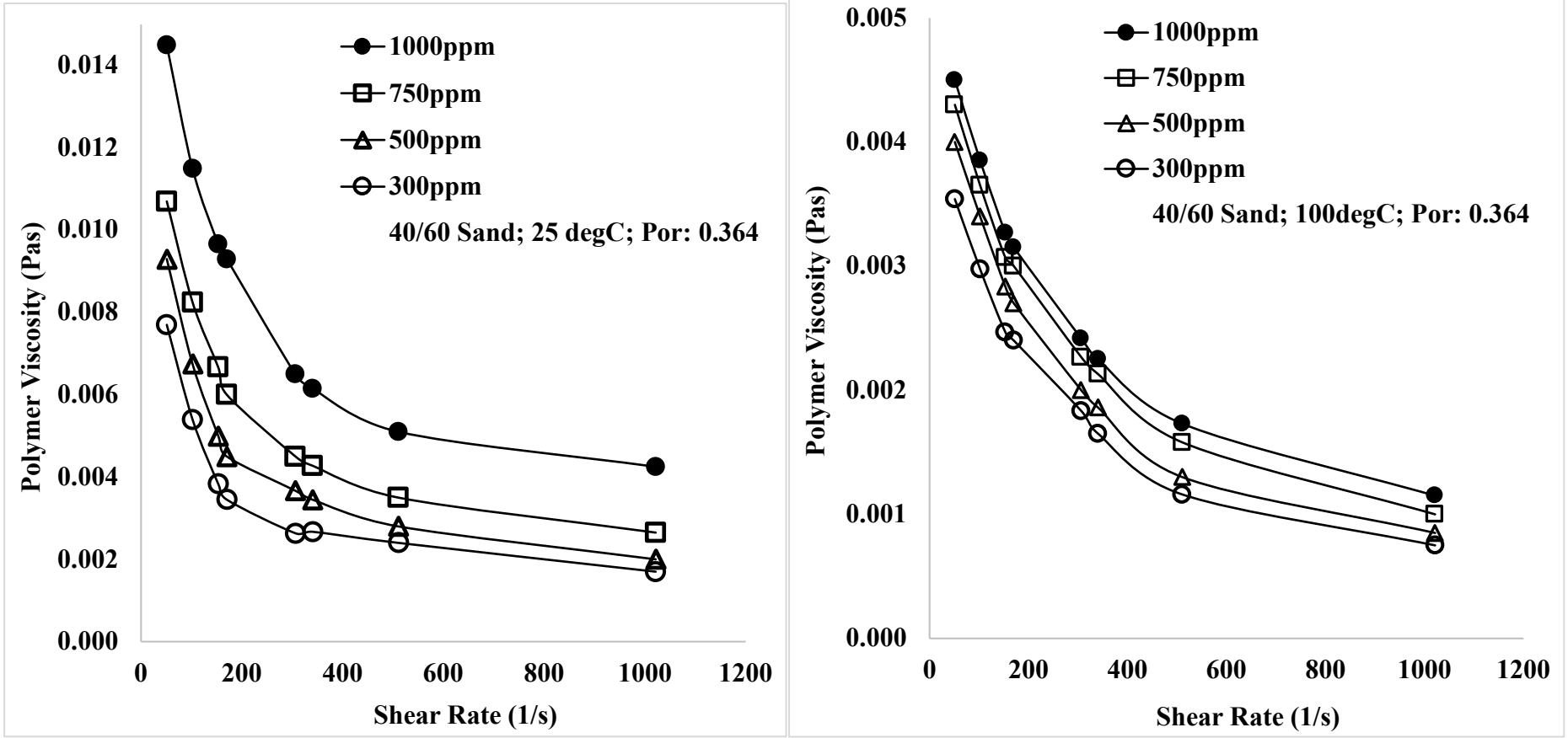

Figure C.1*: Dataset for the bulk rheological analysis of the polymer solution after contacting with 40/60 silica sand, 25 ℃ and 2.45 %TDS.*

C.2. Regresion Fitting of Developed Model for Hydrophobic Interactions

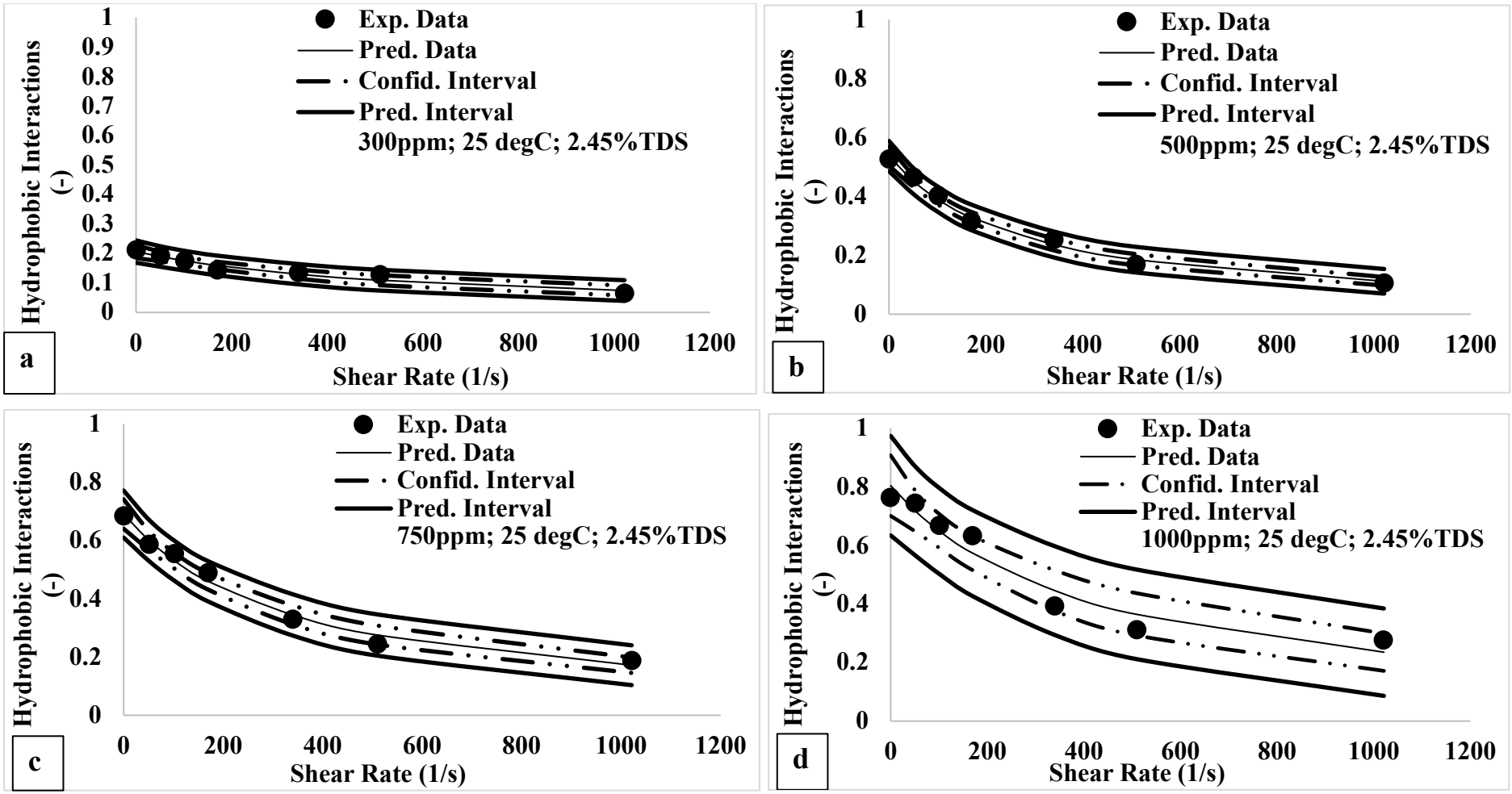

***Figure C.2**: Regression analysis of the developed model in (3.20) under shear thinning (a) 300 ppm (b) 500 ppm (c) 750 ppm (d) 1000 ppm*

APPENDIX D: Dataset for Static and Dynamic Retention

D.1. Static and Dynamic Retention

Table D.1*: Polymer retention values under static and dynamic conditions at different concentration, flowrate and temperature. The dynamic retention was carried out at 25* ℃.

Temperature (℃)	**25**	**25**	**25**	**25**	**50**	**75**	**100**
Flowrate (mL/min)	**1**	**3**	**6**	**0**	**0**	**0**	**0**
Poly. Conc. (ppm)	**Dynamic Retention**	**Dynamic Retention**	**Dynamic Retention**	**Static Retention**	**Static Retention**	**Static Retention**	**Static Retention**
0	0	0	0	0	0	0	0
10	1.645794866	0.544727486	0.263284952	7.68707483	9.608843537	9.608843537	9.608843537
50	7.278868248	2.428048872	1.171797499	33.90022676	46.62698413	48.04421769	48.04421769
220	11.60185091	3.952441294	1.952995832	53.62811791	68.45238095	72.70408163	81.20748299
300	36.76910531	11.27459215	5.510615266	146.1451247	247.8741497	256.377551	304.5634921
500	74.79446199	20.37449705	8.867656749	209.1836735	372.0238095	404.6201814	474.0646259
750	146.5538629	39.74610436	17.26026046	313.4920635	406.037415	491.0714286	590.2777778
1000	185.2706857	54.26161392	22.97145367	395.1247166	451.3888889	506.6609977	635.6292517

***Table D.2**: Polymer retention values under static and dynamic conditions at different concentration, flowrate and temperature. The dynamic retention was carried out at 100 ℃.*

Temperature (℃)	**100**	**100**	**100**	**25**	**50**	**75**	**100**
Flowrate (mL/min)	**1**	**3**	**6**	**0**	**0**	**0**	**0**
Poly. Conc. (ppm)	**Dynamic Retention**	**Dynamic Retention**	**Dynamic Retention**	**Static Retention**	**Static Retention**	**Static Retention**	**Static Retention**
0	0	0	0	0	0	0	0
10	2.48611091	0.836093351	0.424380716	7.68707483	9.608843537	9.608843537	9.608843537
50	13.05340187	4.286034095	2.149351088	33.90022676	46.62698413	48.04421769	48.04421769
220	22.19025534	7.347487021	3.652630042	53.62811791	68.45238095	72.70408163	81.20748299
300	83.89436689	27.71142734	13.80820837	146.1451247	247.8741497	256.377551	304.5634921
500	149.905626	47.18860199	23.01368061	209.1836735	372.0238095	404.6201814	474.0646259
750	206.4105459	65.55731954	31.03679862	313.4920635	406.037415	491.0714286	590.2777778
1000	233.4093937	74.74167832	35.68176168	395.1247166	451.3888889	506.6609977	635.6292517

D.2. Dataset for Modelling Hydrophobic Interactions lost to Polymer Retention in Porous Media

Table D.3*: Dataset for predicting hydrophobic interactions lost to polymer retention mechanisms in the porous media at a flowrate of 1 mL/min (50.83/s) and 25* ℃.

PV-PRL	PV-DL	DPV	Deborah Number	Dilute	Semi-Dilute	Hydrodynamic Size (nm)
0	0	0	0	0	0	0
0.009809093	0.204289885	0.214098978	4.670736913	0.954184307	0.045815693	368.3135801
0.010424556	0.204289885	0.214714441	4.657348588	0.951449208	0.048550792	394.8154948
0.012049069	0.204289885	0.216338954	4.62237606	0.944304674	0.055695326	424.0391348
0.047303217	0.204289885	0.251593102	3.974671766	0.811985238	0.188014762	445.1449675
0.153264128	0.204289885	0.357554013	2.796780242	0.571353914	0.428646086	586.5656354
0.263198386	0.204289885	0.467488271	2.139091098	0.436994675	0.563005325	814.83066
0.264601778	0.204289885	0.468891664	2.132688802	0.43568675	0.56431325	959.9017595

Table D.4: *Dataset for predicting hydrophobic interactions lost to polymer retention mechanisms in the porous media at a flowrate of 1mL/min (50.83/s) and 100* ℃.

PV-PRL	PV-DL	DPV	Deborah Number	Dilute	Semi-Dilute	Hydrodynamic Size (nm)
0	0	0	0	0	0	0
0.003026418	0.258731542	0.258731542	3.865010004	0.066158981	0.011697135	410.3079285
0.015990461	0.271695586	0.271695586	3.680589793	0.069473954	0.058854328	388.5393259
0.0175487	0.273253825	0.273253825	3.659601106	0.069872403	0.064221243	423.7731102
0.019752601	0.255705125	0.275457726	3.630321121	0.928291715	0.071708285	433.0649792
0.060508357	0.255705125	0.316213482	3.162420508	0.80864713	0.19135287	491.2423424
0.093978624	0.255705125	0.349683748	2.859726838	0.731246807	0.268753193	580.4215657
0.111504838	0.255705125	0.367209963	2.723237662	0.696345826	0.303654174	659.4101923

APPENDIX E: Statistical Dataset of used in Developing and Validating the Proxy Model

***Table E.1**: Statistical data used in the development and evaluation of the proxy model for the resistance factor*

Run Order	RF	Q/Qdg	NRV	Cpd	Cp	Pred. Fits	Lower Limit CI	Upper Limit CI	Lower Limit PI	Upper Limit PI
1	32.45	0.046	0.11922	0.022	300	32.901	30.646	35.330	29.398	36.830
2	33.23	0.139	0.50358	0.093	300	32.769	30.917	34.724	29.501	36.390
3	34.78	0.279	0.67629	0.115	300	34.993	32.508	37.668	31.213	39.231
4	51.97	0.056	0.04547	0.097	500	51.488	48.876	54.238	46.507	57.001
5	53.81	0.170	0.15367	0.225	500	52.736	49.933	55.696	47.571	58.462
6	55.12	0.340	0.28866	0.330	500	56.294	52.417	60.457	50.287	63.018
7	151.4	0.066	0.03933	0.198	1000	156.938	146.159	168.50	140.20	175.65
8	173.6	0.2	0.08634	0.259	1000	167.398	159.105	176.12	151.30	185.20
9	184.1	0.4	0.14154	0.349	1000	184.723	171.039	199.50	164.41	207.53

	S	R-sq	R-sq(adj)	R-sq(pred)
Regression Model	0.0314838	99.91%	99.81%	99.47%

In(RF) = 2.8007 + 0.662(Q/Qdg) - 0.1155(NRV) - 0.303(Cpd) +0.002276(Cp)

Analysis of Variance for Transformed Response

Source	DF	Adj SS	Adj MS	F-Value	P-Value
Q/Qdg	1	0.00782	0.00782	7.89	0.048
NRV	1	0.0015	0.0015	1.51	0.086
Cpd	1	0.00112	0.00112	1.13	0.098
Cp	1	1.34932	1.34932	1361.25	0
Error	4	0.00396	0.00099		
Total	8	4.19141			

***Table E.2**: Experimental data and predicted data using the proxy model for the resistance factor at 2.45 %TDS and 25 ℃.*

300ppm			500ppm			1000ppm		
Flowrate (mL/min)	**Resistance Factor**	**Predicted RF**	**Flowrate (mL/min)**	**Resistance Factor**	**Predicted RF**	**Flowrate (mlLmin)**	**Resistance Factor**	**Predicted RF**
0	0.00	0.00	0	0.00	0.00	0	0.00	0.00
1	32.46	32.91	1	51.97	51.49	1	151.45	156.93
3	33.23	32.77	3	53.82	52.74	3	173.61	167.40
6	34.79	34.99	6	55.12	56.29	6	184.14	187.72
8	38.66	39.66	8	66.64	68.64	8	201.62	207.62
10	46.83	49.83	10	80.64	85.64	10	220.55	229.55
11	58.96	61.96	11	98.79	100.79	11	247.29	257.29

APPENDIX F: Dataset of Polymer Effluent Analysis used in Validating the Degradation Model

Table F.1*: Effluent data used in the validation of the model which predicts the onset of mechanical degradation in associative polymers at 2.45 %TDS and 25* ℃.

		300ppm		500ppm		1000ppm	
Flowrate (mL/min)	**Shear Rate (1/s)**	**Exp. Hydro. Interac.**	**Pred. Hydro. Interac.**	**Exp. Hydro. Interac.**	**Pred. Hydro. Interac.**	**Exp. Hydro. Interac.**	**Pred. Hydro. Interac.**
0	0	0.211	0.211	0.426	0.426	0.763	0.763
1	50.82	0.310	0.366	0.572	0.499	0.803	0.784
3	152.49	0.614	0.567	0.680	0.618	0.850	0.822
6	304.97	0.787	0.736	0.815	0.747	0.905	0.875
8	406.64	0.764	0.806	0.810	0.813	0.925	0.907
10	508.29	0.909	0.859	0.846	0.867	0.942	0.936
11	559.12	0.948	0.880	0.872	0.891	0.958	0.951
12	609.96	0.928	0.899	0.902	0.912	0.968	0.964
13	660.79	0.938	0.916	0.952	0.932	0.958	0.977
14	711.62	0.948	0.931	0.922	0.951	0.988	0.990
15	762.45	0.908	0.945	0.952	0.968	0.998	1.002
16	813.28	0.968	0.957	0.972	0.984		0.749
17	864.11	0.978	0.969	0.992	0.999		0.737
18	914.94	0.988	0.979	0.999	1.013		0.726
19	965.77	0.988	0.988		0.480		0.715
20	1016.60	0.988	0.997		0.467		0.705
21	1067.43		1.005		0.455		0.694
22	1118.26		0.198		0.443		0.684
23	1169.09		0.191		0.433		0.675
24	1219.92		0.185		0.422		0.665
25	1270.75		0.179		0.412		0.656